THE DERIVATION AND UTILITY OF *IN VITRO* ORGANOIDS FROM HUMAN PLURIPOTENT STEM CELLS

THE DERIVATION AND UTILITY OF *IN VITRO* ORGANOIDS FROM HUMAN PLURIPOTENT STEM CELLS

BY
ROHAN R. NADKARNI, B.Sc. (Honours)

A Thesis Submitted to the School of Graduate Studies in Partial Fulfillment of the Requirements for the Degree

Doctor of Philosophy

McMaster University

Descriptive Note

McMaster University Doctor of Philosophy (2018) Hamilton, Ontario

TITLE: The derivation and utility of *in vitro* organoids from human pluripotent stem cells

AUTHOR: Rohan R. Nadkarni, B.Sc. (Honours) (McMaster University)

SUPERVISOR: Dr. Jonathan S. Draper, Ph.D.

NUMBER OF PAGES: xi, 189

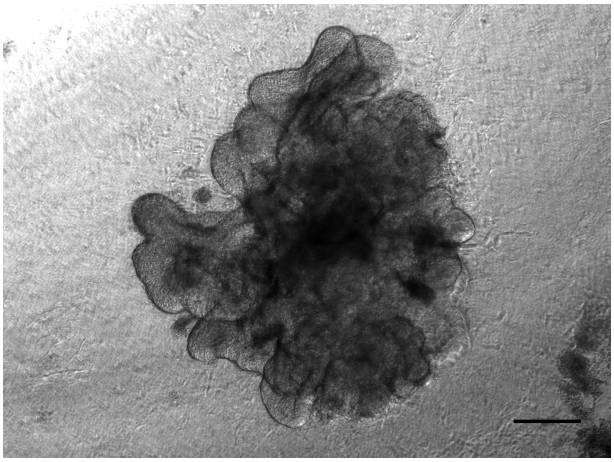

Budding organoids

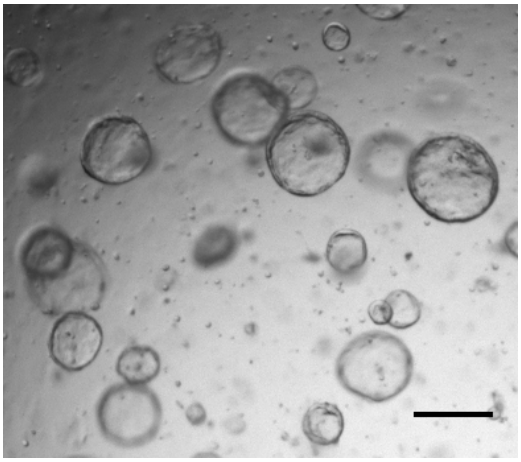

Spheroids

A beauty of nature. Simple yet remarkable structures that self-organize from cells that know exactly what to do. One look under the microscope reinvigorates my enthusiasm for organoids.

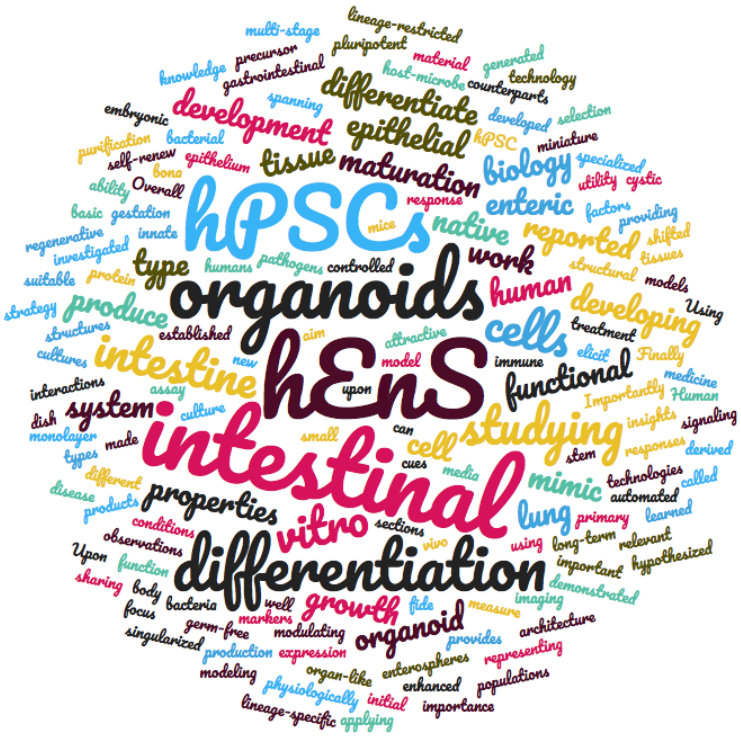

This is a word cloud generated from the main abstract of my thesis. The size of each word is directly proportional to how frequently it appears in the text.

Generated online at https://www.wordclouds.com

ABSTRACT

Human pluripotent stem cells (hPSCs) have the ability to self-renew and differentiate into all specialized body cells, providing material suitable for studying basic biology, modeling disease, and for regenerative medicine. The differentiation of hPSCs into functional cell types has been further enhanced by the production of organoids, miniature 3D organ-like structures that mimic the architecture and function of their *in vivo* counterparts, representing more physiologically relevant models of native tissues than monolayer cultures. Our initial aim was to differentiate hPSCs into lung epithelial organoids *in vitro*, and we hypothesized that applying knowledge of signaling cues during embryonic development to the dish would produce lineage-specific tissue. Using a multi-stage differentiation strategy, we derived organoids sharing properties with the developing lung as well as intestine. From this work, we learned the importance of purification, selection, and using singularized precursor cells to produce populations of bona fide lineage-restricted organoids.

Upon developing a type of intestinal organoid technology from hPSCs not reported before, we shifted our focus to the intestine. We generated cystic intestinal epithelial organoids called enterospheres (hEnS) *in vitro* from hPSCs, which mimic structural and cell type properties of the native small intestinal epithelium. hEnS growth, differentiation, and long-term culture can be controlled by modulating media conditions. Importantly, hEnS are functional in that they elicit an innate immune response upon treatment with enteric pathogens. We established hEnS as an attractive *in vitro* model system for studying human gastrointestinal biology.

We then developed an automated hEnS imaging assay to measure responses to growth factors, bacterial products, and enteric bacteria themselves. In doing so, we demonstrated the utility of hEnS as a germ-free system for studying host-microbe interactions and intestinal maturation. Finally, we investigated the expression of protein markers of intestinal maturation in tissue sections of primary human intestine spanning gestation, and made observations that are different from those reported in mice. Overall, our work provides new and important insights into hPSC differentiation, organoid technologies, and intestinal development in humans.

Acknowledgments

While writing this acknowledgements page, I became emotional as I remembered a number of defining moments, fun times, and the people who have played an important role in my graduate studies experience.

First and foremost, I want to thank my supervisor Dr. Jonathan Draper for giving me the opportunity to pursue a PhD in his lab, and for all his guidance and support throughout my degree. When I first started, he told me that if I work hard and apply myself, he would ensure that I get the best educational experience of my life, which it has been. Jon's door was always open, and I could talk to him any time and get advice, which I think is important for students early in their academic career. He gave me enough freedom to explore project avenues, encouraged me to attend conferences and workshops, and kept my focus on publishing in later years. Also, I appreciate his continuous encouragement and support towards getting my thesis completed and providing feedback.

I want to acknowledge my committee members, Dr. Mick Bhatia and Dr. Jack Gauldie for their support, feedback, as well as keeping me grounded in my expectations. Also, I got the opportunity to TA a number of courses under the supervision of Drs. John Hassell, Boris Zhorov, and Brad Doble.

I want to thank past and present members of the Draper lab for academic collaboration and social experiences. I want to give special thanks to former postdoctoral fellow Dr. Carlos Pilquil for his early insights into the project and for mentoring me when I started. Although our time in the lab overlapped by only 4 months, Carlos trained me extensively during this period, especially in tissue culture, which I consider to be my greatest wet lab skill to date. I want to thank former postdoctoral fellow Dr. Soumeya Abed, who contributed significantly in experimental work and was involved in 3 publications. I want to give a shout out to Jack Huang, with whom I developed a close friendship during our time in the lab that will last forever. I got the opportunity to mentor a number of undergraduate students, including Shirley Zhang and Young-Jin Cheon, and graduate student Amos Lim, who all made valuable contributions to this work.

I want to thank several past and present colleagues in the SCC-RI (there are too many to name), for many fun social experiences, including summer softball league, drinks at the Phoenix, and house parties.

Finally, I can't thank my parents enough for all their love and support, and for taking an interest in my work. I could not have done this without you!

I have spent 10 years at McMaster University and in the city of Hamilton. This is a bittersweet ending. I will miss this place and the people, but I am also happy to be moving on with an excellent graduate education and lots of great memories.

Table of Contents

List of Important Abbreviations

Note: this list excludes gene names and signaling pathways

2D	Two-dimensional
3D	Three-dimensional
AB-PAS	Alcian blue, Periodic acid-Schiff
AFE	Anterior foregut endoderm
ALI	Air-liquid interface
CF	Cystic fibrosis
COPD	Chronic obstructive pulmonary disease
DE	Definitive endoderm
ECAD	E-cadherin
ECM	Extracellular matrix
ESCs	Embryonic stem cells
FACS	Fluorescence-activated cell sorting
FD4	FITC-Dextran-4
FMIA	Familial multiple intestinal atresia
H&E	Haematoxylin and eosin
hEnS	Human enterospheres
hESCs	Human embryonic stem cells
HLFs	Human lung fibroblasts
hPSCs	Human pluripotent stem cells
HUVECs	Human umbilical vein endothelial cells
IBD	Inflammatory bowel disease
iPSCs	Induced pluripotent stem cells
LrGG	*Lactobacillus rhamnosus*
MEF-CM	Mouse embryonic fibroblast conditioned media
NEC	Necrotizing enterocolitis
PSCs	Pluripotent stem cells
SCFA	Short-chained fatty acids
TEM	Transmission electron microscopy
VAFE	Ventral anterior foregut endoderm

SECTION 1 – Generation of definitive endoderm-derived organoids from human pluripotent stem cells

SECTION 1 – Generation of definitive endoderm-derived organoids from human pluripotent stem cells

Preface

This section focuses on strategies for the differentiation of human pluripotent stem cells (hPSCs) into endoderm-derived tissues *in vitro*. This project was initiated by Dr. Jonathan Draper before I joined the lab, and built on preliminary work done by former postdoctoral fellow Dr. Carlos Pilquil. This project was primarily executed by me, with help from undergraduate student Yu Tong (Shirley) Zhang. The section starts off (Chapter 1.1) with an introduction to hPSCs, *in vitro* differentiation into definitive endoderm and downstream lineages, and organoid technologies. It also includes a published review article on the utility of lung organoids. Chapter 1.2 is about the production of early lung and intestinal organoids from hPSCs. Chapter 1.3 is a brief conclusion and transition to Section 2.

Chapter 1.1 – Introduction

1.1.1 - Pluripotent stem cells and in vitro differentiation

Pluripotent stem cells (PSCs) are undifferentiated cells that have the ability to self-renew and differentiate into all specialized body cells. PSCs encompass embryonic stem cells (ESCs) and induced pluripotent stem cells (iPSCs). ESCs are derived from the inner cell mass of the blastocyst stage of a developing embryo upon propagation in culture (Thomson et al., 1998), while iPSCs are derived from somatic cells upon ectopic expression of pluripotency transcription factors that render them ESC-like (Takahashi and Yamanaka, 2006; Takahashi et al., 2007). PSCs differentiated into clinically relevant cell types *in vitro* provide material suitable for studying basic biology, modeling disease and for regenerative medicine.

The embryos and PSCs of triplioblastic organisms, from flat worms to humans, differentiate along three primary germ lineages: the ectoderm, mesoderm, and endoderm. *In vitro* or in-the-dish differentiation of PSCs involves providing specific instructions to cells in order to prompt them to undergo specification and subsequent differentiation towards a lineage or cell type of interest. Directed differentiation of PSCs *in vitro* can be achieved two ways, either through step-by-step differentiation that mimics key stages of native organ development, or by ectopically expressing a key transcription factor(s) of the target lineage in undifferentiated cells (Blij et al., 2015; Séguin et al., 2008). The latter approach has typically been used to interrogate the function and sufficiency of transcription factors in inducing differentiation, while the former approach is the preferred method of producing target cells for characterization and applications that include disease modeling and regenerative medicine.

In vitro differentiation studies have increased our understanding of how stem cells make fate decisions and have contributed to our knowledge of embryonic development. Stage-specific screening of growth factors during differentiation *in vitro* has helped elucidate the role of signaling pathways and their relative dosage in germ layer and organ specification (Loh et al., 2014; Pagliuca et al., 2014). Also, these studies have provided the best direct evidence of intermediate cell states, such as transient mesendoderm progenitors during gastrulation (Tada et al., 2005). Conversely, PSC differentiation protocols themselves have been designed by extrapolating from development studies in animals. This work has been instrumental in the success of directed differentiation into clinically relevant cell types.

1.1.2 – Differentiation of PSCs towards the definitive endoderm lineage and its derivatives

One of the first cell fate decisions made in embryonic development is gastrulation, which is when the segregation of the three primordial germ layers, the ectoderm, mesoderm, and endoderm, occurs. Nodal growth factor signaling is necessary and sufficient to induce definitive endoderm (DE) specification from migrating cells of the inner cell mass (Zorn and Wells, 2009). The DE germ layer then differentiates into a primitive gut tube, along which organs lining the future alimentary canal develop from. The anterior-posterior axis of the primitive gut tube is sub-divided into the foregut, midgut, and hindgut. The lungs, thyroid, esophagus, liver, pancreas, and stomach develop from the foregut, the small intestine develops from the midgut, and the large intestine develops from the hindgut. The morphogenesis of organ domains and the establishment

of cellular identity are regulated by signaling pathways including FGF, BMP, Wnt, retinoic acid, Hedgehog, and Notch in a stage-specific manner (Zorn and Wells, 2009).

Over the past decade, various protocols have been designed for differentiating ESCs and iPSCs *in vitro* into DE-specified cells and their derivatives with varying efficiencies by mimicking native endoderm organogenesis (D'Amour et al., 2005, 2006; Loh et al., 2014). These protocols have either involved the production of transient DE cells that are volatile to subsequent differentiation (Green et al., 2011), or the production of more stable DE stem-like cells that can be maintained and propagated (Cheng et al., 2012). As mentioned earlier, Nodal signaling is necessary for DE specification in the embryo. In the dish, most protocols use Activin A, a surrogate of Nodal, to induce DE specification from undifferentiated PSCs. The production of functional DE cells is marked by co-expression of the transcription factors FOXA2 and SOX17 (Zorn and Wells, 2009). DE cells can be subsequently differentiated into foregut, midgut, and hindgut derivatives by exogenous addition of growth factors in a dose-dependent manner of the signaling pathways mentioned above. For example, dual inhibition of BMP and TGFβ signaling in DE cells leads to foregut specification (Green et al., 2011), while dual activation of Wnt and FGF signaling leads to mid/hindgut specification (Spence et al., 2011). Step-by-step PSC differentiation via the endoderm lineage has been used for producing monolayer cultures of pulmonary, thyroid, pancreatic and intestinal cells (Antonica et al., 2012; D'Amour et al., 2006; Green et al., 2011; Huang et al., 2014; Longmire et al., 2012; Spence et al., 2011).

PSC differentiation strategies have most often focused on producing populations of a single cell type or a mixture of cell types within a tissue (Lanza et al., 2009).

However, important limitations of monolayer cultures are that they are supported by a simple 2D extracellular matrix (ECM), and that cells have a random distribution in the dish, which in turn does not accurately recapitulate native organ architecture and function. *In vivo* tissues are supported by a complex 3D ECM, and consist of spatially arranged cell types that interact with each other and constitute organ function. In recent years, to address these pitfalls, the differentiation of PSCs into functional cell types has been further enhanced by the production of miniature 3D organ-like structures called organoids, which are discussed in Chapter 1.1.3.

1.1.3 – Organoids as a model system for studying human lung development and disease

Preface

This sub-chapter is an original published review article from the scientific journal *Biochemical and Biophysical Research Communications*, and is presented in its published form. At the time of publication, it became the first ever review article that was explicitly about lung organoids.

Nadkarni, R.R., Abed, S., Draper J.S. (2015). Organoids as a model system for studying human lung development and disease. *Biochemical and Biophysical Research Communications*. **473**(3), 675-682.

I conceived the idea of the subject of this review article. Dr. Jonathan Draper, Dr. Soumeya Abed, and I contributed to the writing of the manuscript. I generated all the figures. This review includes an introduction to organoid technologies in general, principles of organoid formation, and the derivation and utility of lung organoids from primary cells and PSCs.

Title

Organoids as a model system for studying human lung development and disease

Authors

Rohan R. Nadkarni[1, 3, 4], Soumeya Abed[1, 2, 4] & Jonathan S. Draper [1, 2, 3 *]

Affiliations

[1] McMaster Stem Cell and Cancer Research Institute, Michael G. DeGroote School of Medicine, McMaster University, Hamilton, ON L8N 3Z5, Canada

[2] Department of Pathology and Molecular Medicine, McMaster University, Hamilton, ON L8N 3Z5, Canada

[3] Department of Biochemistry and Biomedical Sciences, McMaster University, Hamilton, ON L8N 3Z5, Canada

[4] These authors contributed equally.

* Corresponding author at: McMaster Stem Cell and Cancer Research Institute, Michael G. DeGroote School of Medicine, McMaster University, Hamilton, ON L8N 3Z5, Canada. draperj@mcmaster.ca

ABSTRACT

The lung is a complex organ comprising multiple cell types that perform a variety of vital processes, including immune defense and gas exchange. Diseases of the lung, such as chronic obstructive pulmonary disease, asthma and lung cancer, together represent one of the largest causes of patient suffering and mortality. Logistical barriers that hamper access to embryonic, normal adult or diseased lung tissue currently hinder the study of lung disease. *In vitro* lung modeling represents an attractive and accessible avenue for investigating lung development, function and disease pathology, but accurately modeling the lung *in vitro* requires a system that recapitulates the structural features of the native lung. Organoids are stem cell-derived three-dimensional structures that are supported by an extracellular matrix and contain multiple cell types whose spatial arrangement and interactions mimic those of the native organ. Recently, organoids representative of the respiratory system have been generated from adult lung stem cells and human pluripotent stem cells. Ongoing studies are showing that organoids may be used to model human lung development, and can serve as a platform for interrogating the function of lung-related genes and signalling pathways. In a therapeutic context, organoids may be used for modeling lung diseases, and as a platform for screening for drugs that alleviate respiratory disease. Here, we summarize the organoid-forming capacity of respiratory cells, current lung organoid technologies and their potential use in future therapeutic applications.

INTRODUCTION

One of the major goals of regenerative medicine is to utilize stem cells in the generation of tissues for therapeutic transplantation or drug screening. In adult organs, tissue function is derived from the synergistic interaction of multiple cell types that are distributed and organized within a three-dimensional (3D) structure, and supported by a complex extracellular matrix (Hynds and Giangreco, 2013). The spatial arrangement of organ cell types is crucial for normal cellular interaction and function, but most *in vitro* approaches for the generation of tissues from stem cell sources have focused on cell culture in a monolayer format. Although a broad range of cell types can emerge in monolayer differentiation environments, the lack of structural organization hinders the emergence of cell-cell interactions that govern tissue function in the native organ (Hynds and Giangreco, 2013).

To address the pitfalls associated with modelling *in vivo* tissues using monolayer cultures, strategies have been recently developed for the production of miniature 3D structures, termed "organoids". Organoids share important features with *in vivo* organs that make them attractive prospects for exploring multiple avenues of developmental, disease and therapeutic biology. First, they contain multiple cell types that are found within that organ; second, they approximate the cellular organization within the organ; and finally, they share some level of native organ functionality (Hynds and Giangreco, 2013). The term "organoid" has been inconsistently applied throughout the literature, but for this review we use the term to encompass 3D tissue structures containing multiple cell types in an organized manner. This definition of organoids includes multicellular spheroids, which arise from tissue-specific stem cell populations. It does not extend to

disorganized aggregates of cells in sphere-like structures, such as those often described in tumour sphere biology (Weiswald et al., 2015). Organoid production capitalizes on the processes that regulate organogenesis during embryonic development: the self-organization of cells, via similarities in adhesion properties, and spatially restricted progenitor differentiation (Hynds and Giangreco, 2013; Lancaster and Knoblich, 2014). Experiments with embryonic tissues demonstrated that aggregates of progenitor cells self-organize into 3D structures typical of early organogenesis (Auerbach and Grobstein, 1958; Lancaster and Knoblich, 2014; Weiss and Taylor, 1960), while single cells dissociated from adult organs can re-aggregate and reconstruct the original architecture to some extent (Hynds and Giangreco, 2013; Lancaster and Knoblich, 2014).

The application of these approaches has now enabled the production of organoids from primary tissue-specific cells taken from the mammary gland (Dontu et al., 2003), bone (Kale et al., 2000), small intestine (Sato et al., 2009), stomach (Barker et al., 2010), colon (Sato et al., 2011), liver (Huch et al., 2015), pancreas (Huch et al., 2013), lung (Barkauskas et al., 2013; Lee et al., 2014; Rock et al., 2009) and prostate (Gao et al., 2014). In addition, the establishment of differentiation protocols recapitulating organ development has enabled the production of pluripotent stem cell-derived organoids representative of retinal (Eiraku et al., 2011), pituitary (Suga et al., 2011), cerebral (Lancaster et al., 2013), small intestine (Spence et al., 2011), thyroid (Antonica et al., 2012), liver (Takebe et al., 2013), stomach (McCracken et al., 2014), lung (Dye et al., 2015) and cardiac tissues (Stevens et al., 2009).

The increasing activity and interest focusing on the development of organoid technologies reflects the growing sentiment that *in vit*ro organoids will play a major role

in modelling organ development and disease pathobiology, as well as in toxicology and drug discovery. In this review, we discuss the advances that have been made in using 3D cultures to model the lung, including the organoid-forming capacity of pulmonary cells, current lung organoid technologies and their utility in therapeutic applications.

ORGANOID-FORMING STEM CELLS OF THE ADULT LUNG EPITHELIUM

The adult lung comprises two zones, each having a unique cell type composition and function. The trachea, bronchi and bronchioles are epithelial tubules that constitute the conducting zone (airways), which assist in moistening air and protecting the lung by expelling foreign particulates and pathogens via the mucociliary escalator. The conducting epithelial tubules are lined with a mixture of cell types, including club, goblet, ciliated, basal and neuroendocrine cells. The bronchioles terminate into the respiratory zone (alveoli) of the lung. This is the site of gas exchange, facilitated by type I alveolar epithelial cells (AEC1s) with the associated vasculature. Type II alveolar epithelial cells (AEC2s) secrete surfactant which reduces surface tension, enabling alveoli expansion and preventing collapse.

The ability of the lung to regenerate following disease or damage is a major research focus, and it is now understood that the lung epithelium of the conducting and respiratory zones contain distinct stem cell populations. Basal cells are stem cells of the airway epithelium, and in humans, are present throughout the airways, including small bronchioles near the distal region (Boers et al., 1998; Evans et al., 2001; Nakajima et al., 1998; Rock et al., 2009). Basal cells self-renew and are capable of mucociliary differentiation, giving rise to secretory and ciliated cells in response to normal wear-and-

tear or injury (Borthwick et al., 2001; Hong et al., 2004; Rock et al., 2009; Schoch et al., 2004). Alongside basal cells, pulmonary neuroendocrine cells (PNECs) are distributed throughout the conducting airways and can self-renew and differentiate into club and ciliated cells (Cutz, 1982; Song et al., 2012). In the respiratory zone of the lung, AEC2s can serve in a stem cell capacity, undergoing self-renewal and differentiating into AEC1s when required (Barkauskas et al., 2013). A distinct stem cell population, termed bronchioalveolar stem cells (BASCs), exists at the border of the conducting and respiratory zones (Kim et al., 2005). BASCs are located at the bronchioalveolar duct junction of the distal lung, and can self-renew and differentiate into bronchiolar Clara cells and AEC2s (Kim et al., 2005).

The stem cell types described above are essential for lung epithelial maintenance and repair *in vivo,* and are now known to be capable of organogenesis *in vitro* when cultured in a suitable microenvironment. In the next section, we discuss lung organoid technologies developed over the last decade.

CURRENT LUNG ORGANOID TECHNOLOGIES

The microenvironment supporting lung organoid formation

The most common 3D environment used in the formation of organoids are hydrogels, such as Matrigel, that contain gelatinous mixtures of extracellular matrix components, including laminin and collagen (Kleinman and Martin, 2005). The air-liquid interface (ALI) culture system is favoured when culturing primary human bronchial epithelial cell (HBECs) lines (Bals et al., 2004; Fessart et al., 2013; Pageau et al., 2011; Vaughan et al., 2006), due to retention of polarized apical-basal organization, as well as

functional differentiation properties like cilliogenesis (Bérubé et al., 2010; Vaughan et al., 2006). The ALI system utilizes an insert with a permeable culture membrane that can be submerged in media, and can be combined with a 3D extracellular matrix layer (or a "3D ALI") to create an environment that supports 3D growth, polarization and differentiation (Delgado et al., 2011; Rock et al., 2009; Van Haute et al., 2009). Supplementing cultures with supporting stromal cell types, including fibroblasts, endothelial cells or smooth muscle cells, can also assist in organoid formation by secreting factors that are important for determining cell fate (Kimura and Deutsch, 2007). These are often used in combination with media components that are necessary for lung epithelial culture, including factors like EGF and retinoic acid that are involved in lung development (Malpel et al., 2000; Miettinen et al., 1997; You et al., 2002).

Interestingly, the positioning of organoids-forming cells in the 3D growth environment impacts the structures derived: HBECs embedded within Matrigel organize into spheroids containing cuboidal epithelial cells, while HBECs plated on top of the Matrigel layer self-organize into tubular structures that undergo branching and budding (Delgado et al., 2011).

Lung organoids derived from primary respiratory cells and cell lines

Primary basal cells harvested from mouse and human lungs can self-organize into organoids termed tracheospheres or bronchospheres when cultured in a 3D ALI (Rock et al., 2009). These organoids are derived from basal cells expressing p63 and NGFR, which proliferate to establish a layer of basal cells in a spherical organization, covered on the luminal side by a second layer of differentiated goblet and ciliated cells (Rock et al.,

2009). Under normal physiological conditions, basal cells undergo mucociliary differentiation in a salt-and-pepper distribution, and *in vivo* experiments suggest that Notch signalling is an important controller in secretory versus ciliated differentiation (Guseh et al., 2009; Rock et al., 2011). Recent work utilizing human bronchospheres as a model system revealed that the Notch pathway has diverse actions on basal cell differentiation: blocking the NOTCH1 receptor leads to increases in basal cell markers, but blocking NOTCH2 receptor facilitated the induction of ciliated markers at the expense of goblet markers (Danahay et al., 2015). It remains to be determined whether PNECs, which are capable of Clara and ciliated cell differentiation, can produce organoids in a similar manner to basal cells.

Alveolar spheroids or "alveolospheres" that capture properties of the alveolar compartment of the lung have also been developed by isolating primary SFTPC-expressing AEC2s from mouse lungs, and co-culturing them with lung stromal cells in a 3D ALI (Barkauskas et al., 2013). During alveolosphere production, AEC2s proliferate to form 3D aggregates, and also differentiate into AEC1s, establishing organoids composed of both alveolar epithelial cell types (Barkauskas et al., 2013).

Other complex *in vitro* organoids have also been generated that contain cell types from both zones of the lung or that have multipotent differentiation potential. For example, immortalized airway basal cells and HBECs can produce embryonic-like branching structures when co-cultured with fibroblasts or endothelial cells in 3D conditions (Franzdóttir et al., 2010; Kaisani et al., 2014). These structures contain multipotent cells and structurally resemble the branching epithelia of lung development. Similarly, single BASCs harvested from mouse lungs give rise to bronchiolar, alveolar

and bronchioalveolar structures when co-cultured with mouse lung endothelial cells (LuMECs) in 3D conditions, with the latter structure containing both airway and alveolar cell types (Lee et al., 2014). The clonal nature of this study highlights the multipotent potential of BASCs.. The lung organoid types described above, their precursor cells and pulmonary zone representation are schematized in **Figure 1**, and their properties are summarized in **Table 1**.

Lung organoids derived from human pluripotent stem cells

Producing lung organoids from primary cells can be hampered by logistical challenges in accessing patient tissue, so recent attention has focused on utilising human pluripotent stem cells (hPSCs). HPSCs can be derived from the developing embryo (embryonic stem cells), or patient tissue samples via the process of reprogramming adult somatic cells into induced pluripotent stem cells (iPSCs) by ectopic expression of pluripotency transcription factors (Takahashi and Yamanaka, 2006; Takahashi et al., 2007). HPSCs provide an accessible source of potentially unlimited starting material that can differentiate into all specialized cell types of the body. Importantly, iPSCs permit disease modeling via the capture of patient genotypes containing disease-causing mutations, and provide an attractive avenue for modeling both monogenic and polygenic diseases. Although human iPSC-derived lung organoids have yet to be used to model patient diseases, a similar approach has been successfully employed using cerebral organoids for modeling and recapitulating disease phenotypes for hereditary brain mutations (Lancaster et al., 2013).

To date, mouse and human PSCs have been differentiated via step-by-step protocols into lung progenitors (Green et al., 2011; Longmire et al., 2012; Mou et al., 2012), mature airway and alveolar cells (Huang et al., 2014), and even an organized airway epithelium (Firth et al., 2014; McIntyre et al., 2014; Wong et al., 2012). These protocols capitalize on current knowledge of embryonic lung development. Within the developing embryo, the endoderm germ layer produces a primitive gut tube along which the lung, thyroid and organs lining the gastrointestinal tract emerge (Zorn and Wells, 2009). The lung arises from cells expressing the transcription factor NKX2.1 (TTF-1) in the ventral wall of the anterior foregut endoderm (Zorn and Wells, 2009). Hence current protocols include discrete steps to differentiate hPSCs through an initial definitive endoderm (DE) specification, then anterior foregut endoderm (AFE), and finally into ventral anterior foregut endoderm (VAFE) and NKX2.1+ lung progenitors. Each step uses stage-specific growth factors to recapitulate signalling pathways involved in lung development (Morrisey and Hogan, 2010). Importantly, since organoids develop from tissue-specific stem cells or progenitors, hPSC differentiation into these cell types has been employed as a strategy en route to producing organoids.

So far, two studies have reported the generation of lung organoids *in vitro* from hPSCs (summarized in **Table 1**). The first study identified Carboxypeptidase M (CPM) as a cell-surface marker of VAFE cells that coincided with NKX2.1 expression, and then showed that culturing purified CPM expressing cells in 3D conditions, supplemented with alveolar-related growth factors and human lung fibroblasts, produced alveolar epithelial spheroids (Gotoh et al., 2014). These spheroids contained cells expressing NKX2.1 and CPM, as well as differentiated cells that stained positive for AQP5 and

SFPTC, markers of AEC1s and AEC2s respectively (Gotoh et al., 2014). The hPSC-derived alveolar spheroids reported in this study are similar in structure and composition to alveolospheres generated from primary mouse AEC2s (Barkauskas et al., 2013), and also contained lamellar-body-like subcellular structures characteristic of AEC2s.

In the second study, step-by-step differentiation of hPSCs into multi-lineage organoids with both epithelial and mesenchymal components was reported (Dye et al., 2015). Here, hPSCs were also initially differentiated into DE and AFE cells, followed by formation of VAFE spheroids. By stimulating the Hedgehog (HH) signaling pathway during spheroid generation, the authors were able to enhance NKX2.1 expression and expand spheroids in media containing FGF10. This allowed VAFE spheroids to grow into more complex structures that the authors termed human lung organoids (HLOs) (Dye et al., 2015). HLOs persisted in culture for over 100 days and developed organized proximal airway-like epithelial tubules containing numerous cell types found in the native airway epithelium, including basal, ciliated and club cells. Moreover, proximal airway structures were often surrounded by smooth muscle actin (SMA)-expressing mesenchymal tissue. HLOs also possessed distal-like epithelial cells that co-expressed progenitor markers, SFTPC/SOX9 and HOPX/SOX9, consistent with early bipotent alveolar progenitor cells. Thus, HLOs are multi-lineage in that they contain both airway and alveolar cells types. Whole transcriptome analysis showed that HLOs are similar to fetal lung tissue (Dye et al., 2015).

Both these studies showcase the potential of hPSCs to generate tissues that are analogous to those observed in the developing fetus. However, further work is required to evaluate the maturation and functionality of these hPSC-derived organoids before their

utility in biomedical applications can be properly assessed. It remains to be determined if other types of lung organoids like bronchospheres can also be generated *in vitro* from hPSCs.

APPLICATIONS/THERAPEUTIC POTENTIAL OF LUNG ORGANOIDS

There is a need to create human lung models that aid in further understanding human lung development and pathobiology, both of which are crucial for generating new therapeutic approaches to tackle respiratory diseases. Below, we discuss current and potential applications of lung organoids.

Modeling human lung development

Historically, several important aspects of human lung development, repair and regeneration have been extrapolated from mouse models (Morrisey and Hogan, 2010). The developmental functions of lung-related transcription factors like NKX2.1, FOXA2 and GATA6 were elucidated using genetic ablation experiments in mice (Wan et al., 2004; Yang et al., 2002; Yuan et al., 2000). Indeed, the mouse has been a critical model for understanding developmental processes like tracheo-esophageal separation and branching morphogenesis, as well as interrogating which signalling pathways function during lung development (Bellusci et al., 1997; Weaver et al., 2000; Xing et al., 2008). However, there are intrinsic differences between human and mouse lung tissue that make establishing human models of lung development a worthwhile endeavour (Rock and Hogan, 2011; Rock et al., 2010). For example, basal cells are present throughout the human airways but are confined to the trachea in mice (Boers et al., 1998; Nakajima et

al., 1998), and mucin-secreting goblet cells are common in human airways but rare in mice (Rock et al., 2010). To this end, human lung epithelial cell lines that capture some phenotypic traits of the adult lung are in use, but these cell lines are cultured as a monolayer and can struggle to provide insights into the process that govern the development and organization of the lung, including epithelial-mesenchymal interactions and branching morphogenesis.

Identifying factors that control the proliferation of lung stem cells during development and adult lung homeostasis should assist in devising strategies for encouraging endogenous stem cells to repair damaged lung tissue. Since basal cells govern the formation and growth of bronchospheres, these organoids represent a useful model for exploring factors that potentiate basal cell expansion. The addition of fibroblast growth factors (FGF2, FGF9 and FGF10) to basal cells in sphere-forming cultures increases sphere production and size, whereas the addition of chemical FGF inhibitors blocks basal cell proliferation (Hegab et al., 2015). A number of newly identified factors that positively regulate human basal cell marker expression in bronchospheres have recently been described, suggesting that additional pathways may also control basal cell expansion in humans (Danahay et al., 2015). In mice, FGFs and transforming growth factors (TGFs) exert a strong effect on lung branching morphogenesis (Bellusci et al., 1997; Weaver et al., 2000; Xing et al., 2008), but it remains to be determined whether these processes are fully conserved in humans. The branching structures produced from immortalized HBECs (Franzdóttir et al., 2010; Kaisani et al., 2014) mimic the developing lung in structure and contain cells with multipotent potential, providing a model that may serve as a starting point to begin addressing these questions.

Modelling lung diseases

The mouse have proved to be an imperfect model for several diseases affecting the lung and airways, providing a strong rationale for developing and investigating human organoid models of disease. One conspicuous example is the modeling of cystic fibrosis (CF) in mice, via mutation of the causative gene CFTR: Mouse models of CF, including CFTR gene deletion, have failed to fully recapitulate the human symptoms of the disease (Cohen and Prince, 2012; Ratjen and Döring, 2003). CFTR functions as an anion channel that is essential for fluid and electrolyte homeostasis at the epithelial surfaces of many organs, including the lung and intestine (Gadsby et al., 2006). The addition of forskolin activates CFTR by raising the amount of intracellular cyclic AMP, thus mediating fluid secretion into the lumen (Dekkers et al., 2013). To date, organoid-based modeling of CF has been best achieved by using intestinal organoids, which manifest key CF phenotypes when mutant CFTR is present. Forskolin induces rapid swelling of normal intestinal organoids, but not of organoids derived from CF patients with CFTR mutations (Dekkers et al., 2013). Exposure to both forskolin and drugs that restore function for specific CFTR mutations results in CF intestinal organoid swelling close to wild-type controls. This study highlights organoids as tractable models for generating simple yet robust functional assays for testing CFTR drug efficacy *in vitro*. Indeed, given the large number of mutations documented to impact the CTFR gene, and the need to evaluate new drugs that target specific CFTR mutations, the development of similar assays using lung organoids should yield important insights.

In vitro human models of goblet cell metaplasia, a phenotype associated with CF, asthma and chronic obstructive pulmonary disease (COPD), are needed for developing

new treatments (Boucherat et al., 2013). The normal distribution of airway cell types is disrupted in goblet cell metaplasia, leading to increased goblet cells numbers, overproduction of mucus, and concomitant illness due to airway obstruction. A strong component of goblet cell metaplasia appears to be signalling via T Helper 2 cytokines, such as Interleukin 13, in response to acute or chronic injury (Boucherat et al., 2013). A recent high-throughput screen on human bronchospheres sought to identify secreted factors that could alter their cellular composition by assaying markers of basal, ciliated and goblet cells (Danahay et al., 2015). Both Il-13 and IL-17A elicited a mucosal hypersecretory phenotype, in which ciliated cell markers were depleted and goblet cell markers were increased. Importantly, modulation of Notch signalling was shown to be a controlling element in the IL-13 induced mucosal hypersecretory phenotype, with chemical inhibition of Notch2 preventing goblet cell metaplasia (Danahay et al., 2015). The Notch pathway is now a potential therapeutic intervention target in the treatment of goblet cell metaplasia, and highlights the value that organoids can bring to respiratory research.

It is highly likely that the near future will see human iPSC-derived lung organoids that capture disease-associated mutations used in similar approaches to understand how genetic predisposition and environmental exposure contribute to other aspects lung disease (Noble et al., 2012; Ryu et al., 2014).

Modelling lung cancer

Studying tumorigenesis and the characteristics of early stage human lung tumours could greatly improve the ability to diagnose lung cancer at earlier stages, but access to

early stage lung tumours is sporadic and often the result of accidental discovery via tests for other medical conditions. Animal models of lung cancer have been informative, but there are important differences, including the differing oncogenic and tumour suppressor changes required in the transformation of human cells in comparison to rodent (Akagi, 2004), that can hinder the translation of research in mice to humans. Cancer cell lines acquired from patient tumours often represent later stage tumours, with numerous genetic lesions that contribute to aggressive or metastatic phenotypes, making the study of driver mutations in tumorigenesis difficult. Modeling lung cancer genesis *ex vivo* with human lung organoids offers a distinct advantage over lung cancer cell lines: they contain multiple normal lung cell types, including precursor cells that can be genetically engineered to test the ability of specific mutations in driving transformation. This approach has permitted the identification of genetic alterations that enable HBECs to acquire a fully transformed phenotype: immortalization with hTERT and CDK4 overexpression, loss of normal p53 function, and over expression of oncogenic K-RAS and c-MYC (Sasai et al., 2011; Sato et al., 2006). Normal HBECs form organized networks of tubules that branch and bud when cultured in 3D conditions. Once HBECs are transformed they form tubular structures that fail to branch/bud, and instead develop an invasive phenotype indicative of malignant transformation (Kaisani et al., 2014). Exploring the oncogenic transformation in lung organoid culture systems will allow the development of accessible models for studying tumorigenesis, and provide new pre-clinical models for evaluating treatments in a human-specific context.

THE NEXT STEPS IN LUNG ORGANOID RESEARCH

Advances in multipotent stem and progenitor cell isolation have allowed researchers to develop highly reproducible lung organoids from primary cells isolated from the lungs of patients (Barkauskas et al., 2013; Kim et al., 2005; Rock and Hogan, 2011; Rock et al., 2009). Similarly, protocols have now been described that permit the production of lung cell types and organoids from hPSCs. Together, primary cell- and hPSC-derived lung organoids represent a powerful resource that will supercharge the study of human lung biology.

The deployment of recent advances in genome editing, via the CRISPR/Cas9 system (Cong and Zhang, 2015; Cong et al., 2013), in lung organoid models will allow the genetics of lung development and disease to be explored in a human context. A range of experiments that were until recently practical only in the mouse is now tractable using human organoids, allowing human-centric evaluations of genetic contribution to lung disease. Similarly, the production of lung organoids from patient-derived iPSCs is a key advance that will permit lung disease phenotypes to be accurately evaluated on a patient-by-patient basis, opening up plausible personalised medicine applications.

These advances are close to being implemented, but there is further work that needs to be done to exploit the full potential of lung organoids. Although gene expression profiles have been published, proteomic and epigenomic profiles have not been described. The factors that control stem cell proliferation and differentiation have not been fully explored, and could lead to optimization of organoid protocols that allow consistent, efficient and reproducible formation. These, and other advances are vital if

organoids are going to become a driving force in applications such as drug or toxicology screening.

There are currently a number of outstanding questions that need to be addressed before the benefits of lung organoids derived from pluripotent stem cell sources are realised. It is unclear whether lung organoids derived from hPSCs most closely mimic fetal or adult lung tissue, and if it is the former, then maturation strategies will likely be needed. The functionality of cell types found in hPSC-derived lung organoids remains to be determined, in addition to establishing if all of the cell types that populate the adult lung epithelium are represented in organoids. Finally, it will be interesting to see if incorporating supporting cell types into human lung organoids, such as vasculature and mesenchymal cells, demonstrably improves replication of the *in vivo* organ phenotype (Takebe et al., 2013). This could significantly extend their utility, and provide systems for modeling the interaction of the respiratory epithelium with surrounding host tissues.

The future for organoid models of the lung is arriving quickly and will lead to tangible benefits to researchers, clinicians and patients.

REFERENCES

Akagi, T. (2004). Oncogenic transformation of human cells: shortcomings of rodent model systems. Trends Mol. Med. *10*, 542–548.

Antonica, F., Kasprzyk, D.F., Opitz, R., Iacovino, M., Liao, X.-H., Dumitrescu, A.M., Refetoff, S., Peremans, K., Manto, M., Kyba, M., et al. (2012). Generation of functional thyroid from embryonic stem cells. Nature *491*, 66–71.

Auerbach, R., and Grobstein, C. (1958). Inductive interaction of embryonic tissues after dissociation and reaggregation. Exp. Cell Res. *15*, 384–397.

Bals, R., Beisswenger, C., Blouquit, S., and Chinet, T. (2004). Isolation and air-liquid interface culture of human large airway and bronchiolar epithelial cells. J. Cyst. Fibros. Off. J. Eur. Cyst. Fibros. Soc. *3 Suppl 2*, 49–51.

Barkauskas, C.E., Cronce, M.J., Rackley, C.R., Bowie, E.J., Keene, D.R., Stripp, B.R., Randell, S.H., Noble, P.W., and Hogan, B.L.M. (2013). Type 2 alveolar cells are stem cells in adult lung. J. Clin. Invest. *123*, 3025–3036.

Barker, N., Huch, M., Kujala, P., van de Wetering, M., Snippert, H.J., van Es, J.H., Sato, T., Stange, D.E., Begthel, H., van den Born, M., et al. (2010). Lgr5(+ve) stem cells drive self-renewal in the stomach and build long-lived gastric units in vitro. Cell Stem Cell *6*, 25–36.

Bellusci, S., Grindley, J., Emoto, H., Itoh, N., and Hogan, B.L. (1997). Fibroblast growth factor 10 (FGF10) and branching morphogenesis in the embryonic mouse lung. Dev. Camb. Engl. *124*, 4867–4878.

Bérubé, K., Prytherch, Z., Job, C., and Hughes, T. (2010). Human primary bronchial lung cell constructs: the new respiratory models. Toxicology *278*, 311–318.

Boers, J.E., Ambergen, A.W., and Thunnissen, F.B. (1998). Number and proliferation of basal and parabasal cells in normal human airway epithelium. Am. J. Respir. Crit. Care Med. *157*, 2000–2006.

Borthwick, D.W., Shahbazian, M., Krantz, Q.T., Dorin, J.R., and Randell, S.H. (2001). Evidence for stem-cell niches in the tracheal epithelium. Am. J. Respir. Cell Mol. Biol. *24*, 662–670.

Boucherat, O., Boczkowski, J., Jeannotte, L., and Delacourt, C. (2013). Cellular and molecular mechanisms of goblet cell metaplasia in the respiratory airways. Exp. Lung Res. *39*, 207–216.

Cohen, T.S., and Prince, A. (2012). Cystic fibrosis: a mucosal immunodeficiency syndrome. Nat. Med. *18*, 509–519.

Cong, L., and Zhang, F. (2015). Genome engineering using CRISPR-Cas9 system. Methods Mol. Biol. Clifton NJ *1239*, 197–217.

Cong, L., Ran, F.A., Cox, D., Lin, S., Barretto, R., Habib, N., Hsu, P.D., Wu, X., Jiang, W., Marraffini, L.A., et al. (2013). Multiplex genome engineering using CRISPR/Cas systems. Science *339*, 819–823.

Cutz, E. (1982). Neuroendocrine cells of the lung. An overview of morphologic characteristics and development. Exp. Lung Res. *3*, 185–208.

Danahay, H., Pessotti, A.D., Coote, J., Montgomery, B.E., Xia, D., Wilson, A., Yang, H., Wang, Z., Bevan, L., Thomas, C., et al. (2015). Notch2 is required for

inflammatory cytokine-driven goblet cell metaplasia in the lung. Cell Rep. *10*, 239–252.

Dekkers, J.F., Wiegerinck, C.L., de Jonge, H.R., Bronsveld, I., Janssens, H.M., de Winter-de Groot, K.M., Brandsma, A.M., de Jong, N.W.M., Bijvelds, M.J.C., Scholte, B.J., et al. (2013). A functional CFTR assay using primary cystic fibrosis intestinal organoids. Nat. Med. *19*, 939–945.

Delgado, O., Kaisani, A.A., Spinola, M., Xie, X.-J., Batten, K.G., Minna, J.D., Wright, W.E., and Shay, J.W. (2011). Multipotent capacity of immortalized human bronchial epithelial cells. PloS One *6*, e22023.

Dontu, G., Abdallah, W.M., Foley, J.M., Jackson, K.W., Clarke, M.F., Kawamura, M.J., and Wicha, M.S. (2003). In vitro propagation and transcriptional profiling of human mammary stem/progenitor cells. Genes Dev. *17*, 1253–1270.

Dye, B.R., Hill, D.R., Ferguson, M.A.H., Tsai, Y.-H., Nagy, M.S., Dyal, R., Wells, J.M., Mayhew, C.N., Nattiv, R., Klein, O.D., et al. (2015). In vitro generation of human pluripotent stem cell derived lung organoids. eLife *4*.

Eiraku, M., Takata, N., Ishibashi, H., Kawada, M., Sakakura, E., Okuda, S., Sekiguchi, K., Adachi, T., and Sasai, Y. (2011). Self-organizing optic-cup morphogenesis in three-dimensional culture. Nature *472*, 51–56.

Evans, M.J., Van Winkle, L.S., Fanucchi, M.V., and Plopper, C.G. (2001). Cellular and molecular characteristics of basal cells in airway epithelium. Exp. Lung Res. *27*, 401–415.

Fessart, D., Begueret, H., and Delom, F. (2013). Three-dimensional culture model to distinguish normal from malignant human bronchial epithelial cells. Eur. Respir. J. *42*, 1345–1356.

Firth, A.L., Dargitz, C.T., Qualls, S.J., Menon, T., Wright, R., Singer, O., Gage, F.H., Khanna, A., and Verma, I.M. (2014). Generation of multiciliated cells in functional airway epithelia from human induced pluripotent stem cells. Proc. Natl. Acad. Sci. U. S. A. *111*, E1723-1730.

Franzdóttir, S.R., Axelsson, I.T., Arason, A.J., Baldursson, O., Gudjonsson, T., and Magnusson, M.K. (2010). Airway branching morphogenesis in three dimensional culture. Respir. Res. *11*, 162.

Gadsby, D.C., Vergani, P., and Csanády, L. (2006). The ABC protein turned chloride channel whose failure causes cystic fibrosis. Nature *440*, 477–483.

Gao, D., Vela, I., Sboner, A., Iaquinta, P.J., Karthaus, W.R., Gopalan, A., Dowling, C., Wanjala, J.N., Undvall, E.A., Arora, V.K., et al. (2014). Organoid cultures derived from patients with advanced prostate cancer. Cell *159*, 176–187.

Gotoh, S., Ito, I., Nagasaki, T., Yamamoto, Y., Konishi, S., Korogi, Y., Matsumoto, H., Muro, S., Hirai, T., Funato, M., et al. (2014). Generation of Alveolar Epithelial Spheroids via Isolated Progenitor Cells from Human Pluripotent Stem Cells. Stem Cell Rep. *3*, 394–403.

Green, M.D., Chen, A., Nostro, M.-C., d'Souza, S.L., Schaniel, C., Lemischka, I.R., Gouon-Evans, V., Keller, G., and Snoeck, H.-W. (2011). Generation of anterior foregut endoderm from human embryonic and induced pluripotent stem cells. Nat. Biotechnol. *29*, 267–272.

Guseh, J.S., Bores, S.A., Stanger, B.Z., Zhou, Q., Anderson, W.J., Melton, D.A., and Rajagopal, J. (2009). Notch signaling promotes airway mucous metaplasia and inhibits alveolar development. Dev. Camb. Engl. *136*, 1751–1759.

Hegab, A.E., Arai, D., Gao, J., Kuroda, A., Yasuda, H., Ishii, M., Naoki, K., Soejima, K., and Betsuyaku, T. (2015). Mimicking the niche of lung epithelial stem cells and characterization of several effectors of their in vitro behavior. Stem Cell Res. *15*, 109–121.

Hong, K.U., Reynolds, S.D., Watkins, S., Fuchs, E., and Stripp, B.R. (2004). In vivo differentiation potential of tracheal basal cells: evidence for multipotent and unipotent subpopulations. Am. J. Physiol. Lung Cell. Mol. Physiol. *286*, L643-649.

Huang, S.X.L., Islam, M.N., O'Neill, J., Hu, Z., Yang, Y.-G., Chen, Y.-W., Mumau, M., Green, M.D., Vunjak-Novakovic, G., Bhattacharya, J., et al. (2014). Efficient generation of lung and airway epithelial cells from human pluripotent stem cells. Nat. Biotechnol. *32*, 84–91.

Huch, M., Bonfanti, P., Boj, S.F., Sato, T., Loomans, C.J.M., van de Wetering, M., Sojoodi, M., Li, V.S.W., Schuijers, J., Gracanin, A., et al. (2013). Unlimited in vitro expansion of adult bi-potent pancreas progenitors through the Lgr5/R-spondin axis. EMBO J. *32*, 2708–2721.

Huch, M., Gehart, H., van Boxtel, R., Hamer, K., Blokzijl, F., Verstegen, M.M.A., Ellis, E., van Wenum, M., Fuchs, S.A., de Ligt, J., et al. (2015). Long-term culture of genome-stable bipotent stem cells from adult human liver. Cell *160*, 299–312.

Hynds, R.E., and Giangreco, A. (2013). Concise review: the relevance of human stem cell-derived organoid models for epithelial translational medicine. Stem Cells Dayt. Ohio *31*, 417–422.

Kaisani, A., Delgado, O., Fasciani, G., Kim, S.B., Wright, W.E., Minna, J.D., and Shay, J.W. (2014). Branching morphogenesis of immortalized human bronchial epithelial cells in three-dimensional culture. Differ. Res. Biol. Divers. *87*, 119–126.

Kale, S., Biermann, S., Edwards, C., Tarnowski, C., Morris, M., and Long, M.W. (2000). Three-dimensional cellular development is essential for ex vivo formation of human bone. Nat. Biotechnol. *18*, 954–958.

Kim, C.F.B., Jackson, E.L., Woolfenden, A.E., Lawrence, S., Babar, I., Vogel, S., Crowley, D., Bronson, R.T., and Jacks, T. (2005). Identification of bronchioalveolar stem cells in normal lung and lung cancer. Cell *121*, 823–835.

Kimura, J., and Deutsch, G.H. (2007). Key mechanisms of early lung development. Pediatr. Dev. Pathol. Off. J. Soc. Pediatr. Pathol. Paediatr. Pathol. Soc. *10*, 335–347.

Kleinman, H.K., and Martin, G.R. (2005). Matrigel: basement membrane matrix with biological activity. Semin. Cancer Biol. *15*, 378–386.

Lancaster, M.A., and Knoblich, J.A. (2014). Organogenesis in a dish: modeling development and disease using organoid technologies. Science *345*, 1247125.

Lancaster, M.A., Renner, M., Martin, C.-A., Wenzel, D., Bicknell, L.S., Hurles, M.E., Homfray, T., Penninger, J.M., Jackson, A.P., and Knoblich, J.A. (2013). Cerebral organoids model human brain development and microcephaly. Nature *501*, 373–379.

Lee, J.-H., Bhang, D.H., Beede, A., Huang, T.L., Stripp, B.R., Bloch, K.D., Wagers, A.J., Tseng, Y.-H., Ryeom, S., and Kim, C.F. (2014). Lung stem cell differentiation in mice directed by endothelial cells via a BMP4-NFATc1-thrombospondin-1 axis. Cell *156*, 440–455.

Longmire, T.A., Ikonomou, L., Hawkins, F., Christodoulou, C., Cao, Y., Jean, J.C., Kwok, L.W., Mou, H., Rajagopal, J., Shen, S.S., et al. (2012). Efficient derivation of purified lung and thyroid progenitors from embryonic stem cells. Cell Stem Cell *10*, 398–411.

Malpel, S., Mendelsohn, C., and Cardoso, W.V. (2000). Regulation of retinoic acid signaling during lung morphogenesis. Dev. Camb. Engl. *127*, 3057–3067.

McCracken, K.W., Catá, E.M., Crawford, C.M., Sinagoga, K.L., Schumacher, M., Rockich, B.E., Tsai, Y.-H., Mayhew, C.N., Spence, J.R., Zavros, Y., et al. (2014). Modelling human development and disease in pluripotent stem-cell-derived gastric organoids. Nature *516*, 400–404.

McIntyre, B.A.S., Alev, C., Mechael, R., Salci, K.R., Lee, J.B., Fiebig-Comyn, A., Guezguez, B., Wu, Y., Sheng, G., and Bhatia, M. (2014). Expansive generation of functional airway epithelium from human embryonic stem cells. Stem Cells Transl. Med. *3*, 7–17.

Miettinen, P.J., Warburton, D., Bu, D., Zhao, J.S., Berger, J.E., Minoo, P., Koivisto, T., Allen, L., Dobbs, L., Werb, Z., et al. (1997). Impaired lung branching morphogenesis in the absence of functional EGF receptor. Dev. Biol. *186*, 224–236.

Morrisey, E.E., and Hogan, B.L.M. (2010). Preparing for the first breath: genetic and cellular mechanisms in lung development. Dev. Cell *18*, 8–23.

Mou, H., Zhao, R., Sherwood, R., Ahfeldt, T., Lapey, A., Wain, J., Sicilian, L., Izvolsky, K., Musunuru, K., Cowan, C., et al. (2012). Generation of multipotent lung and airway progenitors from mouse ESCs and patient-specific cystic fibrosis iPSCs. Cell Stem Cell *10*, 385–397.

Nakajima, M., Kawanami, O., Jin, E., Ghazizadeh, M., Honda, M., Asano, G., Horiba, K., and Ferrans, V.J. (1998). Immunohistochemical and ultrastructural studies of basal cells, Clara cells and bronchiolar cuboidal cells in normal human airways. Pathol. Int. *48*, 944–953.

Noble, P.W., Barkauskas, C.E., and Jiang, D. (2012). Pulmonary fibrosis: patterns and perpetrators. J. Clin. Invest. *122*, 2756–2762.

Pageau, S.C., Sazonova, O.V., Wong, J.Y., Soto, A.M., and Sonnenschein, C. (2011). The effect of stromal components on the modulation of the phenotype of human bronchial epithelial cells in 3D culture. Biomaterials *32*, 7169–7180.

Ratjen, F., and Döring, G. (2003). Cystic fibrosis. Lancet Lond. Engl. *361*, 681–689.

Rock, J.R., and Hogan, B.L.M. (2011). Epithelial progenitor cells in lung development, maintenance, repair, and disease. Annu. Rev. Cell Dev. Biol. *27*, 493–512.

Rock, J.R., Onaitis, M.W., Rawlins, E.L., Lu, Y., Clark, C.P., Xue, Y., Randell, S.H., and Hogan, B.L.M. (2009). Basal cells as stem cells of the mouse trachea and human airway epithelium. Proc. Natl. Acad. Sci. U. S. A. *106*, 12771–12775.

Rock, J.R., Randell, S.H., and Hogan, B.L.M. (2010). Airway basal stem cells: a perspective on their roles in epithelial homeostasis and remodeling. Dis. Model. Mech. *3*, 545–556.

Rock, J.R., Gao, X., Xue, Y., Randell, S.H., Kong, Y.-Y., and Hogan, B.L. (2011). Notch-dependent differentiation of adult airway basal stem cells. Cell Stem Cell *8*, 639–648.

Ryu, J.H., Moua, T., Daniels, C.E., Hartman, T.E., Yi, E.S., Utz, J.P., and Limper, A.H. (2014). Idiopathic pulmonary fibrosis: evolving concepts. Mayo Clin. Proc. *89*, 1130–1142.

Sasai, K., Sukezane, T., Yanagita, E., Nakagawa, H., Hotta, A., Itoh, T., and Akagi, T. (2011). Oncogene-mediated human lung epithelial cell transformation produces adenocarcinoma phenotypes in vivo. Cancer Res. *71*, 2541–2549.

Sato, M., Vaughan, M.B., Girard, L., Peyton, M., Lee, W., Shames, D.S., Ramirez, R.D., Sunaga, N., Gazdar, A.F., Shay, J.W., et al. (2006). Multiple oncogenic changes (K-RAS(V12), p53 knockdown, mutant EGFRs, p16 bypass, telomerase) are not sufficient to confer a full malignant phenotype on human bronchial epithelial cells. Cancer Res. *66*, 2116–2128.

Sato, T., Vries, R.G., Snippert, H.J., van de Wetering, M., Barker, N., Stange, D.E., van Es, J.H., Abo, A., Kujala, P., Peters, P.J., et al. (2009). Single Lgr5 stem cells build crypt-villus structures in vitro without a mesenchymal niche. Nature *459*, 262–265.

Sato, T., Stange, D.E., Ferrante, M., Vries, R.G.J., Van Es, J.H., Van den Brink, S., Van Houdt, W.J., Pronk, A., Van Gorp, J., Siersema, P.D., et al. (2011). Long-term expansion of epithelial organoids from human colon, adenoma, adenocarcinoma, and Barrett's epithelium. Gastroenterology *141*, 1762–1772.

Schoch, K.G., Lori, A., Burns, K.A., Eldred, T., Olsen, J.C., and Randell, S.H. (2004). A subset of mouse tracheal epithelial basal cells generates large colonies in vitro. Am. J. Physiol. Lung Cell. Mol. Physiol. *286*, L631-642.

Song, H., Yao, E., Lin, C., Gacayan, R., Chen, M.-H., and Chuang, P.-T. (2012). Functional characterization of pulmonary neuroendocrine cells in lung development, injury, and tumorigenesis. Proc. Natl. Acad. Sci. U. S. A. *109*, 17531–17536.

Spence, J.R., Mayhew, C.N., Rankin, S.A., Kuhar, M., Vallance, J.E., Tolle, K., Hoskins, E.E., Kalinichenko, V.V., Wells, S.I., Zorn, A.M., et al. (2011). Directed differentiation of human pluripotent stem cells into intestinal tissue in vitro. Nature *470*, 105–109.

Stevens, K.R., Pabon, L., Muskheli, V., and Murry, C.E. (2009). Scaffold-free human cardiac tissue patch created from embryonic stem cells. Tissue Eng. Part A *15*, 1211–1222.

Suga, H., Kadoshima, T., Minaguchi, M., Ohgushi, M., Soen, M., Nakano, T., Takata, N., Wataya, T., Muguruma, K., Miyoshi, H., et al. (2011). Self-formation of functional adenohypophysis in three-dimensional culture. Nature *480*, 57–62.

Takahashi, K., and Yamanaka, S. (2006). Induction of pluripotent stem cells from mouse embryonic and adult fibroblast cultures by defined factors. Cell *126*, 663–676.

Takahashi, K., Tanabe, K., Ohnuki, M., Narita, M., Ichisaka, T., Tomoda, K., and Yamanaka, S. (2007). Induction of pluripotent stem cells from adult human fibroblasts by defined factors. Cell *131*, 861–872.

Takebe, T., Sekine, K., Enomura, M., Koike, H., Kimura, M., Ogaeri, T., Zhang, R.-R., Ueno, Y., Zheng, Y.-W., Koike, N., et al. (2013). Vascularized and functional human liver from an iPSC-derived organ bud transplant. Nature *499*, 481–484.

Van Haute, L., De Block, G., Liebaers, I., Sermon, K., and De Rycke, M. (2009). Generation of lung epithelial-like tissue from human embryonic stem cells. Respir. Res. *10*, 105.

Vaughan, M.B., Ramirez, R.D., Wright, W.E., Minna, J.D., and Shay, J.W. (2006). A three-dimensional model of differentiation of immortalized human bronchial epithelial cells. Differ. Res. Biol. Divers. *74*, 141–148.

Wan, H., Xu, Y., Ikegami, M., Stahlman, M.T., Kaestner, K.H., Ang, S.-L., and Whitsett, J.A. (2004). Foxa2 is required for transition to air breathing at birth. Proc. Natl. Acad. Sci. U. S. A. *101*, 14449–14454.

Weaver, M., Dunn, N.R., and Hogan, B.L. (2000). Bmp4 and Fgf10 play opposing roles during lung bud morphogenesis. Dev. Camb. Engl. *127*, 2695–2704.

Weiss, P., and Taylor, A.C. (1960). RECONSTITUTION OF COMPLETE ORGANS FROM SINGLE-CELL SUSPENSIONS OF CHICK EMBRYOS IN ADVANCED STAGES OF DIFFERENTIATION. Proc. Natl. Acad. Sci. U. S. A. *46*, 1177–1185.

Weiswald, L.-B., Bellet, D., and Dangles-Marie, V. (2015). Spherical cancer models in tumor biology. Neoplasia N. Y. N *17*, 1–15.

Wong, A.P., Bear, C.E., Chin, S., Pasceri, P., Thompson, T.O., Huan, L.-J., Ratjen, F., Ellis, J., and Rossant, J. (2012). Directed differentiation of human pluripotent stem cells into mature airway epithelia expressing functional CFTR protein. Nat. Biotechnol. *30*, 876–882.

Xing, Y., Li, C., Hu, L., Tiozzo, C., Li, M., Chai, Y., Bellusci, S., Anderson, S., and Minoo, P. (2008). Mechanisms of TGFβ Inhibition of Lung Endodermal Morphogenesis: The role of TβRII, Smads, Nkx2.1 and Pten. Dev. Biol. *320*, 340–350.

Yang, H., Lu, M.M., Zhang, L., Whitsett, J.A., and Morrisey, E.E. (2002). GATA6 regulates differentiation of distal lung epithelium. Dev. Camb. Engl. *129*, 2233–2246.

You, Y., Richer, E.J., Huang, T., and Brody, S.L. (2002). Growth and differentiation of mouse tracheal epithelial cells: selection of a proliferative population. Am. J. Physiol. Lung Cell. Mol. Physiol. *283*, L1315-1321.

Yuan, B., Li, C., Kimura, S., Engelhardt, R.T., Smith, B.R., and Minoo, P. (2000). Inhibition of distal lung morphogenesis in Nkx2.1(-/-) embryos. Dev. Dyn. Off. Publ. Am. Assoc. Anat. *217*, 180–190.

Zorn, A.M., and Wells, J.M. (2009). Vertebrate endoderm development and organ formation. Annu. Rev. Cell Dev. Biol. *25*, 221–251.

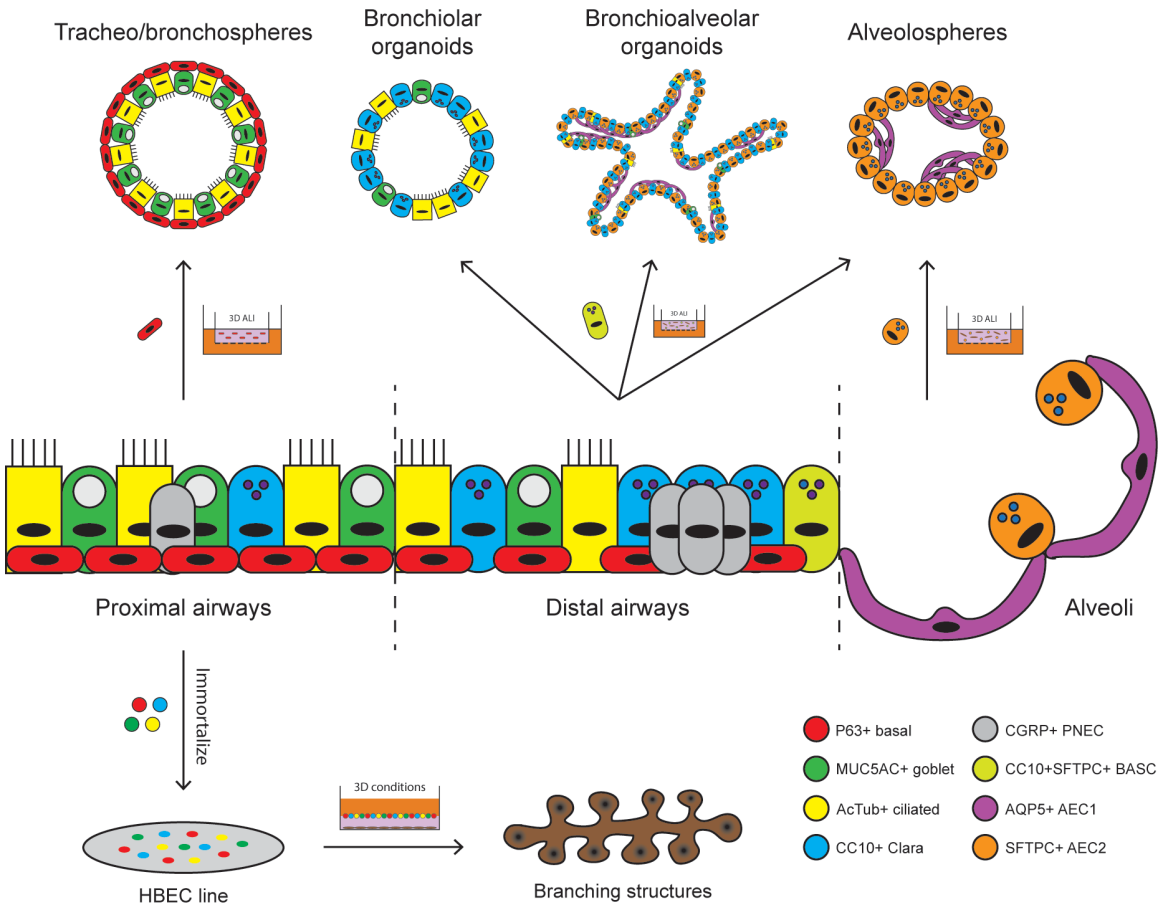

Figure 1 - Schematic of the types of lung organoids generated from epithelial cells within different respiratory compartments

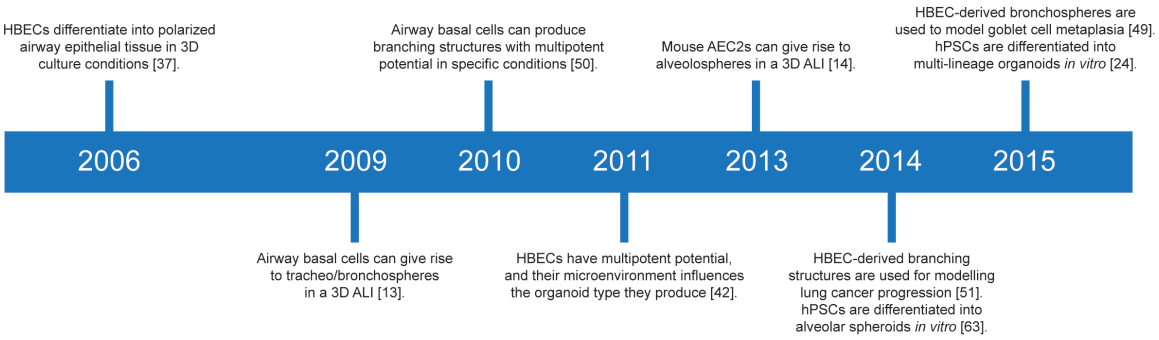

Figure 2 - A timeline of significant events in the last decade that contributed to current lung organoid technologies

Table 1 – Properties of different types of lung organoids that have been derived from primary cells, cell lines and hPSCs

Type of lung organoid	Compartment representation	Cell type composition or markers detected	Principal organoid-forming cell type(s)	Supporting cell types	References
Lung organoids derived from primary cells and cell lines *in vitro*					
Tracheo/ bronchospheres (mouse and human)	Proximal airway epithelium	Basal, ciliated and goblet	Basal cells	±HLFs or HUVECs	[13,48,49,72]
Bronchiolar organoids (mouse)	Distal airway epithelium	Club, ciliated and goblet	BASCs	LuMECs	[15]
Bronchioalveolar organoids (mouse)	Bronchioalveolar epithelium	Club, ciliated, goblet, AEC1s and AEC2s	BASCs	HLFs, HUVECs or LuMECs	[15,72]
Alveolospheres (mouse)	Alveolar epithelium	AEC1s and AEC2s	AEC2s or BASCs	PDGFRα+ lung stromal cells or LuMECs	[14,15,72]
Branching structures (human)	Embryonic-like; multipotent potential	NKX2.1, P63, CC10, SFTPA, SFTPC	Immortalized basal cells or HBECs	HLFs or HUVECs	[42,50,51]
Lung organoids derived from hPSCs *in vitro*					
Alveolar spheroids (human)	Alveolar epithelium	AEC1s and AEC2s	NKX2.1+ SFTPC+ CPM+ alveolar progenitors	HLFs	[63]
Multi-lineage organoids (human)	Unclear; both airway and alveolar components detected	NKX2.1, SOX2, SOX9, P63, SCGB1A1, MUC5AC, HOPX, SFTPC, ECAD, VIM, αSMA	NKX2.1+FOXA2+ lung progenitors in VAFE spheroids	hPSC-derived fibroblasts and myofibroblasts detected	[24]

1.1.4 - Summary of Intent and Research Hypothesis

From the various endoderm derivatives, we were particularly interested in generating lung epithelial organoids from human PSCs (hPSCs). My role in this project commenced in September 2012, at which point there had been some success in deriving lung epithelium from PSCs in the field (Green et al., 2011; Longmire et al., 2012; Mou et al., 2012; Wong et al., 2012), and our understanding of cellular and molecular mechanisms controlling lung development that could be applied in the dish was still lacking. Also, most research groups had focused their efforts on making monolayer cultures of lung epithelial cells, which did not recapitulate *in vivo* lung architecture and function, and which contained contaminating lineages. There had been no report of the generation of hPSC-derived lung organoids. The ability to derive lung organoids from hPSCs would expand our knowledge of exogenous factors and mechanical cues required for differentiation and 3D complexity. This approach may ultimately provide tissue that better recapitulates the structure and function of the native lung, and that is suitable for studying basic lung biology and modeling lung disease.

We hypothesized that mimicking in vivo patterns of lung organogenesis by modulating growth factor conditions would produce functional 3D lung tissue in vitro. The goals of this project were to i) establish a step-by-step differentiation protocol for producing lung organoids from hPSCs, ii) to quantify and characterize the organoid populations, and iii) to design simple *in vitro* assays to test the functionality and utility of the organoids.

Chapter 1.2 – *In vitro* generation of early lung and intestinal tissues from human pluripotent stem cells

Preface

This chapter addresses the research goal of Section 1. It includes results of two hPSC differentiation schemes for generating early lung and intestinal tissues, and their characterization. Experimental work began in September 2012, and was performed primarily by me with major contributions from postdoctoral fellow Dr. Carlos Pilquil in Fall 2012. Undergraduate student Yu Tong (Shirley) Zhang and postdoctoral fellow Dr. Soumeya Abed from the Draper lab assisted with experimental work from Fall 2016 to Spring 2017.

BACKGROUND

hPSC-derived organoids:

hPSC differentiation strategies most often focus on producing a population comprising a single cell type (Lanza et al., 2009) as opposed to the complete set of cell types of an organ. Cells differentiated *in vitro* as a monolayer are supported by a simple attachment substrate and do not achieve the 3D properties and complexity of *in vivo* organs. These single cells typically have a random distribution in the dish along with contaminating cell types, suggesting that differentiation and interaction of multiple cell types of a particular organ/tissue may not recapitulate that of their native counterpart (Hynds and Giangreco, 2013). *In vivo* organs have a 3D architecture, contain multiple interacting cell types, and are supported by a complex ECM. The normal spatial arrangement of different cells within an organ is important for proper cellular interaction and function, especially when multiple cell types work together to provide a function. *In vitro*-generated organoids do have a 3D structure, and contain multiple cell types whose spatial arrangement and interactions are similar to those of the native organ (Hynds and Giangreco, 2013; Lancaster and Knoblich, 2014).

Organoids may be generated from hPSCs if the latter are differentiated into organoid-forming progenitors equivalent to those that give rise to their primary counterparts (Lancaster and Knoblich, 2014). Also, hPSCs can be expanded indefinitely in culture, enabling potential large-scale production of organoids. As opposed to primary adult organoids, hPSC-derived organoids may be used to model human organ development, which is the case for intestinal, brain and retinal organoid models that have been shown to exhibit similar developmental properties to their native organs (Eiraku et

al., 2011; Lancaster et al., 2013; Nakano et al., 2012; Spence et al., 2011). In a therapeutic context, hPSC-derived organoids have the potential to be used for modeling genetic disorders and complex diseases *ex vivo* (Dekkers et al., 2013; Lancaster et al., 2013; Matano et al., 2015; Takebe et al., 2013). This is especially true for certain functional assays that are unique to organoids, or disease phenotypes that can only be recapitulated in organoids but not in monolayer cultures. For example, cystic fibrosis (CF) is a disease that affects multiple organs including the intestine and is caused by mutations in the CFTR gene, which encodes the cystic fibrosis transmembrane conductance regulator. The addition of forskolin induces rapid swelling of normal intestinal organoids but not of organoids derived from CF-infected hosts, due to a failure of the CFTR protein in transporting ions properly across the organoid epithelial membrane (Dekkers et al., 2013). This is a simple yet robust functional assay using primary CF intestinal organoids, which cannot be performed on intestinal monolayer cultures.

Organoids may also be used as an alternative system for small-scale drug screening (Dekkers et al., 2013; van de Wetering et al., 2015), and since these tissues are derived from human cells, they may better recapitulate effects in human patients (Lancaster and Knoblich, 2014). Eventually, *in vitro* patient-derived tissues have the potential to be used in regenerative medicine.

Lung development:

The entire lung arises from a subset of cells in the ventral wall of the anterior foregut which express homeodomain transcription factor NKX2.1 (Minoo et al., 1999;

Morrisey and Hogan, 2010; Yuan et al., 2000). This is the earliest known step in lung development. By E9.5 in the mouse or ~28 days in the human, the two primary lung buds arise while the foregut tube begins to separate into a dorsal esophagus that connects to the stomach and a ventral trachea that is attached to the lung buds. From E9.5 to E16.5 in the mouse, the primary lung buds branch in a highly stereotyped pattern (Metzger et al., 2008) to produce a complex tree-like structure with thousands of terminal airway tubules. This largely depends on activity of the surrounding lung mesenchyme, which secretes growth factors like Wnts, FGFs and BMPs towards the branching epithelium. From E16.5 to E17.5 in the mouse, the terminal buds become narrower, and from E18.5 to postnatal day 5, they form sacs at their terminal ends that develop into alveoli. Meanwhile, blood vessels that develop during branching morphogenesis become closely associated with the alveoli, allowing for functional gas exchange to occur, the principal function of the lung (Morrisey and Hogan, 2010).

The utility of airway epithelial organoids:

Basal cells are stem cells of the airway epithelium, which give rise to secretory and ciliated cells (known as mucociliary differentiation) in response to wear-and-tear or injury. In 2009, Brigid Hogan's group showed that primary basal cells harvested from mouse lungs, when cultured in a 3D ALI growth condition, generate organoids termed tracheospheres (Rock et al., 2009), or bronchospheres in the human system. These organoids are clonal, each derived from a single P63+NGFR+ basal cell that initially proliferates to establish a single layer of basal cells in a spherical organization (at 1-2 weeks in culture), followed by differentiation into ciliated and goblet cells which

constitute a second layer facing the sphere lumen (at 3-4 weeks in culture) (Rock et al., 2009, 2011).

In the last decade, studies have reproducibly generated bronchospheres *in vitro* from purified adult mouse and human basal cells, and have used this system to further investigate basal cell function. For example, the ability of basal cells to differentiate into ciliated verus goblet cells has been shown to be Notch-dependent (Guseh et al., 2009; Morrisey and Hogan, 2010; Rock et al., 2011). Under normal conditions, basal cells undergo mucociliary differentiation in a salt-and-pepper distribution in the native airway epithelium and in bronchospheres. Notch hyperactivation favours goblet cell differentiation whereas Notch inhibition favours ciliated cell differentiation (Guseh et al., 2009). In either case, a measurable change in proportion of one cell type over the other is observed. This phenomenon has been recapitulated *in vitro* using the bronchosphere-forming assay, in which exogenous Notch signaling molecules are added to basal cells in culture and their resulting impact on mucociliary differentiation is manifested in the spheres (Rock et al., 2011). Similarly, one study used primary human basal cell-derived bronchospheres to create an experimentally induced model of goblet cell metaplasia, a phenotype associated with asthma, chronic obstructive pulmonary disease (COPD) and cystic fibrosis. The authors found that exposure to cytokines such as Il-13 and IL-17A via the Notch2 receptor results in a hypersecretory phenotype in bronchospheres, and which is prevented when Notch2 is inhibited (Danahay et al., 2015).

In vitro-generated bronchospheres can also be used as a functional assay to test the effect of exogenous growth factors on basal cells. Since bronchospheres develop from single basal cells, it is these cells that control sphere size and sphere-forming efficiency.

For example, the addition of FGF2, FGF9 and FGF10 to basal cells in culture significantly increases sphere production and size, whereas the opposite is observed upon addition of FGF inhibitors, showing that FGF signaling promotes basal cell proliferation (Hegab et al., 2015). These observations are consistent with growth factor-dependent basal cell behaviour during embryonic lung development (Morrisey and Hogan, 2010).

RESULTS

Multi-stage differentiation is the traditional approach to generate specialized cell types from PSCs. For example, D'Amour et al (2006) mimicked *in vivo* pancreatic organogenesis by directing human ESCs through stages resembling definitive endoderm, gut-tube endoderm, pancreatic endoderm, endocrine precursors and finally hormone-producing cells. Similarly, we attempted to differentiate human ESCs (hESCs) towards a pulmonary epithelial fate by taking advantage of current knowledge on stages of vertebrate development through which the mature lung arises (Morrisey and Hogan, 2010; Zorn and Wells, 2009). Also, we timely incorporated a 3D culture system in our differentiation protocol to promote formation of 3D tissue.

hESC differentiation into definitive endoderm and foregut endoderm:

Previous studies have achieved intermediate stages of differentiation in culture (prior to lung development) through timely addition of endoderm- and foregut-specifying growth factors at strict doses. D'Amour et al (2005) found that adding exogenous Activin A for 4-5 days, acting as a surrogate for Nodal signaling (Zorn and Wells, 2009), resulted in definitive endoderm cells. Green et al (2011) found that dual inhibition of BMP4 and

TGFβ signalling using Noggin and SB431542, respectively, promoted anterior foregut specification from endoderm cells while attenuating CDX2-expressing hindgut cells (Goessling et al., 2008). Subsequent stages employing Wnt, FGF, BMP, and retinoic acid signalling have been attempted by various studies (Green et al., 2011; Longmire et al., 2012; Mou et al., 2012) to yield putative lung progenitors that express NKX2.1.

We aggregated work from the above studies into a differentiation protocol **(Figure 1)** and confirmed expression of specific markers during each main stage. We found that hESCs on a monolayer treated with Activin A for 5 days resulted in cells expressing endoderm markers FOXA2 and GATA4 **(Figure 2A)**. Following this, we replaced Activin with Noggin and SB431542 for 2 days and found a subset of SOX2+FOXA2+ cells **(Figure 2B)**, an anterior foregut profile. Subsequently treating cells with WNT3A, FGF10, KGF10, BMP4, EGF (WFKBE), and retinoic acid (RA) for 6 days resulted in a subset of NKX2.1+ cells that co-expressed FOXA2 **(Figure 2C)**, indicative of putative lung progenitors within the ventral foregut. Overall, this protocol captures three early stages of development prior to lung differentiation: 1) definitive endoderm formation, 2) anterior patterning, and 3) ventral foregut and lung specification. All factors in this protocol are added exogenously and no genetic modification of cells was performed.

Development of 3D lung tissue in a 3D culture system:

At the time, there had been almost no success in generating 3D lung tissue from hESCs. The air-liquid interface (ALI) culture system has been used for promoting differentiation and maturation of lung epithelium (Coraux et al., 2005; Van Haute et al.,

2009; Wong et al., 2012). The ALI growth condition mimics the *in vivo* airway epithelial niche, since the apical surface of cells is exposed to air while the basal surface is in contact with fluid. Cells experience this condition after respiratory specification and during the stereotyped process of branching morphogenesis (Metzger et al., 2008). In addition, although NKX2.1 expression also marks thyroid and neuroectodermal cells, these cells do not rely on an ALI growth condition *in vivo*. We hypothesized that timely adaptation of lung progenitors to an ALI would promote their maturation into airway epithelium.

Following our three-stage differentiation protocol, we adapted cells to an ALI and sustained culture for 20-25 days. We observed growth of 3D structures having epithelial morphology that exhibited primary lung-like budding **(Figure 3C)**, compared to cells that were adapted to an ALI prematurely **(Figures 3A and 3B)**. Through immunofluorescence of organoid cryo-sections, we observed tubular patterns that contained club cells and goblet cells of the native airways, identified by positive staining for club cell secretory protein (CC10) and mucin-5B (MUC5B), respectively **(Figure 4A)**. Cells expressing lung transcription factor NKX2.1, and airway epithelial markers SOX2 and P63 were also seen **(Figure 4B)**. We also found tissues containing cells that stained positive for aquaporin 5 (AQP5) and surfactant protein C (SPC) **(Figure 5)**, markers for alveolar type I and type II cells, respectively. The epithelial marker E-cadherin (ECAD) was expressed throughout the tubular structures **(Figures 4 and 5)**. Although the ALI growth condition mimics the airway niche, the appearance of alveolar cells in our organoids suggests that the differentiation protocol captures a broader spectrum of lung epithelial cell types. Importantly, CC10 and SPC are pulmonary-specific markers since they are expressed

exclusively in club cells and alveolar type II cells, which only reside in the lung. This suggests that adapting putative specified lung cells (by stage 3) to an ALI promotes growth of 3D lung epithelium. 3D ALI culture for 20-25 days represented stage 4 of our differentiation protocol **(Figure 1)**.

Molecular characterization of 3D tissue:

Although hESC-derived organoids in stage 4 stained positive for pulmonary markers, it was important to further characterize the structures morphologically to convincingly demonstrate that the obtained tissue is lung epithelium and which is comparable to native lung tissue. Through haematoxylin and eosin (H&E) staining of paraffin-embedded organoid sections, we observed pseudostratified columnar and simple cuboidal epithelial patterns resembling those of the native proximal and distal airways, respectively **(Figures 6)**. In addition, we captured ultrastructures of organoid tissue using transmission electron microscopy (TEM), in which we observed tubules with visible lumen lined with polarized epithelial cells, which contained microvilli-like protrusions on their apical surface, suggesting the presence of club cells **(Figure 7)**.

Survival and growth of organoid epithelium requires interaction with mesenchyme:

During embryonic development, the mesenchyme plays a critical role in patterning the primitive gut tube into distinct organ domains (Zorn and Wells, 2009). Signals from the mesenchyme are received and interpreted by the epithelium, initiating organ development via budding from the gut tube. We attempted to recapitulate this behaviour *in vitro* using our hESC-derived organoids through a simple assay to further

support the importance of mesenchyme in epithelial growth. We hypothesized that organ-like epithelial budding occurs only in the presence of surrounding mesenchymal cells. To test this, organoids obtained from our differentiation protocol were micro-dissected to separate epithelium from mesenchyme (del Moral and Warburton, 2010). Epithelium and mesenchyme were re-plated both together and alone, and tissue growth was compared between the three cultures. When treated as above, we observed that mesenchyme plated alone showed further growth, whereas epithelium plated alone collapsed by day 5 **(Figure 8, left)**. Conversely, when epithelium and mesenchyme were plated together, organ-like buds developed as outgrowths from the epithelium by day 5 **(Figure 8, right)**. These results support the role of mesenchyme in enriching the epithelium during development.

Microarray analysis revealed lineage heterogeneity in 3D tissues:

To determine the average expression of various lineage-related transcripts in our stage 4 tissue and determine how much lineage heterogeneity was present at this stage, we opted to perform RNA microarray analysis. We harvested the tissue from transwells, dissociated into single cells and sorted cells using E-cadherin (ECAD) to separate epithelial from non-epithelial cell types. We included both ECAD+ and ECAD- samples in the RNA microarray experiment to determine transcript expression levels in ECAD+ cells relative to ECAD- cells. Since our hPSC differentiation protocol was designed to produce airway tissue, we had anticipated that majority of the tissue was of this lineage with the presence of contaminating cell types. However, the RNA microarray data showed that within the ECAD+ population, there was a mixture of lung, liver and

intestine-related transcript expression **(Figure 9)**. This data suggests that tissue obtained from our hPSC differentiation protocol only contained a fraction of pulmonary tissue plus other lineages.

Production of spheroids from ECAD+ cells isolated from stage 4 tissues:

Interestingly, aside from the dense mixture of tissues we produced in stage 4, we also observed spheroids via immunohistochemistry that resembled bronchospheres in structure and lineage marker expression **(Figure 10A)**. We found that these spheroids contained a basal layer of P63+ cells and a luminal layer, similar to the spatial organization of cell types in bronchospheres (Danahay et al., 2015; Rock et al., 2009). It is worth mentioning that although esophageal spheroids also contain P63+ basal cells, they contain a highly stratified squamous epithelium (DeWard et al., 2014), unlike the pseudostratified epithelium we observed in these spheroids **(Figures 10A and B).** A similar number of putative bronchospheres were observed in stage 4 cultures derived from H1 and H9 wild-type hESC lines **(Figure 10C).** Based on this finding, as well as the observation of P63+ cells in epithelial tubules **(Figure 4B)**, we attempted to purify these sphere-forming cells from the stage 4 tissue mixture and passage them to form new spheres. This advantage of producing spheroids from singularized cells was purity in lineage combined with a 3D airway epithelial architecture.

Initially, we explored strategies for purifying basal cells via fluorescence activated cell sorting (FACS). Nerve growth factor receptor (NGFR) is a surface marker expressed by airway basal cells. If the P63+ basal cells that were produced co-expressed NGFR, then performing a dual sort using ECAD and NGFR may be used to enrich for these cells.

However, through immunohistochemistry of tissue sections, we found that P63+ basal cells stained negative for NGFR (data not shown). In fact, Hans-Willem Snoeck's group found that NGFR is not expressed in fetal-like airway tissue differentiated from hPSCs (Huang et al., 2014), but is expressed in adult basal cells, indicating that NGFR expression is developmentally regulated.

Since we could not further enrich for these cells using NGFR, we sorted cells only by ECAD positivity like we had done for the RNA microarray experiment, and determined whether the basal cells within the ECAD+ population could give rise to bronchospheres when re-seeded in a 3D ALI culture system with MTEC lung media (Rock et al., 2009). We found that when ECAD+ cells were cultured alone, no spheres developed within 2 weeks post-seeding (data not shown). However, when sorted ECAD+ cells were co-cultured with human lung fibroblasts (HLFs) or human endothelial cells (HUVECs) at a ratio of 1:1, spheroids were observed within the first 6 days post-seeding and continued to grow in size until day 20 **(Figure 11A)**. Surprisingly, we found that >95% (n=4) of spheroids showed ubiquitous expression of intestinal marker CDX2 and <5% were P63+MUC5AC+ **(Figure 11B)**, even though cells were cultured in MTEC lung media. Studies have shown that both fetal and intestinal spheroids require a cocktail of factors to develop, including WNT3a, Noggin, R-spondin and nicotinamide (Mustata et al., 2013; Sato et al., 2009, 2011), all of which are not present in MTEC lung media. Thus, we had developed a population of intestinal spheroids capable of growing in the absence of the above factors, a phenotype that has not been reported previously in the literature. We further characterized this spheroid population. We found that average sphere diameter is 288 ± 166 μm (n=43) by day 18 in culture **(Figure 11C).** Similar to

FGF response experiments performed on primary basal cell-derived bronchospheres by Hegab et al (2015), we tested the effect of different growth factors and compounds on sphere size and number. We found that MTEC supplemented with 20ng/ml FGF10 for 18 days in culture did not change sphere count but almost tripled the average sphere size (**Figure 11C)**. However, MTEC supplemented with PD173074, a specific FGFR inhibitor, did not decrease sphere count or size **(Figure 11D)**. Therefore, interestingly gut sphere size but not sphere-forming efficiency is increased upon exogenous FGF addition, but neither size nor count is affected by inhibiting endogenous FGF signaling. In addition, MTEC supplemented with Y-27632, an inhibitor of the rho-associated protein kinase (ROCK) signaling pathway, doubled sphere count **(Figure 11D)**. Inhibition of the ROCK pathway is known to promote cell survival and proliferation, and in this case, sphere formation provided a functional output for ROCK inhibition-mediated cell proliferation by increasing sphere-forming efficiency.

Generation of early lung and intestinal spheroids using an alternative differentiation scheme:

Due to the inability of the original differentiation protocol in producing bronchospheres, we used a different protocol as a starting point. In a recent study, hPSCs were differentiated into complex lung organoids containing airway and alveolar epithelium, as well as mesenchyme (Dye et al., 2015). These organoids were derived from anterior foregut endoderm (AFE) cell clumps **(Figure 12)**. When we tried to reproduce the protocol, we found that these organoids contain contaminating CDX2+ mid-hindgut cells (data not shown). We hypothesized that contaminating lineages were

present because the organoids were derived from multicellular clumps as opposed to single cells. We tested this hypothesis by dissociating AFE clumps and seeding them as single cells in 3D conditions to determine if organoids representing different lineages would arise. We tested two different airway epithelial media formulations, MTEC and B-ALI (Lonza), with or without the presence of support cells (human lung fibroblasts, HLFs; human endothelial cells; HUVECs). Cystic organoids or spheroids formed with varying efficiencies in these conditions **(Figures 13A and B)**. To determine the proportion of phenotypes present in these spheroid populations, we performed immunohistochemistry for lung basal cell marker P63 and intestinal marker CDX2. We found that spheroids were made up of either P63- or CDX2-expressing cells, with the expression of the markers being mutually exclusive, and both phenotypes were present in the populations **(Figure 14)**. *In situ* immunostaining for CDX2 and SOX2 (SOX2 being used a surrogate of P63 in this case) showed that the two phenotypes could be distinguished by morphology, with SOX2-expressing spheroids having a relatively thin epithelium and larger lumen **(Figure 15A)**, and CDX2-expressing spheroids having a thicker epithelium and dark-coloured lumen **(Figure 15B)**. Scoring of spheroid phenotypes by morphology and marker expression revealed that the morphology could be used to predict the phenotype **(Figure 15C)**.

Overall, these data show that using this protocol as a starting point (Dye et al., 2015) was also not suitable for generating a pure population of airway epithelial spheroids or bronchospheres. This underscores the importance of generating spheroids/organoids from singularized cells to avoid contaminating lineages emerging within the same organoid unit and the need for purification of phenotypes.

DISCUSSION

An important limitation of *in vitro* differentiation of PSCs is that the process is fast-tracked and lacks the complete barrage of signaling factors and extracellular matrix components present in native organ development, which can affect the purity, maturation status and functionality of the end-product cells. The purity of tissue derived from PSC differentiation is critical for downstream applications. In our case, this largely depends on the differentiation prolife of cells during each of the first three stages of the protocol. It is worth noting that since Wnt, FGF, BMP, and RA signalling participate in differentiation of tissue derived from all three germ lineages, the earliest stages of development, such as endoderm formation and anterior-posterior patterning, are critical before responses to downstream signalling occur as desired. Therefore, optimization of the differentiation protocol may be required to produce a near homogeneous population of putative specified lung cells before adaptation to an ALI to produce a high proportion of 3D lung epithelium. This may partly be achieved by FACS-sorting Activin-treated cells using the endoderm cell surface marker CXCR4 (D'Amour et al., 2005). Then re-plating CXCR4+ cells may allow subsequent anterior patterning and lung specification to occur from a near pure population of endoderm cells, thus limiting heterogeneity. Recent studies discovered that NKX2.1+ lung progenitors express the cell surface marker carboxypeptidase M (CPM) (Gotoh et al., 2014; Konishi et al., 2016), which can be used to FACS-purify the cells, re-seed them and continue with differentiation. However, this work has not been reproducible due to the antibody used in the above study no longer being commercially available. An alternative is to use an NKX2.1-GFP reporter cell line

(Longmire et al., 2012) to FACS-isolate GFP+ cells allowing a pure population of NKX2.1-expressing cells to be adapted to an ALI.

Although stage 2 in our differentiation protocol was meant for specifying an anterior foregut fate and mitigating mid/hindgut, we were still producing the latter at the end of the protocol. To determine why this may be occurring, we looked more closely at the design of the protocol. During stage 3 of the protocol to produce lung progenitors, we were adding a high dose of WNT3A. Other studies have shown that a high dose of Wnt signaling during this stage is necessary to produce at least 30-40% of NKX2.1+FOXA2+ lung progenitors (Green et al., 2011; Huang et al., 2014; Longmire et al., 2012). However, during embryonic development, Wnt signaling is also involved in the development of midgut/hindgut-related lineages. In fact, one study showed that treating foregut cells with a high dose of exogenous Wnt could dedifferentiate them to an intestinal fate (Sherwood et al., 2011). Hence, there is a tradeoff between Wnt addition for lung specification and producing undesired intestinal cells. It is unclear whether the above lung differentiation studies from which our protocol was derived from also faced a similar problem, but such data was not shown.

We found that the epithelial tubules in stage 4 contained microvilli on their apical surface, which we thought marked club cells, but after determining that CDX2-expressing cells were also present in stage 4, the microvilli-containing cells may represent early enterocytes.

Some studies have generated complex organoids from multicellular clumps (Dye et al., 2015; McCracken et al., 2014; Spence et al., 2011), which are not pure in lineage-restricted progenitors. The advantage of producing bronchospheres compared to the

mixture of tissues we produced at the end of stage 4 is that they develop from single cells. This allows for both lineage purity and a 3D airway epithelial architecture. For example, the intestinal organoids developed by Hans Clevers' group come from single LGR5+ intestinal stem cells, and in the right culture conditions, this yields a pure population of intestinal organoids (Sato et al., 2009, 2011). Another advantage of producing bronchospheres is that it is easier to immunostain spheres *in situ* and collect quantitative data on the whole population which cannot be done with the more dense tissue we produced in stage 4. Measuring sphere count, size, and the proportion of ciliated versus secretory cells inside spheres is a simple but powerful method of determining whether phenotypic changes occur in response to stimuli (Danahay et al., 2015; Hegab et al., 2015; Rock et al., 2011). *In vitro*-generated bronchospheres have the potential to be used for small-scale drug screening in a similar manner. They may be used for modeling airway diseases where basal, ciliated or goblet cells are the affected cell types, and which show cell metaplasia or increased mucous production, phenotypes observed in lung diseases like asthma, COPD and CF.

Compared to the lung, other endoderm derivatives like the thyroid and pancreas secrete specific hormones or bioactive peptides that can be measured, and this in fact has been demonstrated recently in hESC-derived thyroid follicular cells and pancreatic cells (Antonica et al., 2012; D'Amour et al., 2006), confirming basic functionality of these cells. In lieu of this hormone secreting behaviour, the primary function of the lung is gas exchange, which occurs in the respiratory zone between alveolar type I cells and the supporting vasculature. This gas exchange behaviour of the lung has been challenging to reproduce *in vitro*. In addition, it is unclear if lung epithelial cells injected into

immunodeficient mice can form an intimate connection with the host vasculature and perform gas exchange. Therefore, aside from the difficulty in producing lung tissue from hPSCs, there is almost a complete of lack of functional assays that may be used to test the functionality of hPSC-derived lung epithelium.

EXPERIMENTAL PROCEDURES

Maintenance and differentiation of hESCs

H1 and H9 wt hESCs (Wicell Research Institute) were cultured on Matrigel (Corning; #354234) in mouse embryonic fibroblast-conditioned medium (MEF-CM) as previously described (Tomishima, 2008). In preparation for differentiation, hESCs were passaged and seeded in a 48-well format. After seeding, cells were cultured for 2-3 days in MEF-CM, and were then subjected to a 4-stage differentiation protocol.

Differentiation of hESCs into 3D endoderm-derived tissues

In preparation for differentiation, hESCs were passaged and seeded in a 48-well format. After seeding, cells were cultured for 2-3 days in MEF-CM, and were then subjected to a 4-stage differentiation protocol. The basal media used in stage 1 consisted of RPMI 1640 (ThermoFisher; 11875093), 1X non-essential amino acids, 1X GlutaMAX, and 0.05% BSA. In stage 1, hESCs were treated for 3 days with 100ng/ml Activin A (R&D Systems; 338-AC-010), with 25ng/ml WNT3a (R&D Systems; 5036-WN-010), which was supplemented with, 0.2% FBS on day 2, and 2% FBS on day 3. The basal media used in stage 2 and 3 consisted of DMEM/F12 (ThermoFisher; 11320033), 1X non-essential amino acids, 1X GlutaMAX, 0.05% BSA, 0.4μM monothioglycerol

(Sigma; M6145), 1X N-2 supplement (ThermoFisher; 17502048), 1X B-27 supplement (ThermoFisher; 17504044), and 50µg/ml L-ascorbic acid. In stage 2, the media was supplemented for 2 days with 200ng/ml Noggin (Peprotech; 120-10C) and 10µM SB431542 (Tocris; 1614). In stage 3, the media was supplemented for 6 days with 100ng/ml WNT3a, 10ng/ml FGF10 (Peprotech; 100-26), 10ng/ml KGF (Peprotech; 100-19B), 10ng/ml BMP4 (Peprotech; 120-05), 20ng/ml EGF (Peprotech; AF-100-15), and 0.05µM all-trans retinoic acid (Sigma; R2625). Cells were washed once with DMEM/F12 between each differentiation stage. Monolayer cultures from stage 3 were collected as aggregates by mechanical scraping followed by gentle trituration. Aggregates were seeded within a 3D matrix of growth factor-reduced Matrigel (GFRM; Corning; #356231; Thick Gel Method, as per manufacturers instructions) diluted in a 1:1 ratio with 100µl MTEC media in a 24-well format. MTEC media (You et al., 2002), comprised DMEM/F12 with HEPES (ThermoFisher; 11330032), 1X non-essential amino acids, 1X GlutaMAX, 1X Insulin-Transferrin-Selenium (ThermoFisher; 51500056), 30µg/ml Bovine Pituitary Extract (ThermoFisher; 13028014), 5% FBS, 25ng/ml EGF, and 10nM all-trans retinoic acid. The 3D matrix was permitted to solidify at 37°C for 30 mins, and then covered with 500µl MTEC media. Cells were cultured at 37°C in a 5% CO_2/air environment, and media was changed every 2 days. Endoderm-derived 3D tissues were typically cultured for 15-20 days.

Histological staining

Stage 4 tissues were prepared for histological staining by making formalin-fixed, paraffin-embedded sections. Tissues were harvested from their gel matrix as described,

washed twice with PBS, fixed for 1-2 hours at room temperature in 10% neutral-buffered formalin, and then washed again with PBS. Tissues were collected and embedded in HistoGel (ThermoFisher; HG-4000-012) as a plug, then transferred to histology cassettes. Cassettes were taken through an ethanol wash series of increasing concentration and xylene to dehydrate tissue, and then embedded in paraffin at 58°C. 5µm-thick sections were cut using a rotary microtome, floated in a 56°C water bath, mounted onto gelatin-coated histological slides and allowed to dry. H&E and immunostaining were performed essentially as described in available protocols from R&D Systems for fluorescent and chromogenic IHC staining of paraffin-embedded tissue sections.

Note: See Chapter 2.2 for additional information about immunostaining as well as microarray analysis.

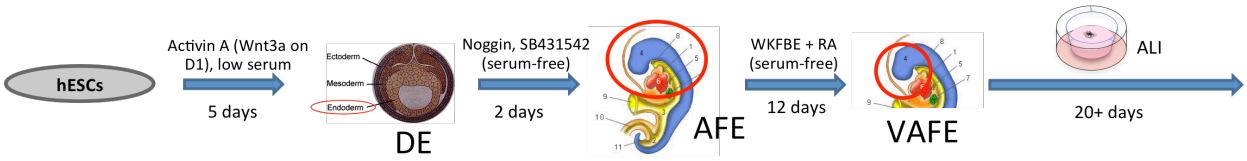

Figure 1 – Differentiation protocol with four principal stages that led to the development of 3D organoid tissue. Activin A and low serum treatment was used to form definitive endoderm (D'Amour et al, 2005). Noggin and SB431542, as dual inhibitors of BMP and TGFβ signalling, respectively, patterned definitive endoderm into anterior foregut endoderm (Green et al, 2011). WKFBE + RA specified ventral foregut endoderm and the lung field (Green et al, 2011; Mou et al, 2012). Air-liquid interface culture was used for 3D maturation of monolayer cells (Coraux et al, 2005; Van Haute et al, 2009; Wong et al, 2012). Doses: Activin A, 100 ng/ml (Wnt3A on d1, 25 ng/ml); Noggin, 200 ng/ml; SB431542, 10 uM; Wnt3A, 100 ng/ml; FGF10, 10 ng/ml; KGF10, 10 ng/ml; BMP4, 10 ng/ml; EGF, 20 ng/ml; RA, 0.5 um. DE = definitive endoderm; AFE = anterior foregut endoderm; VAFE = ventral anterior foregut endoderm; RA = retinoic acid; ALI = air-liquid interface.

A)

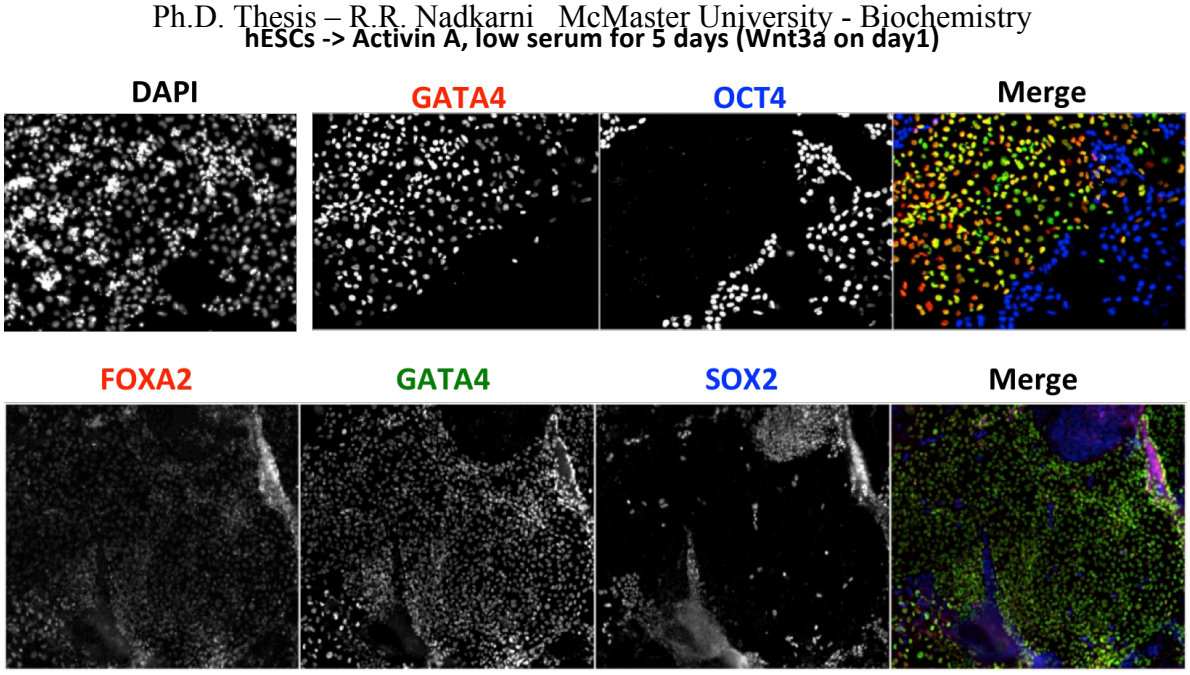

B)

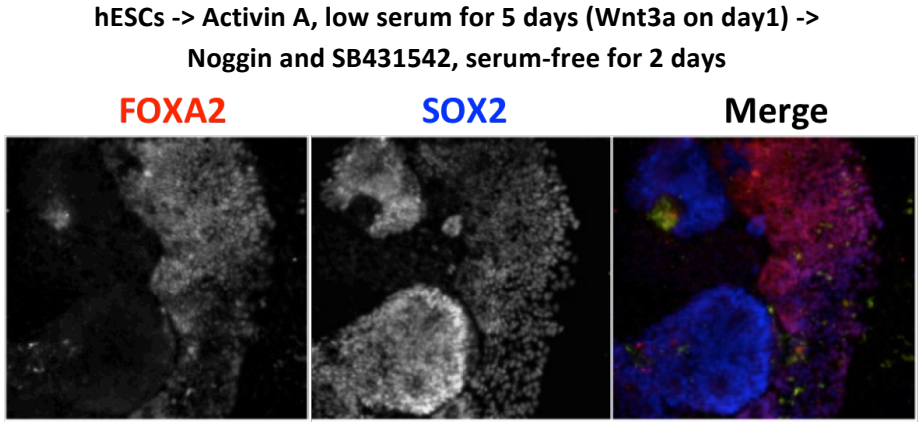

C)

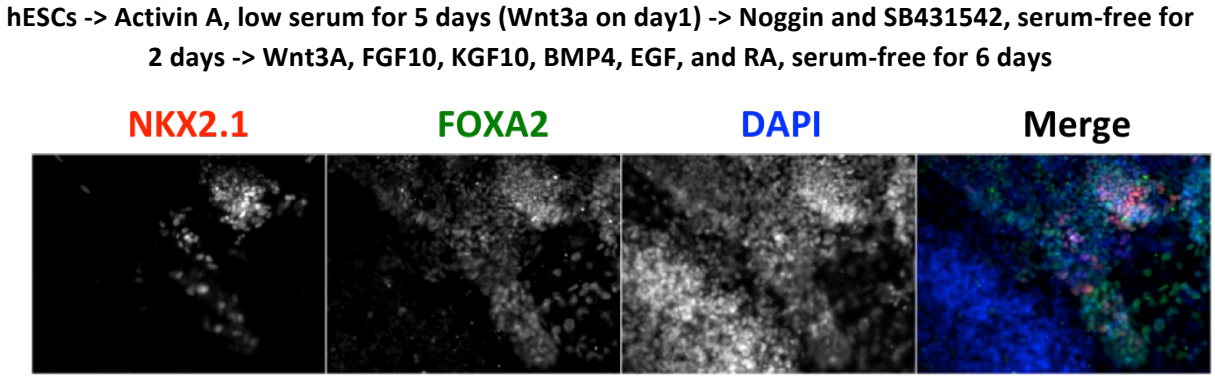

Figure 2 – Immunofluorescent staining of cells at different stages of hESC differentiation. **A)** Activin A, low serum-treated cells for 5 days were stained with definitive endoderm markers GATA4 and FOXA2 (10x mag) as well as pluripotency markers OCT4 and SOX2 (4x mag). **B)** Cells treated at day 6 with inhibitors Noggin and SB431542 for 2 days and stained with SOX2 and FOXA2 (4x mag). **C)** Cells treated at day 8 with WKFBE + RA cocktail, and stained with NKX2.1 and FOXA2 (10x mag).

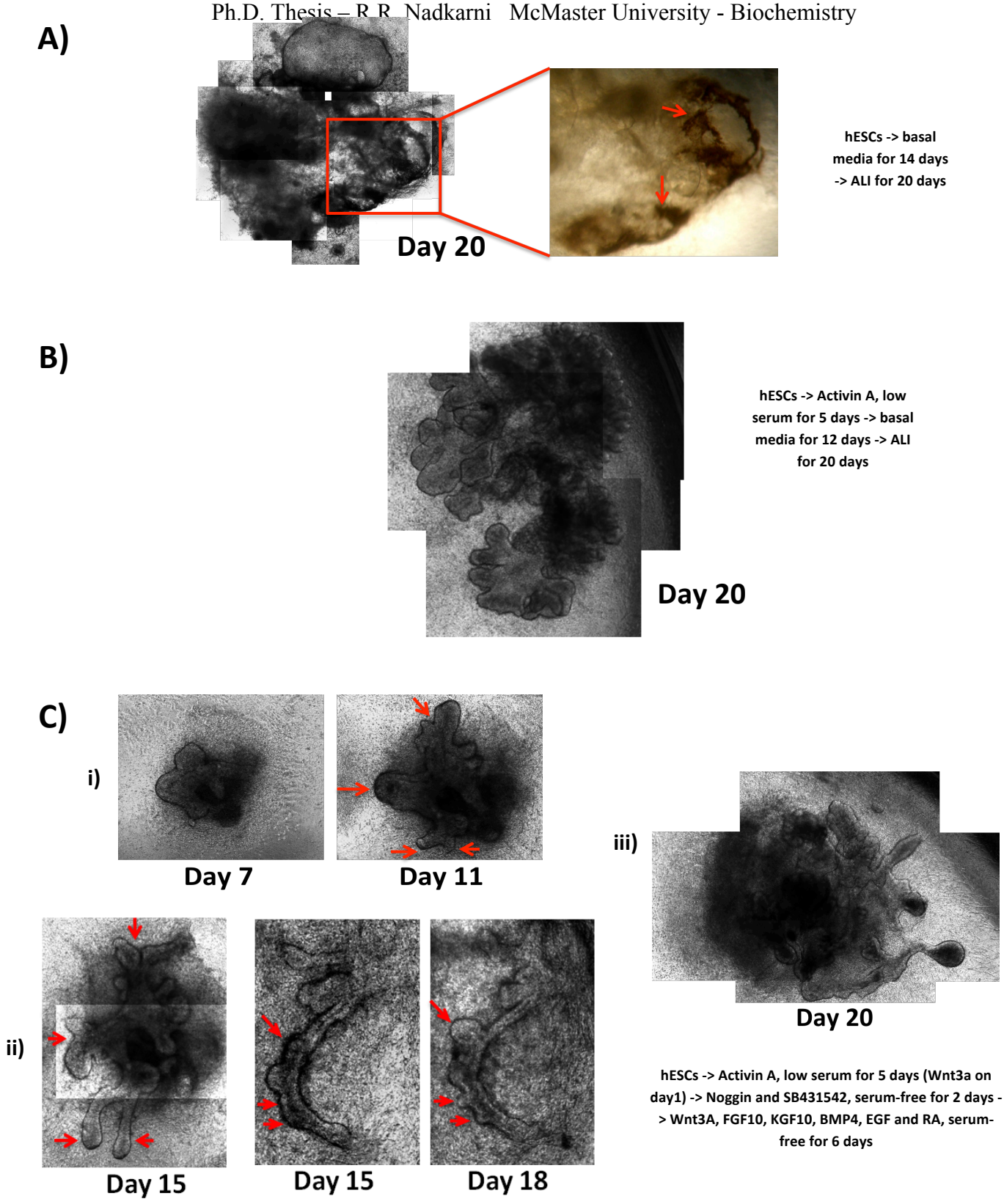

Figure 3 – Structures obtained days after adaptation to air-liquid interface culture system from varying protocols at monolayer level. **A)** Organoid with epithelial-like branching. Arrows in inlet point to pigmentation. **B)** Organoid showing cleaner epithelial growth compared to **(A)**. **C)** Three different organoids (i, ii and iii) with organ-like buds developing as outgrowths from epithelium. Arrows point to budding locations.

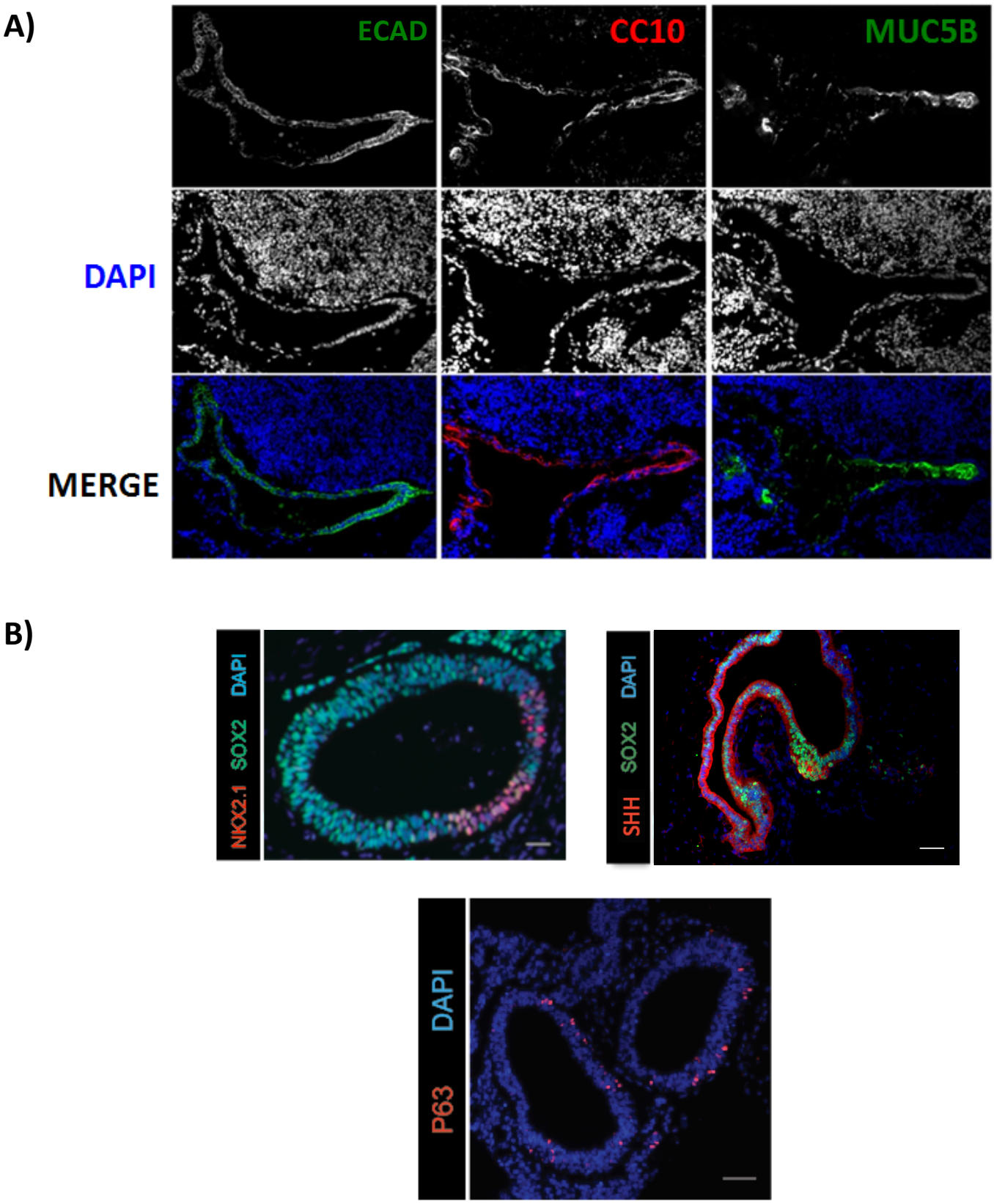

Figure 4 – Immunofluorescent IHC staining of organoids in stage 4 shows that tubular structures contain cells expressing airway markers. **A)** E-cadherin (ECAD), club cell secretory protein (CC10), and mucin-5B (MUC5B) staining in tubular structures (10x mag). **B)** NKX2.1, SOX2, SHH and P63 staining in tubular structures. Scale bars: 50µm (left); 100 µm (right and bottom).

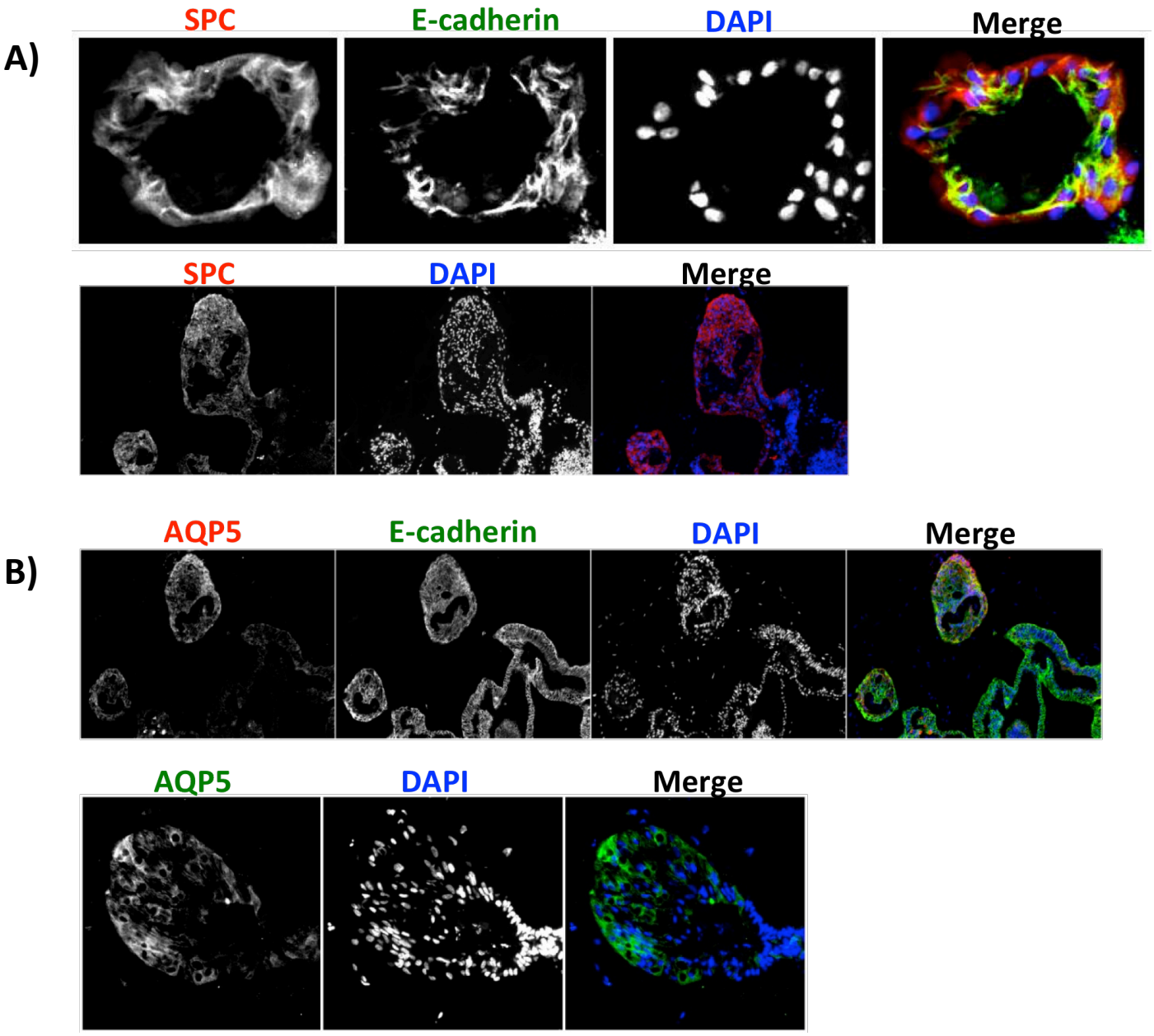

Figure 5 – Immunofluorescent IHC staining of organoids in stage 4 shows that tubular structures contain cells expressing alveolar markers. **A)** Surfactant protein C (SPC) and E-cadherin staining (20x and 4x mag top and bottom). **B)** Aquaporin 5 (AQP5) and E-cadherin staining (4x and 10x mag top and bottom).

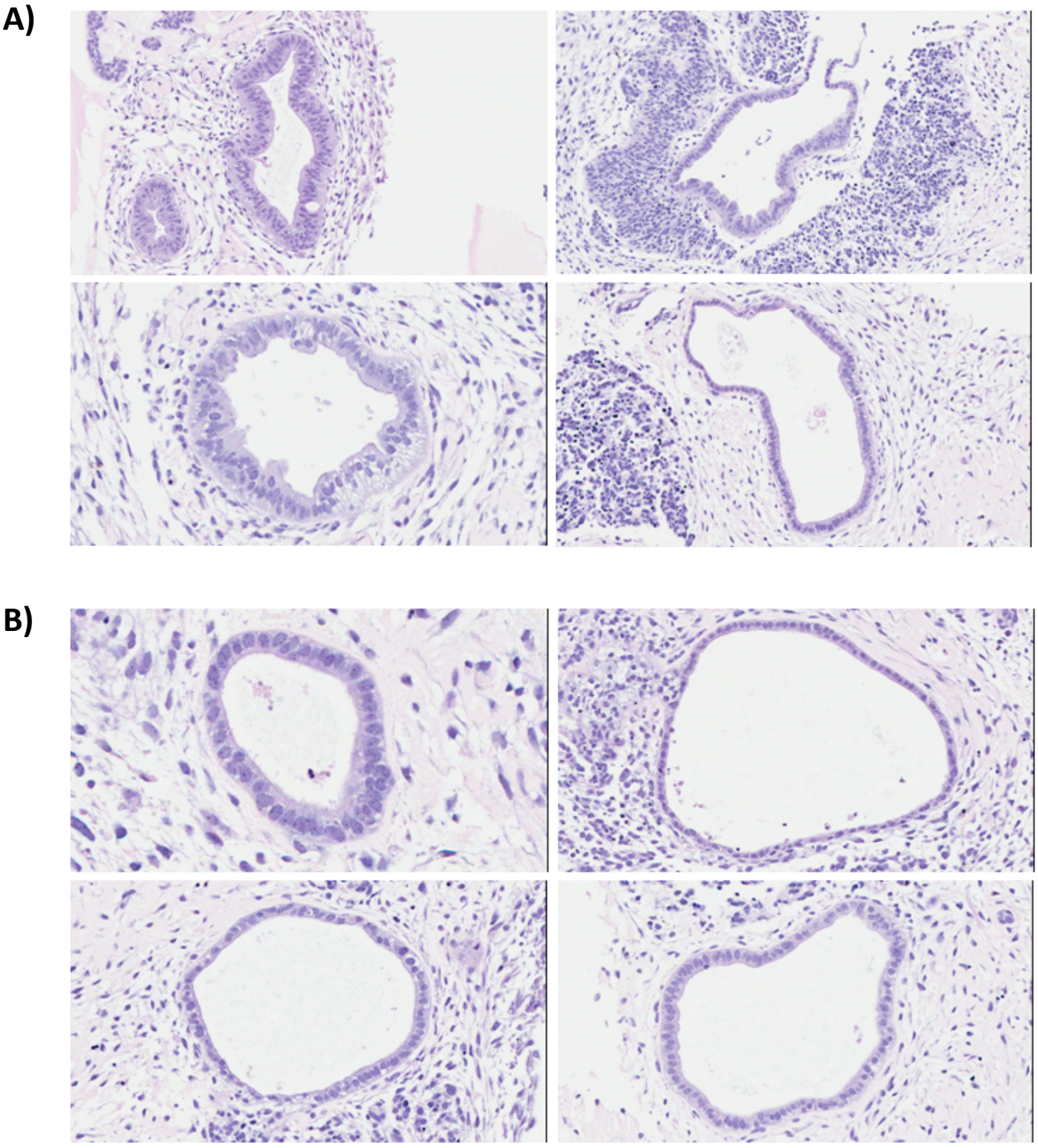

Figure 6 – Haematoxylin and eosin (H&E) staining of organoids in stage 4. **A)** Pseudostratified columnar epithelium reminiscent of the native proximal airways. **B)** Simple cuboidal epithelium reminiscent of the native terminal airways.

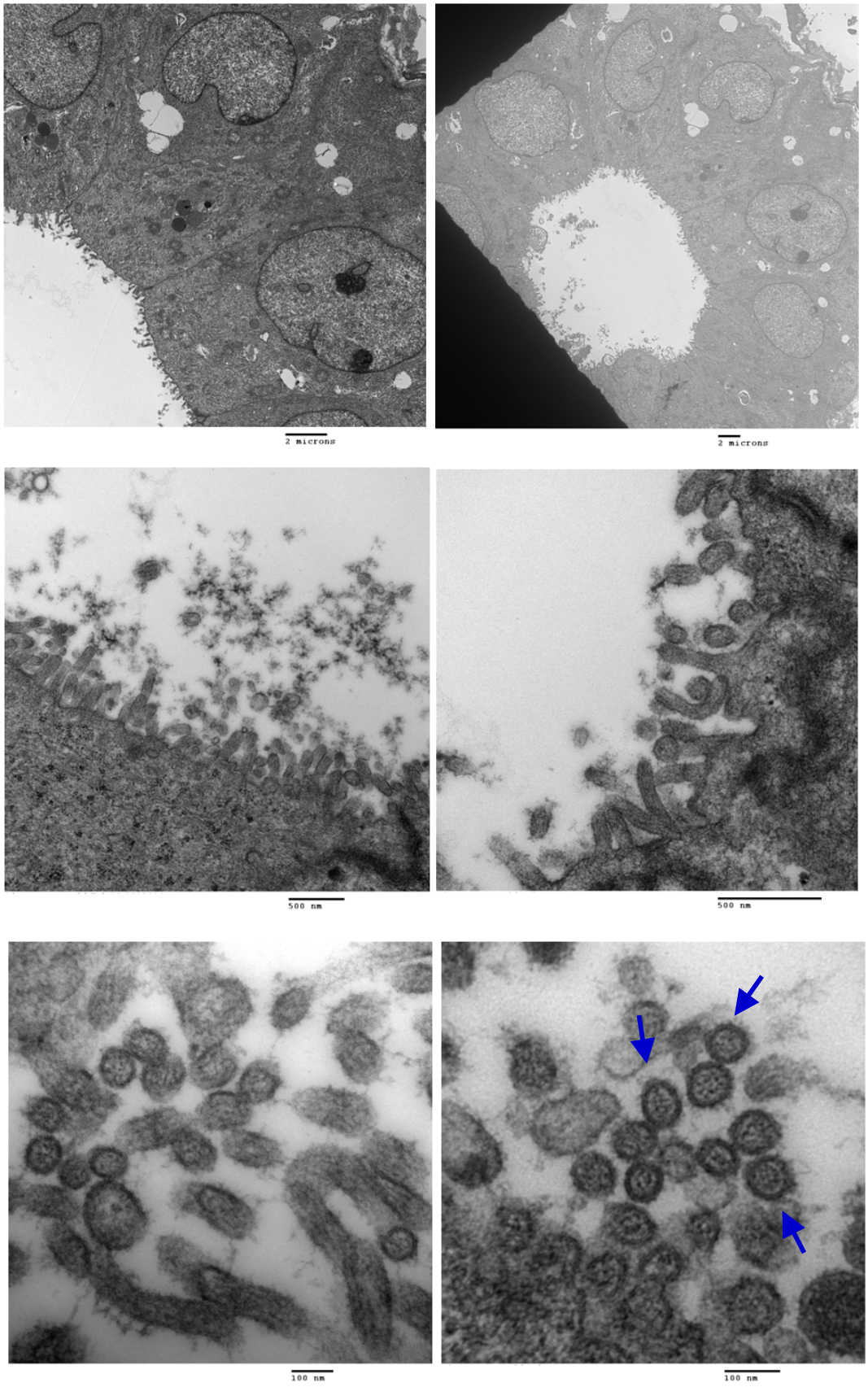

Figure 7 – Transmission electron microscopy ultrastructures of organoids in stage 4. Note polarized epithelium with visible lumen and microvilli (blue arrows) protruding from the apical surface of epithelial cells.

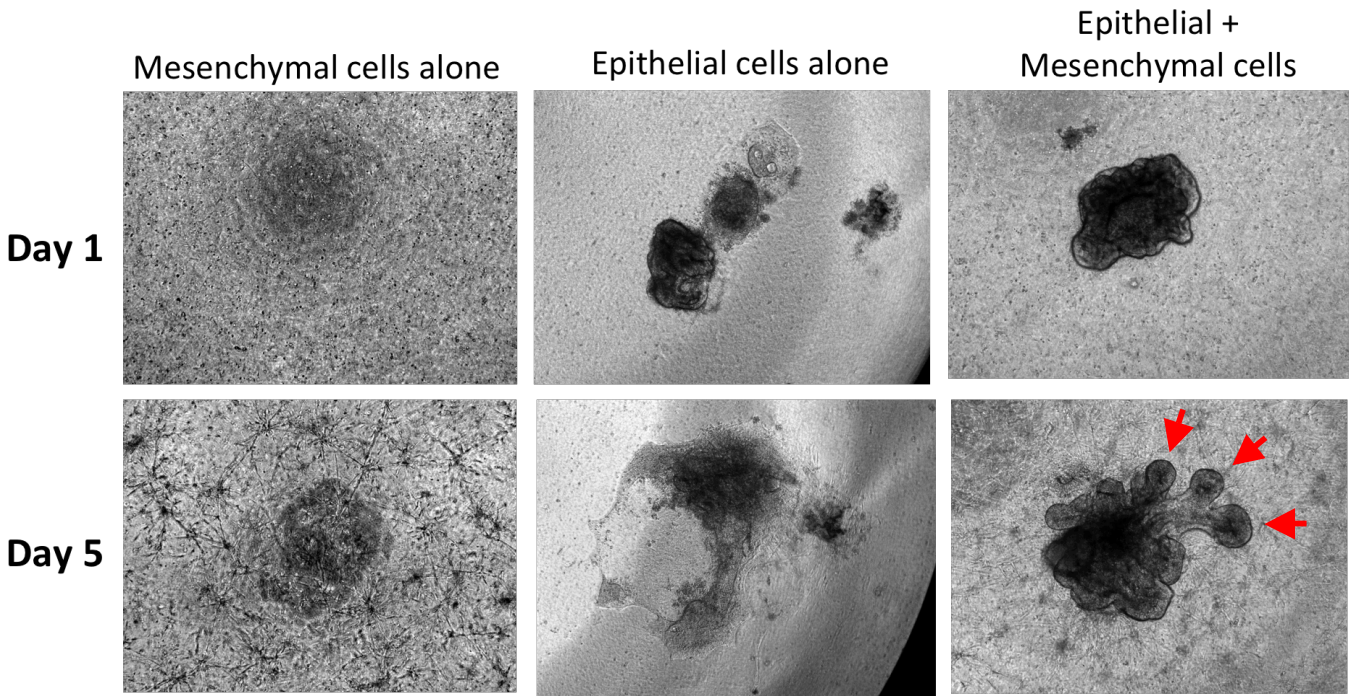

Figure 8 – Segregation and culture of organoid epithelium and mesenchyme. Growth of mesenchyme alone (left), epithelium alone (middle), and epithelium and mesenchyme together (right) were compared. From left to right, note proliferation of mesenchymal cells, collapse of epithelium, and epithelial outgrowths (arrows). Scale: 2x mag.

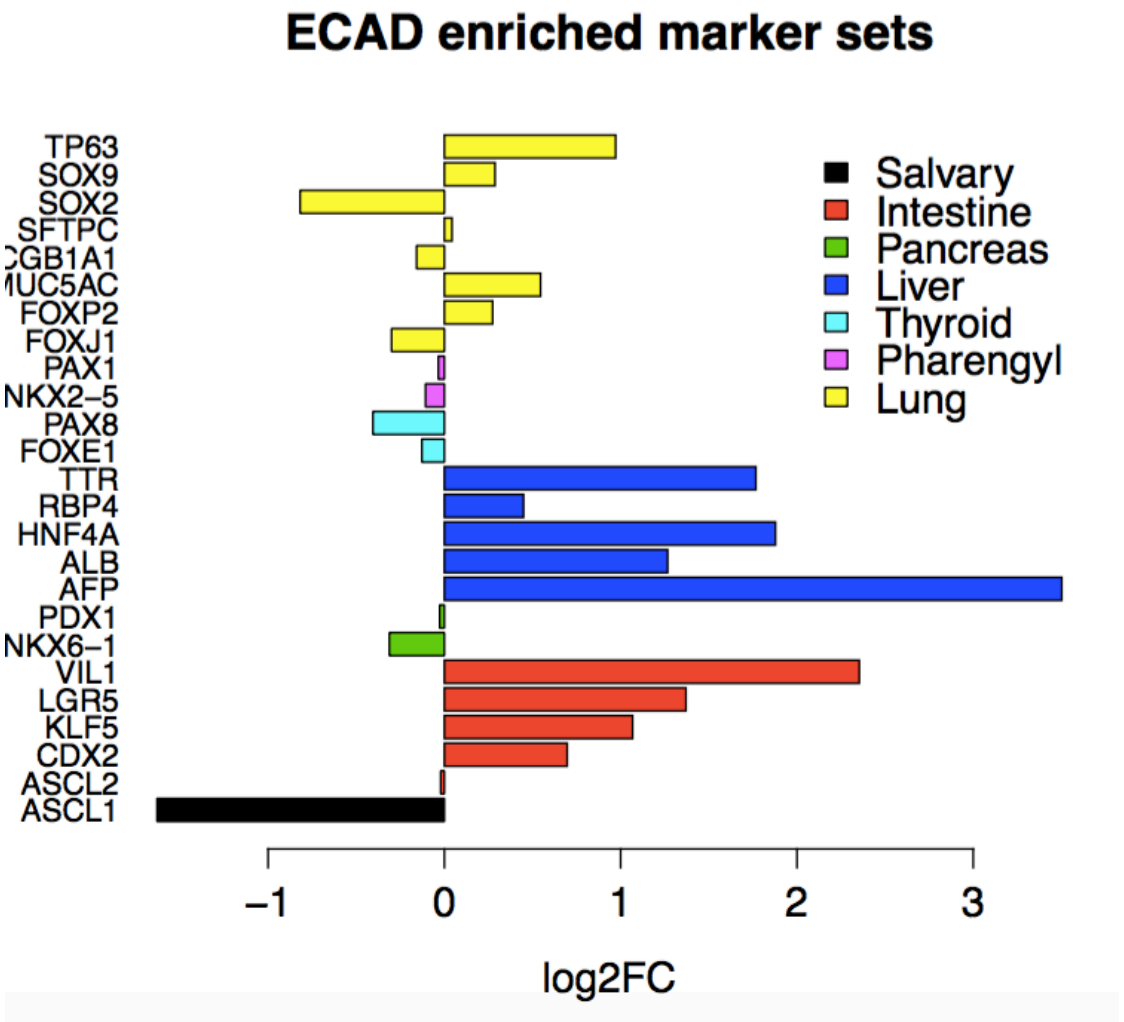

Figure 9 – Microarray analysis of ECAD+ and ECAD- cells from stage 4 tissue. Lineage-related transcript expression levels of ECAD+ cells sorted from stage 4 tissue; done using Affymetrix Human Gene 2.0 RNA microarray.. Expression levels are relative to those of ECAD- cells.

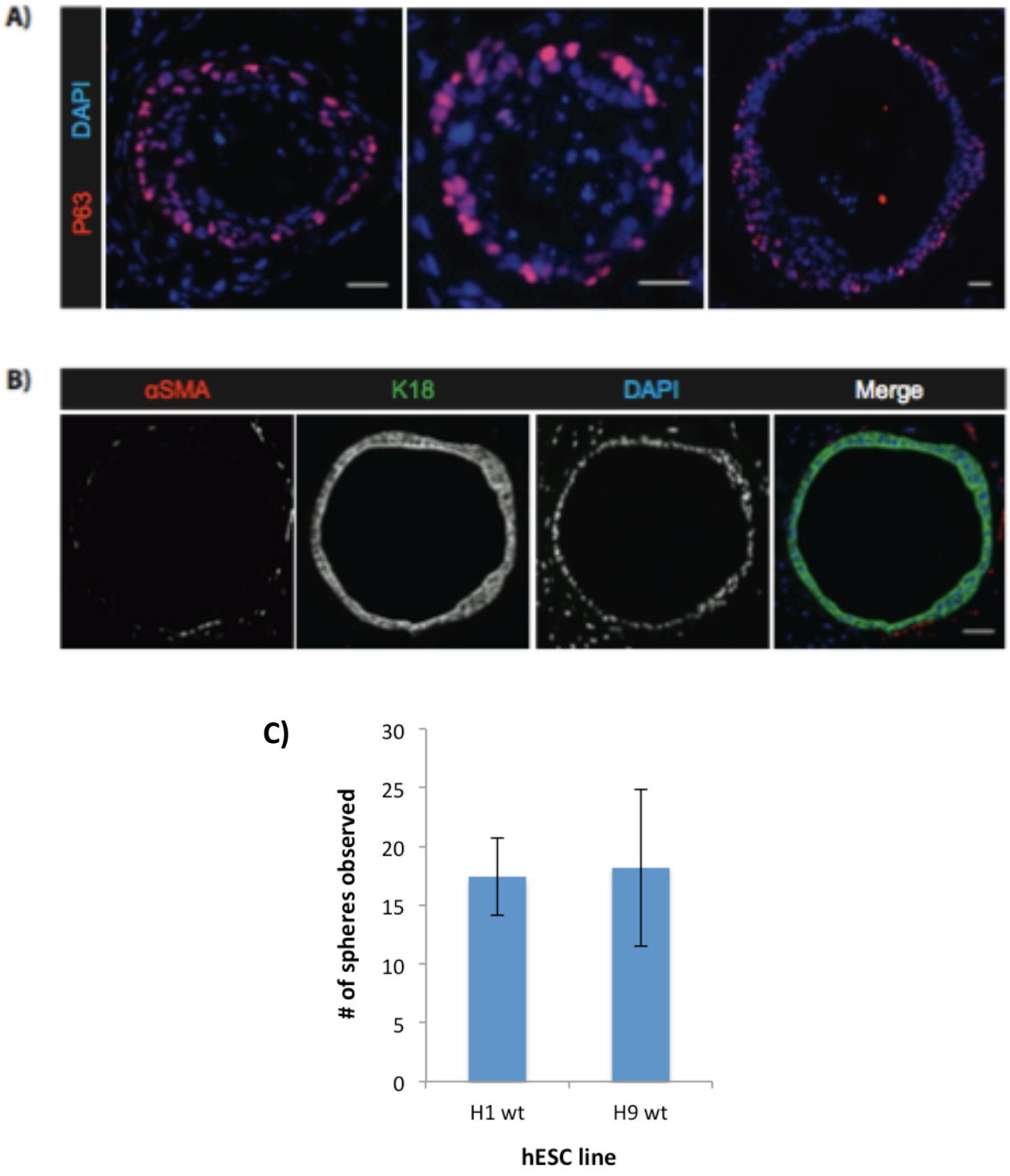

Figure 10 – Bronchosphere-like structures observed in stage 4 cultures. **A)** Representative IF images of spheres containing a pseudostratified epithelium and expression of basal cell marker P63 ubiquitously in the basal layer. **B)** Spheres show ubiquitous expression of epithelial marker K18. **C)** Average number of bronchosphere-like structures observed in stage 4 cultures derived from H1 and H9 wt hESC lines. 17.4 ± 3.3 (n=5) spheres from H1 wt; 18.2 ± 6.7 (n=5) spheres from H9 wt. Scale bars 100µm.

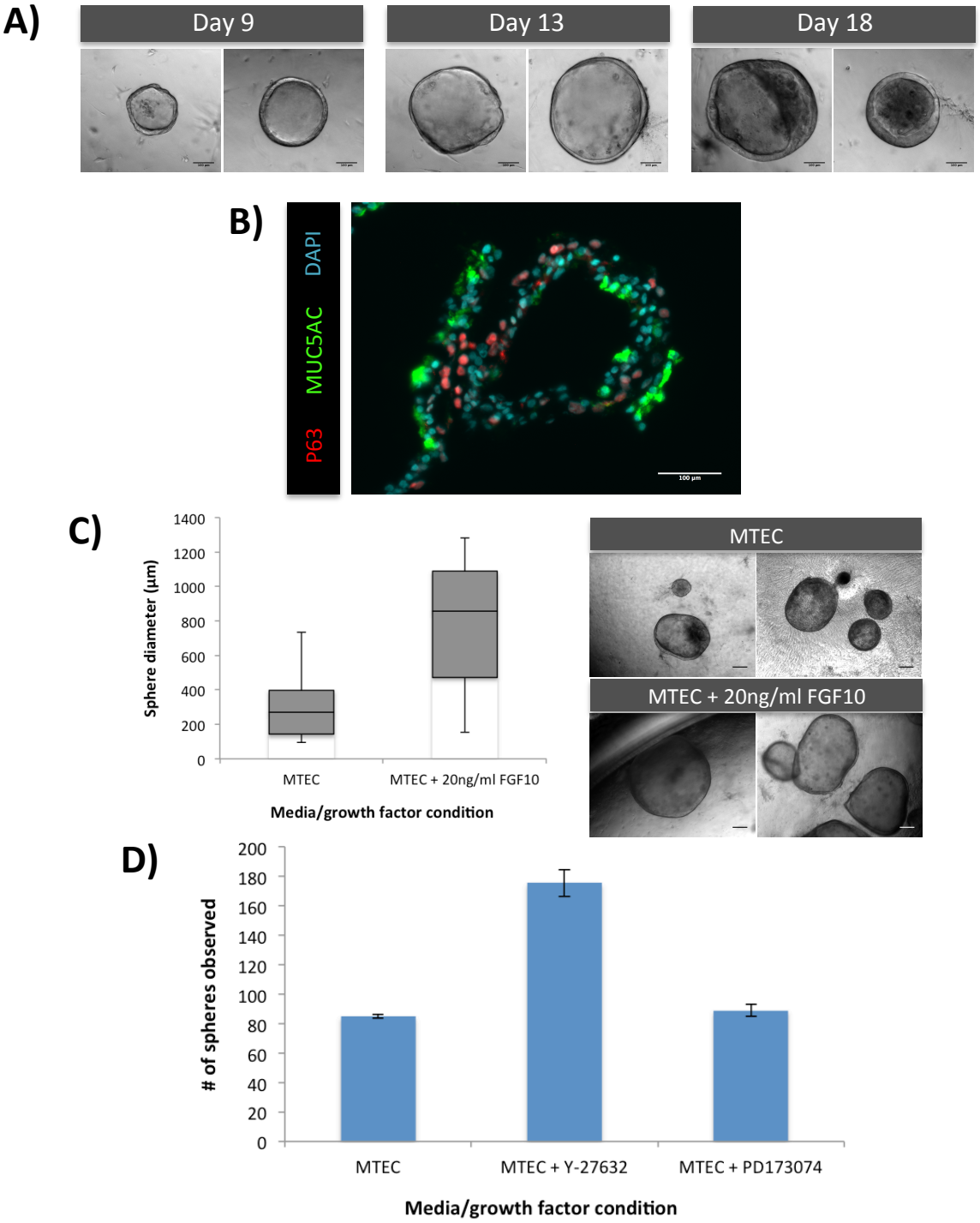

Figure 11 – ECAD+ cells purified from stage 4 tissue, when co-cultured with human lung fibroblasts in a 3D ALI system, gave rise to spheroids.

A) Representative images of spheroids derived from stage 4 tissue-purified ECAD+ cells. Images were taken on day 9, 13 and 18 post-seeding. Spheroids of variable morphology and size were observed, and became more dense with time.

B) Immunofluorescent staining of bronchospheres showing P63+ cells in the basal layer and MUC5AC expression by a subset of goblet cells.

C) On day 18 post-seeding, spheroids had an average diameter of 288 ± 166 µm (n=43). Upon addition of 20ng/ml FGF10 for 18 days post-seeding, the average spheroid diameter was significantly larger: 769 ± 363 µm (n=18).

D) Upon addition of 10UM Y-27632, double the # of spheroids were observed, while addition of 100nM PD173074, an FGFR inhibitor, had no noticeable effect on spheroid count.

Scale bars 100µm.

A)

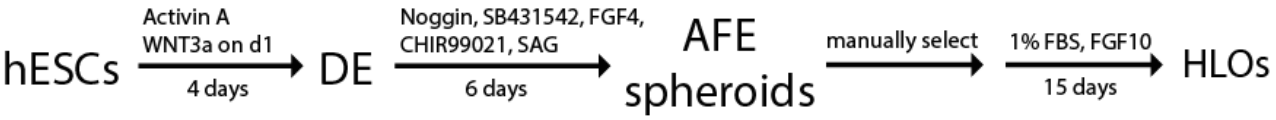

B)

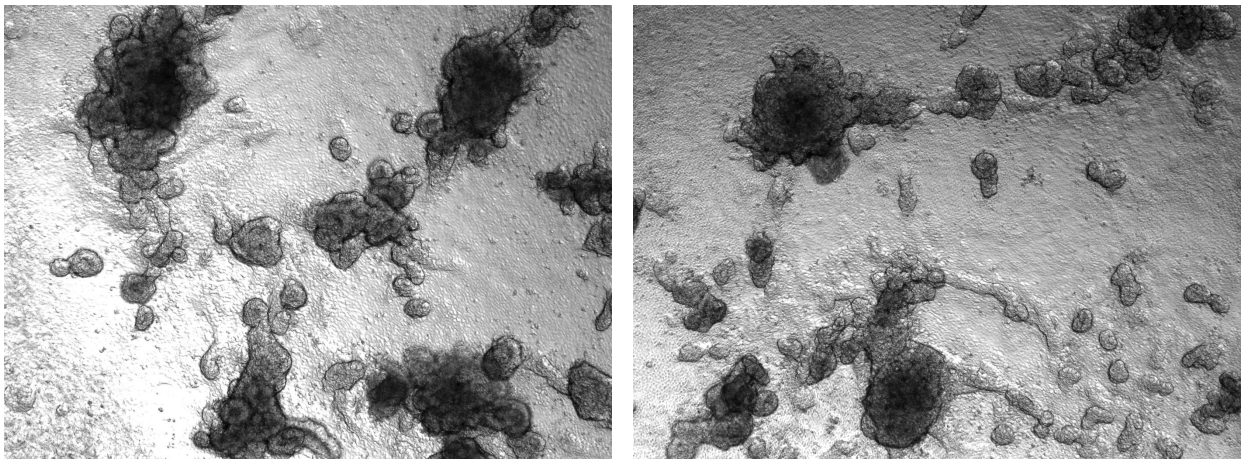

C)

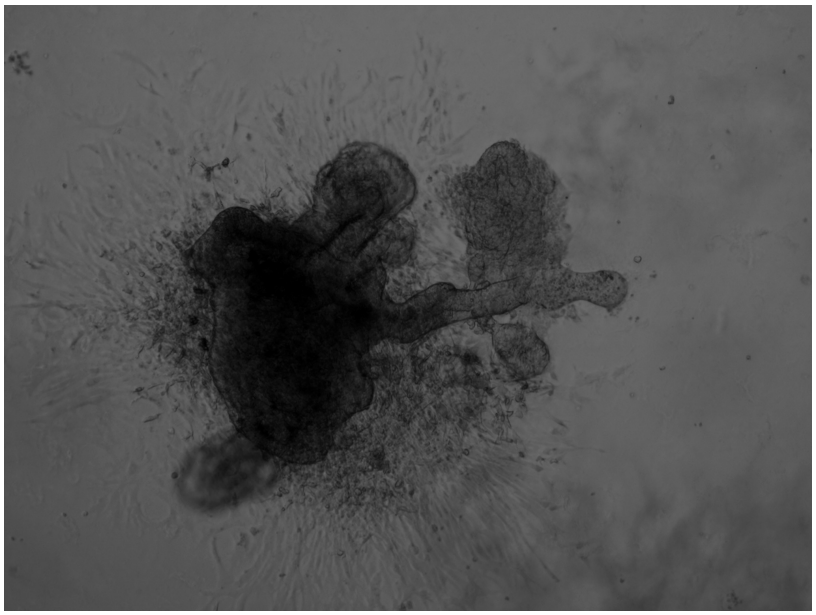

Figure 12 - In vitro generation of lung organoids from hPSCs. **A)** Schematic of *in vitro* differentiation protocol. **B)** Phase images of anterior foregut endoderm (AFE) spheroids/clumps. **C)** Representative phase image of more complex organoid derived from AFE clumps. Scale: 4x mag.

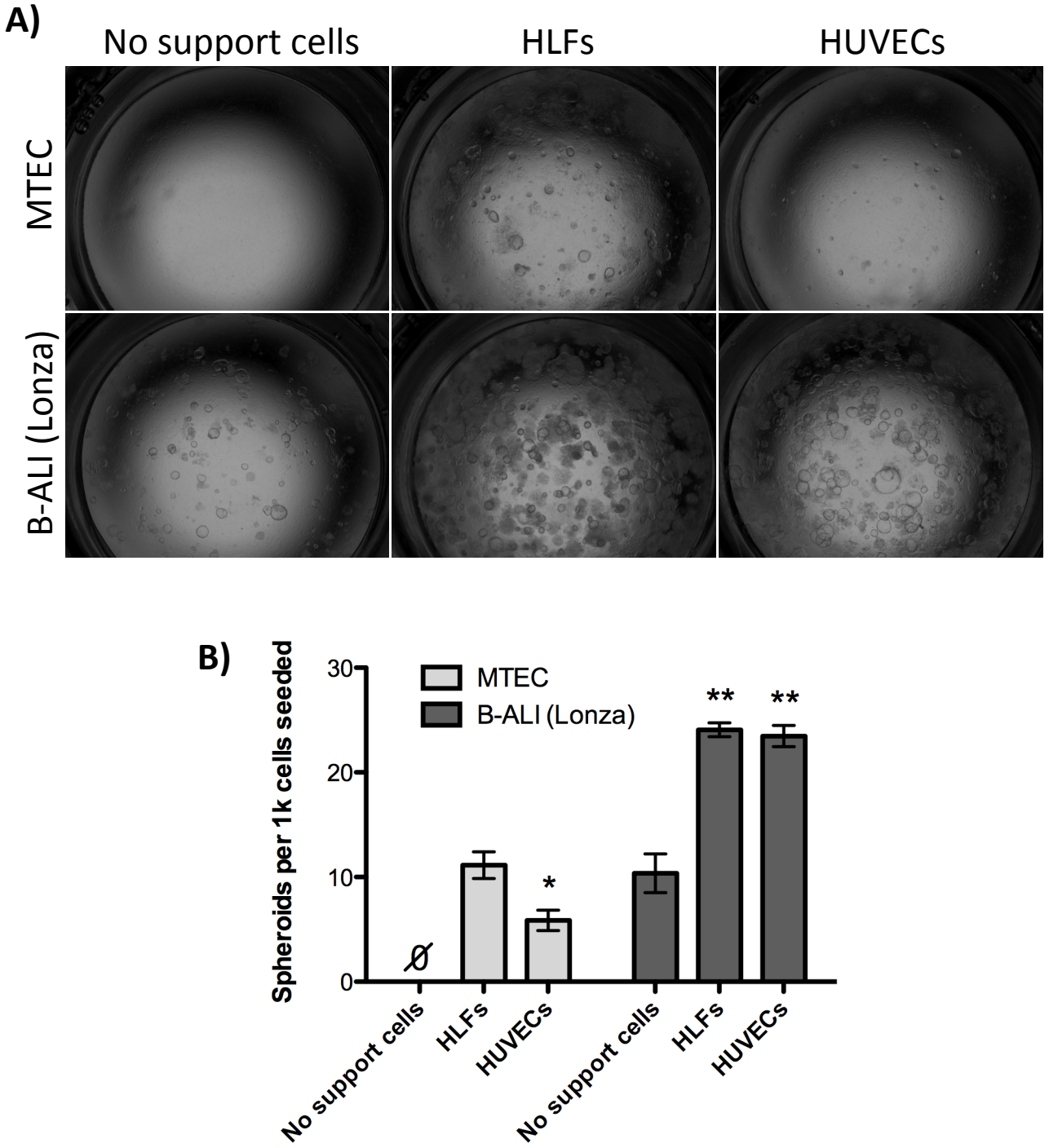

Figure 13 – Cystic epithelial spheroids derived from singularized AFE cells in different conditions. **A)** Representative whole-well scans of spheroids in different conditions; 2x mag. **B)** Number of spheroids produced per 1k AFE cells seeded in different media and co-culture conditions. Scale: 2x mag.

A)

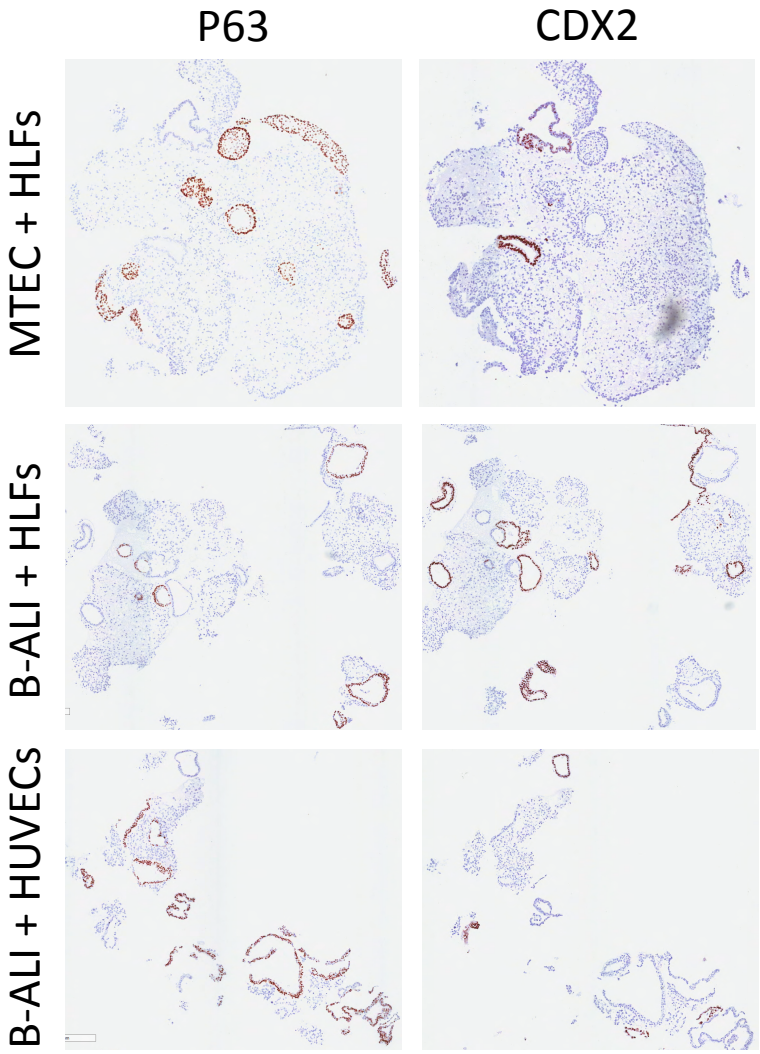

B)

Condition	P63+ spheroids	CDX2+ spheroids
MTEC + HLFs	64%	36%
MTEC + HUVECs	Too few spheres produced	
B-ALI	Too few spheres produced	
B-ALI + HLFs	54%	62%
B-ALI + HUVECs	68%	39%

Figure 14 – Molecular characterization of spheroid populations in different conditions. **A)** IHC staining for P63 and CDX2 of spheroid populations reveals that both phenotypes are present in spheroid populations and are mutually exclusive. **B)** Proportion of spheroids expressing P63 or CDX2 in individually stained tissue sections.

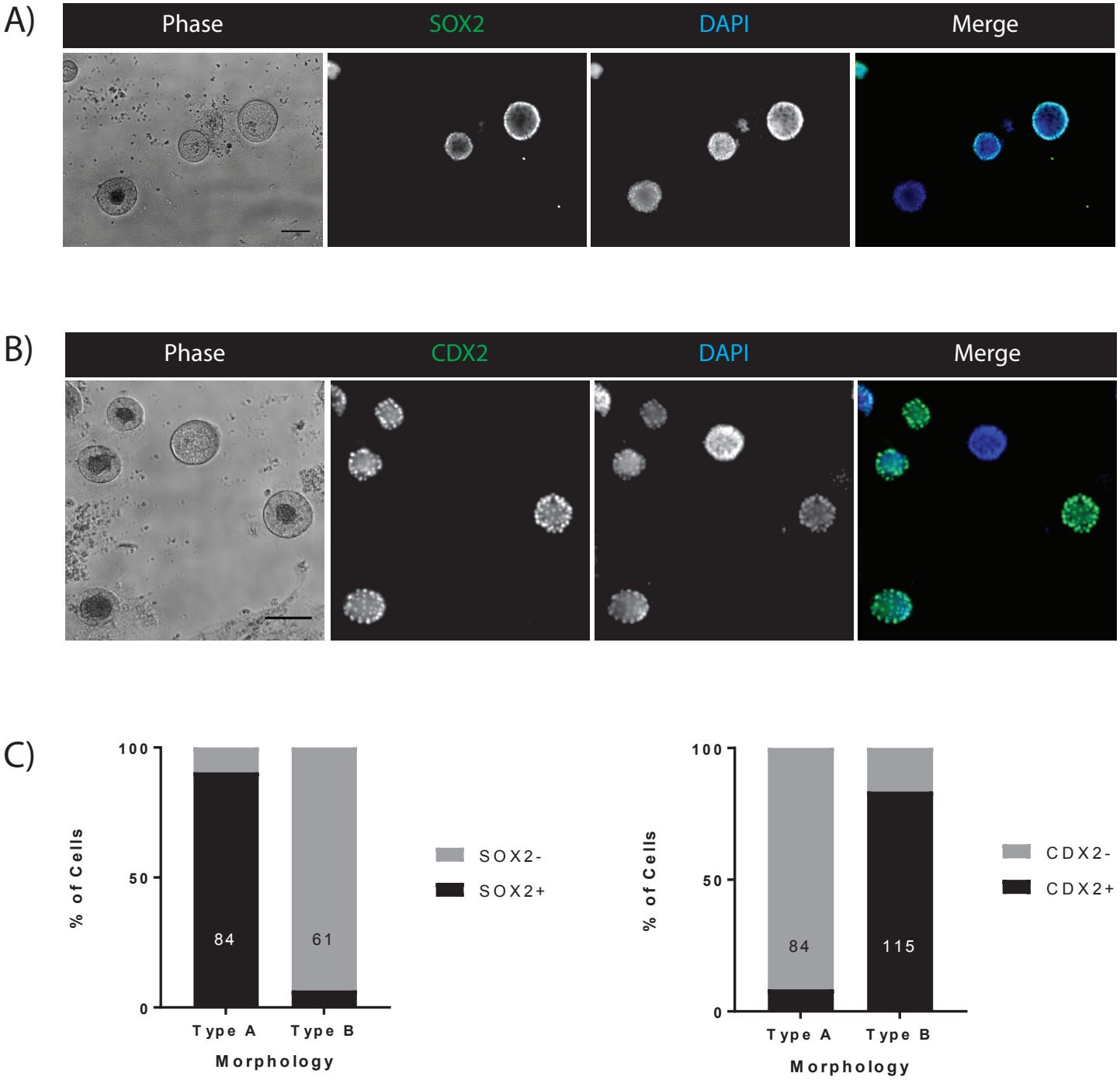

Figure 15 - Analysis of populations of spheroids expressing SOX2 and P63. **A)** *In situ* immunostaining of spheroids for SOX2 and **B)** CDX2. **C)** Scoring of phenotypes by morphology and marker expression. Type A is spheroids with colourless lumen; type B is spheroids with thicker epithelium and dark lumen. Scale bars 100µm.

Chapter 1.3 – Conclusion and Introduction to SECTION 2

In Chapter 1.2, I described strategies for differentiation of hPSCs into early lung and intestinal tissues *in vitro*, and discussed the importance of obtaining a pure population for downstream applications. During our attempts to optimize the hPSC differentiation protocol for deriving lung epithelium, at the time there was greater success by other groups in generating hPSC-derived lung epithelium and lung organoids (Chen et al., 2017; Dye et al., 2015; Konishi et al., 2016). This led us to change our focus going forward, but apply what we had learned in the process, towards the production and characterization of intestinal organoids that were being generated in parallel via our differentiation schemes. Nevertheless, we were successful in publishing the review article about lung organoids mentioned previously (Nadkarni et al., 2015), and later another review article about stem cells in pulmonary disease and regeneration in the scientific journal *Chest* (Nadkarni et al., 2018).

Since we had success in producing intestinal organoids from the original differentiation protocol, I changed my focus from the lung to the intestine during the second half of my degree in the interest of being able to publish novel work. We wanted to show that using a combination of selection and extended culture time we could produce intestinal organoids that were more mature than had been described in the literature. SECTION 2 involves using the original differentiation protocol as a starting point for producing pure populations of cystic intestinal epithelial organoids called enterospheres from hPSCs *in vitro*, and their utility in modeling bacterial-host interactions and intestinal maturation.

REFERENCES

Antonica, F., Kasprzyk, D.F., Opitz, R., Iacovino, M., Liao, X.-H., Dumitrescu, A.M., Refetoff, S., Peremans, K., Manto, M., Kyba, M., et al. (2012). Generation of functional thyroid from embryonic stem cells. Nature *491*, 66–71.

Blij, S., Parenti, A., Tabatabai-Yazdi, N., and Ralston, A. (2015). Cdx2 efficiently induces trophoblast stem-like cells in naïve, but not primed, pluripotent stem cells. Stem Cells Dev. *24*, 1352–1365.

Chen, Y.-W., Huang, S.X., de Carvalho, A.L.R.T., Ho, S.-H., Islam, M.N., Volpi, S., Notarangelo, L.D., Ciancanelli, M., Casanova, J.-L., Bhattacharya, J., et al. (2017). A three-dimensional model of human lung development and disease from pluripotent stem cells. Nat. Cell Biol. *19*, 542–549.

Cheng, X., Ying, L., Lu, L., Galvão, A.M., Mills, J.A., Lin, H.C., Kotton, D.N., Shen, S.S., Nostro, M.C., Choi, J.K., et al. (2012). Self-Renewing Endodermal Progenitor Lines Generated from Human Pluripotent Stem Cells. Cell Stem Cell *10*, 371–384.

Coraux, C., Nawrocki-Raby, B., Hinnrasky, J., Kileztky, C., Gaillard, D., Dani, C., and Puchelle, E. (2005). Embryonic stem cells generate airway epithelial tissue. Am. J. Respir. Cell Mol. Biol. *32*, 87–92.

D'Amour, K.A., Agulnick, A.D., Eliazer, S., Kelly, O.G., Kroon, E., and Baetge, E.E. (2005). Efficient differentiation of human embryonic stem cells to definitive endoderm. Nat. Biotechnol. *23*, 1534–1541.

D'Amour, K.A., Bang, A.G., Eliazer, S., Kelly, O.G., Agulnick, A.D., Smart, N.G., Moorman, M.A., Kroon, E., Carpenter, M.K., and Baetge, E.E. (2006). Production of pancreatic hormone-expressing endocrine cells from human embryonic stem cells. Nat. Biotechnol. *24*, 1392–1401.

Danahay, H., Pessotti, A.D., Coote, J., Montgomery, B.E., Xia, D., Wilson, A., Yang, H., Wang, Z., Bevan, L., Thomas, C., et al. (2015). Notch2 is required for inflammatory cytokine-driven goblet cell metaplasia in the lung. Cell Rep *10*, 239–252.

Dekkers, J.F., Wiegerinck, C.L., de Jonge, H.R., Bronsveld, I., Janssens, H.M., de Winter-de Groot, K.M., Brandsma, A.M., de Jong, N.W.M., Bijvelds, M.J.C., Scholte, B.J., et al. (2013). A functional CFTR assay using primary cystic fibrosis intestinal organoids. Nat. Med. *19*, 939–945.

DeWard, A.D., Cramer, J., and Lagasse, E. (2014). Cellular heterogeneity in the mouse esophagus implicates the presence of a nonquiescent epithelial stem cell population. Cell Rep *9*, 701–711.

Dye, B.R., Hill, D.R., Ferguson, M.A.H., Tsai, Y.-H., Nagy, M.S., Dyal, R., Wells, J.M., Mayhew, C.N., Nattiv, R., Klein, O.D., et al. (2015). In vitro generation of human pluripotent stem cell derived lung organoids. Elife *4*.

Eiraku, M., Takata, N., Ishibashi, H., Kawada, M., Sakakura, E., Okuda, S., Sekiguchi, K., Adachi, T., and Sasai, Y. (2011). Self-organizing optic-cup morphogenesis in three-dimensional culture. Nature *472*, 51–56.

Goessling, W., North, T.E., Lord, A.M., Ceol, C., Lee, S., Weidinger, G., Bourque, C., Strijbosch, R., Haramis, A.-P., Puder, M., et al. (2008). APC mutant zebrafish uncover a changing temporal requirement for wnt signaling in liver development. Dev. Biol. *320*, 161–174.

Gotoh, S., Ito, I., Nagasaki, T., Yamamoto, Y., Konishi, S., Korogi, Y., Matsumoto, H., Muro, S., Hirai, T., Funato, M., et al. (2014). Generation of Alveolar Epithelial Spheroids via Isolated Progenitor Cells from Human Pluripotent Stem Cells. Stem Cell Reports *3*, 394–403.

Green, M.D., Chen, A., Nostro, M.-C., d'Souza, S.L., Schaniel, C., Lemischka, I.R., Gouon-Evans, V., Keller, G., and Snoeck, H.-W. (2011). Generation of anterior foregut endoderm from human embryonic and induced pluripotent stem cells. Nat. Biotechnol. *29*, 267–272.

Guseh, J.S., Bores, S.A., Stanger, B.Z., Zhou, Q., Anderson, W.J., Melton, D.A., and Rajagopal, J. (2009). Notch signaling promotes airway mucous metaplasia and inhibits alveolar development. Development *136*, 1751–1759.

Hegab, A.E., Arai, D., Gao, J., Kuroda, A., Yasuda, H., Ishii, M., Naoki, K., Soejima, K., and Betsuyaku, T. (2015). Mimicking the niche of lung epithelial stem cells and characterization of several effectors of their in vitro behavior. Stem Cell Res *15*, 109–121.

Huang, S.X.L., Islam, M.N., O'Neill, J., Hu, Z., Yang, Y.-G., Chen, Y.-W., Mumau, M., Green, M.D., Vunjak-Novakovic, G., Bhattacharya, J., et al. (2014). Efficient generation of lung and airway epithelial cells from human pluripotent stem cells. Nat. Biotechnol. *32*, 84–91.

Hynds, R.E., and Giangreco, A. (2013). Concise review: the relevance of human stem cell-derived organoid models for epithelial translational medicine. Stem Cells *31*, 417–422.

Konishi, S., Gotoh, S., Tateishi, K., Yamamoto, Y., Korogi, Y., Nagasaki, T., Matsumoto, H., Muro, S., Hirai, T., Ito, I., et al. (2016). Directed Induction of Functional Multi-ciliated Cells in Proximal Airway Epithelial Spheroids from Human Pluripotent Stem Cells. Stem Cell Reports *6*, 18–25.

Lancaster, M.A., and Knoblich, J.A. (2014). Organogenesis in a dish: modeling development and disease using organoid technologies. Science *345*, 1247125.

Lancaster, M.A., Renner, M., Martin, C.-A., Wenzel, D., Bicknell, L.S., Hurles, M.E., Homfray, T., Penninger, J.M., Jackson, A.P., and Knoblich, J.A. (2013). Cerebral organoids model human brain development and microcephaly. Nature *501*, 373–379.

Loh, K.M., Ang, L.T., Zhang, J., Kumar, V., Ang, J., Auyeong, J.Q., Lee, K.L., Choo, S.H., Lim, C.Y.Y., Nichane, M., et al. (2014). Efficient endoderm induction from human pluripotent stem cells by logically directing signals controlling lineage bifurcations. Cell Stem Cell *14*, 237–252.

Longmire, T.A., Ikonomou, L., Hawkins, F., Christodoulou, C., Cao, Y., Jean, J.C., Kwok, L.W., Mou, H., Rajagopal, J., Shen, S.S., et al. (2012). Efficient derivation of purified lung and thyroid progenitors from embryonic stem cells. Cell Stem Cell *10*, 398–411.

Matano, M., Date, S., Shimokawa, M., Takano, A., Fujii, M., Ohta, Y., Watanabe, T., Kanai, T., and Sato, T. (2015). Modeling colorectal cancer using CRISPR-Cas9-mediated engineering of human intestinal organoids. Nat. Med. *21*, 256–262.

McCracken, K.W., Catá, E.M., Crawford, C.M., Sinagoga, K.L., Schumacher, M., Rockich, B.E., Tsai, Y.-H., Mayhew, C.N., Spence, J.R., Zavros, Y., et al. (2014). Modelling human development and disease in pluripotent stem-cell-derived gastric organoids. Nature *516*, 400–404.

Metzger, R.J., Klein, O.D., Martin, G.R., and Krasnow, M.A. (2008). The branching programme of mouse lung development. Nature *453*, 745–750.

Minoo, P., Su, G., Drum, H., Bringas, P., and Kimura, S. (1999). Defects in tracheoesophageal and lung morphogenesis in Nkx2.1(-/-) mouse embryos. Dev. Biol. *209*, 60–71.

del Moral, P.-M., and Warburton, D. (2010). Explant Culture of Mouse Embryonic Whole Lung, Isolated Epithelium, or Mesenchyme Under Chemically Defined Conditions as a System to Evaluate the Molecular Mechanism of Branching Morphogenesis and Cellular Differentiation. Methods Mol Biol *633*, 71–79.

Morrisey, E.E., and Hogan, B.L.M. (2010). Preparing for the first breath: genetic and cellular mechanisms in lung development. Dev. Cell *18*, 8–23.

Mou, H., Zhao, R., Sherwood, R., Ahfeldt, T., Lapey, A., Wain, J., Sicilian, L., Izvolsky, K., Musunuru, K., Cowan, C., et al. (2012). Generation of multipotent lung and airway progenitors from mouse ESCs and patient-specific cystic fibrosis iPSCs. Cell Stem Cell *10*, 385–397.

Mustata, R.C., Vasile, G., Fernandez-Vallone, V., Strollo, S., Lefort, A., Libert, F., Monteyne, D., Pérez-Morga, D., Vassart, G., and Garcia, M.-I. (2013). Identification of Lgr5-independent spheroid-generating progenitors of the mouse fetal intestinal epithelium. Cell Rep *5*, 421–432.

Nadkarni, R.R., Abed, S., and Draper, J.S. (2015). Organoids as a model system for studying human lung development and disease. Biochem. Biophys. Res. Commun.

Nadkarni, R.R., Abed, S., and Draper, J.S. (2018). Stem Cells in Pulmonary Disease and Regeneration. Chest *153*, 994–1003.

Nakano, T., Ando, S., Takata, N., Kawada, M., Muguruma, K., Sekiguchi, K., Saito, K., Yonemura, S., Eiraku, M., and Sasai, Y. (2012). Self-formation of optic cups and storable stratified neural retina from human ESCs. Cell Stem Cell *10*, 771–785.

Pagliuca, F.W., Millman, J.R., Gürtler, M., Segel, M., Van Dervort, A., Ryu, J.H., Peterson, Q.P., Greiner, D., and Melton, D.A. (2014). Generation of functional human pancreatic β cells in vitro. Cell *159*, 428–439.

Rock, J.R., Onaitis, M.W., Rawlins, E.L., Lu, Y., Clark, C.P., Xue, Y., Randell, S.H., and Hogan, B.L.M. (2009). Basal cells as stem cells of the mouse trachea and human airway epithelium. Proc. Natl. Acad. Sci. U.S.A. *106*, 12771–12775.

Rock, J.R., Gao, X., Xue, Y., Randell, S.H., Kong, Y.-Y., and Hogan, B.L. (2011). Notch-dependent differentiation of adult airway basal stem cells. Cell Stem Cell *8*, 639–648.

Sato, T., Vries, R.G., Snippert, H.J., van de Wetering, M., Barker, N., Stange, D.E., van Es, J.H., Abo, A., Kujala, P., Peters, P.J., et al. (2009). Single Lgr5 stem cells build crypt-villus structures in vitro without a mesenchymal niche. Nature *459*, 262–265.

Sato, T., Stange, D.E., Ferrante, M., Vries, R.G.J., Van Es, J.H., Van den Brink, S., Van Houdt, W.J., Pronk, A., Van Gorp, J., Siersema, P.D., et al. (2011). Long-term expansion of epithelial organoids from human colon, adenoma, adenocarcinoma, and Barrett's epithelium. Gastroenterology *141*, 1762–1772.

Séguin, C.A., Draper, J.S., Nagy, A., and Rossant, J. (2008). Establishment of endoderm progenitors by SOX transcription factor expression in human embryonic stem cells. Cell Stem Cell *3*, 182–195.

Sherwood, R.I., Maehr, R., Mazzoni, E.O., and Melton, D.A. (2011). Wnt Signaling Specifies and Patterns Intestinal Endoderm. Mech Dev *128*, 387–400.

Spence, J.R., Mayhew, C.N., Rankin, S.A., Kuhar, M., Vallance, J.E., Tolle, K., Hoskins, E.E., Kalinichenko, V.V., Wells, S.I., Zorn, A.M., et al. (2011). Directed differentiation of human pluripotent stem cells into intestinal tissue in vitro. Nature *470*, 105–109.

Tada, S., Era, T., Furusawa, C., Sakurai, H., Nishikawa, S., Kinoshita, M., Nakao, K., Chiba, T., and Nishikawa, S.-I. (2005). Characterization of mesendoderm: a diverging point of the definitive endoderm and mesoderm in embryonic stem cell differentiation culture. Development *132*, 4363–4374.

Takahashi, K., and Yamanaka, S. (2006). Induction of pluripotent stem cells from mouse embryonic and adult fibroblast cultures by defined factors. Cell *126*, 663–676.

Takahashi, K., Tanabe, K., Ohnuki, M., Narita, M., Ichisaka, T., Tomoda, K., and Yamanaka, S. (2007). Induction of pluripotent stem cells from adult human fibroblasts by defined factors. Cell *131*, 861–872.

Takebe, T., Sekine, K., Enomura, M., Koike, H., Kimura, M., Ogaeri, T., Zhang, R.-R., Ueno, Y., Zheng, Y.-W., Koike, N., et al. (2013). Vascularized and functional human liver from an iPSC-derived organ bud transplant. Nature *499*, 481–484.

Thomson, J.A., Itskovitz-Eldor, J., Shapiro, S.S., Waknitz, M.A., Swiergiel, J.J., Marshall, V.S., and Jones, J.M. (1998). Embryonic stem cell lines derived from human blastocysts. Science *282*, 1145–1147.

Van Haute, L., De Block, G., Liebaers, I., Sermon, K., and De Rycke, M. (2009). Generation of lung epithelial-like tissue from human embryonic stem cells. Respir. Res. *10*, 105.

van de Wetering, M., Francies, H.E., Francis, J.M., Bounova, G., Iorio, F., Pronk, A., van Houdt, W., van Gorp, J., Taylor-Weiner, A., Kester, L., et al. (2015). Prospective derivation of a living organoid biobank of colorectal cancer patients. Cell *161*, 933–945.

Wong, A.P., Bear, C.E., Chin, S., Pasceri, P., Thompson, T.O., Huan, L.-J., Ratjen, F., Ellis, J., and Rossant, J. (2012). Directed differentiation of human pluripotent stem cells into mature airway epithelia expressing functional CFTR protein. Nat. Biotechnol. *30*, 876–882.

Yuan, B., Li, C., Kimura, S., Engelhardt, R.T., Smith, B.R., and Minoo, P. (2000). Inhibition of distal lung morphogenesis in Nkx2.1(-/-) embryos. Dev. Dyn. *217*, 180–190.

Zorn, A.M., and Wells, J.M. (2009). Vertebrate endoderm development and organ formation. Annu. Rev. Cell Dev. Biol. *25*, 221–251.

SECTION 2 – The production and utility of human pluripotent stem cell-derived intestinal organoids

SECTION 2 – The production and utility of human pluripotent stem cell-derived intestinal organoids

Preface

This section focuses on the *in vitro* generation and characterization of cystic intestinal organoids or enterospheres (hEnS) from human pluripotent stem cells, and their deployment for studying bacterial-host interactions and intestinal maturation. This project was initiated by Dr. Jonathan Draper and myself halfway through my tenure in the lab, and was primarily executed by me. The section starts off (Chapter 2.1) with an introduction to intestinal organoids, intestinal development and organogenesis, as well as the current knowledge on maturation of the intestine. Chapter 2.2 is a published research study that was a result of this project, and is explicitly about hEnS derivation. Chapter 2.3 is a draft of a manuscript about the assessment of protein markers of intestinal maturation during human gestation. Chapter 2.4 builds on the work in Chapter 2.2 and focuses on our efforts to model bacteria-host interactions and intestinal maturation with hEnS *in vitro*. Chapter 2.5 is a brief conclusion, provides an update on ongoing work, and describes future directions in the project.

Chapter 2.1 – Introduction

2.1.1 – Intestinal organoid technologies

The production of intestinal organoid cultures in recent years represents a major advance towards creating an *ex vivo* model system of the human intestine and providing simplified access to human intestinal tissues for research. Intestinal organoids were first derived from primary mouse and human intestinal stem cells (Sato et al., 2009, 2011), but there has also been recent success in the production of similar tissues from human pluripotent stem cells (hPSCs) (Finkbeiner et al., 2015; Fordham et al., 2013; Forster et al., 2014; Nadkarni et al., 2017; Spence et al., 2011). Like most organoid types of the definitive endoderm germ layer, intestinal organoids require a three-dimensional (3D) extracellular matrix (ECM) to form and grow, similar to their *in vivo* counterparts that are also supported by a complex 3D ECM. As opposed to a liquid medium suspension, a 3D gel layer allows organoid-forming cells to mostly remain in position and divide and form individual structures in that position. Hans Clevers and colleagues, who pioneered intestinal organoid technology, first made them in the animal-derived hydrogel Matrigel (Sato et al., 2009, 2011), but they can also grow in laminin, collagen, fibronectin and polyethylene glycol (PEG)-based hydrogels (Gjorevski et al., 2016). Intestinal organoids have been shown to require a cocktail of growth factors in the culture media including WNT, EGF, Noggin and R-spondin (Sato et al., 2011), which are members of signaling pathways active in native intestinal organogenesis (Zorn and Wells, 2009).

Primary mouse and human intestinal organoids are generated by harvesting intestinal biopsies, then either purifying LGR5+ intestinal stem cells or separating crypt fragments, followed by culturing in a 3D gel layer with medium containing the above

growth factors (Mustata et al., 2013; Sato et al., 2009, 2011). hPSC-derived intestinal organoids have been made using the following methods: The traditional approach has been to differentiate hPSCs into definitive endoderm using Activin A, then into mid-hindgut endoderm domains using high doses of Wnt and FGF signaling, followed by manually isolating the domains and culturing in Matrigel drops with medium containing intestinal growth factors to produce organoids (Forbester et al., 2015; Fordham et al., 2013; Spence et al., 2011). One study used a unique approach where hPSCs equipped with an LGR5-GFP reporter were transplanted into immunocompromised mice to generate teratomas. Teratomas were then harvested, LGR5-GFP+ve cells were FACS-purified, and cultured in 3D conditions with intestinal medium to produce organoids (Forster et al., 2014).

There are two types of intestinal epithelial organoids that are structurally distinct: enterospheres and enteroids. Enterospheres are cystic organoids or spheroids that have a simple uniform structure and mimic a cross-section of the intestinal tube (Stelzner et al., 2012). In general, enterospheres develop from single precursor cells, which initially divide to form a small aggregate of cells and then expand into a spheroid with a visible lumen. They have been shown to contain intestinal progenitor cells, enterocytes, goblet cells and Paneth cells. In contrast to enterospheres, enteroids are complex multilobulated structures that have crypt-villus asymmetry. Enteroids tend to develop from larger cellular fragments or from enterospheres themselves by formation of budding crypts (Stelzner et al., 2012). They have been shown to contain intestinal stem/progenitor cells, enterocytes, goblet cells, Paneth cells and enteroendocrine cells. The formation of enterospheres versus enteroids can be used to gauge the maturation status and position

along the intestine of their precursor cells. In mice, fetal intestinal stem/progenitor cells from embryonic day 16 (E16) almost exclusively give rise to enterospheres, while adult intestinal stem cells from post-natal day 15 (P15) typically give rise to enteroids, with the ratio of enteroids to enterospheres increasing with development (Fordham et al., 2013; Mustata et al., 2013). The same trend is true along the proximal-distal axis of the intestine, with proximal progenitors giving rise to enterospheres and distal progenitors giving rise to enteroids (Fordham et al., 2013). It is unknown if these trends are the same in humans. While enterospheres have been successfully made from primary mouse and human intestinal cells (Fordham et al., 2013; Mustata et al., 2013), there was only one report of the generation of enterosphere-like structures from hPSCs but which did not display molecular hallmarks of their primary counterparts (Fordham et al., 2013). Similarly, while primary mouse and human enteroids have been made (Sato et al., 2009, 2011), hPSC-derived complex structures resembling enteroids are not identical in architecture and cellular identity (Finkbeiner et al., 2015; Forster et al., 2014; Spence et al., 2011).

2.1.2 – Utility of intestinal organoids in studying basic biology and modeling disease

The applications of intestinal organoids are only just beginning to be explored. Intestinal organoids have been used to determine the effects of various growth factors on proliferation and differentiation of intestinal stem cells (Forster et al., 2014; Kaiko et al., 2016; Mustata et al., 2013; Sato et al., 2011). hPSC-derived intestinal organoids have been used to model the interaction of pathogenic bacteria with the intestine *ex vivo* (Forbester et al., 2015; Hill et al., 2017). Intestinal organoids have also been used to

model cancer. Organoids derived from patients with colorectal carcinoma closely recapitulate properties of the original tumour, and are amenable to high-throughput drug screening, which has led to the identification of gene-drug associations (van de Wetering et al., 2015).

Organoid technologies are already being utilized in personalized medicine. In the Netherlands, less than a decade after Hans Clevers and colleagues pioneered and optimized the production of intestinal organoids from patient biopsies (Sato et al., 2011), they are now capitalizing on their work for treatment of cystic fibrosis (CF) in a patient-specific manner (Dekkers et al., 2013). Organoids derived from CF patients are being subjected to an *in vitro* drug testing assay to determine which drug(s) may ultimately be given to those patients, a test which is actually being covered by Dutch insurance companies (Sinha, 2017).

Primary or iPSC-derived intestinal organoids have the potential to model genetic disorders like familial multiple intestinal atresia (Bigorgne et al., 2014), as well as complex diseases like inflammatory bowel syndrome. Finally, primary fetal or hPSC-derived intestinal organoids may be used to study intestinal development and maturation *in vitro*, such as identifying factors that induce maturation of the fetal intestine. Intestinal maturation is covered in detail in Chapters 2.3 and 2.4.

2.1.3 – Summary of intent

As mentioned at the end of Section 1, while differentiating hPSCs into lung epithelium, we were also producing intestinal tissue. We planned to use our differentiation protocol as a starting point for generating populations of intestinal

organoids. Although hPSCs have been differentiated into various types of intestinal organoids before (Fordham et al., 2013; Forster et al., 2014; Spence et al., 2011), the generation of bona fide enterospheres entirely *in vitro* has not been reported.

Our strategy was to produce pure populations of enterospheres from singularized progenitor cells that were functional and could be expanded and cultured long-term. Enterospheres provide some important advantages over other types of hPSC-derived intestinal tissues made previously. While other groups have noted the presence of contaminating lineages in their organoids (Forster et al., 2014; Spence et al., 2011), enterospheres are composed entirely of intestinal epithelium because they develop from singularized cells. Also, compared to complex intestinal organoids derived from multicellular fragments that vary in structure (Spence et al., 2011), enterospheres have a simple spherical structure, which makes their populations amenable to easier measurement of sphere numbers and sizes, as well as *in situ* staining. Generating bona fide enterospheres from hPSCs will add to the repertoire of epithelial organoid types made in the dish. hPSC-derived enterospheres may be used for studying basic intestinal biology like interrogating the function of intestine-related genes and signaling pathways, modeling host-microbe interactions, and modeling intestinal development and disease. *We hypothesized that differentiating hPSCs into intestinal progenitors and culturing in intestine-specific 3D conditions would produce organoids mimicking the human intestinal epithelium.* Our goals were to I) to differentiate hPSCs into enterospheres *in vitro*, II) to quantify and characterize enterosphere populations and control properties like long-term culture and differentiation, and III) to use *in vitro* assays to demonstrate their functionality and utility.

Aims I and II were addressed by developing a novel protocol to differentiate hPSCs into enterospheres (hEnS) entirely *in vitro*, followed by their characterization at the molecular and functional level. Aim III was addressed by establishing an automated hEnS imaging assay to measure hEnS numbers and sizes in response to treatment with compounds and enteric pathogens that have not been previously tested in this context on human intestinal tissues. We demonstrated the utility of the imaging assay for characterizing bacterial strains in their impact on hEnS formation. Also, preliminary results suggested that hEnS maturation at the molecular level could be induced *in vitro* when treated with probiotic bacteria. As an aside, we assessed the expression of protein markers of intestinal maturation during human gestation in primary samples.

Chapter 2.2 – Functional enterospheres derived *in vitro* from human pluripotent stem cells

Preface

This chapter is an original published article from the scientific journal *Stem Cell Reports*, and is presented in its published form. Some sections have been moved around, and supplemental information has been incorporated. At the time of publication, it became one of the first studies reporting the production of cystic intestinal organoids or enterospheres from human pluripotent stem cells.

Nadkarni, R. R., Abed, S., Cox, B. J., Bhatia, S., Lau, J. T., Surette, M. G., & Draper, J. S. (2017). Functional Enterospheres Derived In Vitro from Human Pluripotent Stem Cells. *Stem Cell Reports*. **9**(3), 897-912.

Dr. Jonathan Draper and I designed this study, and I primarily took part in executing it. Dr. Soumeya Abed, Sonam Bhatia and Jennifer Lau assisted with experimental work. Dr. Jonathan Draper and I contributed to the writing of the manuscript. I primarily generated all the figures with help from Dr. Jonathan Draper, Dr. Soumeya Abed and Dr. Brian Cox.

Title

Functional enterospheres derived *in vitro* from human pluripotent stem cells

Authors

Rohan R. Nadkarni[1, 3], Soumeya Abed[1, 2], Brian J. Cox[4], Sonam Bhatia[1, 3], Jennifer T. Lau[3, 6], Michael G. Surette[5, 6, 7], Jonathan S. Draper[1, 2, 3 *]

Affiliations

[1] McMaster Stem Cell and Cancer Research Institute, Michael G. DeGroote School of Medicine, McMaster University, Hamilton, ON L8N 3Z5, Canada.
[2] Department of Pathology and Molecular Medicine, McMaster University, Hamilton, ON L8N 3Z5, Canada.
[3] Department of Biochemistry and Biomedical Sciences, McMaster University, Hamilton, ON L8N 3Z5, Canada.
[4] Department of Physiology, University of Toronto, Toronto, Canada; Department of Obstetrics and Gynaecology, University of Toronto, Toronto, Canada.
[5] Michael G. DeGroote Institute for Infectious Disease Research, McMaster University, Hamilton, ON L8N 3Z5, Canada.
[6] Farncombe Family Digestive Health Research Institute, McMaster University, Hamilton, ON L8N 3Z5, Canada.
[7] Department of Medicine, McMaster University, Hamilton, ON L8N 3Z5, Canada.
* Corresponding author. Electronic address: draperj@mcmaster.ca

ABSTRACT

Intestinal organoids derived from human pluripotent stem cells (hPSCs) are valuable *in vitro* research models that enable simplified access to human gastrointestinal tissues. Here we report the *in vitro* generation of enterospheres (hEnS) from hPSC-derived gastrointestinal epithelial precursors. hEnS are cystic spheroids with a simple uniform structure composed entirely of intestinal epithelium. hEnS express markers of mature brush border cells, and share a similar transcriptome profile to more mature intestinal organoids. Modulation of signaling cues enables control of hEnS growth and differentiation, including long-term propagation. We show that hEnS can be exploited for functional studies: hEnS display an innate immune response when treated with enteric pathogens, and transgenic modification of hEnS with a fluorescence cell cycle reporter enables hEnS-forming stem cell enrichment. Our work establishes hEnS as an accessible and tractable *in vitro* modeling system for studying human gastrointestinal biology.

INTRODUCTION

Human pluripotent stem cells (hPSCs) can differentiate into all specialized cell types of the body, providing material suitable for a range of applications, including regenerative medicine. hPSCs facilitate research questions that are impractical or difficult using tissue samples derived from patients, including the study of developmental lineage specification. Differentiation studies using hPSCs have helped uncover novel information about human development, such as the roles of signaling pathways in lineage commitment, and have provided evidence of intermediate cell populations during differentiation (Murry and Keller, 2008; Zhu and Huangfu, 2013; Zorn and Wells, 2009).

The differentiation of hPSCs into functional cell types has been enhanced by the production of organoids, 3D structures mimicking the structural and functional properties of *in vivo* organs (Lancaster and Knoblich, 2014). Organoids can be derived from primary adult stem cells as well as hPSC sources (Fatehullah et al., 2016; Huch and Koo, 2015; Nadkarni et al., 2015), but hPSC-derived organoids offer some important advantages, including increased accessibility and an unlimited supply of the starting material. Therefore, the recent establishment of intestinal organoid cultures from hPSCs represents a major advance towards creating a model system of the human intestine (Fordham et al., 2013; Forster et al., 2014; Spence et al., 2011). Organoids generated using various methods have been shown to contain cell types with properties of intestinal stem and differentiated epithelial cells, as well as stromal components. Most studies have relied upon *in vivo* engraftment either to achieve maturation of organoids (Finkbeiner et al., 2015; Spence et al., 2011; Watson et al., 2014) or to derive the organoid precursor cells themselves (Forster et al., 2014). Although these reports have been highly

instructive, a completely *in vitro* approach for the *de novo* production of uniform intestinal organoids containing differentiated cell types would advance gastrointestinal (GI) research.

Here, we report the *in vitro* generation from hPSCs of enterospheres (hEnS) with intestinal cell maturation features akin to those previously obtained via *in vivo* engraftment. hEnS express markers of intestinal epithelial cells types and are similar in gene expression to primary human intestine. We provide detailed insights into the properties of hEnS, and show that they respond to signaling cues during growth and differentiation comparably to primary and hPSC-derived intestinal organoids generated by other methods (Fordham et al., 2013; Forster et al., 2014; Sato et al., 2011). In doing so, we establish hEnS as a research tool that will have utility to the broader stem cell and gastrointestinal research communities.

RESULTS

Spheroid production from hESC-derived endoderm tissues

Since *in vitro* culture duration for the differentiation of other cell types from hPSCs appears to correlate with maturation status (Lundy et al., 2013; Nicholas et al., 2013; Yang et al., 2014; Zhang et al., 2009), we tested if the combination of extended *in vitro* differentiation with an unbiased method for isolating the gut-tube progenitor populations would enhance the maturation status of hPSC-derived tissues compared to current *in vitro* methods. To obtain tissue to evaluate this strategy, we employed a multistage 11-day monolayer differentiation protocol (D'Amour et al., 2005; Green et al., 2011) that produced a mixture of posterior (CDX2-expressing mid/hindgut cells) and

anterior (NKX2-1-expressing putative lung progenitors) endoderm-derived lineages (Figure S1). This population was then used to initiate the production of 3D tissues: the day 11 monolayer cultures were mechanically dissociated and seeded into a Matrigel-based 3D growth environment (Figures 1A and S2). Small cellular aggregates obtained via mechanical dissociation of the monolayer cultures gave rise to multiple organized epithelial "buds" (Figures 1B and S2B) that migrated out of the cell aggregates (Movie S1) during the first 4 days of culture; the transfer of singularized cells (seeded at 50k or 70k per well) from the day-11 monolayer into 3D cultures did not facilitate appreciable bud formation (Figure S2A). By day 15 of 3D culturing, the buds had extensively self-organized to form complex structures (Figure 1C). These structures comprised E-cadherin (ECAD)- and cytokeratin 18 (K18)-expressing epithelial tubules surrounded by mesenchymal tissues that stained positive for α-smooth muscle actin (αSMA) (Figures 1D-E). The mesenchymal component appeared to be necessary for epithelial integrity and growth, as epithelial tubules isolated by micro-dissection degenerated when not co-cultured with mesenchymal cells isolated from the 3D structures (Figure S2C). Analysis of protein expression within the epithelial tubules revealed the presence of CDX2+ cells (Figure 1E), as well as cells expressing markers consistent with an early lung bud fate, including the transcription factors NKX2.1, SOX2, and p63 (Figure 1E). Therefore, the 3D culture environment generated complex 3D structures with organized epithelial tubules containing gastrointestinal and lung cell populations resembling those of the developing fetal gut tube.

We next evaluated fluorescence-activated cell sorting (FACS)-based isolation as a strategy for purifying progenitor populations, using clonal organoid formation and long-

term propagation as a stringent assay for the presence of self-renewing progenitor populations. We opted to perform an unbiased isolation of epithelial cells from dissociated day-15 3D tissues by performing FACS using the pan-epithelium marker ECAD (Figures 2A and S2D). We cultured the sorted cells in the same 3D Matrigel-based growth environment supplemented with MTEC medium containing components compatible with the growth of a range of cell types (Baten et al., 1992; Jumarie and Malo, 1991; Takenaka et al., 2014). No structures formed within 2 weeks post-plating for either ECAD+ or ECAD- cells obtained from the 3D endoderm-enriched tissues (Figure 2B). However, when sorted ECAD+ cells were co-cultured with human lung fibroblasts (HLFs) or human endothelial cells (HUVECs) at a ratio of 1:1, cystic organoids (herein, spheroids) were observed within 6 days at a frequency of ~ 1 per 200 seeded ECAD+ cells from H1 hESCs (Figures 2B-C). The spheroid-forming frequency of ECAD+ cells derived from H9 hESCs was ~1:2500 and ~1:2000 cells when co-cultured with HLFs and HUVECs, respectively (data not shown). These spheroids had a uniform epithelial structure and the morphology was consistent across spheroid units (Figure 2C). Examination of spheroid growth kinetics showed that when co-cultured with HLFs, spheroids were maintained and grew in size over the course of the following 2 weeks (Figure 2D). In contrast, spheroids that formed with the assistance of HUVECs did not grow in size and cultures collapsed after 2 weeks (Figure 2D), so subsequent experiments utilized the HLF co-culture method. No structures were observed in ECAD- cultures with or without supporting cell types despite prolonged culture over 2 weeks (Figure 2B). These data show that FACS-based purification of ECAD+ cells isolated spheroid

precursor cells from the 3D endoderm-derived tissues capable of forming spheroids when co-cultured with HLFs.

Molecular characterization of spheroids reveals intestinal lineage enrichment

E-cadherin expression is not restricted to a particular cell lineage during development, so we next sought to clarify the identity of the spheroids generated from ECAD+ cells. A mixture of cells expressing CDX2 or NKX2.1 were present within the endoderm-enriched 3D tissues used to isolate the ECAD+ cells, however, immunohistochemistry revealed that all assayed spheroids expressed the intestinal transcription factor CDX2 (Figures 3A-B). No spheroids were observed that expressed NKX2-1 (Fig S3A) or SOX2 (data not shown). Almost all spheroids also robustly expressed cytokeratin 20 (CK20), which is expressed in mature intestinal and gastric epithelium (Moll et al., 1990), as well as SOX9, which is found within the proliferating compartment of the intestine (Figures 3A-B and S3A). These data show that the ECAD+ population generated spheroids with features consistent with a gastrointestinal lineage.

Strikingly, this outcome was obtained by culturing cells in growth medium that is not optimized for gastrointestinal organoid growth (Sato et al., 2011). Omitting specific MTEC medium constituents during ECAD+ cell co-culture with HLFs was performed to identify key components. Insulin-transferrin-selenium (ITS) and bovine pituitary extract (BPE) have been used as mitogenic supplements in low-serum media and intestinal epithelial cultures (Baten et al., 1992; Jumarie and Malo, 1991; Takenaka et al., 2014), but only ITS removal significantly reduced both spheroid number and size (Figures S3B-C). Removal of epidermal growth factor (EGF) and retinoic acid (RA) from MTEC

media also had no visible effect (data not shown). Finally, addition of Y-27632 for the duration of spheroid culture, to inhibit the rho-associated protein kinase (ROCK) pathway, which is known to promote survival of single cells and cloning efficiency (Watanabe et al., 2007), almost doubled the spheroid-forming frequency to 1:100 cells in MTEC medium without impacting size (Figures S3B-C).

For further characterization, we performed global mRNA expression profiling on the ECAD+ and ECAD- populations isolated from the 3D endoderm-derived tissues at day 15, as well as spheroids isolated at day 20 of culture. We first assessed the similarity of ECAD+ cells, ECAD- cells and spheroids to *in vivo* tissues by contrasting them with custom gene sets comprising EMAPA ontology and single cell RNA-seq data from primary adult intestinal organoids (Grün et al., 2015). Gene Set Enrichment mapping of our gene expression profiling data onto the custom gene set revealed that a broad range of processes associated with organ development and morphogenesis were enriched in the ECAD+ cells over the ECAD- cells (Figure S3F), supporting their organ precursor status. Also, the transcript levels of markers associated with intestine or stomach development were enriched in the ECAD+ cells when compared to the ECAD- cells, but lung-related transcripts were not (Figure 3C). Analysis of the spheroids over ECAD+ cells demonstrated increased expression of intestine and stomach-associated genes, but not lung (Figure 3D). Gene Set Enrichment of the spheroids over ECAD+ cells highlighted the intestinal identity of the spheroids, displaying enrichment for nodes representative of general intestinal development, as well as specific intestinal epithelial cell types (Figure S3G). Indeed, markers of enterocytes (*VIL1, APOA1, FABP2*) and intestinal stem cells (*LGR5, OLFM4, TACSTD2*) were all elevated in the spheroids when contrasted to the

ECAD+ cells (Figure 3E). However, markers of goblet cells (*MUC2*), enteroendocrine cells (*CHGA, NEUROG3, NKX2-2*) and general commitment to the secretory lineage (*ATOH1*) were depleted (Figure 3E). Immunofluorescence staining (IF) for intestinal brush border markers villin (VIL1) and the digestive enzyme sucrose-isomaltase (SI) demonstrated expression and protein localization consistent with that observed in human fetal small intestine (Figure 3F). A combination of CDX2, VIL1 and SI is restricted to the small intestine (Beaulieu et al., 1990; Gorvel et al., 1991; Moskaluk et al., 2003), providing a regional identity for the spheroids.

Finally, we assayed the similarity of the ECAD cells and spheroids to other tissues. Principle component analysis (PCA) on the transcript profiles of hESCs, ECAD-, ECAD+ cells and spheroids demonstrated that the ECAD- and ECAD+ samples showed large variance with undifferentiated hESCs, but that the ECAD+ cells were closest to the spheroids in the second PC (Figure S3E). Comparison of the spheroid expression profiles with those of endoderm-derived human adult organs (liver, lung, pancreas, stomach, small intestine and colon) revealed the highest similarity to gastrointestinal tissues (Figure 3G). We obtained expression profiles for hPSC-derived intestinal organoids produced by others (Finkbeiner et al., 2015; Forster et al., 2014; Spence et al., 2011) , as well as the control human adult and fetal intestinal tissues included in these studies, and contrasted them with our spheroids. The *in vitro* methodology utilized to generate the hPSC-derived intestinal organoids described in Spence et al, 2011 produces tissues that most closely resemble human fetal intestinal samples (Finkbeiner et al., 2015), but a period of *in vivo* engraftment is sufficient to produce a more mature phenotype (Finkbeiner et al., 2015; Watson et al., 2014). The Forster et al, 2014 study demonstrated

that LGR5+ intestinal progenitors could be isolated from teratomas produced by *in vivo* engraftment of LGR5-GFP reporter hPSCs, and that LGR5+ cells isolated from these teratomas formed intestinal organoids that displayed more mature properties (Forster et al., 2014). Comparison with these organoid and primary human datasets demonstrated that the ECAD+ cell-derived spheroids clustered closely with the more mature Forster organoids (Figure 3H), which together more closely resembled primary human adult intestinal tissues than fetal intestinal tissues.

Together these data support a small intestinal identity for the ECAD+ cell-derived spheroids, and show that they retain properties that are similar to hPSC-derived intestinal tissues that have undergone *in vivo* engraftment. The cystic morphology and expression of some intestinal epithelial markers in the spheroids resembles primary enterospheres (Stelzner et al., 2012), so, herein, they are referred to as hPSC-derived enterospheres (hEnS).

Growth and differentiation of hEnS in different media conditions

The derivation and culture of primary human GI organoids requires a cocktail of factors such as WNT3a, EGF, Noggin and R-Spondin (McCracken et al., 2014; Mustata et al., 2013; Sato et al., 2009, 2011), most of which are absent in MTEC medium. Therefore, widely used intestinal-specific media conditions were utilized to determine if structures that were more representative of mature intestinal epithelium could be generated. ECAD+ cells cultured in intestinal medium containing EGF, Noggin and R-Spondin (ENR) gave rise to a similar number of hEnS (Figure 4A), but those that did form were larger (Figures 4B and S4) and expressed CK20 in similar numbers as MTEC

spheroids (Figure 4C). Combined Periodic acid-Schiff (PAS) and Alcian Blue (AB) staining discriminates glycoproteins and neutral mucins (stained magenta) from acid mucins (blue), with the latter present in functional goblet cells. MTEC medium produced homogeneous hEnS, with >90% comprised of PAS+ AB- cuboidal epithelium. ENR medium resulted in greater heterogeneity, with ~40% of spheroids displaying a PAS-AB- phenotype (Figures 4D-E), and small numbers of AB+ structures indicative of secretory lineages. The addition of WNT3a to ENR is thought to induce intestinal maturation in culture (Fordham et al., 2013). Similar hEnS numbers, sizes and percentage of structures expressing CDX2 or CK20 seen in ENR were observed when ENR was supplemented with WNT3a halfway through the 20 day culture period (ENR-to-WENR) or when WNT3a was supplemented from the start (WENR) (Figures 4A-C). Both ENR-to-WENR and WENR conditions produced hEnS similar to ENR alone, but with a reduction in the fraction of PAS- AB- structures (Figures 4D-E). The gamma-secretase inhibitor DAPT inhibits NOTCH signaling, promoting goblet cell differentiation in intestinal tissues (van Es et al., 2005; Forster et al., 2014; Mustata et al., 2013). Culturing ECAD+ cells in WENR for 10 days, followed by withdrawal of WNT3a and addition of DAPT (WENR-to-ENR+DAPT) for 10 days, produced about the same, but larger, structures than MTEC, but nearly all expressed CDX2 and CK20 (Figures 4A-C). The WENR-to-ENR+DAPT condition also elicited almost 40% of hEnS to express acid mucins (AB+) in a pattern consistent with a goblet cell phenotype (Figures 4D-E). IF staining demonstrated that MTEC spheroids did not express MUC2 or the marker lysozyme (LYZ) at the protein level, however, spheroids expressing MUC2 and LYZ

could be observed in all of the intestine-specific media conditions (Figure 4G and data not shown).

Secondary spheroid formation and long-term propagation indicate the presence of functional stem cells, so we tested the capacity of the different media to enable passaging of hEnS. MTEC medium formed hEnS in 2° assays, but efficiency was less than half that of 1° MTEC hEnS formation (Figure 4F). Insufficient hEnS formed in 3° assays in MTEC medium for continued passage (data not shown). Significantly lower 2° hEnS formation efficiencies were observed for ENR, WENR, WENR-to-ENR and WENR-to-ENR+DAPT (Figure 4F), showing that they were not suitable for long-term propagation.

Long term propagation of hEnS

Gastrin and nicotinamide (WENRg+Nic) have been shown to improve plating efficiency and long-term maintenance of primary human intestinal organoids (Sato et al., 2011), so we tested if this medium could support hEnS derivation and maintenance. Primary cultures of hEnS grown from H1 hESC-derived ECAD+ cells in WENRg+Nic were observed at a higher frequency (1:100 cells) and smaller size to WENR (Figures S5A-B). The WENRg+Nic hENS expressed SOX9 (Figure S5C), but only about half as many structures displayed CK20 reactivity as observed in WENR (Figure 5A). Only a few spheroids with AB+ cells were present in WENRg+Nic, but about 50% of hEnS were of a more complex "budding" structure that were AB-, PAS+, and displayed low/no expression of CK20 and CDX2 (Figures 5B, S5D-E). The lack of AB and CK20, as well as low/no CDX2 suggested that they were composed of cells that were less differentiated compared to those produced in other media conditions (Silberg et al., 2000). In support of

this, and in contrast to other media conditions tested, WENRg+Nic yielded significantly more 2° hEnS than were produced in 1° derivation assays from ECAD+ cells (Figure 5C), and supported their continued passage (more than 8 months; >13 passages) and cryopreservation, avoiding the need to derive *de novo* cultures from hESCs. Primary hEnS from H9 hESCs were produced in WENRg+Nic media at a lower frequency (~1:2000 cells) than from H1 hESCs, but could be subsequently expanded upon passaging (data not shown). WENRg+Nic elicited robust expression of the cell proliferation marker Ki67 (Basak et al., 2014), with 90% of WENRg+Nic hEnS containing Ki67+ cells, compared to 10-30% Ki67+ for other media (Figures 5A and S5F). Since WENRg+Nic enabled robust hEnS expansion, we evaluated the necessity of the HLF support cells in this condition. Substituting the HLFs with human dermal fibroblasts (HDFs) led to a large decline in hEnS formation efficiency, although, unlike HUVECs (Fig 2D), those hEnS that did form were larger than those found in HLF conditions (Figures S5G-I). HLFs removal led to an almost total loss of hEnS formation in WENRg+Nic, WENR, and basal medium, underscoring the necessity of these cells in supporting the propagation of the hEnS (Figure 5D). Inhibition of the TGF-b and p38 signaling (usually via addition of the small molecule inhibitors of Alk4/5/7 (A83-01) and p38 (SB202190)) has been demonstrated to overcome the window of growth arrest/crisis that occurs after ~3 months when adult primary intestinal organoids are grown in WENRg+Nic (Sato et al., 2011). Derivation of 1° hEnS from ECAD+ cells in the presence of HLFs was twice as efficient in WENRg+Nic supplemented with A83-01 and SB202190 (WENRg+Nic+A83+SB2), than for WENRg+Nic only (Figure 5E). Spheroid size was smaller in the presence of the inhibitors, but complex budding structures were

present at a similar frequency to that observed in WENRg+Nic (Figures S5B, D & I). The frequency of Ki67+ hEnS in the presence of the inhibitors was similar to WENRg+Nic without inhibitors, but the fraction of CDX2+ hEnS was substantially reduced (Figures S5J & L). Transfer of hEnS established and propagated in WENRg+Nic with HLFs for over 10 passages to WENRg+Nic+A83+SB2 with HLFs yielded a 2-fold increase in hEnS-forming efficiency (Figure S5K). hEnS derived in WENRg+Nic+A83+SB2 with HLFs generated 2-fold more hEnS in 2° assays, elevating the hEnS-forming efficiency to ~1:30 cells (Figure 5F). Growth of hEnS in WENRg+Nic was reliant upon the presence of HLFs (Figure 5D), however hEnS previously cultured in WENRg+Nic+A83+SB2 formed 2° hEnS in the absence of feeders, albeit with a moderate reduction in efficiency (Figure 5G). Previous culture with the inhibitors inured the 2° hEnS formation efficiency to removal of gastrin + nicotinamide or A83-01 + SB202190, but not both, showing that sustained increases in efficiency were not mediated solely by the presence of the inhibitors.

Next, we assayed how the different media conditions influenced the expression of key intestinal stem cell and differentiation markers. hEnS generated in ENR, WENR and WENR-to-ENR+DAPT expressed higher levels of *VIL1, LYZ* and *MUC2* (Figure 5H), implying a more differentiated phenotype. hEnS grown in WENRg+Nic clustered separately and expressed higher levels of the stem cell markers *OLFM4* and *ASCL2*, whereas WENRg+Nic+A83+SB2 had relatively lower OLMF4 and higher LGR5. hEnS grown in WENR-to-ENR+DAPT showed the highest expression of *MUC2*.

Finally, we tested how media conditions might be eliciting altered hEnS behavior. Since Wnt signaling is recognized to be the dominant mechanism for driving the

proliferation of intestinal stem cells (Fevr et al., 2007; Krausova and Korinek, 2014), we assayed levels of the active form of the Wnt signal mediator β-catenin. Phosphorylation at Ser33/37/Thr41 by GSK-3 inactivates β-catenin (Yost et al., 1996), so we looked at active, nuclear β-catenin using an antibody that recognizes only the non-phosphorylated form (NP-β-catenin). Membrane-bound NP-β-catenin was observable in all conditions tested. Nuclear NP-β-catenin was most frequent in the WENRg+Nic, WENR and MTEC conditions (Figures 5I-K), but levels for ENR were much lower, and similar to those observed in the human intestinal villi. WENRg+Nic+A83+SB2 displayed nuclear NP-β-catenin levels that were lower than for WENRg+Nic alone, but were more equivalent to those seen in the human crypts, despite all three samples displaying higher Ki67 expression levels that other conditions (Figures 5I-J).

Collectively, these observations demonstrate that specific culture conditions allow for the long-term culture of hEnS, and that the most efficient culture conditions elicit Wnt signaling levels that match those observed in the intestinal crypts.

Cell cycle analysis of hEnS equipped with a fluorescence cell cycle reporter

Genetic modification experiments can provide fundamental insights into tissue function. We reasoned that the population of singularized precursor cells used to form hEnS would be amenable to transgenic alteration, avoiding the laborious process of creating stable genetically modified hPSC lines. We took advantage of this utility by infecting dissociated hEnS cells with a lentivirus carrying the H2BGFP-FUCCI reporter (Calder et al., 2013) (Figure 6A). This reporter consists of H2B-GFP, which decorates chromatin, linked via a 2A sequence to mKO2-Cdt1, the expression of which is restricted

to cells in G1/G0 (Sakaue-Sawano et al., 2008). Following puromycin selection, we derived hEnS that ubiquitously expressed H2B-GFP, with cells in G1/G0 transiently expressing mKO2-Cdt1 (Figure 6B). Flow quantification indicated that ~92% of cells were mKO2+ (data not shown).

We utilized the H2BGFP-FUCCI reporter for cell cycle analysis of hEnS cells. As described earlier, hEnS produced in WENRg+Nic consist of Ki67-expressing cells, which may be capable of spheroid propagation. Since cells that are actively cycling are more likely to represent proliferative or stem cells (Calder et al., 2013), we hypothesized that the mKO2- cell fraction would be enriched for hEnS-forming stem cells, while the mKO2+ fraction, or cells in G1/G0, would contain a greater proportion of non-proliferative or differentiated cells.

To show proof of principle, we tested this hypothesis by FACS-separating FUCCI-equipped hEnS cells by mKO2-Cdt1 expression, and comparing the frequency at which each fraction generates new hEnS in culture. We found that while mKO2+ and unsorted cells produced hEnS in similar numbers, mKO2- cells produced hEnS with almost double the frequency (Figure 6C). This indicates that the occurrence of hEnS-propagating cells was higher in the actively cycling population than in cells in G1/G0. Therefore, transgenic modification of hEnS with the H2BGFP-FUCCI reporter permitted cell cycle analysis and enabled further enrichment for hEnS-forming stem cells.

hEnS elicit a functional innate immune response to bacterial infection

Establishing robust assays that test the functionality of *in vitro*-derived intestinal tissues is necessary if they are to be used in downstream biomedical applications. We

sought to test if the hEnS provided a model for studying functional gastrointestinal responses. To functionally interrogate the hEnS, we tested their ability to demonstrate an innate immune response to bacterial infection. Mucin glycoproteins like MUC2, whose expression was detected in hEnS, are the main component of the first barrier that bacteria encounter in the intestine (Lindén et al., 2008), and increased expression of MUC2 is a well documented innate response by intestinal cell types confronted with pathogenic bacteria (Forbester et al., 2015; Lindén et al., 2008; Möndel et al., 2009; Vora et al., 2004; Xue et al., 2014). We tested the response of hEnS to bacterial interaction by incubating hEnS with either 100ng/ml bacterial lipopolysaccharide (LPS), the pathogenic *E. coli* strain O157:H7, or the non-pathogenic probiotic strain Nissle 1917 (both bacteria strains at an MOI of ~1:50) (Figure 6D). The Nissle 1917 strain serves as a negative control, as it contains a defect in LPS biosynthesis that leads to the production of truncated O-antigen polysaccharide chains (Güttsches et al., 2012). After infection, O157:H7 bacteria could be observed in close association with the hEnS (Figure 6E). Relative to uninfected hEnS, transcript levels for genes associated with an innate immune response, including *MUC2, DEFB4A, TNF, IL6,* and *IL8,* were significantly higher in hEnS treated with pathogenic strain O157:H7, but were not significantly changed for non-pathogenic Nissle 1917 (Figure 6F). LPS treatment induced significant changes only in *MUC2, DEFB4A*, and *TNF*. No significant changes in *CDX2* levels were detected in any of the treatments, indicating that the transcript changes were not global events. No changes in *MUC2* or *CDX2* transcripts were observed in undifferentiated H1 hESCs for any of the treatments (data not shown), supporting the specificity of this response to *bona*

fide intestinal cell types. Therefore, hEnS elicited a functional innate immune response to treatment with LPS and enteric pathogens.

DISCUSSION

We have established an *in vitro* method for generating enterospheres, or hEnS, from hPSCs. Intestinal organoids have been generated *in vitro* from hPSCs by endoderm differentiation protocols that produce raised aggregates of mid/hindgut cells on the culture surface at around day 7 (Fordham et al., 2013; Spence et al., 2011; Watson et al., 2014). Subsequent 3D culture of these progenitor units produces complex organoids that contain multiple intestinal cells types organized in a manner similar to that of native intestine. Our approach uses ECAD expression to isolate singularized epithelial progenitors from hPSC-derived 3D tissues comprising a mixture of endoderm lineages generated via a 4-stage, 26-day differentiation process. Subsequent hEnS formation in a 3D growth environment demonstrates the presence of intestinal stem cells within the ECAD+ population that display resilient growth in a variety of media conditions.

In our multistage differentiation strategy, we routinely derived monolayer cultures containing CDX2+ cells. CDX2 expression was absent at stages 1 and 2, but emerged by the end of stage 3, following treatment consisting of WNT, FGF, BMP and RA signaling. The emergence of CDX2 at stage 3 may be due to exposure to WNT and FGF signaling, which have been utilized in previous work to specify the mid/hindgut lineage from endoderm (Spence et al., 2011). Despite the extensive presence of CDX2+ cells at the end of stage 3 (day 11), we were unable to isolate spheroids by seeding singularized cells into 3D culture conditions, with or without support cells. However, subsequent culture of

cell clumps from stage 3 in a 3D growth environment produced complex structures, composed of mesenchymal cells that we showed supported the integrity and growth of epithelial tubules. Isolation of ECAD+ epithelial cells from the 3D tissues enabled the formation of hEnS, showing that functional hEnS-forming stem cells were specified within the 3D structures produced in stage 4.

The differentiation of hPSCs often yields tissues that have an immature fetal phenotype, although several studies have shown correlations between extending the duration hPSC-derived cell types are in culture with the extent of maturation achieved (Lundy et al., 2013; Nicholas et al., 2013; Yang et al., 2014; Zhang et al., 2009). *In vivo* engraftment enables hPSC-derived intestinal organoids to manifest features associated with maturation (Finkbeiner et al., 2015; Forster et al., 2014). Although the *in vitro* generation of fetal enterosphere-like structures was previously reported (Fordham et al., 2013), they failed to display robust expression of intestinal epithelial markers. We have shown that our methodology produces hEnS that are more similar in gene expression profile to hPSC-derived intestinal organoids derived via *in vivo* engraftment, than to those made by previously described *in vitro* differentiation protocols, and that our hEnS show greater transcriptional similarity to primary adult intestine than to fetal intestine. The hEnS express markers of enterocytes (VIL1), goblet cells (MUC2), mature brush border proteins (CK20 and SI), as well as the antimicrobial enzyme LYZ. Of note, the detection of SI expression has only been described in hPSC-derived intestinal organoids after a period of maturation by *in vivo* engraftment (Finkbeiner et al., 2015). We were unable to detect other maturation indicators in the hEnS, such as enteroendocrine marker CHGA and ubiquitous OLMF4 expression (data not shown), indicating that the hEnS

achieved an intermediate stage of maturation that surpasses previous *in vitro* methods for generating intestinal tissues, but does not fully attain the maturation level observed following *in vivo* engraftment. Cystic spheroids, as opposed to crypt-villus structures or enteroids, represented the most prevalent phenotype. Taken together, the hEnS display hallmarks of proximal intestinal tissue at around E16-E18 in the mouse or 10-12 gestational weeks in the human (Fordham et al., 2013; Mustata et al., 2013).

Strikingly, hEnS can initially form from ECAD+ cells in the absence of growth factors thought to be essential for the formation of intestinal or gastric organoids (McCracken et al., 2014; Sato et al., 2009, 2011; Spence et al., 2011), but do require specific media conditions for long-term propagation and differentiation induction. hEnS grown in MTEC display relatively low expression of both intestinal stem and differentiation-related genes, whereas hEnS grown in ENR, WENR or ENR+DAPT express higher levels. MTEC produces CK20-expressing structures that are devoid of MUC2, suggesting that they may be mainly composed of enterocytes. In the native intestine, Notch inhibition promotes goblet cell differentiation (van Es et al., 2005; Forster et al., 2014; Mustata et al., 2013), and high expression of *MUC2,* along with CK20 and AB positivity in ENR+DAPT, recapitulates this phenomenon. Since expansion of intestinal organoids is a qualitative measure for the presence of intestinal stem cells, we profiled conditions that might enable long-term propagation of the hEnS. We found that WENRg+Nic facilitated long-term passaging, but unlike the primary adult intestinal organoids reported by Sato et al, 2011, we did not see a window of arrest/crisis for the hEnS when cultured in this medium. We showed that this difference was mediated entirely by the presence of the HLFs in our culture system, which outperformed other

support cells in maintaining hEnS. Addition of the Alk4/5/7 (A83-01) and p38 (SB202190) inhibitors to WENRg+Nic not only improved hEnS-forming efficacy but also enabled feeder-free growth. The observation that WENRg+Nic+A83+SB2 allows robust, feeder-free growth of the hEnS, and that it produces nuclear β-catenin levels similar to endogenous crypts is intriguing. WENRg+Nic supplemented with feeders generated the highest levels of nuclear β-catenin, but cultures expanded at half the rate, and quickly crashed upon feeder removal. These observations may be related to the "just-right" model of Wnt signaling (Albuquerque et al., 2002; Cadigan and Peifer, 2009) that proposes that optimal Wnt signaling levels, but not levels too high or low, enable Wnt-driven expansion. Our findings suggest that correct Wnt signaling levels may also be required for the robust *in vitro* expansion of intestinal organoids. Finally, expression of adult stem cell marker *LGR5* was highest in WENR, suggesting that hEnS grown in this condition may have the most mature phenotype (Fordham et al., 2013; Forster et al., 2014). Although *LGR5* is a Wnt target gene, LGR5 expression was depleted in hEnS cultured in WENRg+Nic relative to WENR or WENRg+Nic+A83+SB2, implying that the modulation of LGR5 expression is influenced by other interactions.

Generating populations of organoids with homogeneous structure and cell-type composition simplifies the interpretation of cell-specific responses, and enables consistency in applications such as screening, where similarity in material across replicate wells is desirable. The more variable and complex intestinal organoids reported by others contain multiple cell types, including mesenchymal components, and are less amenable to high-throughput assays. The method we used produces functional intestinal organoid units that can be utilized in spheroid-forming assays, and can be enumerated by

automated imaging of calcein green (data not shown). In combination with the long-term propagation potential of hEnS, these spheroids represent attractive screening tools for exploring human-specific gastrointestinal biology. Indeed, although the activation of an innate immune response by the hEnS after treatment with LPS and enteric pathogens does not describe the absolute maturation status of the hEnS, it does demonstrate important aspects concerning their utility: first, they contain functional intestinal cell types that respond to external stimuli in a manner characteristic of native intestinal tissues; and second, they recapitulate aspects of gastrointestinal biology.

Our work establishes hEnS as an *in vitro* model system for studying human intestinal biology, development and disease.

EXPERIMENTAL PROCEDURES

Maintenance and differentiation of hESCs

H1 and H9 wt hESCs (Wicell Research Institute) were cultured on Matrigel (Corning; #354234) in mouse embryonic fibroblast-conditioned medium (MEF-CM) as previously described (Tomishima, 2008). In preparation for differentiation, hESCs were passaged and seeded in a 48-well format. After seeding, cells were cultured for 2-3 days in MEF-CM, and were then subjected to a 4-stage differentiation protocol.

Differentiation of hESCs into 3D endoderm-derived tissues

In preparation for differentiation, hESCs were passaged and seeded in a 48-well format. After seeding, cells were cultured for 2-3 days in MEF-CM, and were then subjected to a 4-stage differentiation protocol. The basal media used in stage 1 consisted

of RPMI 1640 (ThermoFisher; 11875093), 1X non-essential amino acids, 1X GlutaMAX, and 0.05% BSA. In stage 1, hESCs were treated for 3 days with 100ng/ml Activin A (R&D Systems; 338-AC-010), with 25ng/ml WNT3a (R&D Systems; 5036-WN-010), which was supplemented with, 0.2% FBS on day 2, and 2% FBS on day 3. The basal media used in stage 2 and 3 consisted of DMEM/F12 (ThermoFisher; 11320033), 1X non-essential amino acids, 1X GlutaMAX, 0.05% BSA, 0.4μM monothioglycerol (Sigma; M6145), 1X N-2 supplement (ThermoFisher; 17502048), 1X B-27 supplement (ThermoFisher; 17504044), and 50μg/ml L-ascorbic acid. In stage 2, the media was supplemented for 2 days with 200ng/ml Noggin (Peprotech; 120-10C) and 10μM SB431542 (Tocris; 1614). In stage 3, the media was supplemented for 6 days with 100ng/ml WNT3a, 10ng/ml FGF10 (Peprotech; 100-26), 10ng/ml KGF (Peprotech; 100-19B), 10ng/ml BMP4 (Peprotech; 120-05), 20ng/ml EGF (Peprotech; AF-100-15), and 0.05μM all-trans retinoic acid (Sigma; R2625). Cells were washed once with DMEM/F12 between each differentiation stage. Monolayer cultures from stage 3 were collected as aggregates by mechanical scraping followed by gentle trituration. Aggregates were seeded within a 3D matrix of growth factor-reduced Matrigel (GFRM; Corning; #356231; Thick Gel Method, as per manufacturers instructions) diluted in a 1:1 ratio with 100μl MTEC media in a 24-well format. MTEC media (You et al., 2002), comprised DMEM/F12 with HEPES (ThermoFisher; 11330032), 1X non-essential amino acids, 1X GlutaMAX, 1X Insulin-Transferrin-Selenium (ThermoFisher; 51500056), 30μg/ml Bovine Pituitary Extract (ThermoFisher; 13028014), 5% FBS, 25ng/ml EGF, and 10nM all-trans retinoic acid. The 3D matrix was permitted to solidify at 37°C for 30 mins, and then covered with 500μl MTEC media. Cells were cultured at 37°C in a 5% CO_2/air

environment, and media was changed every 2 days. Endoderm-derived 3D tissues were typically cultured for 15-20 days.

Generation and culture of hEnS

At the end of stage 4, the gel matrix containing endoderm-derived 3D tissues was dissolved with Cell Recovery Solution (Corning; #354253) for 1 – 1.5 hours on ice. Tissues were washed twice with cold PBS, and dissociated into single cells using TrypLE (ThermoFisher). For ECADHERIN-based FACS, dissociated cells were diluted to 1-5 x 10^6 cells/ml in 1%BSA, 2mM EDTA in PBS, and incubated with mouse anti-ECAD PE (1:100; Santa Cruz; sc-21791 PE) for 1 hour on ice. Sorting was performed on BD FACSAria II, and data was analyzed using FACS DIVA (BD Biosciences). For generation of hEnS, ECAD+ cells were counted (typically 20-30k cells per well), mixed with an equal number of human lung fibroblast (HLF) support cells, and seeded within a 3D matrix (Thick Gel Method) in 75µl MTEC or intestinal media diluted 1:1 with GFRM (total volume 150µl) in a 48-well format. For different intestinal media formulations, the basal media and growth factor concentrations used were exactly as described in other studies (Sato et al., 2009, 2011). After allowing the gel mixture to solidify at 37°C for 30 mins, the gel was covered with 250µl culture media. Cells were cultured at 37°C in a 5% CO_2/air environment, and spheroid formation was observed as early as 5 days post-seeding. With media changes every 4 days, hEnS could be cultured up to 30 days within the same gel matrix without collapsing. For passaging of hEnS, the gel matrix was dissolved with Cell Recovery Solution, then hEnS were dissociated into single cells, counted and seeded as described.

Bacterial and lentiviral infection of hEnS

For infection of hEnS with bacterial cells and LPS, the day before infection, starter cultures of *E. coli* strains Nissile 1917 and O157:H7 were grown overnight in 5ml of LB media at 37°C with shaking. The next morning, bacterial cultures were diluted 1:100 in 3ml of LB and incubated for 3 hours as above to reach their exponential growth phase. The OD_{600} was adjusted to $1x10^8$ cfu/ml in antibiotic-free Advanced DMEM/F12 (ThermoFisher; 12634010). In parallel, hEnS were manually plucked out of their gel matrix and also collected in antibiotic-free Advanced DMEM/F12 in culture tubes with the final volume adjusted to about 500ul. hEnS in solution were treated with bacterial cells at an MOI of ~1:50, or 100ng/ml LPS (Sigma, L4391), and incubated for 4 hours at 37°C, 5% CO_2. Supernatant was collected and plated on MacConkey agar to confirm *E. coli* viability. hEnS were washed twice with cold PBS, allowed to settle each time and supernatant aspirated to remove bacteria in solution, then processed for RNA isolation using Trizol LS Reagent (ThermoFisher; 10296010).

For infection of hEnS with H2BGFP-FUCCI virus, hEnS were dissociated into single cells and passaged as described. The day after seeding cells, lentivirus titre was added to the culture media. The media was changed the next day, then 3 days were allowed for transgene integration and hEnS growth, following which 2µg/ml puromycin was supplemented for 10 days, added fresh every 2 days, for selection. For FACS by MKO2-Cdt1 expression, the gel matrix containing spheroids was dissolved, and tissues were dissociated into single cells as described. Cells were diluted in 1%BSA, 2mM

EDTA in PBS, and then sorting was performed on BD FACSAria III, with data analyzed using FACS DIVA (BD Biosciences).

Histological staining

Endoderm-derived tissues and hEnS were prepared for histological staining by making formalin-fixed, paraffin-embedded sections. Tissues were harvested from their gel matrix as described, washed twice with PBS, fixed for 1-2 hours at room temperature in 10% neutral-buffered formalin, and then washed again with PBS. Tissues were collected and embedded in HistoGel (ThermoFisher; HG-4000-012) as a plug, then transferred to histology cassettes. Cassettes were taken through an ethanol wash series of increasing concentration and xylene to dehydrate tissue, and then embedded in paraffin at 58°C. 5µm-thick sections were cut using a rotary microtome, floated in a 56°C water bath, mounted onto gelatin-coated histological slides and allowed to dry. H&E, AB/PAS and immunostaining were performed essentially as described in available protocols from R&D Systems for fluorescent and chromogenic staining of paraffin-embedded tissue sections. Antibody usage information is provided below.

RNA extraction and qRT-PCR

RNA from cultured samples was isolated using either Trizol LS Reagent or PicoPure RNA Isolation Kit (ThermoFisher; KIT0204). cDNA was made from total RNA using iScript cDNA Synthesis Kit (Bio-Rad; 1708891). Either SYBR Green-based detection using GoTaq qPCR Master Mix (Promega; A6001) for analysis of *SOX2* and *CDX2* expression, or FAM-based detection using PerfeCTa MultiPlex qPCR SuperMix

(Quanta BioSciences; 97065-230) and optimized probes from Universal Probe Library (Roche) for analysis of all other genes, with optimized primer pairs was used for qRT-PCR on a Bio-Rad CFX96. Values were normalized to *GAPDH* using the ΔCt method and to calculate fold-change relative to reference samples. Primer sequences are provided below. For generation of the clustergram, z-scores calculated from ΔCt values were used to create a heatmap in NetWalker, and non-supervised hierarchical clustering of heatmap samples was done using SABiosciences qPCR Array data analysis web portal: http://pcrdataanalysis.sabiosciences.com/pcr/arrayanalysis.php

Microarray and PCA

Microarray data was processed from CEL files using the *oligo* package from Bioconductor. Samples were batch corrected using the *limma* package method *removeBatchEffect*. Differential gene expression was calculated using linear models by the *limma* package. Ranked gene expression data was assessed by Gene Set Enrichment Analysis to identify enriched developmental and biological processes in the different samples. A custom gene set was developed using the EMAPA ontology to assess enrichment of gene sets annotated to different anatomical structures, combined with markers identifying specific intestinal lineages obtained from a dataset profiling single intestinal cell types (GSE62270). GSEA data files were processed in Cytoscape using the Enrichment Map plugin to develop network graphs of ontology term enrichments.

To compare our enterospheres (GSE89254) with other human major organ systems, we used two different array data sets GSE2361 and GSE30803. To merge the data sets collected on different platforms, we mapped all probe IDs to gene symbols and

merged redundant symbols by their mean signal. Data sets were then joined by gene symbol on rows and samples on columns. Data were all log2 transformed, normalized and batch corrected. To compare our enterospheres with other hPSC-derived intestinal organoids, we used data sets obtained from (https://github.com/hilldr/Finkbeiner_StemCellReports2015) and GSE56930. RNA-seq data was transformed into log2 counts per million expression values. Data sets were then merged similar to above on gene symbols. Data was normalized and batch corrected.

Heat maps and PCA and correlation plots were all generated from the top 10th centile of genes (1684 genes) filtered with a standard deviation filter. These highly variable genes should be enriched in information and enable separation of different cell types with out using a biased selection system. Heat maps were generated using the R package *pheatmap* using Euclidian distance metrics and complete clustering. PCA was performed and graphed using the R functions *prcomp* and *plot*. Correlation plots were generated using the R package *corrplot* with hierarchical clustering.

Image processing, data analysis and statistics

ImageJ was used for counting spheroids, diameter measurements and processing of histology staining montages. Whole-well phase images of spheroids were stitched together from individual fields using Grid/Collection Stitching plugin on ImageJ (Preibisch et al., 2009). Automated image analysis was performed using the CellProfiler software package. Graphs from quantitative data were created on GraphPad Prism 5, and significant differences in sample means were assessed using two-tailed unpaired t-test.

Antibody usage for IHC-P/IF and ICC/IF

Antibody/protein	Usage	Vendor	Catalog no.
IHC-P/IF			
ECAD	1:100	Santa Cruz	sc-21791
NCAD	1:500	Abcam	ab18203
αSMA	1:200	Abcam	ab5694
SHH	1:100	Santa Cruz	sc-1194
P63	1:100	Santa Cruz	sc-8431
NKX2.1	1:100	Santa Cruz	sc-13040
SOX2	1:400	BD	#561469
CDX2	1:800	Biogenex	CDX2-88
SOX9	1:500	Abcam	ab76997
VIL1	1:100	Santa Cruz	sc-7672
SI	1:100	Santa Cruz	sc-27603
MUC2	1:100	Santa Cruz	sc-15334
LYZ	1:100	Santa Cruz	sc-27956
P21	1:400	Cell Signaling	#2947
Non-phospho β-catenin	1:400	Cell Signaling	#8814
Ki67	1:400	Cell Signaling	#9449
ICC/IF			
SOX2	1:400	BD	#561469
FOXA2	1:200	Santa Cruz	sc-9187
NKX2.1	1:200	Santa Cruz	sc-13040
CDX2	1:1000	Biogenex	CDX2-88

Chromogenic IHC-P was performed by technical staff at the HRLMP in St. Joseph's Hospital (Hamilton, Ontario, Canada). Antibody information:

NKX2.1/TTF-1: Clone – 8G7G3/1; Isotype – IgG1, kappa
CDX2: Clone – DAK-CDX2; Isotype – IgG1, kappa
CK20: Clone – Ks20.8; Isotype – IgG2a, kappa

QRT-PCR primer sequences

Primer name / gene	Sequence (5' -> 3')
For use with GoTaq qPCR Master Mix	
SOX2-F	TACAGCATGTCCTACTCGCAG
SOX2-R	GAGGAAGAGGTAACCACAGGG
CDX2-F	TCCGTGTACACCACTCGATATT
CDX2-R	GGAACCTGTGCGAGTGGAT
GAPDH-F	GGTATCGTGGAAGGACTCATGAC

GAPDH-R		ATGCCAGTGAGCTTCCCGTTCAG
For use with PerfeCTa MultiPlex qPCR SuperMix and probes from UPL		
Primer name / gene	**Probe #**	**Sequence (5' -> 3')**
LGR5-F	78	accagactatgcctttggaaac
LGR5-R		ttcccagggagtggattctat
OLFM4-F	24	atcaaaacacccctgtcgtc
OLFM4-R		gctgatgttcaccacaccac
ASCL2-F	55	gcaccaacacttggagatttt
ASCL2-R		aatggattctctgtgcccttag
VIL1-F	87	ttgccacaattccctgagat
VIL1-R		cttggtcatggtgagtgagc
LYZ-F	68	ccgctactggtgtaatgatgg
LYZ-R		catcagcgatgttatcttgcag
MUC2-F	1	gctgctatgtcgaggacacc
MUC2-R		gggaggagttggtacacacg
GAPDH-F	60	agccacatcgctcagacac
GAPDH-R		gcccaatacgaccaaatcc
TNFα-F	29	cagcctcttctccttcctgat
TNFα-R		gccagagggctgattagaga
IL6-F	40	gatgagtacaaaagtcctgatcca
IL6-R		ctgcagccactggttctgt
IL8-F	72	gagcactccataaggcacaaa
IL8-R		atggttccttccggtggt
DEFB4A-F	35	tcagccatgagggtcttgta
DEFB4A-R		ggatcgcctataccaccaaa

ACCESSION NUMBERS

The NCBI GEO accession number for the microarray data reported in this paper is GEO: GSE89254.

AUTHOR CONTRIBUTIONS

R.R.N. and J.S.D. conceived and designed the study, prepared the figures, and wrote the manuscript. R.R.N., S.A., S.B. and J.L. performed experimental work. R.R.N.,

S.A., B.J.C. and J.S.D. analyzed the data. B.J.C. and M.G.S. gave conceptual advice. J.S.D. supervised the project.

ACKNOWLEDGEMENTS

This work was funded by Canadian Institutes of Health Research (#130499), Ontario Thoracic Society, and Canadian Cancer Society Research Institute (#703434) awards to JSD. B.J.C and J.S.D. are supported by Canada Research Chairs. We thank technicians Kennedy Makondo, Hong Liang and Zoya Shapovalova for FACS assistance. We are grateful to Dr Ivan Damjanov (University of Kansas), Drs. Jean-Claude Cutz and Dr. Brigitte Courteau (St. Joseph's Hospital, Hamilton) for histology analysis. We thank post-doctoral fellow Carlos Pilquil and research assistant Garrett Bullivant for intellectual contributions. We thank Victor Gordon, Nadeem Murtaza and Yu Tong Zhang for technical assistance.

REFERENCES

Albuquerque, C., Breukel, C., van der Luijt, R., Fidalgo, P., Lage, P., Slors, F.J.M., Leitão, C.N., Fodde, R., and Smits, R. (2002). The "just-right" signaling model: APC somatic mutations are selected based on a specific level of activation of the beta-catenin signaling cascade. Hum. Mol. Genet. *11*, 1549–1560.

Basak, O., van de Born, M., Korving, J., Beumer, J., van der Elst, S., van Es, J.H., and Clevers, H. (2014). Mapping early fate determination in Lgr5+ crypt stem cells using a novel Ki67-RFP allele. EMBO J. *33*, 2057–2068.

Baten, A., Sakamoto, K., and Shamsuddin, A.M. (1992). Long-term culture of normal human colonic epithelial cells in vitro. FASEB J. Off. Publ. Fed. Am. Soc. Exp. Biol. *6*, 2726–2734.

Beaulieu, J.F., Weiser, M.M., Herrera, L., and Quaroni, A. (1990). Detection and characterization of sucrase-isomaltase in adult human colon and in colonic polyps. Gastroenterology *98*, 1467–1477.

Cadigan, K.M., and Peifer, M. (2009). Wnt signaling from development to disease: insights from model systems. Cold Spring Harb. Perspect. Biol. *1*, a002881.

Calder, A., Roth-Albin, I., Bhatia, S., Pilquil, C., Lee, J.H., Bhatia, M., Levadoux-Martin, M., McNicol, J., Russell, J., Collins, T., et al. (2013). Lengthened G1 phase indicates differentiation status in human embryonic stem cells. Stem Cells Dev. *22*, 279–295.

D'Amour, K.A., Agulnick, A.D., Eliazer, S., Kelly, O.G., Kroon, E., and Baetge, E.E. (2005). Efficient differentiation of human embryonic stem cells to definitive endoderm. Nat. Biotechnol. *23*, 1534–1541.

van Es, J.H., van Gijn, M.E., Riccio, O., van den Born, M., Vooijs, M., Begthel, H., Cozijnsen, M., Robine, S., Winton, D.J., Radtke, F., et al. (2005). Notch/gamma-secretase inhibition turns proliferative cells in intestinal crypts and adenomas into goblet cells. Nature *435*, 959–963.

Fatehullah, A., Tan, S.H., and Barker, N. (2016). Organoids as an in vitro model of human development and disease. Nat. Cell Biol. *18*, 246–254.

Fevr, T., Robine, S., Louvard, D., and Huelsken, J. (2007). Wnt/beta-catenin is essential for intestinal homeostasis and maintenance of intestinal stem cells. Mol. Cell. Biol. *27*, 7551–7559.

Finkbeiner, S.R., Hill, D.R., Altheim, C.H., Dedhia, P.H., Taylor, M.J., Tsai, Y.-H., Chin, A.M., Mahe, M.M., Watson, C.L., Freeman, J.J., et al. (2015). Transcriptome-wide Analysis Reveals Hallmarks of Human Intestine Development and Maturation In Vitro and In Vivo. Stem Cell Rep. *4*, 1140–1155.

Forbester, J.L., Goulding, D., Vallier, L., Hannan, N., Hale, C., Pickard, D., Mukhopadhyay, S., and Dougan, G. (2015). Interaction of Salmonella enterica Serovar Typhimurium with Intestinal Organoids Derived from Human Induced Pluripotent Stem Cells. Infect. Immun. *83*, 2926–2934.

Fordham, R.P., Yui, S., Hannan, N.R.F., Soendergaard, C., Madgwick, A., Schweiger, P.J., Nielsen, O.H., Vallier, L., Pedersen, R.A., Nakamura, T., et al. (2013). Transplantation of expanded fetal intestinal progenitors contributes to colon regeneration after injury. Cell Stem Cell *13*, 734–744.

Forster, R., Chiba, K., Schaeffer, L., Regalado, S.G., Lai, C.S., Gao, Q., Kiani, S., Farin, H.F., Clevers, H., Cost, G.J., et al. (2014). Human Intestinal Tissue with Adult Stem Cell Properties Derived from Pluripotent Stem Cells. Stem Cell Rep. *2*, 838–852.

Gorvel, J.P., Ferrero, A., Chambraud, L., Rigal, A., Bonicel, J., and Maroux, S. (1991). Expression of sucrase-isomaltase and dipeptidylpeptidase IV in human small intestine and colon. Gastroenterology *101*, 618–625.

Green, M.D., Chen, A., Nostro, M.-C., d'Souza, S.L., Schaniel, C., Lemischka, I.R., Gouon-Evans, V., Keller, G., and Snoeck, H.-W. (2011). Generation of anterior foregut endoderm from human embryonic and induced pluripotent stem cells. Nat. Biotechnol. *29*, 267–272.

Grün, D., Lyubimova, A., Kester, L., Wiebrands, K., Basak, O., Sasaki, N., Clevers, H., and van Oudenaarden, A. (2015). Single-cell messenger RNA sequencing reveals rare intestinal cell types. Nature *525*, 251–255.

Güttsches, A.-K., Löseke, S., Zähringer, U., Sonnenborn, U., Enders, C., Gatermann, S., and Bufe, A. (2012). Anti-inflammatory modulation of immune response by probiotic Escherichia coli Nissle 1917 in human blood mononuclear cells. Innate Immun. *18*, 204–216.

Huch, M., and Koo, B.-K. (2015). Modeling mouse and human development using organoid cultures. Dev. Camb. Engl. *142*, 3113–3125.

Jumarie, C., and Malo, C. (1991). Caco-2 cells cultured in serum-free medium as a model for the study of enterocytic differentiation in vitro. J. Cell. Physiol. *149*, 24–33.

Krausova, M., and Korinek, V. (2014). Wnt signaling in adult intestinal stem cells and cancer. Cell. Signal. *26*, 570–579.

Lancaster, M.A., and Knoblich, J.A. (2014). Organogenesis in a dish: modeling development and disease using organoid technologies. Science *345*, 1247125.

Lindén, S.K., Florin, T.H.J., and McGuckin, M.A. (2008). Mucin Dynamics in Intestinal Bacterial Infection. PLOS ONE *3*, e3952.

Lundy, S.D., Zhu, W.-Z., Regnier, M., and Laflamme, M.A. (2013). Structural and functional maturation of cardiomyocytes derived from human pluripotent stem cells. Stem Cells Dev. *22*, 1991–2002.

McCracken, K.W., Catá, E.M., Crawford, C.M., Sinagoga, K.L., Schumacher, M., Rockich, B.E., Tsai, Y.-H., Mayhew, C.N., Spence, J.R., Zavros, Y., et al. (2014). Modelling human development and disease in pluripotent stem-cell-derived gastric organoids. Nature *516*, 400–404.

Moll, R., Schiller, D.L., and Franke, W.W. (1990). Identification of protein IT of the intestinal cytoskeleton as a novel type I cytokeratin with unusual properties and expression patterns. J. Cell Biol. *111*, 567–580.

Möndel, M., Schroeder, B.O., Zimmermann, K., Huber, H., Nuding, S., Beisner, J., Fellermann, K., Stange, E.F., and Wehkamp, J. (2009). Probiotic E. coli treatment mediates antimicrobial human beta-defensin synthesis and fecal excretion in humans. Mucosal Immunol. *2*, 166–172.

Moskaluk, C.A., Zhang, H., Powell, S.M., Cerilli, L.A., Hampton, G.M., and Frierson, H.F. (2003). Cdx2 protein expression in normal and malignant human tissues: an immunohistochemical survey using tissue microarrays. Mod. Pathol. Off. J. U. S. Can. Acad. Pathol. Inc *16*, 913–919.

Murry, C.E., and Keller, G. (2008). Differentiation of Embryonic Stem Cells to Clinically Relevant Populations: Lessons from Embryonic Development. Cell *132*, 661–680.

Mustata, R.C., Vasile, G., Fernandez-Vallone, V., Strollo, S., Lefort, A., Libert, F., Monteyne, D., Pérez-Morga, D., Vassart, G., and Garcia, M.-I. (2013). Identification of Lgr5-independent spheroid-generating progenitors of the mouse fetal intestinal epithelium. Cell Rep. *5*, 421–432.

Nadkarni, R.R., Abed, S., and Draper, J.S. (2015). Organoids as a model system for studying human lung development and disease. Biochem. Biophys. Res. Commun.

Nicholas, C.R., Chen, J., Tang, Y., Southwell, D.G., Chalmers, N., Vogt, D., Arnold, C.M., Chen, Y.-J.J., Stanley, E.G., Elefanty, A.G., et al. (2013). Functional maturation of hPSC-derived forebrain interneurons requires an extended timeline and mimics human neural development. Cell Stem Cell *12*, 573–586.

Preibisch, S., Saalfeld, S., and Tomancak, P. (2009). Globally optimal stitching of tiled 3D microscopic image acquisitions. Bioinformatics *25*, 1463–1465.

Sakaue-Sawano, A., Kurokawa, H., Morimura, T., Hanyu, A., Hama, H., Osawa, H., Kashiwagi, S., Fukami, K., Miyata, T., Miyoshi, H., et al. (2008). Visualizing spatiotemporal dynamics of multicellular cell-cycle progression. Cell *132*, 487–498.

Sato, T., Vries, R.G., Snippert, H.J., van de Wetering, M., Barker, N., Stange, D.E., van Es, J.H., Abo, A., Kujala, P., Peters, P.J., et al. (2009). Single Lgr5 stem cells build crypt-villus structures in vitro without a mesenchymal niche. Nature *459*, 262–265.

Sato, T., Stange, D.E., Ferrante, M., Vries, R.G.J., Van Es, J.H., Van den Brink, S., Van Houdt, W.J., Pronk, A., Van Gorp, J., Siersema, P.D., et al. (2011). Long-term expansion of epithelial organoids from human colon, adenoma, adenocarcinoma, and Barrett's epithelium. Gastroenterology *141*, 1762–1772.

Silberg, D.G., Swain, G.P., Suh, E.R., and Traber, P.G. (2000). Cdx1 and cdx2 expression during intestinal development. Gastroenterology *119*, 961–971.

Spence, J.R., Mayhew, C.N., Rankin, S.A., Kuhar, M., Vallance, J.E., Tolle, K., Hoskins, E.E., Kalinichenko, V.V., Wells, S.I., Zorn, A.M., et al. (2011). Directed differentiation of human pluripotent stem cells into intestinal tissue in vitro. Nature *470*, 105–109.

Stelzner, M., Helmrath, M., Dunn, J.C.Y., Henning, S.J., Houchen, C.W., Kuo, C., Lynch, J., Li, L., Magness, S.T., Martin, M.G., et al. (2012). A nomenclature for intestinal in vitro cultures. Am. J. Physiol. Gastrointest. Liver Physiol. *302*, G1359–G1363.

Takenaka, T., Harada, N., Kuze, J., Chiba, M., Iwao, T., and Matsunaga, T. (2014). Human small intestinal epithelial cells differentiated from adult intestinal stem cells as a novel system for predicting oral drug absorption in humans. Drug Metab. Dispos. Biol. Fate Chem. *42*, 1947–1954.

Tomishima, M. (2008). Conditioning pluripotent stem cell media with mouse embryonic fibroblasts (MEF-CM). In StemBook, (Cambridge (MA): Harvard Stem Cell Institute),.

Vora, P., Youdim, A., Thomas, L.S., Fukata, M., Tesfay, S.Y., Lukasek, K., Michelsen, K.S., Wada, A., Hirayama, T., Arditi, M., et al. (2004). Beta-defensin-2 expression is regulated by TLR signaling in intestinal epithelial cells. J. Immunol. Baltim. Md 1950 *173*, 5398–5405.

Watanabe, K., Ueno, M., Kamiya, D., Nishiyama, A., Matsumura, M., Wataya, T., Takahashi, J.B., Nishikawa, S., Nishikawa, S., Muguruma, K., et al. (2007). A ROCK inhibitor permits survival of dissociated human embryonic stem cells. Nat. Biotechnol. *25*, 681–686.

Watson, C.L., Mahe, M.M., Múnera, J., Howell, J.C., Sundaram, N., Poling, H.M., Schweitzer, J.I., Vallance, J.E., Mayhew, C.N., Sun, Y., et al. (2014). An in vivo model of human small intestine using pluripotent stem cells. Nat. Med. *20*, 1310–1314.

Xue, Y., Zhang, H., Wang, H., Hu, J., Du, M., and Zhu, M.-J. (2014). Host inflammatory response inhibits Escherichia coli O157:H7 adhesion to gut epithelium through augmentation of mucin expression. Infect. Immun. *82*, 1921–1930.

Yang, X., Pabon, L., and Murry, C.E. (2014). Engineering adolescence: maturation of human pluripotent stem cell-derived cardiomyocytes. Circ. Res. *114*, 511–523.

Yost, C., Torres, M., Miller, J.R., Huang, E., Kimelman, D., and Moon, R.T. (1996). The axis-inducing activity, stability, and subcellular distribution of beta-catenin is regulated in Xenopus embryos by glycogen synthase kinase 3. Genes Dev. *10*, 1443–1454.

You, Y., Richer, E.J., Huang, T., and Brody, S.L. (2002). Growth and differentiation of mouse tracheal epithelial cells: selection of a proliferative population. Am. J. Physiol. Lung Cell. Mol. Physiol. *283*, L1315–L1321.

Zhang, J., Wilson, G.F., Soerens, A.G., Koonce, C.H., Yu, J., Palecek, S.P., Thomson, J.A., and Kamp, T.J. (2009). Functional cardiomyocytes derived from human induced pluripotent stem cells. Circ. Res. *104*, e30–e41.

Zhu, Z., and Huangfu, D. (2013). Human pluripotent stem cells: an emerging model in developmental biology. Dev. Camb. Engl. *140*, 705–717.

Zorn, A.M., and Wells, J.M. (2009). Vertebrate endoderm development and organ formation. Annu. Rev. Cell Dev. Biol. *25*, 221–251.

FIGURE LEGENDS

Figure 1 – Generation of endoderm-derived tissues from hESCs in vitro. **A)** Schematic of *in vitro* stepwise differentiation scheme into endoderm-derived tissues. **B)** Emergence of budding structures in the stage-4 3D conditions at day 7. **C)** Budding structures develop into complex organoids by day 10. Images in panels B and C are of structures made from H1 hESCs. **D)** Haematoxylin and eosin (H&E) staining of 3D tissues showed organized tubular epithelia surrounded by cells with mesenchymal properties. Image shown is of H9 hESC-derived tissue. **E)** Immunofluorescence (IF) staining of H1 and H9 hESC-derived 3D tissues shows that tubular structures express epithelial markers ECAD and K18, while subset of surrounding cells express mesenchymal marker αSMA. Expression of CDX2, an intestinal epithelial marker, and early lung epithelial markers NKX2.1 and SOX2 are evident. Scale bars (**A**), 200μm; (**B, E**), 50μm; (**C**)**,** 250μm; (**D**), 100μm. See also Figure S1 and Movie S1.

Figure 2 – Generation of spheroids from purified epithelial progenitors in endoderm-derived tissues. **A)** Schematic of spheroids generation *in vitro*. **B)** Number of spheroids produced from ECAD+ and ECAD- cells with or without supporting cell types HLFs and HUVECs (mean ± SEM, n = 8 and n = 2 independent experiments for HLFs and HUVECs, respectively). **C)** Whole-well scan of d18 spheroids derived from ECAD+ cells with HLFs in MTEC media. **D)** Comparison of spheroid diameter growth between HLF- and HUVEC-assisted spheroids (mean ± SEM, n ≥ 12 individual spheroids tracked). All data shown in Figure 2 is for spheroids derived from H1 hESCs. Scale bars (**C**), 1mm; (**C inlet**), 500μm. See also Figure S2.

Figure 3 – Spheroids express markers of intestinal epithelial cell types and are similar in transcriptome to primary intestinal organoids. **A)** Representative immunohistochemical staining of spheroids and human adult intestine for CDX2 and CK20. **B)** Proportion of spheroids expressing CDX2 and CK20; numbers at the bottom of each bar denote total number of spheres counted. **C)** Relative transcript expression levels of markers of lung, stomach and intestine for ECAD+ cells relative to ECAD- cells (n = 3 biological replicates, 1 from H1 hESCs and 2 from H9 hESCs). **D)** Relative transcript expression levels of markers of lung, stomach and intestine for spheroids relative to ECAD+ cells. **E)** Relative transcript expression levels of markers of intestinal epithelial cell types for spheroids relative to ECAD+ cells. Data in panels D and E is for spheroids derived from H1 hESCs. **F)** Representative IF staining of spheroids and human fetal small intestine shows expression of brush border markers VIL1 and SI. **G)** Correlation plot contrasting the gene expression profile of H1 hESC-derived spheroids with human adult organs. **H)** Gene expression clustergram comparing H1 hESC-derived spheroids with other hPSC-derived intestinal organoids and human fetal and adult intestinal tissues. Scale bars (**A**), 100μm; (**F**), 50μm. See also Figure S3.

Figure 4 – Comparison of hEnS phenotypes produced in different media conditions. **A)** Comparison of number (mean ± SEM, n ≥ 3 independent experiments) and **B)** diameter of hEnS produced in different media conditions (mean ± SEM, n ≥ 40 spheroids spanning 3 independent experiments, ***p < 0.0001). **C)** Proportion of hEnS expressing CDX2, CK20 and Ki67; numbers at the bottom of each bar denote total number of spheres counted. **D)** Representative Alcian Blue and Periodic acid-Schiff (AB-PAS) staining of hEnS; most prevalent phenotype displayed for each media condition. **E)** Proportion of phenotypes identified by AB-PAS staining per tissue section; numbers at the bottom of each bar denote total number of spheres counted in sections. **F)** Number of secondary spheroids produced relative to primary for corresponding media condition (mean ± SEM, n = 3 independent experiments, *p = 0.0142, **p < 0.01, ***p < 0.0001). **G)** Representative IF staining for LYZ and MUC2 of hEnS in different media conditions and human fetal small intestine. All data shown in Figure 4 is for hEnS derived from H1 hESCs. Scale bars (**D**), 100μm; (**G**), 50μm. See also Figure S4.

Figure 5 – Long-term culture requirements of hEnS in specific media conditions and their phenotypic properties. **A)** Comparison of the proportion of hEnS expressing CDX2, CK20 and Ki67 in WENR and WENRg+Nic media; numbers at the bottom of each bar denote total number of spheres counted. **B)** Representative AB-PAS staining of complex budding structures produced in WENRg+Nic. **C)** Number of secondary spheroids produced relative to primary in WENR and WENRg+Nic (mean ± SEM, n = 3 independent experiments, *p = 0.0142, ***p = 0.0008). **D)** Number of hEnS produced upon passaging in WENRg+Nic, WENR and basal media with or without support cells (mean ± SEM, n = 3 independent experiments, ***p < 0.0001). **E)** Comparison of the relative number of hEnS produced in WENRg+Nic and WENRg+Nic+A83+SB2 media (mean ± SEM, n = 3 independent experiments, ***p = 0.0001). **F)** Number of secondary spheroids produced relative to primary in WENRg+Nic+A83+SB2 (mean ± SEM, n = 3 independent experiments, ***p < 0.0001). **G)** Relative number of hEnS produced upon addition or removal of key growth factors or support cells in a WENR media background (mean ± SEM, n = 3 independent experiments, *p < 0.05, ***p < 0.0001). **H)** Clustergram of intestinal gene expression grouped by type of media condition used to culture hEnS. Non-supervised hierarchical clustering was used to display common gene expression on a heat map; normalized to *GAPDH* expression (z-scores calculated from $2^{-\Delta Ct}$ values; n = 2 biological replicates from independent experiments). **I)** Nuclear intensity of NP-β-Catenin and **J)** Ki67 staining in hEnS cells from different media conditions (mean ± SEM, n ≥ 120 cells analyzed per condition). **K)** Representative IF staining for NP-β-Catenin and Ki67 in hEnS in different media conditions as well as human fetal small intestine. White boxes indicate zoomed-in regions. Dashed yellow and red borders indicate absence and presence, respectively, of nuclear NP-β-catenin staining. All data shown in Figure 5 is for hEnS derived from H1 hESCs. Scale bars (**B**), 100μm; (**K**), 50μm. See also Figure S5.

Figure 6 – Genetic modification and functional interrogation of hEnS. **A)** Schematic of infection of hEnS precursor cells with FUCCI lentivirus, and H2B-GFP photograph

showing pure population of FUCCI-expressing hEnS achieved after antibiotic selection and propagation. **B)** Live fluorescence imaging shows that FUCCI-infected hEnS ubiquitously express H2B-GFP, and cells in G1 phase express CTD1-MK02. **C)** Relative number of hEnS propagated from sorted MKO2+, MKO2- and unsorted hEnS cells at the same seeding density (mean ± SEM, n = 3 independent wells of an experiment). **D)** Schematic of bacterial infection of hEnS. **E)** Representative gram staining of uninfected and *E. coli* O157-infected hEnS; red arrows point to areas of bacterial infiltration. **F)** Relative transcript expression levels of *CDX2, MUC2, DEFB4A, TNF, IL6* and *IL8* in hEnS treated with LPS or bacteria; normalized to *GAPDH* expression (values represent linear fold change; n = 2 independent experiments). All data shown in Figure 6 is for hEnS derived from H1 hESCs. Scale bars (**B** top, **E**), 50μm; (**B** bottom), 100μm; (**E** right), 10μm.

Figure S1 – Differentiation of hESCs into endoderm lineages in 2D culture. Related to Figure 1. **A)** Schematic of protocol for *in vitro* differentiation that resulted in foregut and mid/hindgut lineages. **B)** IF staining of stage 3 cells reveals distinct NKX2.1+ domains surrounded by CDX2+ cells. **C)** Phase image of stage 3 cells showing NKX2.1+ domains and surrounding cells. **D)** IF staining of stage 2 cells shows SOX2+FOXA2+ domains and absence of CDX2 expression. **E)** Time-lapse imaging from stage 2 to stage 3 reveals that NKX2.1+domains arise from the SOX2+ domains, whereas CDX2 expression emerges in surrounding cells. **F)** Relative transcript levels of *SOX2* (left) and *CDX2* (right) in cells at each stage of the differentiation protocol; normalized to *GAPDH* expression (values represent linear fold change; n = 2 biological replicates from independent wells of multiple differentiations). All data shown in Figure S1 is for cells derived from H1 hESCs. Scale bars, 500 μm (**B**), 100 μm (**B** inlet), 200 μm (**C**), 150 μm (**D** top), and 300 μm (**D** bottom and **E**).

Figure S2 – Characterization of endoderm-derived tissues made in 3D conditions. Related to Figure 2. **A)** Number of 3D structures produced by input cells (mean ± SEM, n ≥ 3 independent wells of an experiment). **B)** Number of 3D structures produced per well from stage 3 clumps derived from H1 and H9 wt hESCs (mean ± SEM, n = 12 independent wells of an experiment). **C)** Upon separation by micro-dissection of epithelial and mesenchymal components from stage 4 tissues, re-culturing components alone or together shows that epithelium survives and grows in the presence of mesenchyme, but collapses when cultured alone; red arrows point to budding regions in epithelium. **D)** Schematic of FACS-based isolation of ECAD+ and ECAD- cells from endoderm-derived tissues (top), and representative FACS plot of cell separation by ECAD expression (bottom). Scale bar, 300 μm (**C**).

Figure S3 – Characterization and gene expression analysis of spheroids and ECAD+ precursor cells. Related to Figure 3. **A)** Immunohistochemistry of spheroids for lung marker NKX2.1 shows lack of positive staining; adult human lung used as control. **B)** IF staining of spheroids shows co-expression of CDX2 and intestinal crypt marker SOX9.

C) Number (mean ± SEM, n ≥ 2 independent wells of an experiment) and **D)** diameter (mean ± SEM, n ≥ 18 spheroids spanning 3 independent wells of an experiment) of spheroids produced in MTEC media upon depletion or supplementation of factors. **E)** PCA plot of undifferentiated hESCs and hESC-derived samples shows large variation among phenotypes; microarray data is from GSE89254. **F)** Network diagram of EMAPA showing upregulated (red) and depleted (blue) terms for ECAD+ cells relative to ECAD- cells, and **G)** spheroids relative to ECAD+ cells. Scale bars, 100 μm (**A**) and 50 μm (**B**).

Figure S4 – Generation of hEnS populations in different media conditions. Related to Figure 4. **A)** Whole-well scans; MTEC panel re-used from Figure 2C. **B)** Representative phase image of a spheroid (top) and budding structure (bottom). All images shown in Figure S4 are of hEnS derived from H1 hESCs. Scale bars, 1 mm (**A**) and 300 μm (**B**).

Figure S5 – Characterization of hEnS phenotypes observed in WENRg+Nic and WENRg+Nic+A83+SB2 media. Related to Figure 5. **A)** Comparison of number (mean ± SEM, n = 3 independent experiments) and **B)** diameter of hEnS produced in different media conditions (mean ± SEM, n ≥ 40 spheroids spanning 3 independent experiments, ***p < 0.0001). **C)** Representative IF staining for SOX9 in budding structures in WENRg+Nic. **D)** Proportion of phenotypes identified by AB-PAS staining per tissue section; numbers at the bottom of each bar denote total number of spheres in sections. **E)** Immunohistochemistry of spheroids and budding structures in WENR and WENRg+Nic, respectively, for CDX2 and CK20. **F)** Representative IF staining for P21 and Ki67 of hEnS in various media conditions as well as human small intestine. **G)** Comparison of number (mean ± SEM, n = 3 independent wells of an experiment) and **H)** diameter between hEnS grown in the presence of HLFs and HDFs in WENRg+Nic media (mean ± SEM, n = 37 spheroids spanning 3 independent wells of an experiment). **I)** Representative AB-PAS staining of budding structure (left) and whole-well scan of population (right) in WENRg+Nic+A83+SB2. **J)** Proportion of structures in WENRg+Nic+A83+SB2 expressing CDX2 or Ki67 per tissue section; numbers at the bottom of each bar denote total number of structures counted. **K)** Relative number of structures produced when hEnS grown in WENRg+Nic are passaged into WENRg+Nic+A83+SB2 media (mean ± SEM, n = 3 independent wells of an experiment). **L)** Representative IF staining for Ki67 (left) and CDX2 (right) in budding structures in WENRg+Nic+A83+SB2. All data shown in Figure S5 is for hEnS derived from H1 hESCs. Scale bars, 100 μm (**C**, **E**, and **L**), 50 μm (**F** and **I** left), and 500 μm (**I** right).

Movie S1 – Self-organization of stage 3 cells into epithelial buds in stage 4 3D Matrigel-based culture conditions. Related to Figure 1. Images were taken every 6 hours for a total of 8 days. Acquired using a Nikon BioStation CT. Scale bar, 100 μm.

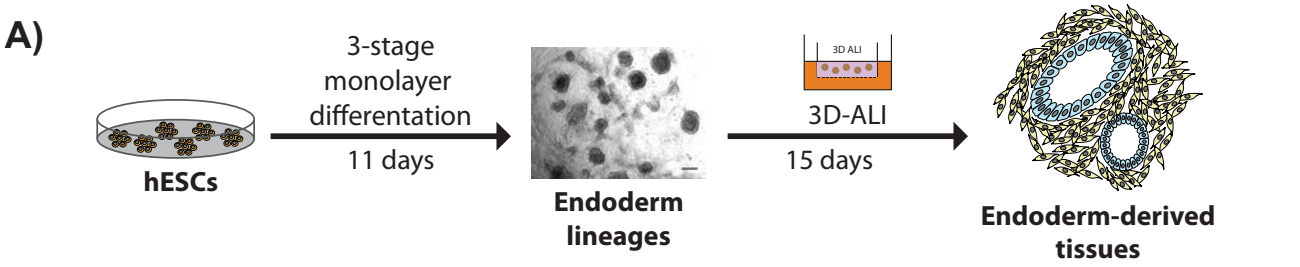
A)
hESCs
3-stage
monolayer
differentation
11 days
Endoderm
lineages
3D ALI
3D-ALI
15 days
Endoderm-derived
tissues

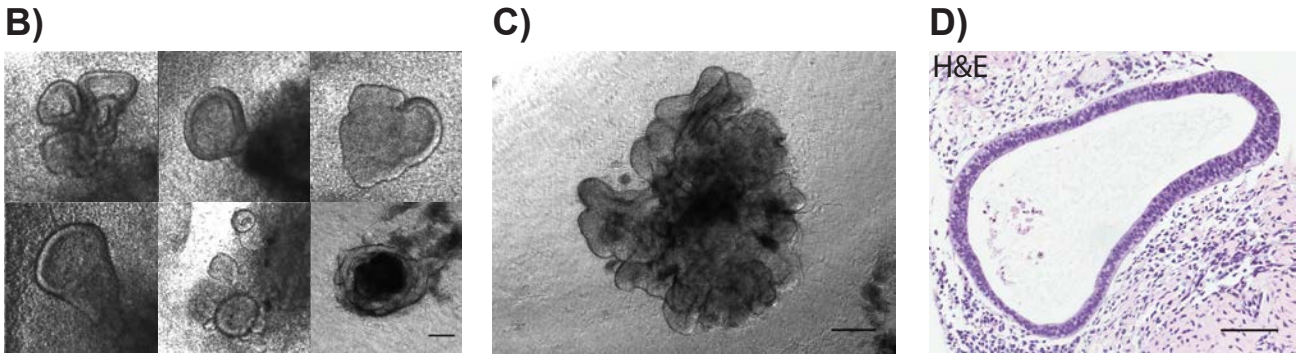
B)
C)
D)
H&E

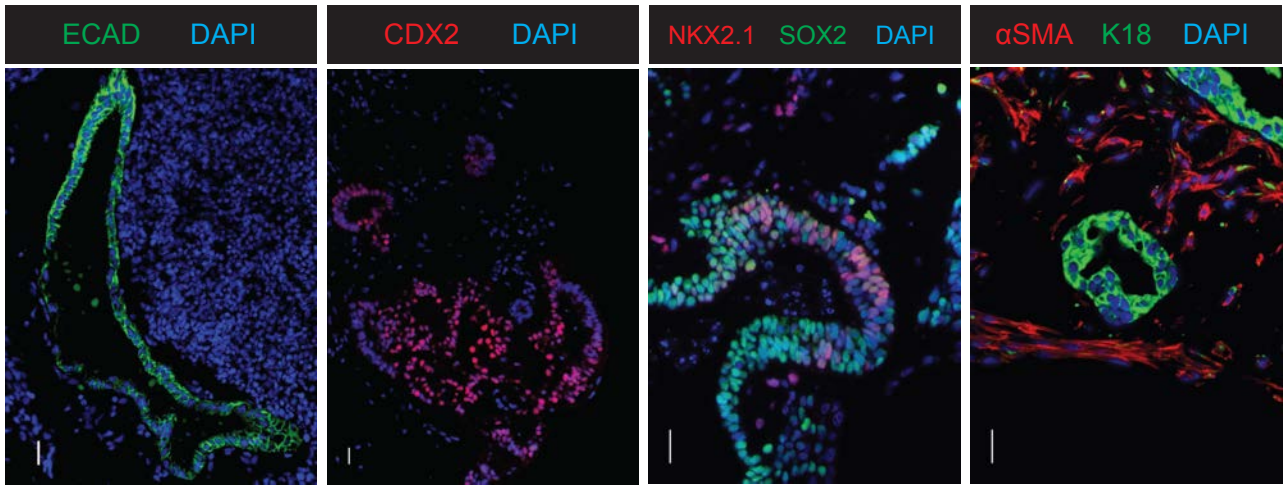
E)
ECAD DAPI
CDX2 DAPI
NKX2.1 SOX2 DAPI
αSMA K18 DAPI

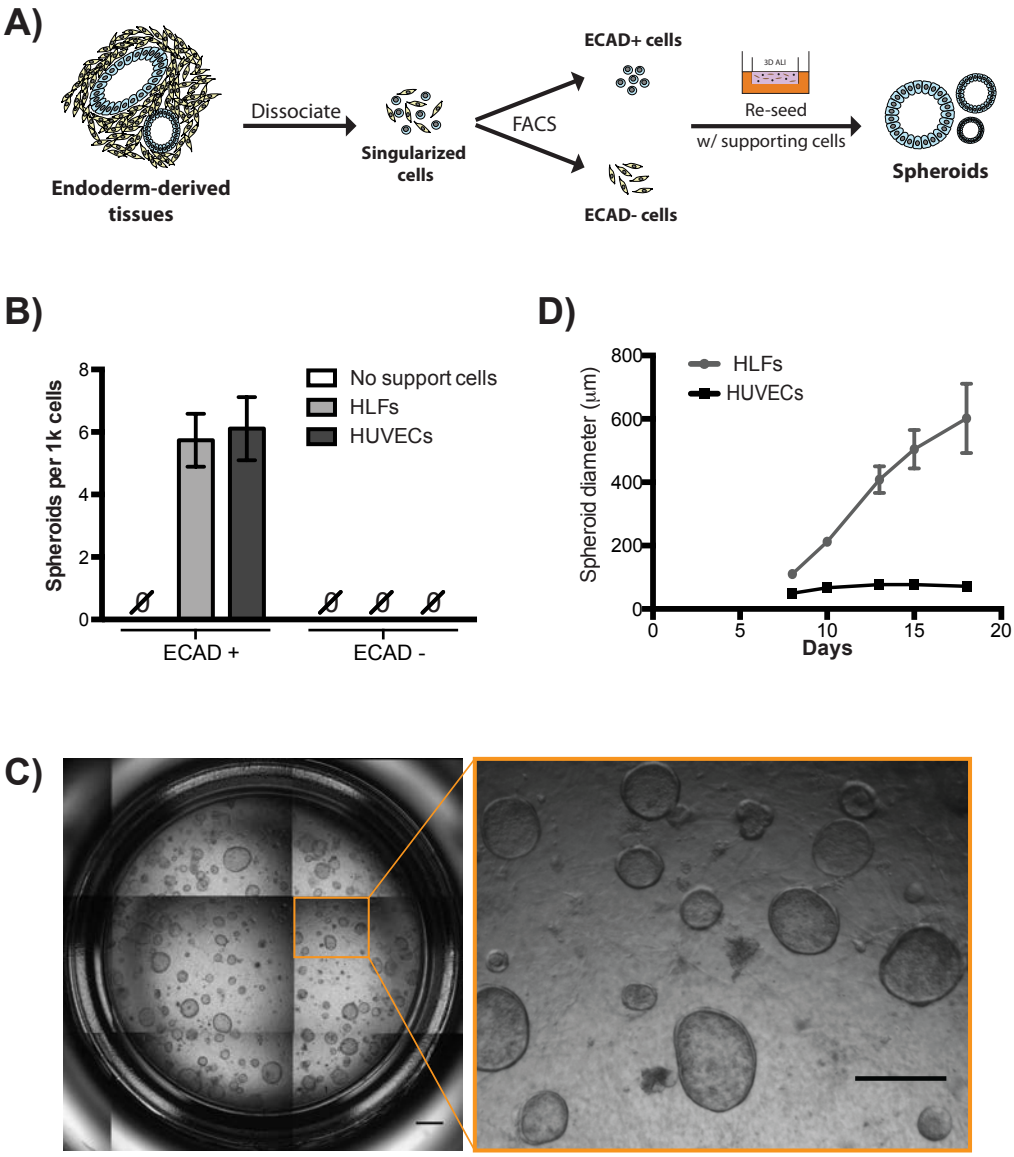
A)
Endoderm-derived tissues
Dissociate
Singularized cells
FACS
ECAD+ cells
ECAD- cells
Re-seed
w/ supporting cells
Spheroids
B)
Spheroids per 1k cells
No support cells
HLFs
HUVECs
ECAD +
ECAD -
D)
Spheroid diameter (µm)
HLFs
HUVECs
Days
C)

Figure 3

Nadkarni et al

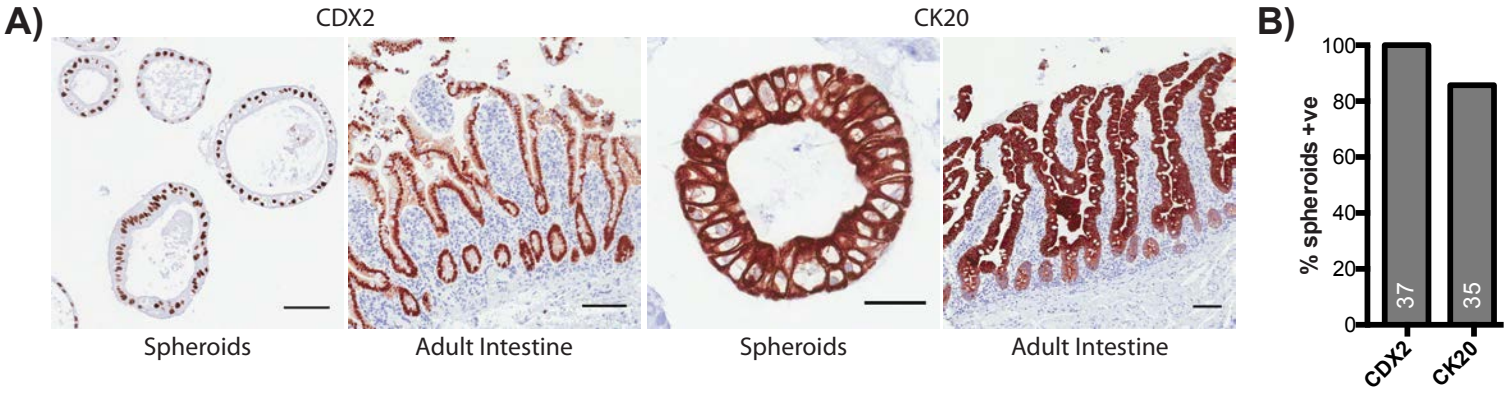

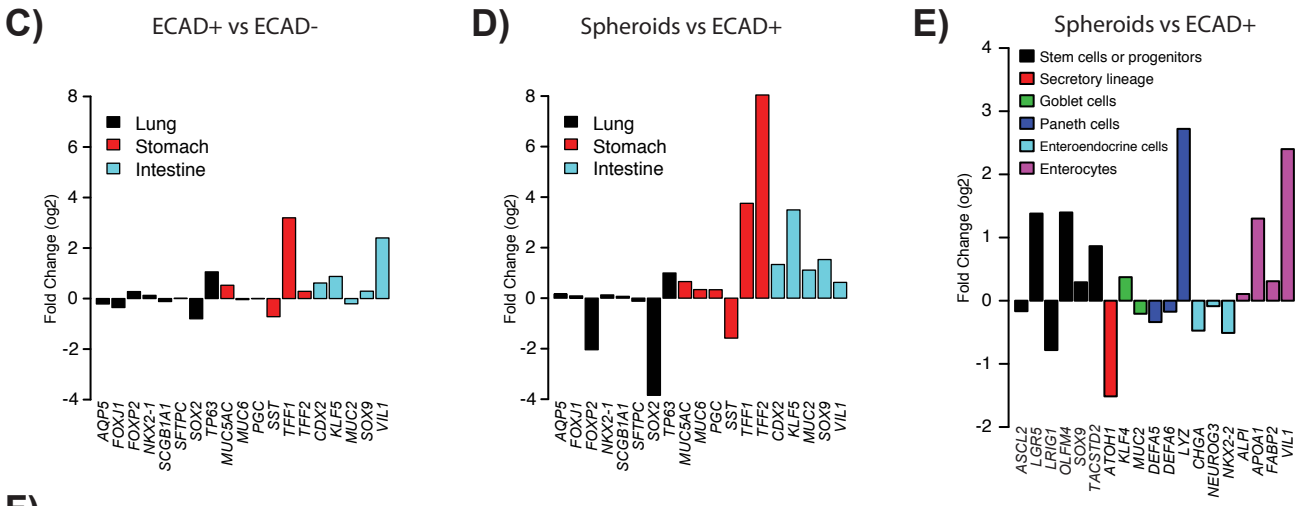

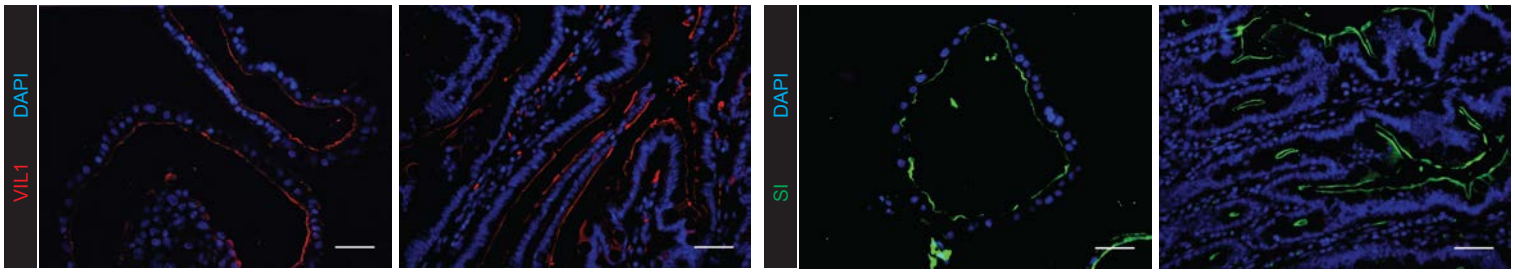

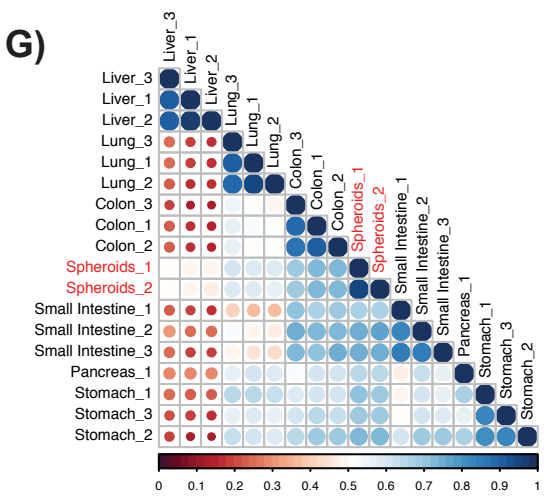

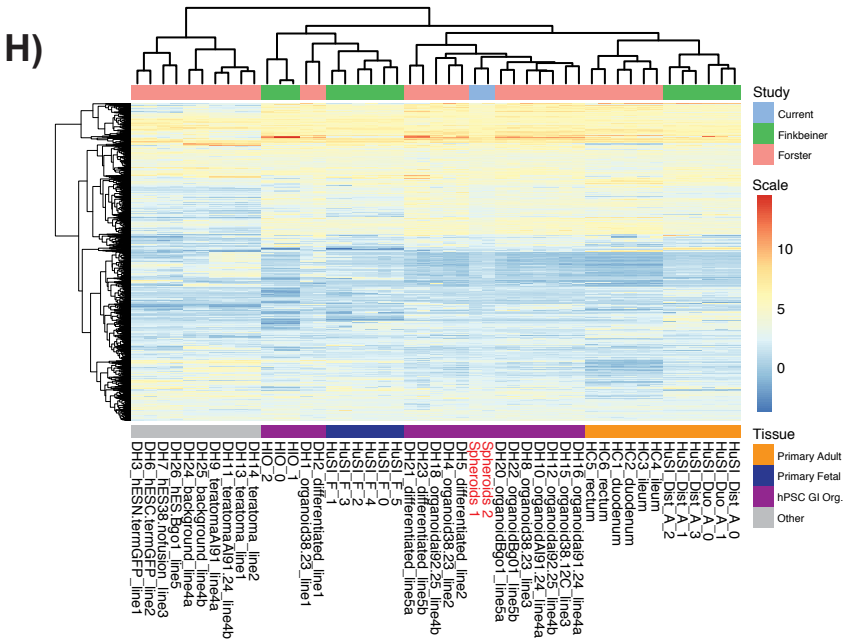

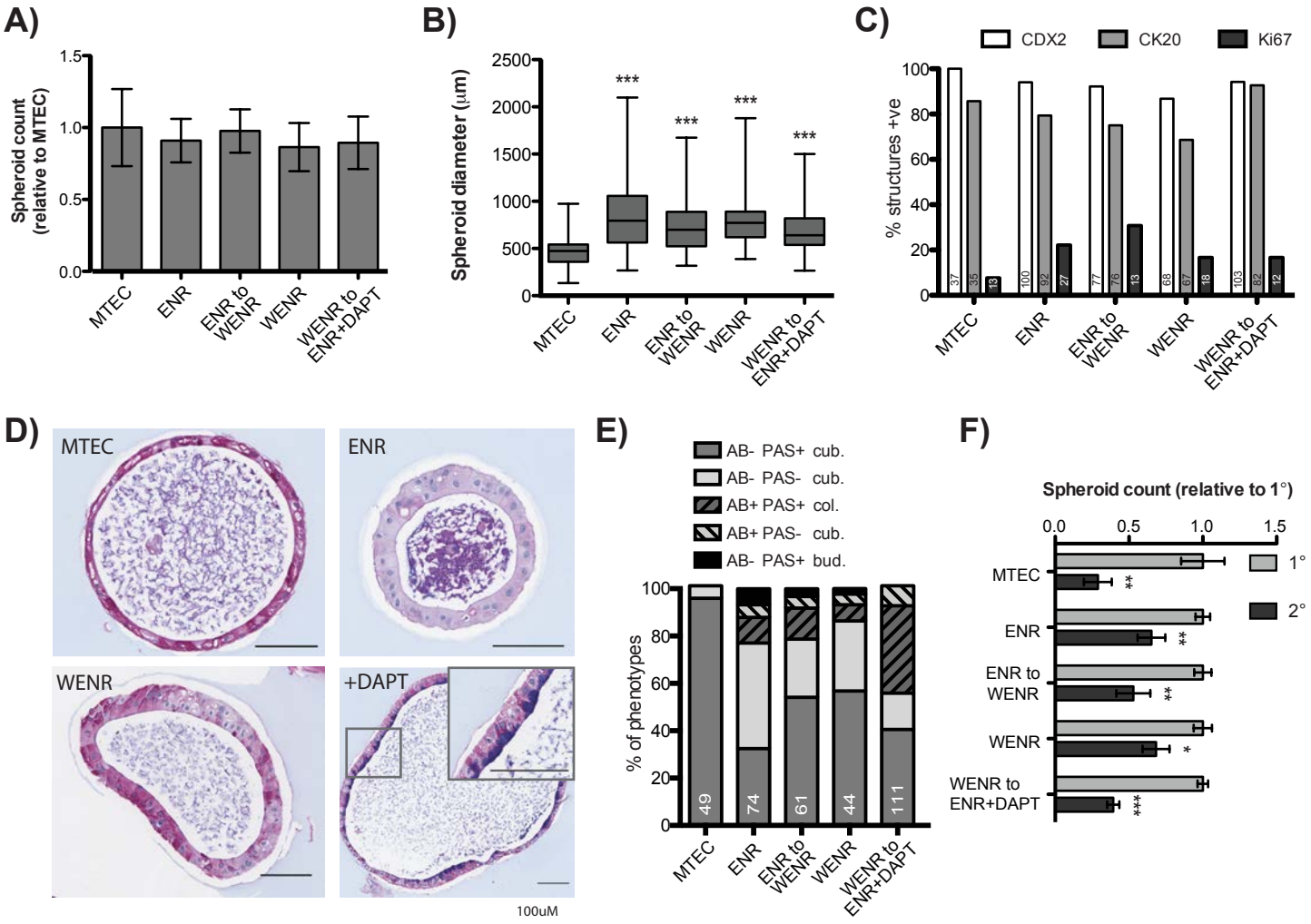
A)
Spheroid count (relative to MTEC)
1.5
1.0
0.5
0.0
MTEC
ENR
ENR to WENR
WENR
WENR to ENR+DAPT
B)
Spheroid diameter (μm)
2500
2000
1500
1000
500
0
***
***
***
***
MTEC
ENR
ENR to WENR
WENR
WENR to ENR+DAPT
C)
CDX2
CK20
Ki67
% structures +ve
100
80
60
40
20
0
37
35
13
100
92
27
77
76
13
68
67
18
103
82
12
MTEC
ENR
ENR to WENR
WENR
WENR to ENR+DAPT
D)
MTEC
ENR
WENR
+DAPT
100uM
E)
AB- PAS+ cub.
AB- PAS- cub.
AB+ PAS+ col.
AB+ PAS- cub.
AB- PAS+ bud.
% of phenotypes
100
80
60
40
20
0
49
74
61
44
111
MTEC
ENR
ENR to WENR
WENR
WENR to ENR+DAPT
F)
Spheroid count (relative to 1°)
0.0
0.5
1.0
1.5
1°
2°
MTEC
ENR
ENR to WENR
WENR
WENR to ENR+DAPT
**
**
**
*
***
G)
MTEC
WENR
ENR+DAPT
Human fetal intestine
MUC2
LYZ
DAPI

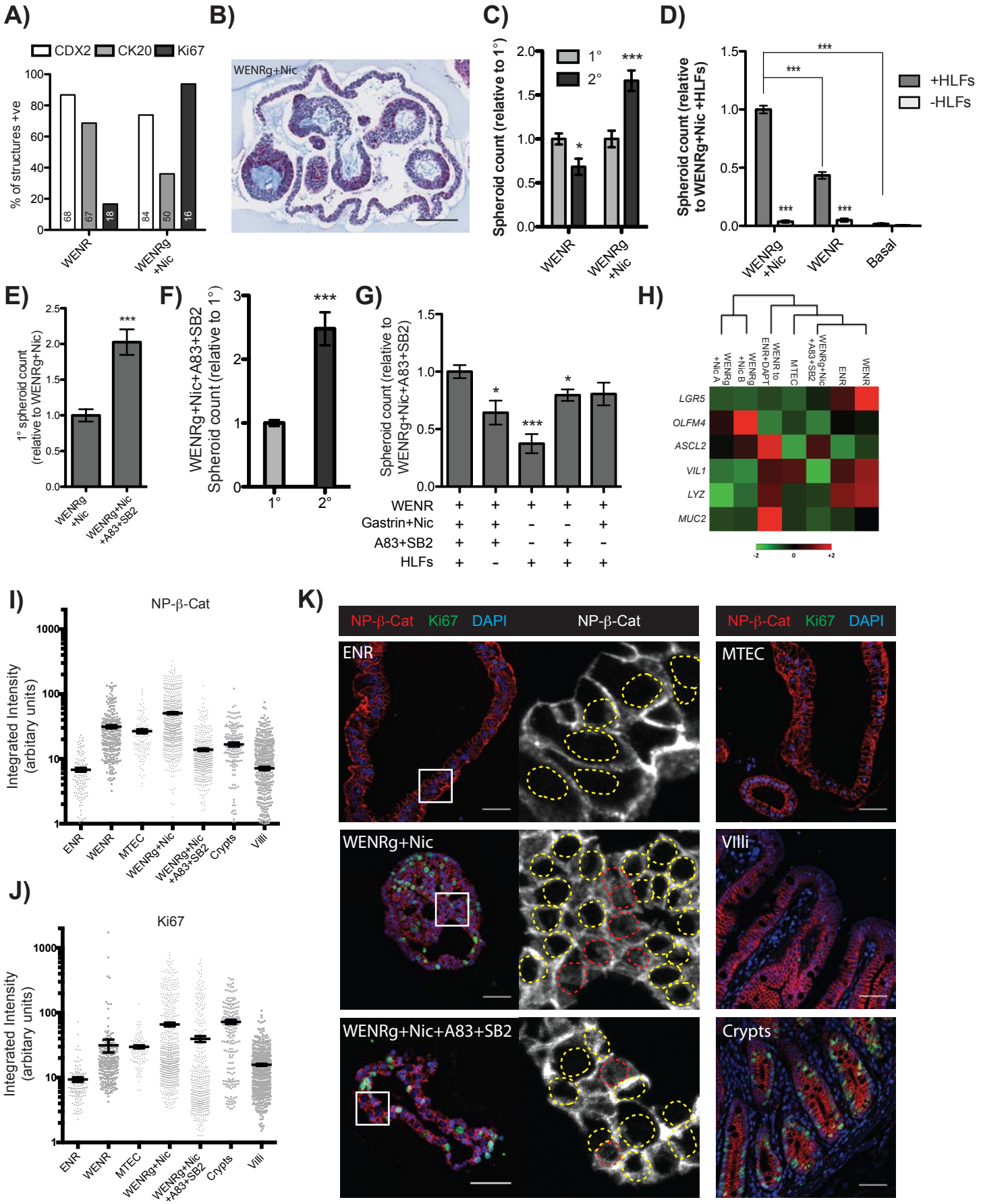
A)
CDX2
CK20
Ki67
% of structures +ve
68
67
18
84
50
16
WENR
WENRg +Nic
B)
WENRg+Nic
C)
1°
2°
Spheroid count (relative to 1°)
WENR
WENRg +Nic
D)
+HLFs
-HLFs
Spheroid count (relative to WENRg+Nic +HLFs)
WENRg +Nic
WENR
Basal
E)
1° spheroid count (relative to WENRg+Nic)
WENRg +Nic
WENRg+Nic +A83+SB2
F)
WENRg+Nic+A83+SB2 Spheroid count (relative to 1°)
1°
2°
G)
Spheroid count (relative to WENRg+Nic+A83+SB2)
WENR
Gastrin+Nic
A83+SB2
HLFs
H)
WENRg +Nic A
WENRg +Nic B
WENR to ENR+DAPT
MTEC
WENRg+Nic +A83+SB2
ENR
WENR
LGR5
OLFM4
ASCL2
VIL1
LYZ
MUC2
I)
NP-β-Cat
Integrated Intensity (arbitary units)
ENR
WENR
MTEC
WENRg+Nic
WENRg+Nic +A83+SB2
Crypts
Villi
J)
Ki67
Integrated Intensity (arbitary units)
ENR
WENR
MTEC
WENRg+Nic
WENRg+Nic +A83+SB2
Crypts
Villi
K)
NP-β-Cat Ki67 DAPI
NP-β-Cat
ENR
MTEC
WENRg+Nic
Villi
WENRg+Nic+A83+SB2
Crypts

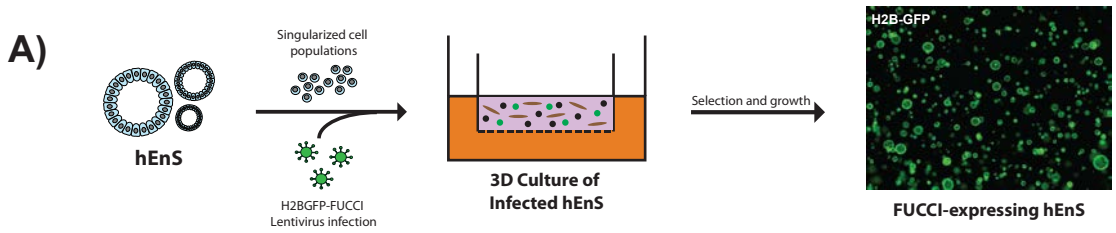
A)
hEnS
Singularized cell populations
H2BGFP-FUCCI Lentivirus infection
3D Culture of Infected hEnS
Selection and growth
H2B-GFP
FUCCI-expressing hEnS

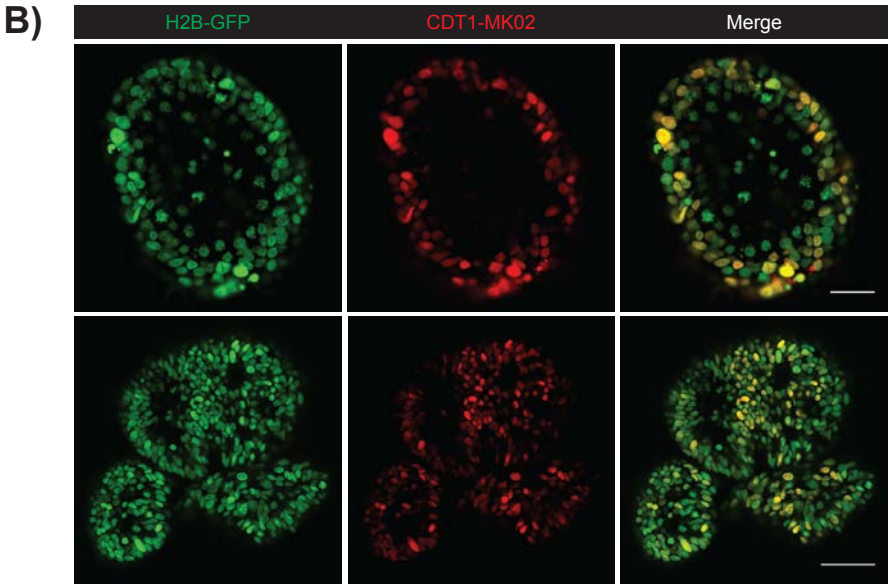
B)
H2B-GFP
CDT1-MK02
Merge

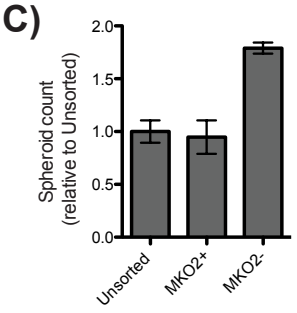
C)
Spheroid count (relative to Unsorted)
2.0
1.5
1.0
0.5
0.0
Unsorted
MKO2+
MKO2-

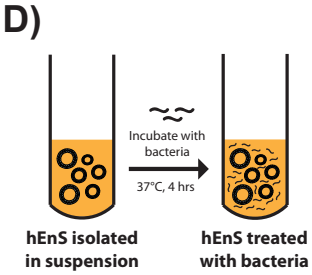
D)
Incubate with bacteria
37°C, 4 hrs
hEnS isolated in suspension
hEnS treated with bacteria

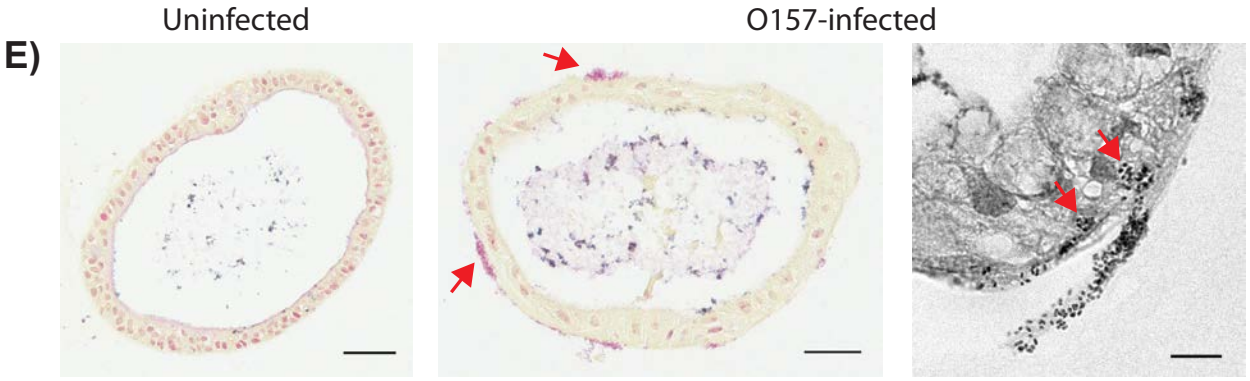
E)
Uninfected
O157-infected

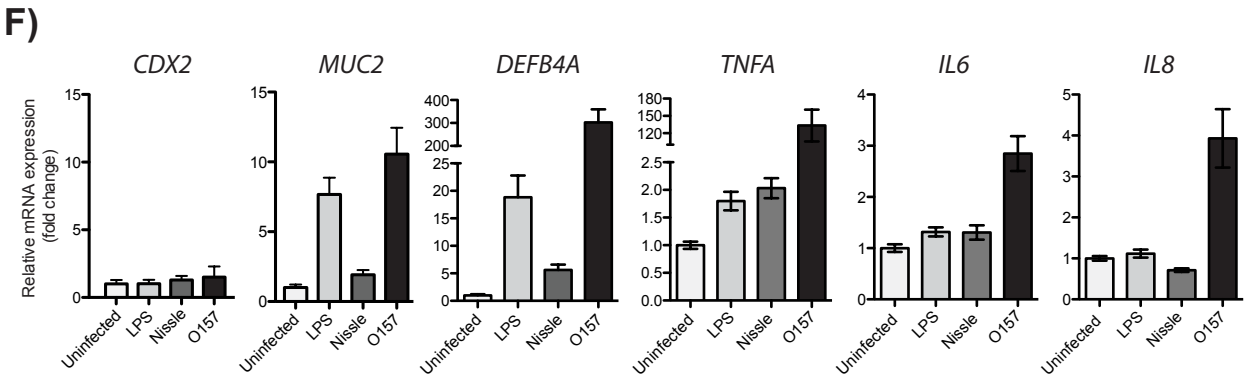
F)
CDX2
MUC2
DEFB4A
TNFA
IL6
IL8
Relative mRNA expression (fold change)
Uninfected
LPS
Nissle
O157

Figure S1

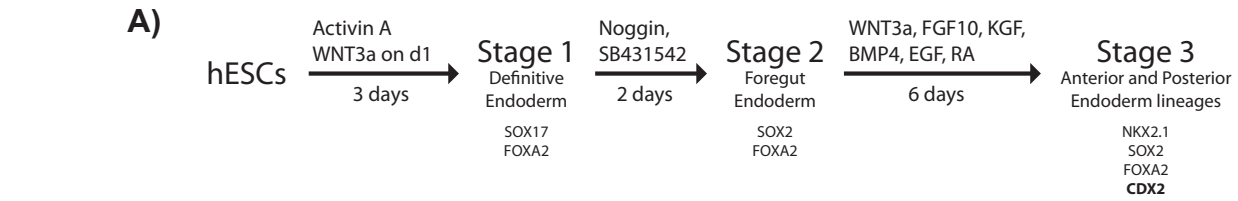
A)
hESCs
Activin A
WNT3a on d1
3 days
Stage 1
Definitive
Endoderm
SOX17
FOXA2
Noggin,
SB431542
2 days
Stage 2
Foregut
Endoderm
SOX2
FOXA2
WNT3a, FGF10, KGF,
BMP4, EGF, RA
6 days
Stage 3
Anterior and Posterior
Endoderm lineages
NKX2.1
SOX2
FOXA2
CDX2

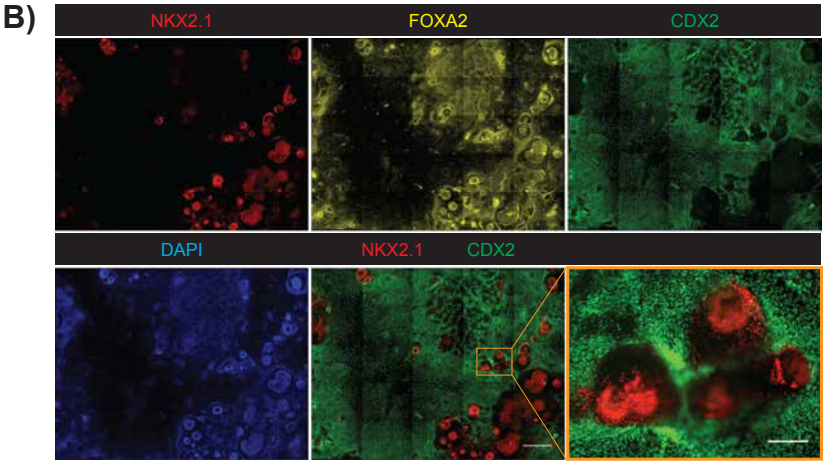
B)
NKX2.1
FOXA2
CDX2
DAPI
NKX2.1
CDX2

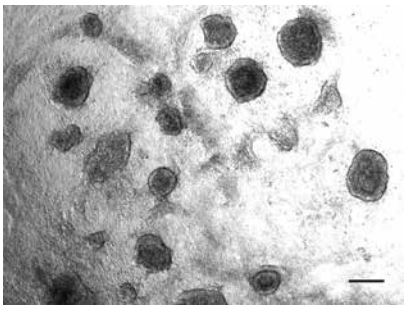
C)

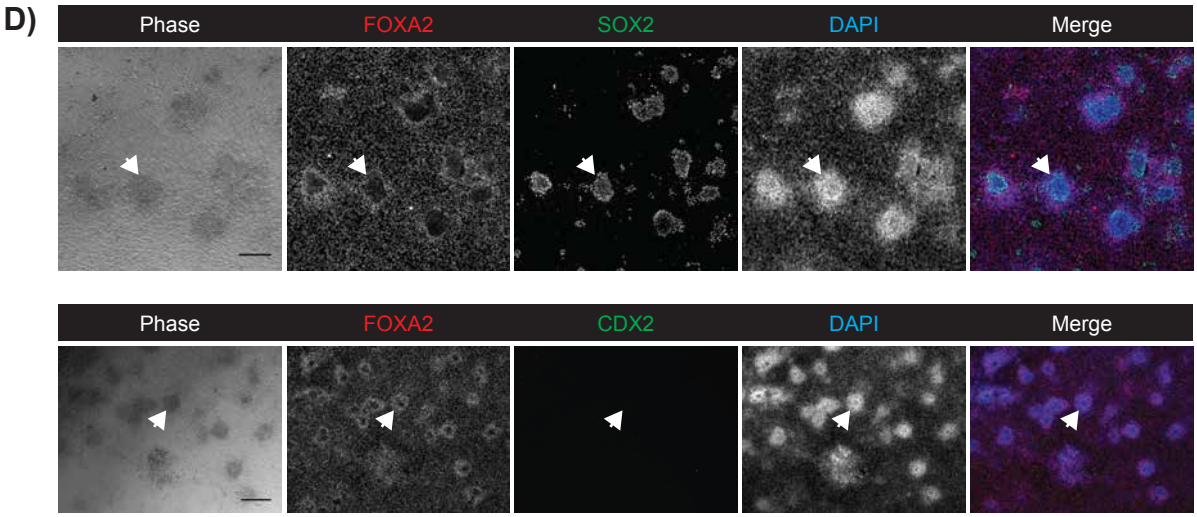
D)
Phase
FOXA2
SOX2
DAPI
Merge
Phase
FOXA2
CDX2
DAPI
Merge

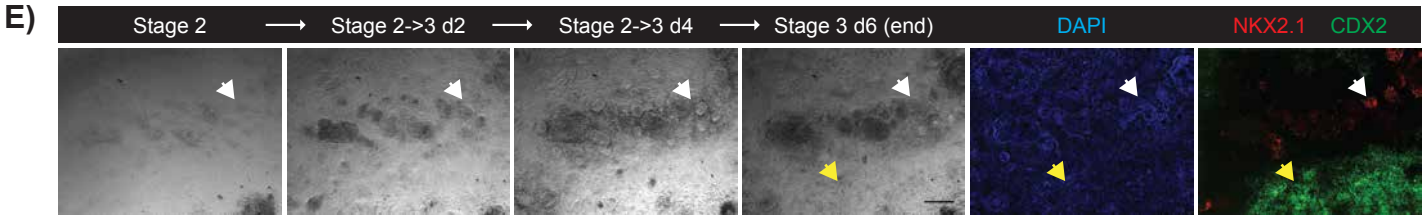
E)
Stage 2
Stage 2->3 d2
Stage 2->3 d4
Stage 3 d6 (end)
DAPI
NKX2.1
CDX2

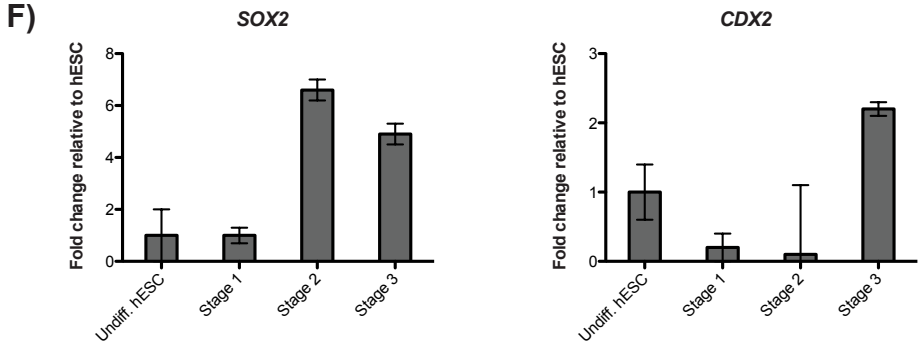
F)
SOX2
Fold change relative to hESC
0
2
4
6
8
Undiff. hESC
Stage 1
Stage 2
Stage 3
CDX2
Fold change relative to hESC
0
1
2
3
Undiff. hESC
Stage 1
Stage 2
Stage 3

Figure S2

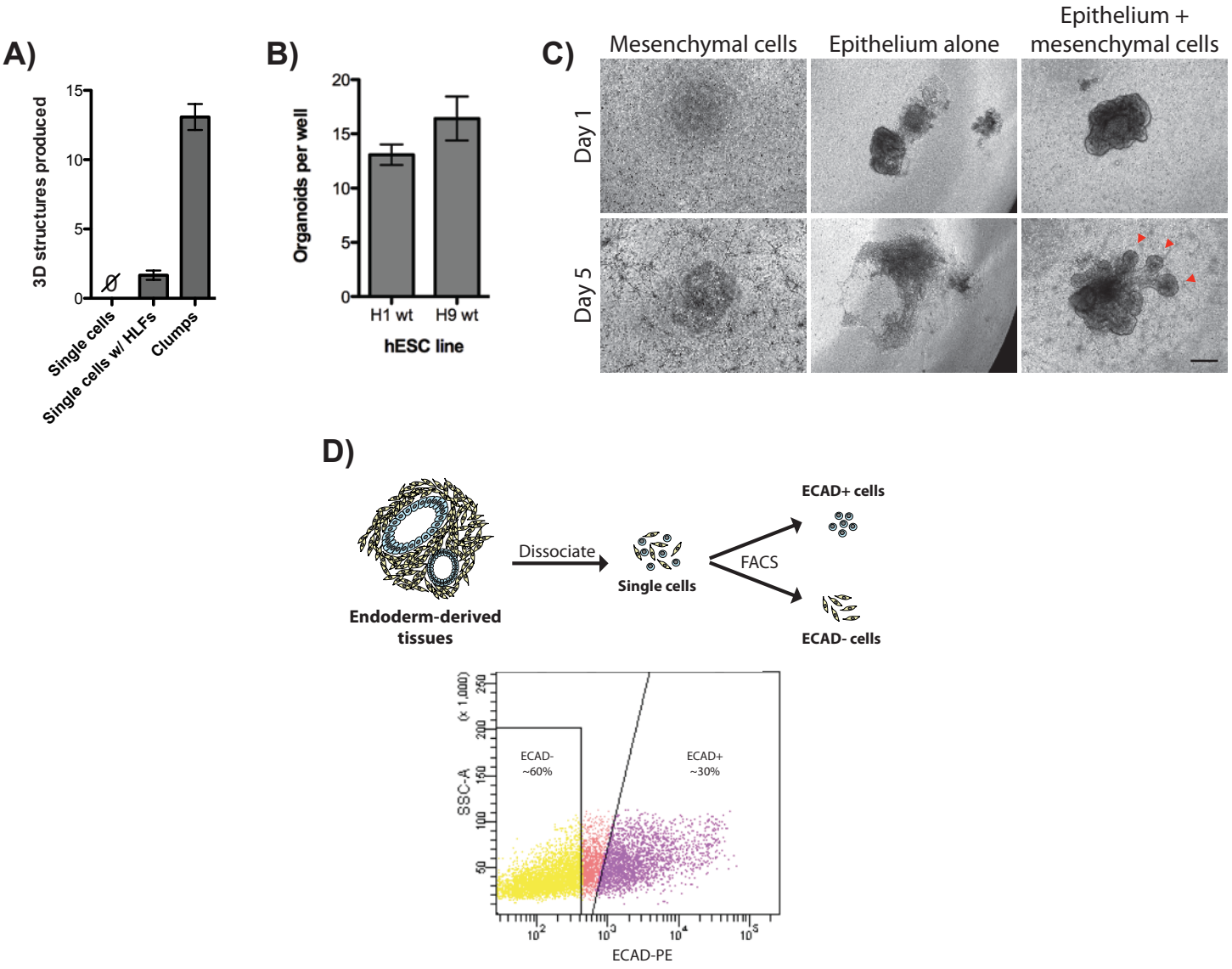
A)
3D structures produced
15
10
5
0
Single cells
Single cells w/ HLFs
Clumps
B)
Organoids per well
20
15
10
5
0
H1 wt
H9 wt
hESC line
C)
Mesenchymal cells
Epithelium alone
Epithelium + mesenchymal cells
Day 1
Day 5
D)
Endoderm-derived tissues
Dissociate
Single cells
FACS
ECAD+ cells
ECAD- cells
ECAD-
~60%
ECAD+
~30%
SSC-A
(x 1,000)
250
200
150
100
50
10^2
10^3
10^4
10^5
ECAD-PE

Figure S3

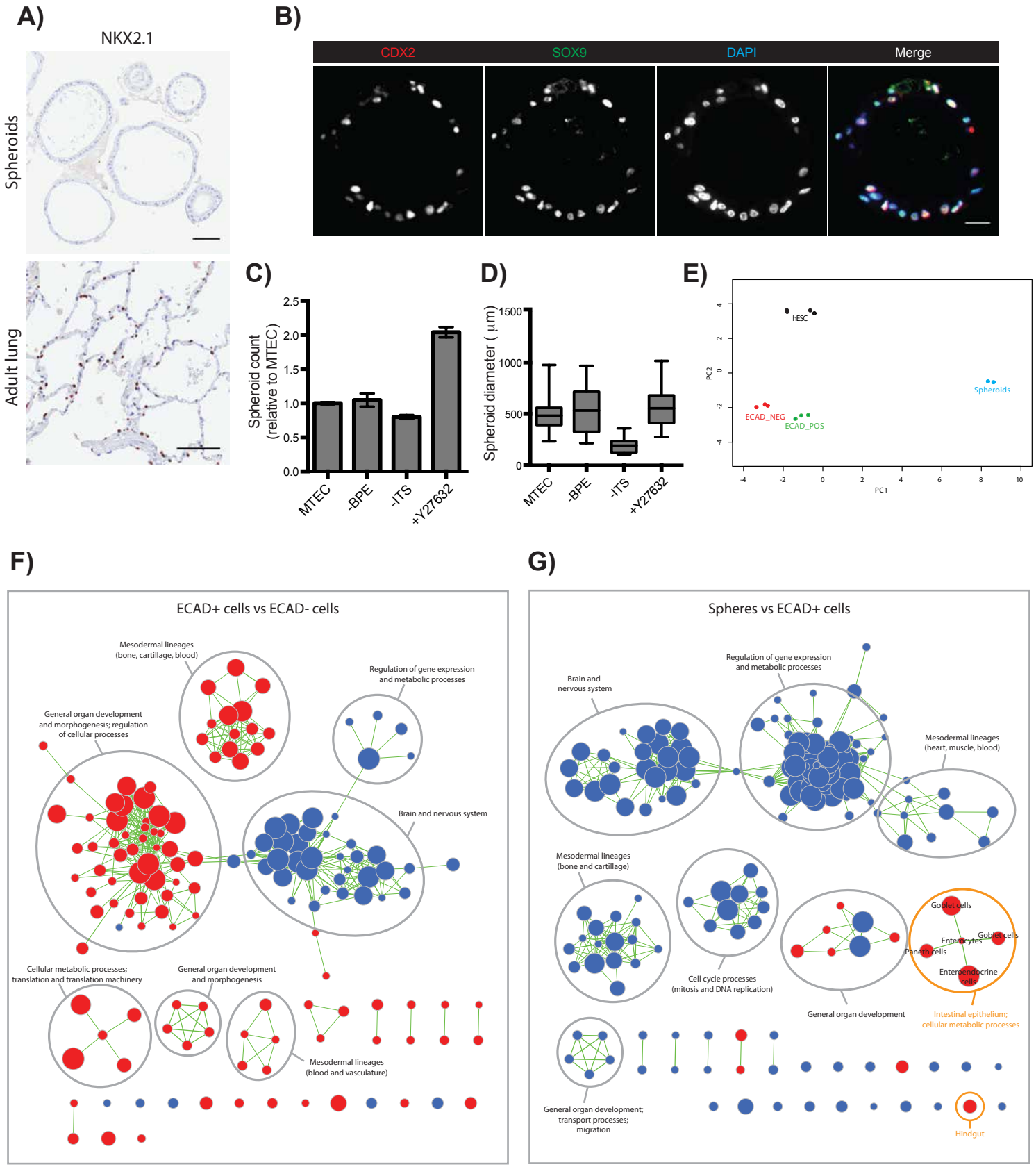
A)
NKX2.1
Spheroids
Adult lung
B)
CDX2
SOX9
DAPI
Merge
C)
Spheroid count (relative to MTEC)
2.5
2.0
1.5
1.0
0.5
0.0
MTEC
-BPE
-ITS
+Y27632
D)
Spheroid diameter (µm)
1500
1000
500
0
MTEC
-BPE
-ITS
+Y27632
E)
hESC
Spheroids
ECAD_NEG
ECAD_POS
PC1
PC2
F)
ECAD+ cells vs ECAD- cells
Mesodermal lineages (bone, cartillage, blood)
Regulation of gene expression and metabolic processes
General organ development and morphogenesis; regulation of cellular processes
Brain and nervous system
Cellular metabolic processes; translation and translation machinery
General organ development and morphogenesis
Mesodermal lineages (blood and vasculature)
G)
Spheres vs ECAD+ cells
Brain and nervous system
Regulation of gene expression and metabolic processes
Mesodermal lineages (heart, muscle, blood)
Mesodermal lineages (bone and cartillage)
Cell cycle processes (mitosis and DNA replication)
General organ development
Goblet cells
Enterocytes
Goblet cells
Paneth cells
Enteroendocrine cells
Intestinal epithelium; cellular metabolic processes
General organ development; transport processes; migration
Hindgut

Figure S4

A)

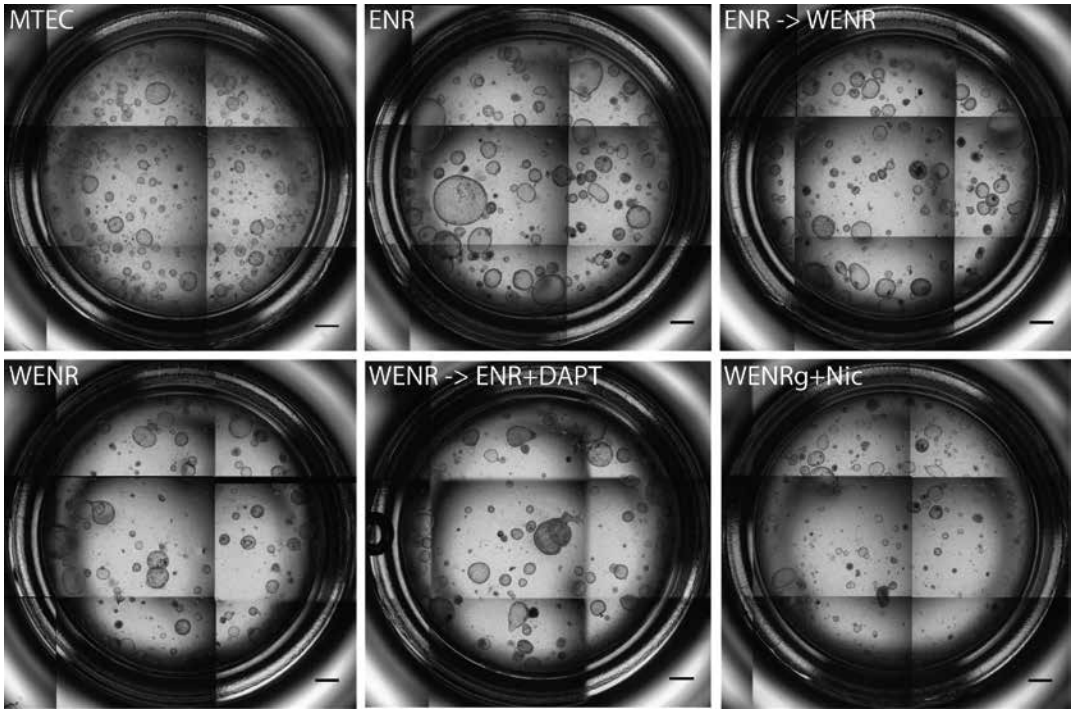
MTEC
ENR
ENR -> WENR
WENR
WENR -> ENR+DAPT
WENRg+Nic

B)

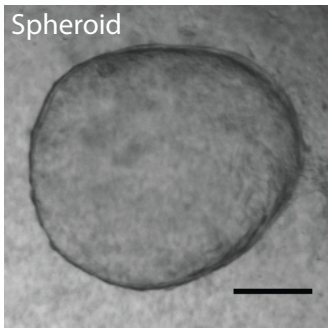
Spheroid

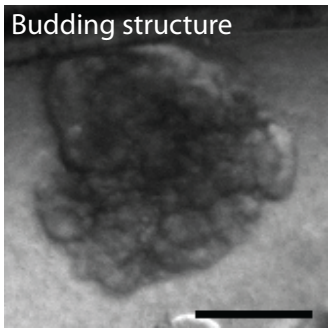
Budding structure

Figure S5

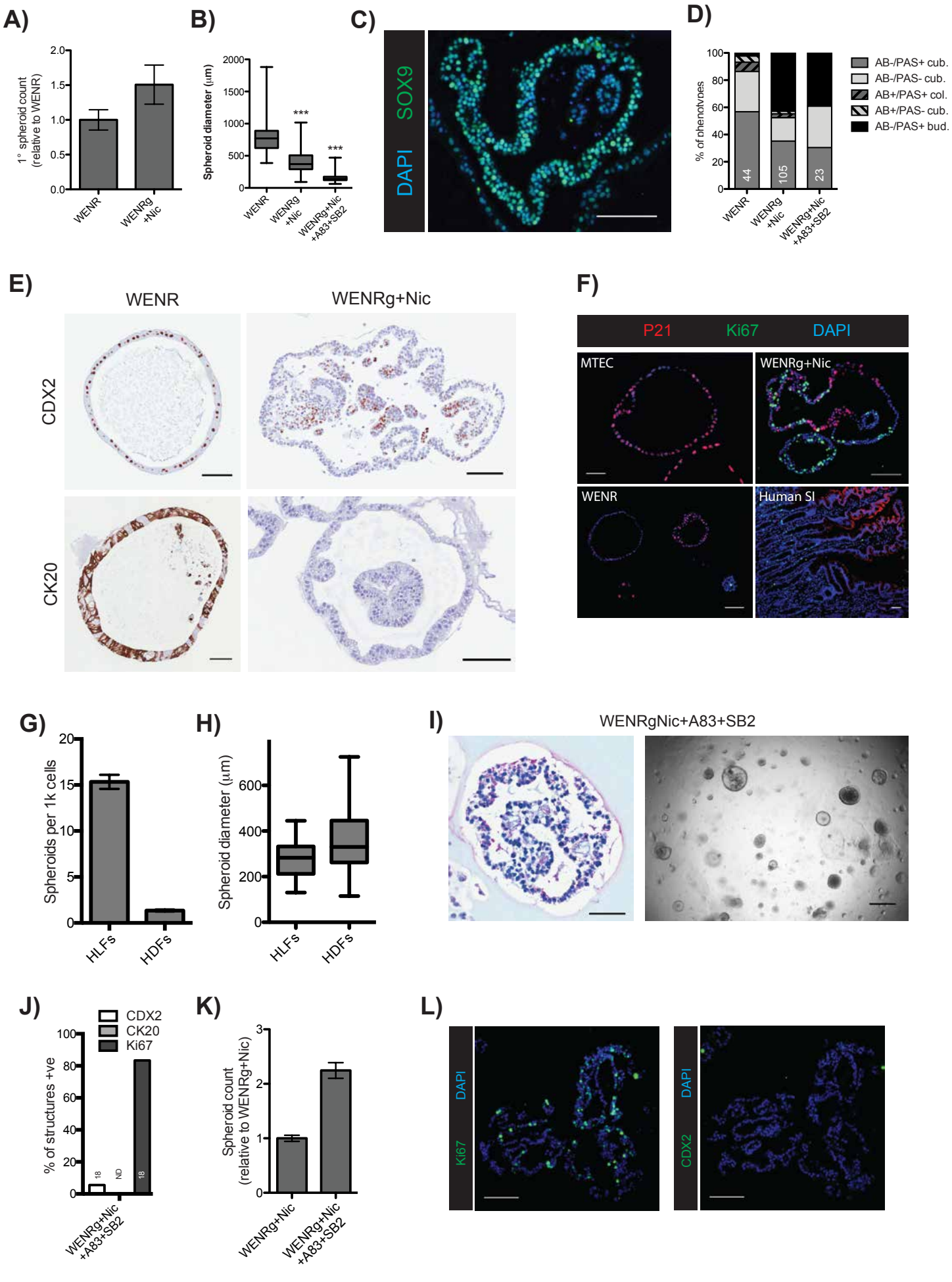
A)
1° spheroid count (relative to WENR)
WENR
WENRg +Nic
B)
Spheroid diameter (µm)
***
***
WENR
WENRg +Nic
WENRg+Nic +A83+SB2
C)
DAPI
SOX9
D)
% of phenotypes
AB-/PAS+ cub.
AB-/PAS- cub.
AB+/PAS+ col.
AB+/PAS- cub.
AB-/PAS+ bud.
44
105
23
E)
WENR
WENRg+Nic
CDX2
CK20
F)
P21
Ki67
DAPI
MTEC
WENRg+Nic
WENR
Human SI
G)
Spheroids per 1k cells
HLFs
HDFs
H)
Spheroid diameter (µm)
HLFs
HDFs
I)
WENRgNic+A83+SB2
J)
CDX2
CK20
Ki67
% of structures +ve
18
ND
18
WENRg+Nic +A83+SB2
K)
Spheroid count (relative to WENRg+Nic)
WENRg+Nic
WENRg+Nic +A83+SB2
L)
Ki67
DAPI
CDX2
DAPI

Chapter 2.3 – Assessment of protein markers of intestinal maturation during human gestation

Preface

This chapter is a draft of a manuscript focusing on intestinal development and maturation in humans using primary tissue samples. Dr. Jonathan Draper and I designed this study, and it was primarily executed by me. Master's student Amos Lim took part in experimental work, and pathology resident Dr. Brigitte Courteau helped in gaining access to, searching for and providing tissue sections. I wrote the manuscript and generated all the figures.

TITLE

Assessment of protein markers of intestinal maturation during human gestation

ABSTRACT

Studying intestinal development and maturation are important for understanding what constitutes a healthy intestine, and for preventing and treating neonatal disease. Most of the current understanding of intestinal maturation in humans has been extrapolated from mouse models, but the timeline is different between the two species. The emergence of maturation indicators in the gestational human intestine has not been explored much in the field due to ethical and logistical barriers in accessing such material for research use. Here, we assess the expression of protein markers of maturation by staining tissue sections of human intestine spanning gestation. These include markers of cell type emergence, functionality, structural integrity, and protective role that overall constitute intestinal maturation. Our work suggests that majority of intestinal maturation in humans occurs before birth. We provide new insights into intestinal development and maturation.

INTRODUCTION

Intestinal maturation plays an important role in the overall normal development and function of the native intestine. Failure of the intestine to properly mature is implicated in the pathogenesis of neonatal intestinal diseases like necrotizing enterocolitis (NEC) and early-onset inflammatory bowel disease (IBD), in which bacteria invade the intestine, resulting in inflammation and potential destruction of the wall of the intestine (Abraham and Cho, 2009; Neu and Walker, 2011). In fact, NEC is the most common disease among premature infants, affecting about 7% of cases, and with a 25% mortality rate (Rich and Dolgin, 2017). The use of breast milk and probiotic bacteria can contribute to proper intestinal maturation in premature infants at risk of NEC or IBD (Alfaleh et al., 2011; Grave et al., 2007; Guandalini, 2010; Klement et al., 2004; Sisk et al., 2007). Studying intestinal development and maturation are important for understanding which factors lead to a healthy intestine, and for preventing and treating disease.

Intestinal maturation can be defined as functional changes that occur beyond morphogenesis and differentiation into intestinal cell types, and is marked by the emergence or loss of key protein markers, improvement of structural integrity, and host defense. For example, when enterocytes first appear in the intestine, they express villin, but become functional upon production of glucosidase enzymes such as sucrase isomaltase, trehalase, and lactase (Finkbeiner et al., 2015). Similarly, emerging Paneth cells secrete lysozyme, but are only considered mature when they secrete α-defensin peptides for host defense (Finkbeiner et al., 2015; Mallow et al., 1996). The expression of tight junction protein Claudin 3 in the intestinal epithelium is an indicator of improved epithelial barrier integrity and reduced intestinal permeability (Günzel and Yu, 2013; Lu

et al., 2013; Milatz et al., 2010; Patel et al., 2012). Failure or untimely emergence of such changes can lead to impaired intestinal function.

Most of the current understanding of human intestinal development and maturation has been extrapolated from mouse models, but the timeline is different between the two species. In humans, intestinal morphogenesis is complete several weeks before birth, and the fetal intestine already structurally resembles that of the adult, whereas in mice it is complete several weeks after birth (McCracken and Lorenz, 2001). This means that the emergence of indicators of intestinal maturation is likely temporally different between humans and mice. For example, in mice, the expression of Claudin 3 in epithelial tight junctions begins several weeks after birth when morphogenesis is complete (Patel et al., 2012), but it is unclear if the same occurs in humans because morphogenesis is complete before birth.

The expression of maturation indicators at the protein level during human intestinal development has not been explored much in the field probably due to difficulty in accessing such material for research use. Here, we assess the expression of protein markers of maturation through staining of tissue sections of human intestine spanning gestation. Our work suggests that majority of intestinal maturation in humans occurs before birth, different from observations in mice. We present novel information about intestinal marker expression in humans, and provide valuable insights into intestinal development and maturation.

RESULTS

To capture most of human gestation across which intestinal organogenesis occurs, we obtained individual cases from 13, 18, 24, and 32 weeks of gestation (as well as

adult), which represent the end of the first trimester, middle and end of the second trimester, and middle of the third trimester. CDX2, the master regulator of intestinal identity (Silberg et al., 2000; Zorn and Wells, 2009), was visible in all cases, confirming that they were intestinal tissue **(Figure S1)**. Haematoxylin and eosin (H&E) staining revealed differences in epithelial structure with age, such as the absence of crypt-resembling domains at 13 and 18 weeks but their presence from 24 weeks onwards **(Figure S2)**, supporting the observation that crypts emerge around week 20 in the human intestine (Chin et al., 2017). A cell length-to-width ratio of 2-2.5, marking cuboidal epithelium, was consistent across 13, 18 and 24 weeks, whereas a ratio of ~3 was seen at 32 weeks, suggesting a transition from cuboidal to columnar epithelium, and columnar epithelium marked by a ratio of >4 was seen in the adult **(Figure S2)**. Alcian blue/periodic acid-Schiff (AB-PAS) staining, which identifies acid and neutral mucins, showed that goblet cells were present in the intestinal epithelium as early as 13 weeks (**Figure S3)**. We then stained for several protein markers of cell type emergence, functionality, structural integrity, and protective role that overall constitute intestinal maturation. A description of the role of each marker assessed in this study is summarized in **Table 1**.

Enteroendocrine cells emerge early during intestinal development in humans

Intestinal enteroendocrine cells (EECs) are specialized cells with endocrine function that produce hormones in response to various stimuli and release them into the bloodstream or to the enteric nervous system. In adults, EECs comprise ~1% of the intestinal epithelium and are located sporadically throughout (Gunawardene et al., 2011;

Noah et al., 2011). EECs emerge at around E16.5 in mice shortly after villus morphogenesis begins (Chin et al., 2017), but it is unclear how early EECs emerge in the human intestine, and are a putative indicator of maturation due to the difficulty in generating them *in vitro* in human pluripotent stem cell (hPSC)-derived intestinal tissues which tend to be fetal-like (Fordham et al., 2013; Forster et al., 2014; Nadkarni et al., 2017). Chromogranin A (CHGA) is a neuroendocrine secretory protein and marker of EECs. We found that CHGA-expressing cells were present in all tested gestational ages, including 13 weeks in the developing epithelium **(Figure 1)**. Also, CHGA-expressing cells were seen at higher frequency in the crypts relative to the villi at 32 weeks of gestation and in the adult **(Figure 1)**. This indicates that intestinal EECs emerge as early as the end of the first trimester in humans.

Intestinal brush border maturation occurs late in gestation but before birth in humans

Villus morphogenesis begins at E15 in mice, and is one of the first signs of differentiation in the developing intestine (Chin et al., 2017; Noah et al., 2011). Absorptive enterocytes are one of the intestinal epithelial cell types that emerge during this period, at around E16.5. Enterocytes comprise more than 80% of the intestinal epithelium, and are responsible for absorbing nutrients from the lumen. Due to the presence of microvilli on their apical surface, enterocytes constitute the brush border of the intestine (Chin et al., 2017). Villin (VIL1) is an actin-binding protein that is expressed in the brush border throughout development and in the adult. However, a fully functional brush border is distinguished by the production of glucosidase enzymes, such as sucrase isomaltase (SI), whose expression is low in the fetal intestine but peaks in the adult

intestine in humans (Finkbeiner et al., 2015). SI expression is thought to be an indicator of brush border maturation, but it is unclear when it emerges at the protein level in the human intestine. We found that VIL1 was expressed in the brush border in all tested gestational ages (data not shown). Interestingly, SI was also clearly expressed in the brush border in all tested gestational ages, including 13 weeks **(Figure 2)**. This shows that SI protein expression in the human intestine begins in the fetus, challenging the notion that it emerges late as a marker of brush border maturation.

OLFM4 becomes expressed in crypt base columnar cells before birth in the human intestine

After villus formation, proliferating cells become confined to the intervillus domains at the base of the villi (at E17 in mice) for the remainder of development. The crypts emerge from the intervillus domains around postnatal day 14, containing all stem and proliferating cells of the mature intestinal epithelium (Chin et al., 2017; Noah et al., 2011). Olfactomedin 4 (OLFM4) is a stem cell marker that is expressed in crypt base columnar cells in the adult intestine, and is an indicator of crypt maturation (Finkbeiner et al., 2015; van der Flier et al., 2009). Since crypt morphogenesis in humans occurs before birth around week 20 of gestation (Chin et al., 2017), we hypothesized that OLFM4 also emerges in the crypts around this time. We found that OLFM4 was expressed in crypt base columnar cells at 32 weeks of gestation, the same as adult **(Figure 3)**. At 24 weeks, OLFM4 was beginning to become localized to developing crypt base columnar cells **(Figure 3)**. OLFM4 staining was not visible at 13 and 18 weeks, concurrent with crypt

absence before week 20. This indicates that OLFM4 localization in the fetal intestine from the end of the second trimester onwards is comparable to that in the adult.

Paneth cell maturation occurs before birth in the human intestine

Paneth cell differentiation coincides with intestinal crypt emergence (Calvert and Pothier, 1990; Chin et al., 2017; Kim et al., 2012), which occurs at postnatal day 14 in mice and 20 weeks of gestation in humans (Mallow et al., 1996; Moxey and Trier, 1978). Lysozyme production marks the presence of Paneth cells in the intestine, but the production of α-defensin peptides for defense against pathogens is an indicator of Paneth cell maturation (Ayabe et al., 2000; Finkbeiner et al., 2015). Since Paneth cells appear during mid-gestation in the human intestine, we hypothesized that their maturation also occurs around this time. We tested this by staining for α-defensin 5 (DEFA5 or HD5). We found that DEFA5-expressing cells were present in the crypts at 24 and 32 weeks of gestation, and progressively migrated downwards to the crypt base **(Figure 4)** (Bjerknes and Cheng, 1981; Kim et al., 2012). DEFA5 staining was not visible at 13 and 18 weeks, concurrent with the absence of crypts and Paneth cells before week 20. This suggests that Paneth cell maturation occurs before birth in the human intestine soon after their differentiation.

Claudin 3 expression begins before birth in the human intestine

In premature infants suffering from NEC or IBD, the immature intestine is vulnerable to invading bacteria that are capable of destroying the intestinal wall. Epithelial barrier integrity is important for reducing systemic entry of gut luminal

pathogens or toxins, and the use of breast milk and probiotics can contribute to proper barrier maturation and prevention of disease (Alfaleh et al., 2011; Clayburgh et al., 2004; Grave et al., 2007; Guandalini, 2010; Klement et al., 2004; Sartor, 2008; Sisk et al., 2007). The tight junction protein Claudin 3 (CLDN3) is a marker of improved epithelial barrier integrity (Günzel and Yu, 2013; Lu et al., 2013; Milatz et al., 2010; Patel et al., 2012). In mice, CLDN3 expression is absent at the protein level throughout gestation, and emerges only several weeks after birth when morphogenesis is complete (Patel et al., 2012). Colonization of the postnatal murine intestine with the probiotic bacterial species *Lactobacillus rhamnosus* induces CLDN3 expression in epithelial tight junctions and reduces intestinal permeability (Patel et al., 2012). We hypothesized that CLDN3 expression also emerges after birth in the human intestine upon exposure to probiotics. Surprisingly, we found that CLDN3 was robustly expressed throughout the intestinal epithelium as early as 18 weeks of gestation, the same as adult **(Figure 5)**. It was weakly present at 13 weeks **(Figure 5)**. This indicates that CLDN3 protein expression in the human intestine emerges before birth as early as the beginning of the second trimester.

Fucosylation in the human intestine occurs during gestation but the localization changes with morphogenesis

Fucosylation is a type of glycosylation in which fucose units are added to glycoproteins and glycolipids, which has a protective role in both intestinal and systemic infection and inflammation through suppressing the virulence of harmful pathogens (Pickard and Chervonsky, 2015). In the intestine, fucosylation is localized to glycoproteins produced by Paneth cells in the crypts, and goblet cells and enterocytes in

the villi (Bry et al., 1996). Fucosylation is marked by increased expression and activity of fucosyltransferase enzymes, and reactivity to the lectin Ulex europaeus agglutinin 1 (UEA1). Fucosylation in the murine intestine occurs primarily after birth and post-weaning, coinciding with the abundance of enteric bacteria and polyamines. Colonization of the gut with the bacterial species *Bacteriodes thetaiotaomicron* or treatment with polyamines has been shown to induce fucosylation of brush border and mucinous glycoproteins in germ-free mouse and rat models (Biol-N'Garagba et al., 2002; Bry et al., 1996; Capano et al., 1994; Dufour et al., 1988). It is poorly understood when fucosylation in the human intestine begins. We investigated this by staining human samples with fluorochrome-conjugated UEA1. In the adult, UEA1 reactivity was clearly observed in Paneth cells, goblet cells, and the brush border, but at 24 and 32 weeks of gestation it was only localized to Paneth and goblet cells **(Figure 6)**. At 18 weeks, UEA1 reactivity was seen in the lumen in patches resembling secreted mucins, and was also seen at 13 weeks but without localization in any obvious morphological structures **(Figure 6**). This indicates that fucosylation in the human intestine begins during gestation but becomes localized to differentiated epithelial cell types later, being absent in mucinous glycoproteins at 13 weeks of gestation, and absent in brush border glycoproteins at 32 weeks and before.

hPSC-derived enterospheres resemble the fetal intestinal epithelium in maturation status

Intestinal organoids made from hPSCs entirely *in vitro* tend to be fetal-like and highly immature compared to primary adult organoids and the native intestine itself (Finkbeiner et al., 2015; Fordham et al., 2013; Spence et al., 2011). We previously

generated hPSC-derived cystic intestinal epithelial organoids or enterospheres (hEnS) *in vitro*, which show robust expression of intestinal genes and are functional in that they elicit an innate immune response when exposed to pathogens (Nadkarni et al., 2017). When hEnS were stained for all the markers described in this study, although VIL1, SI and UEA1 were seen, CHGA, OLFM4, DEFA5 and CLDN3 were not **(Figure 7)**. This suggests that in terms of their maturation status, our *in vitro* hEnS have a phenotype that resembles the fetal intestinal epithelium from before 18 weeks of gestation.

DISCUSSION

While tracking the expression of protein markers of maturation in fixed tissue sections of human intestine from different gestational ages, we made observations not reported before and which are different from those in mice. Although transcript levels of some markers in this study have been compared between the fetal and adult human intestine (Finkbeiner et al., 2015), they have rarely been assessed at the protein level and at multiple gestational ages. Also, as opposed to measuring relative protein expression using western blots, staining of tissue sections provides information about structure and protein localization, which informs about changes that indicate maturation. However, one of the major limitations of this study is that only one case from each age was analyzed due to the difficulty in obtaining human fetal tissue of suitable quality, especially from the first and second trimesters. Nevertheless, one has to start somewhere and this is intended to be a simple descriptive study to determine if protein markers of maturation are expressed in the developing human intestine.

The emergence of EECs, which is marked by CHGA protein expression, is a putative indicator of intestinal maturation. However, we found that CHGA is present in the developing epithelium as early as 13 weeks of gestation, indicating that EECs are one of the first differentiated epithelial cell types that emerge in the human intestine, the same as in mice (Chin et al., 2017; Noah et al., 2011). The difficulty in generating EECs from hPSCs *in vitro* (Fordham et al., 2013; Forster et al., 2014; Nadkarni et al., 2017) may be attributed to deficiencies in exogenous signaling that activate genes responsible for promoting EEC differentiation, such as *Neurogenin-3* (Sinagoga et al., 2018; Spence et al., 2011).

SI, OLFM4, and *DEFA5*, markers of brush border, crypt, and Paneth cell maturation respectively, are expressed at low transcript levels in the fetal intestine and highest in the adult intestine (Finkbeiner et al., 2015). All three are expressed at the protein level in the adult human intestine (Finkbeiner et al., 2015), but we found that they are also present in the fetal intestine mid-gestation onwards, suggesting that brush border and crypt maturation occur before birth.

In the murine intestine, CLDN3 expression is absent at the protein level during gestation, and emerges several weeks after birth upon completion of morphogenesis and exposure to probiotic bacteria (Patel et al., 2012). Similarly, fucosyltransferase activity and in turn fucosylation of brush border and mucinous glycoproteins occurs after birth in mice, and can be triggered by exposure to *Bacteriodes thetaiotaomicron* or polyamines (Biol-N'Garagba et al., 2002; Bry et al., 1996; Capano et al., 1994; Dufour et al., 1988). However, we found that CLDN3 was clearly expressed in the intestinal epithelium as

early as 18 weeks of gestation, and UEA1 reactivity was seen in Paneth and goblet cells at 24 and 32 weeks.

Intestinal organoids derived from hPSCs entirely *in vitro*, including hEnS, are fetal-like and do not express most maturation markers at the protein level. They may be even more immature than previously thought, since we found that majority of maturation markers are expressed in the primary human intestine as early as the middle of the second trimester of development. Strategies to induce maturation of hPSC-derived intestinal organoids have been explored. Spence and colleagues showed that after *in vivo* engraftment under the kidney capsule of mice for 16 weeks, organoids more closely resembled the adult intestine at the structural and molecular level (Finkbeiner et al., 2015; Spence et al., 2011; Watson et al., 2014). Organoid maturation may also be stimulated *in vitro* by co-culture with intestinal stromal cells or exposure to enteric bacteria (Hill et al., 2017).

Our observations underscore the difference in the timeline of intestinal development between humans and mice. Intestinal morphogenesis in humans is complete before birth, whereas in mice it is complete after birth, coinciding with the presence of enteric bacteria (McCracken and Lorenz, 2001). It is important to note that in the fetal intestine there is still systemic access to bacterial products from the maternal microbiota. Although the intestine has long thought to be sterile before birth, recent studies claimed that maternal microbes present in the placenta and amniotic fluid may infiltrate the fetal intestine (Aagaard et al., 2014; Collado et al., 2016; Perez-Muñoz et al., 2017), suggesting that bacteria-mediated maturation may begin *in utero*. On the other hand, although the above markers emerge before birth in the human intestine, additional

maturation likely occurs after birth and post-weaning to contribute to intestinal structure and function.

Overall, this work provides new insights into intestinal development and maturation in humans. It may also be used as a guide by other researchers studying the intestine, including hPSC-derived tissues, to gauge the relative maturation status of their samples.

EXPERIMENTAL PROCEDURES

Obtaining tissue sections of human intestine

Access to fixed tissue sections of human intestine from gestation was gained through Hamilton Health Sciences and St. Joseph's Healthcare Hamilton in Ontario, Canada. Full approval was obtained from the Hamilton Integrated Research Ethics Board (HiREB) for the use of human tissue for research purposes. Archived tissue blocks of fetal autopsies and products of conception were chosen by a staff pathologist using their personal record of completed cases. The gestational age of each sample was determined at the time of diagnosis, based on the patient history and gestational age reference values. Only the tissue blocks containing small bowel were pulled by laboratory staff and identified by the gross description captured on the software Meditech.

Immunostaining of tissue sections

Formalin-fixed paraffin-embedded (FFPE) tissue sections were stained according to protocols from R&D Systems for fluorescent IHC staining (https://www.rndsystems.com/resources/protocols/protocol-preparation-and-fluorescent-ihc-staining-paraffin-embedded-tissue) and chromogenic IHC staining (https://www.rndsystems.com/resources/protocols/protocol-preparation-and-chromogenic-ihc-staining-paraffin-embedded-tissue). For chromogenic IHC staining, reagents from Anti-mouse (CTS002), Anti-rabbit (CTS005), and Anti-rat HRP-DAB Cell & Tissue Staining Kit (CTS017) from R&D Systems were used.

Primary antibody information:

Primary Antibodies			
Antibody/protein	**Vendor**	**Catalog no.**	**Usage**
CLDN3	Abcam	ab15102	1:100
DEFA5	Novus Biologicals	NB110-60002SS	10 µg/ml (1:235)
OLFM4	Abcam	ab85046	5 µg/ml (1:120)
SI	Santa Cruz	sc-27603	1:100
UEA1	Vector Laboratories	DL-1067	1:100

H&E, AB-PAS, and chromogenic IHC staining for CDX2 and CHGA were performed by technical staff in the HRLMP at St. Joseph's Hospital in Hamilton, Ontario, Canada. Antibody information:
CDX2: Clone - DAK-CDX2; Isotype - IgG1, kappa
CHGA: Clone - DAK-A3; Isotype - IgG2b, kappa

REFERENCES

Aagaard, K., Ma, J., Antony, K.M., Ganu, R., Petrosino, J., and Versalovic, J. (2014). The placenta harbors a unique microbiome. Sci Transl Med *6*, 237ra65.

Abraham, C., and Cho, J.H. (2009). Inflammatory Bowel Disease. New England Journal of Medicine *361*, 2066–2078.

Alfaleh, K., Anabrees, J., Bassler, D., and Al-Kharfi, T. (2011). Probiotics for prevention of necrotizing enterocolitis in preterm infants. Cochrane Database Syst Rev CD005496.

Ayabe, T., Satchell, D.P., Wilson, C.L., Parks, W.C., Selsted, M.E., and Ouellette, A.J. (2000). Secretion of microbicidal alpha-defensins by intestinal Paneth cells in response to bacteria. Nat. Immunol. *1*, 113–118.

Biol-N'Garagba, M.-C., Greco, S., George, P., Hugueny, I., and Louisot, P. (2002). Polyamine participation in the maturation of glycoprotein fucosylation, but not sialylation, in rat small intestine. Pediatr. Res. *51*, 625–634.

Bjerknes, M., and Cheng, H. (1981). The stem-cell zone of the small intestinal epithelium. I. Evidence from Paneth cells in the adult mouse. Am. J. Anat. *160*, 51–63.

Bry, L., Falk, P.G., Midtvedt, T., and Gordon, J.I. (1996). A model of host-microbial interactions in an open mammalian ecosystem. Science *273*, 1380–1383.

Calvert, R., and Pothier, P. (1990). Migration of fetal intestinal intervillous cells in neonatal mice. Anat. Rec. *227*, 199–206.

Capano, G., Bloch, K.J., Schiffrin, E.J., Dascoli, J.A., Israel, E.J., and Harmatz, P.R. (1994). Influence of the polyamine, spermidine, on intestinal maturation and dietary antigen uptake in the neonatal rat. J. Pediatr. Gastroenterol. Nutr. *19*, 34–42.

Chin, A.M., Hill, D.R., Aurora, M., and Spence, J.R. (2017). Morphogenesis and maturation of the embryonic and postnatal intestine. Semin. Cell Dev. Biol. *66*, 81–93.

Clayburgh, D.R., Shen, L., and Turner, J.R. (2004). A porous defense: the leaky epithelial barrier in intestinal disease. Lab. Invest. *84*, 282–291.

Collado, M.C., Rautava, S., Aakko, J., Isolauri, E., and Salminen, S. (2016). Human gut colonisation may be initiated *in utero* by distinct microbial communities in the placenta and amniotic fluid. Scientific Reports *6*, 23129.

Dufour, C., Dandrifosse, G., Forget, P., Vermesse, F., Romain, N., and Lepoint, P. (1988). Spermine and spermidine induce intestinal maturation in the rat. Gastroenterology *95*, 112–116.

Finkbeiner, S.R., Hill, D.R., Altheim, C.H., Dedhia, P.H., Taylor, M.J., Tsai, Y.-H., Chin, A.M., Mahe, M.M., Watson, C.L., Freeman, J.J., et al. (2015). Transcriptome-wide

Analysis Reveals Hallmarks of Human Intestine Development and Maturation In Vitro and In Vivo. Stem Cell Reports *4*, 1140–1155.

van der Flier, L.G., Haegebarth, A., Stange, D.E., van de Wetering, M., and Clevers, H. (2009). OLFM4 is a robust marker for stem cells in human intestine and marks a subset of colorectal cancer cells. Gastroenterology *137*, 15–17.

Fordham, R.P., Yui, S., Hannan, N.R.F., Soendergaard, C., Madgwick, A., Schweiger, P.J., Nielsen, O.H., Vallier, L., Pedersen, R.A., Nakamura, T., et al. (2013). Transplantation of expanded fetal intestinal progenitors contributes to colon regeneration after injury. Cell Stem Cell *13*, 734–744.

Forster, R., Chiba, K., Schaeffer, L., Regalado, S.G., Lai, C.S., Gao, Q., Kiani, S., Farin, H.F., Clevers, H., Cost, G.J., et al. (2014). Human Intestinal Tissue with Adult Stem Cell Properties Derived from Pluripotent Stem Cells. Stem Cell Reports *2*, 838–852.

Grave, G.D., Nelson, S.A., Walker, W.A., Moss, R.L., Dvorak, B., Hamilton, F.A., Higgins, R., and Raju, T.N.K. (2007). New therapies and preventive approaches for necrotizing enterocolitis: report of a research planning workshop. Pediatr. Res. *62*, 510–514.

Guandalini, S. (2010). Update on the role of probiotics in the therapy of pediatric inflammatory bowel disease. Expert Rev Clin Immunol *6*, 47–54.

Gunawardene, A.R., Corfe, B.M., and Staton, C.A. (2011). Classification and functions of enteroendocrine cells of the lower gastrointestinal tract. Int J Exp Pathol *92*, 219–231.

Günzel, D., and Yu, A.S.L. (2013). Claudins and the Modulation of Tight Junction Permeability. Physiol Rev *93*, 525–569.

Hill, D.R., Huang, S., Nagy, M.S., Yadagiri, V.K., Fields, C., Mukherjee, D., Bons, B., Dedhia, P.H., Chin, A.M., Tsai, Y.-H., et al. (2017). Bacterial colonization stimulates a complex physiological response in the immature human intestinal epithelium. Elife *6*.

Kim, T.-H., Escudero, S., and Shivdasani, R.A. (2012). Intact function of Lgr5 receptor-expressing intestinal stem cells in the absence of Paneth cells. Proc. Natl. Acad. Sci. U.S.A. *109*, 3932–3937.

Klement, E., Cohen, R.V., Boxman, J., Joseph, A., and Reif, S. (2004). Breastfeeding and risk of inflammatory bowel disease: a systematic review with meta-analysis. Am. J. Clin. Nutr. *80*, 1342–1352.

Lu, Z., Ding, L., Lu, Q., and Chen, Y.-H. (2013). Claudins in intestines. Tissue Barriers *1*.

Mallow, E.B., Harris, A., Salzman, N., Russell, J.P., DeBerardinis, R.J., Ruchelli, E., and Bevins, C.L. (1996). Human enteric defensins. Gene structure and developmental expression. J. Biol. Chem. *271*, 4038–4045.

McCracken, V.J., and Lorenz, R.G. (2001). The gastrointestinal ecosystem: a precarious alliance among epithelium, immunity and microbiota. Cell. Microbiol. *3*, 1–11.

Milatz, S., Krug, S.M., Rosenthal, R., Günzel, D., Müller, D., Schulzke, J.-D., Amasheh, S., and Fromm, M. (2010). Claudin-3 acts as a sealing component of the tight junction for ions of either charge and uncharged solutes. Biochim. Biophys. Acta *1798*, 2048–2057.

Moxey, P.C., and Trier, J.S. (1978). Specialized cell types in the human fetal small intestine. Anat. Rec. *191*, 269–285.

Nadkarni, R.R., Abed, S., Cox, B.J., Bhatia, S., Lau, J.T., Surette, M.G., and Draper, J.S. (2017). Functional Enterospheres Derived In Vitro from Human Pluripotent Stem Cells. Stem Cell Reports.

Neu, J., and Walker, W.A. (2011). Necrotizing Enterocolitis. N Engl J Med *364*, 255–264.

Noah, T.K., Donahue, B., and Shroyer, N.F. (2011). Intestinal development and differentiation. Exp Cell Res *317*, 2702–2710.

Patel, R.M., Myers, L.S., Kurundkar, A.R., Maheshwari, A., Nusrat, A., and Lin, P.W. (2012). Probiotic Bacteria Induce Maturation of Intestinal Claudin 3 Expression and Barrier Function. Am J Pathol *180*, 626–635.

Perez-Muñoz, M.E., Arrieta, M.-C., Ramer-Tait, A.E., and Walter, J. (2017). A critical assessment of the "sterile womb" and "in utero colonization" hypotheses: implications for research on the pioneer infant microbiome. Microbiome *5*, 48.

Pickard, J.M., and Chervonsky, A.V. (2015). Intestinal fucose as a mediator of host-microbe symbiosis. J Immunol *194*, 5588–5593.

Rich, B.S., and Dolgin, S.E. (2017). Necrotizing Enterocolitis. Pediatr Rev *38*, 552–559.

Sartor, R.B. (2008). Microbial influences in inflammatory bowel diseases. Gastroenterology *134*, 577–594.

Silberg, D.G., Swain, G.P., Suh, E.R., and Traber, P.G. (2000). Cdx1 and cdx2 expression during intestinal development. Gastroenterology *119*, 961–971.

Sinagoga, K.L., McCauley, H.A., Múnera, J.O., Reynolds, N.A., Enriquez, J.R., Watson, C., Yang, H.-C., Helmrath, M.A., and Wells, J.M. (2018). Deriving functional human enteroendocrine cells from pluripotent stem cells. Development.

Sisk, P.M., Lovelady, C.A., Dillard, R.G., Gruber, K.J., and O'Shea, T.M. (2007). Early human milk feeding is associated with a lower risk of necrotizing enterocolitis in very low birth weight infants. Journal of Perinatology *27*, 428–433.

Spence, J.R., Mayhew, C.N., Rankin, S.A., Kuhar, M., Vallance, J.E., Tolle, K., Hoskins, E.E., Kalinichenko, V.V., Wells, S.I., Zorn, A.M., et al. (2011). Directed differentiation of human pluripotent stem cells into intestinal tissue in vitro. Nature *470*, 105–109.

Watson, C.L., Mahe, M.M., Múnera, J., Howell, J.C., Sundaram, N., Poling, H.M., Schweitzer, J.I., Vallance, J.E., Mayhew, C.N., Sun, Y., et al. (2014). An in vivo model of human small intestine using pluripotent stem cells. Nat. Med. *20*, 1310–1314.

Zorn, A.M., and Wells, J.M. (2009). Vertebrate endoderm development and organ formation. Annu. Rev. Cell Dev. Biol. *25*, 221–251.

Table 1 – A summary of molecular indicators of intestinal maturation in this study

Protein marker	Type of protein	Description of role in marking maturation
Chromogranin A (CHGA)	Neuroendocine secreted protein	Secreted by enteroendocrine cells. The emergence of enteroendocrine cells is thought to be an indicator maturation.
Claudin 3 (CLDN3)	Tight-junction protein	Indication of improved epithelial barrier integrity and reduced intestinal permeability.
Defensin, alpha 5 (DEFA5)	Host defense peptide	Secreted by functional Paneth cells, and involved in host defense.
Olfactomedin 4 (OLFM4)	Anti-apoptotic factor; extracellular matrix glycoprotein	Mature stem cell marker. Sporadically expressed in immature crypts but becomes ubiquitously expressed in mature crypts.
Sucrase isomaltase (SI)	Glucosidase enzyme	Produced by mature enterocytes.
Ulex Europaeus agglutinin 1 (UEA1)	Glycoprotein-binding lectin	Binds to fucosylated glycoproteins of enterocytes, goblet cells, and Paneth cells. Has protective role in gut infection.

Figure 1

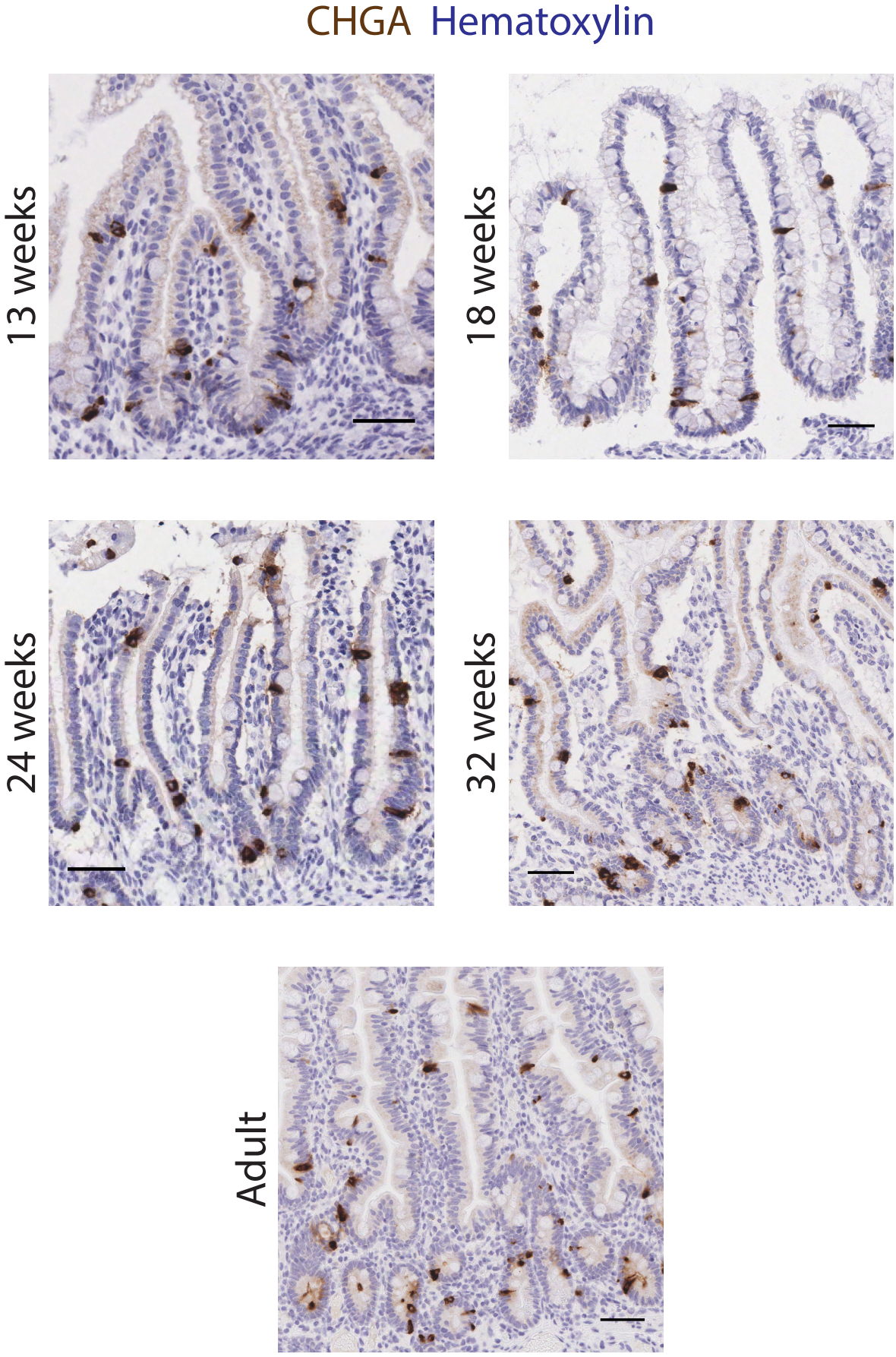

Figure 1 - Chromogenic IHC staining for CHGA of gestational and adult human intestine. Scale bar 50µm.

Figure 2

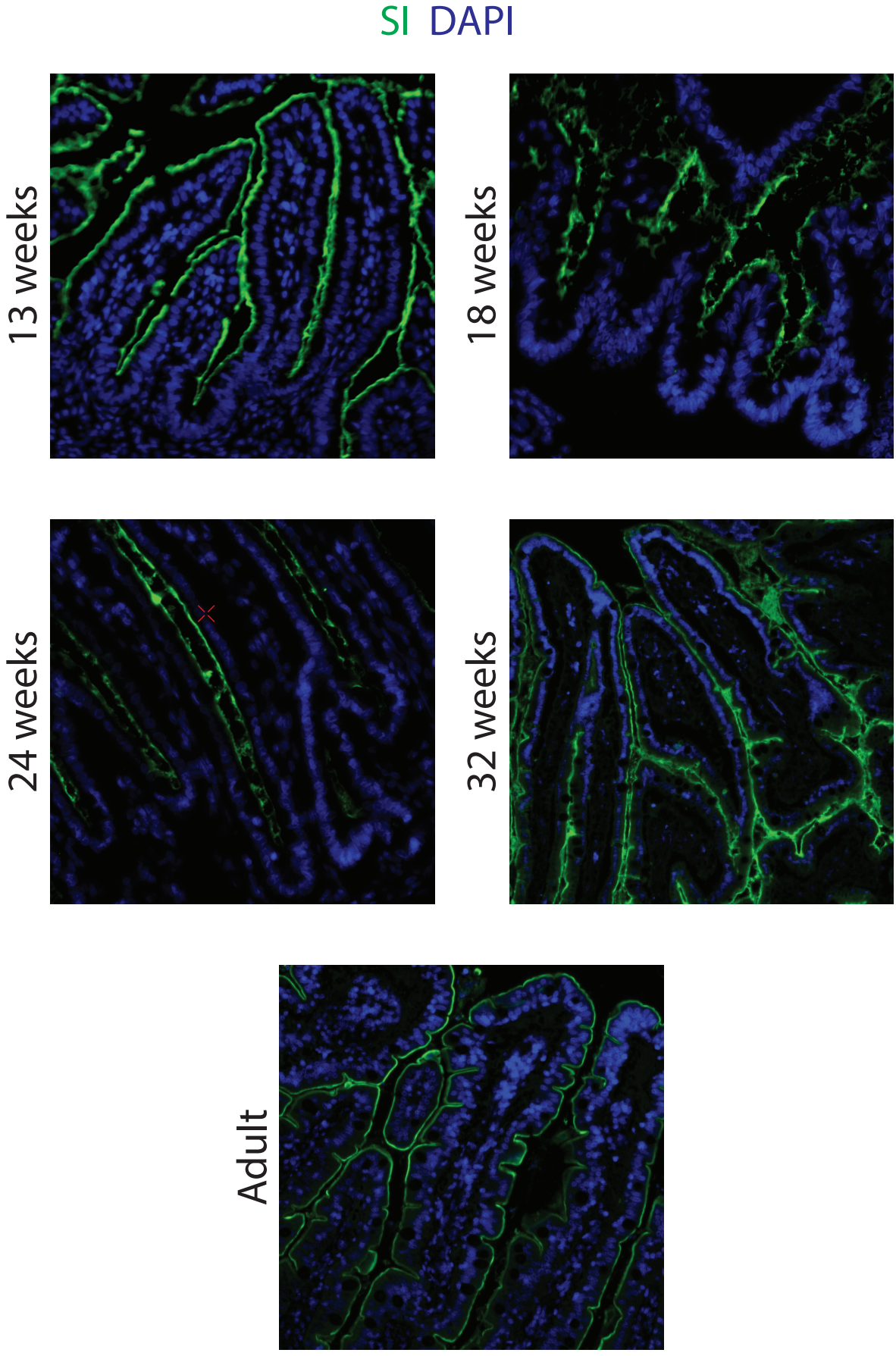

Figure 2 - Immunofluorescent IHC staining for SI of gestational and adult human intestine. Scale bar 50µm.

Figure 3

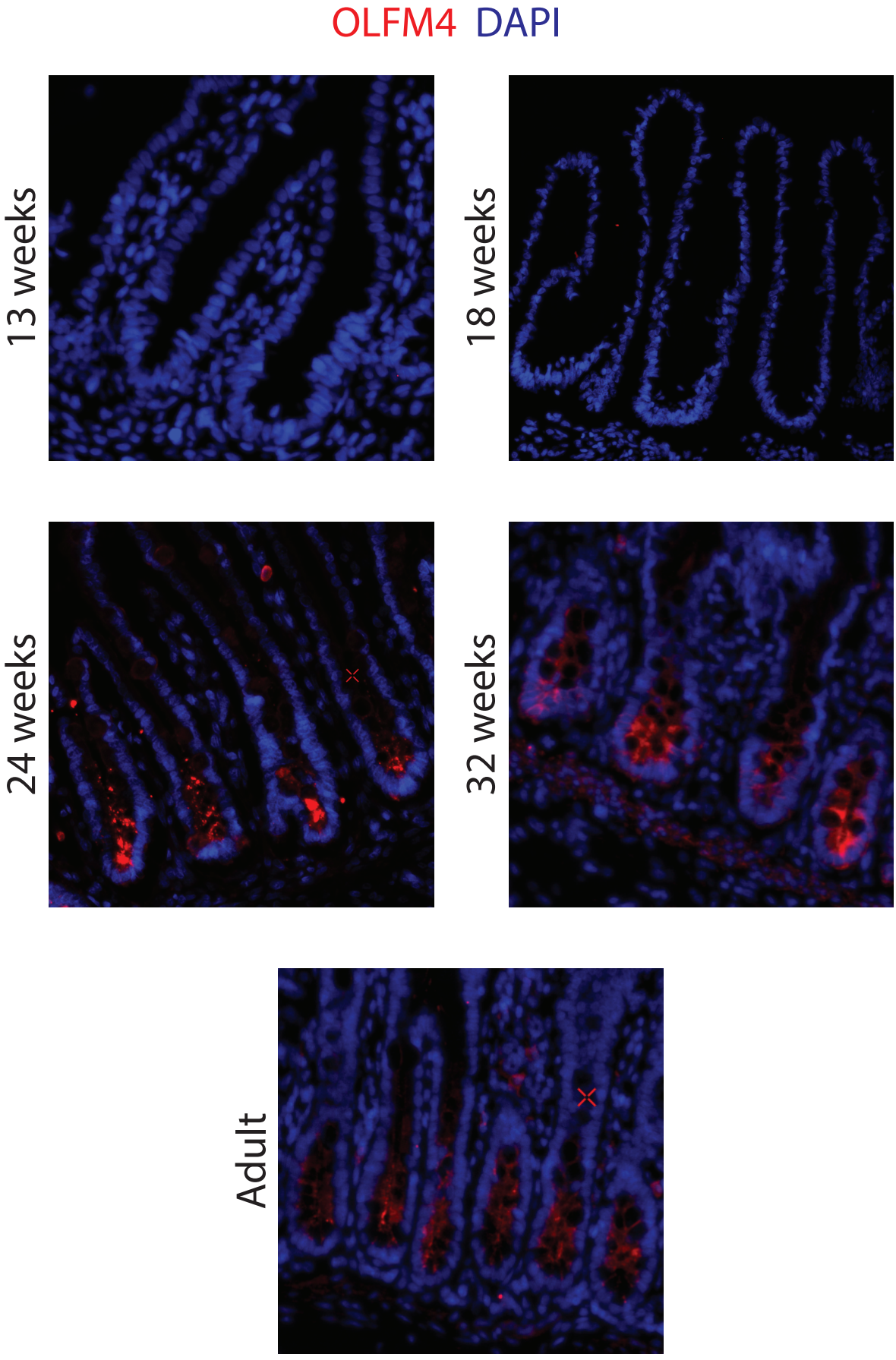

Figure 3 - Immunofluorescent IHC staining for OLFM4 of gestational and adult human intestine. Scale bar 50µm.

Figure 4

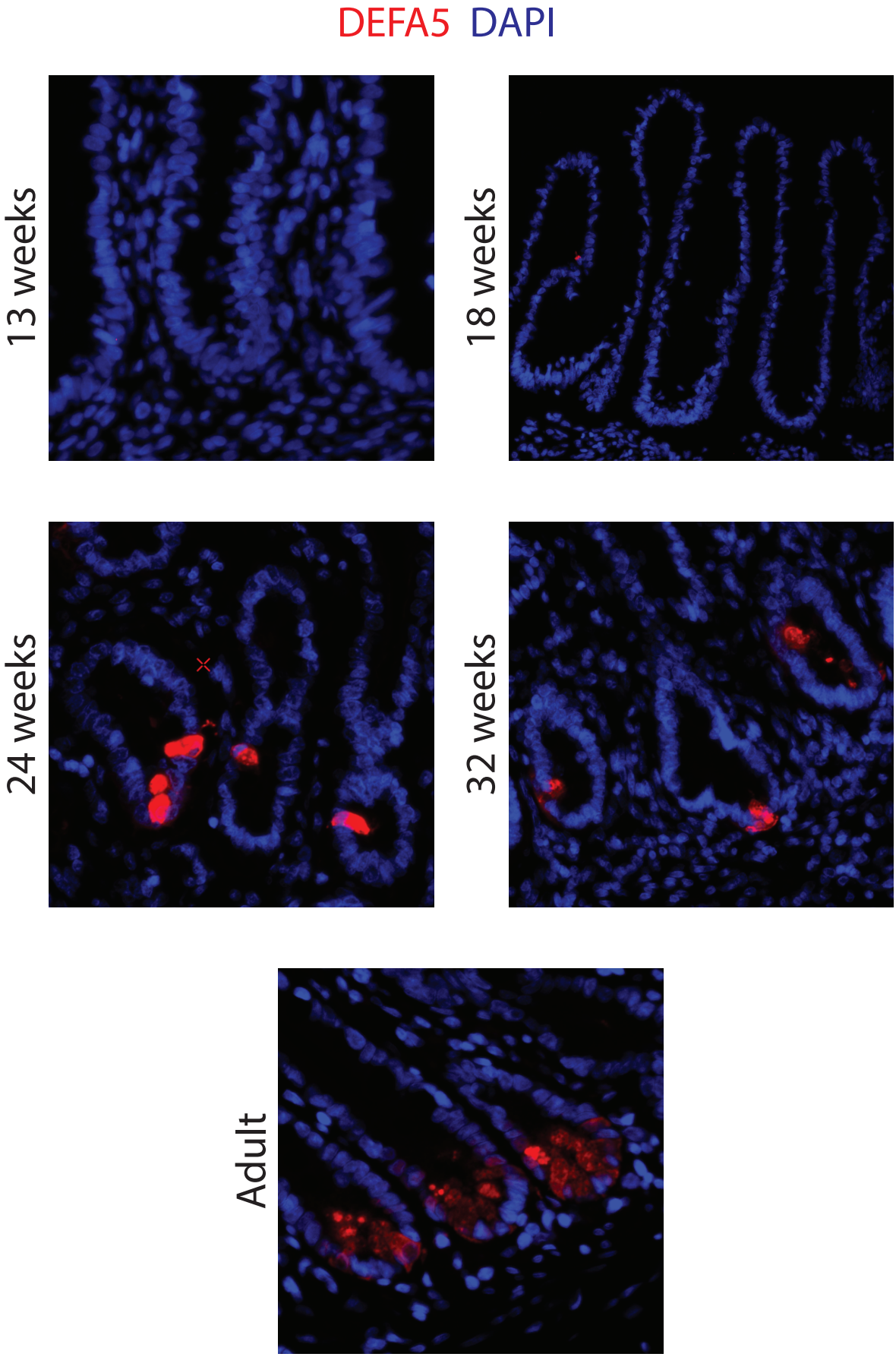

Figure 4 - Immunofluorescent IHC staining for DEFA5 of gestational and adult human intestine. Scale bar 50μm.

Figure 5

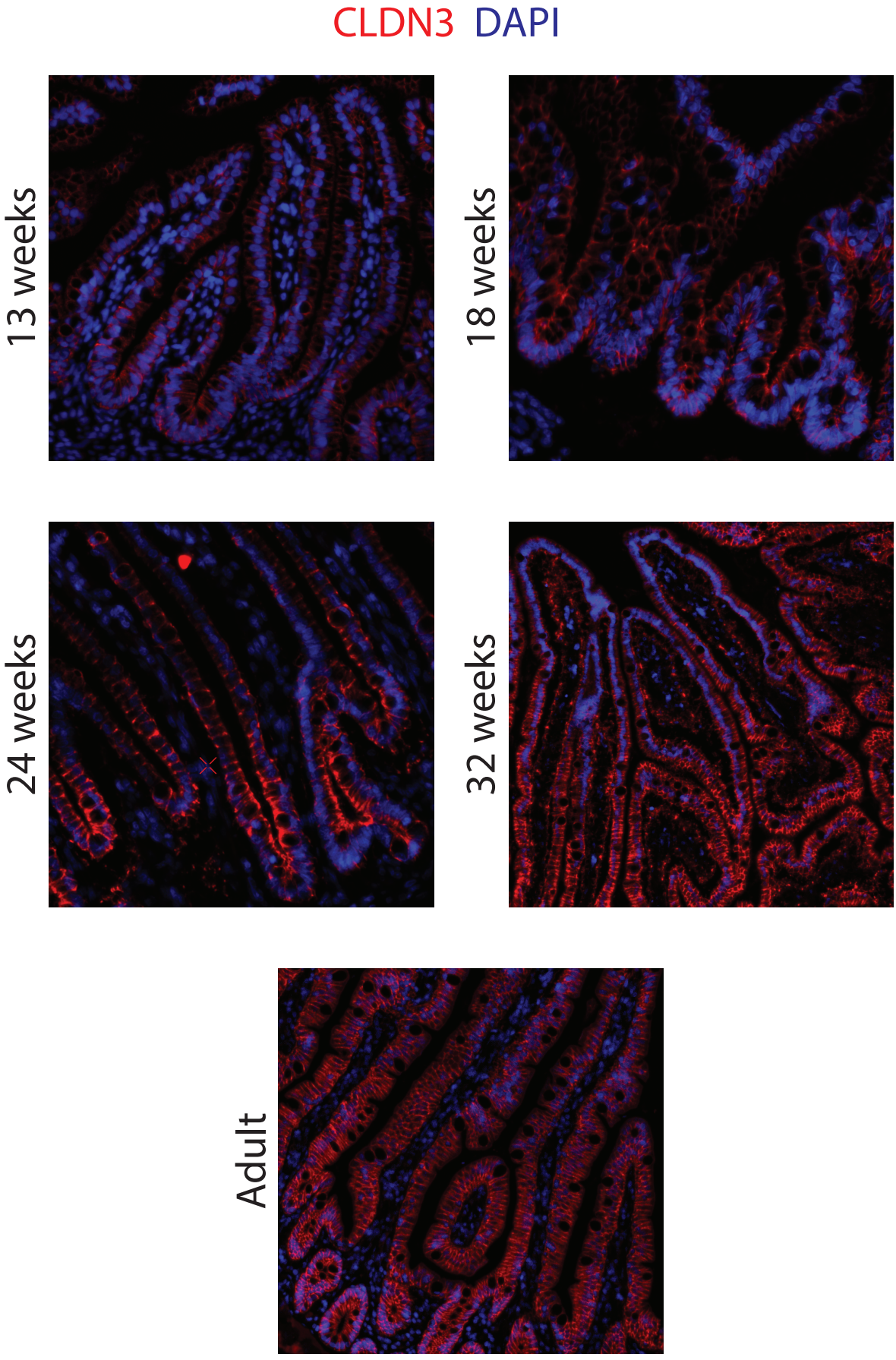

Figure 5 - Immunofluorescent IHC staining for CLDN3 of gestational and adult human intestine. Scale bar 50µm.

Figure 6

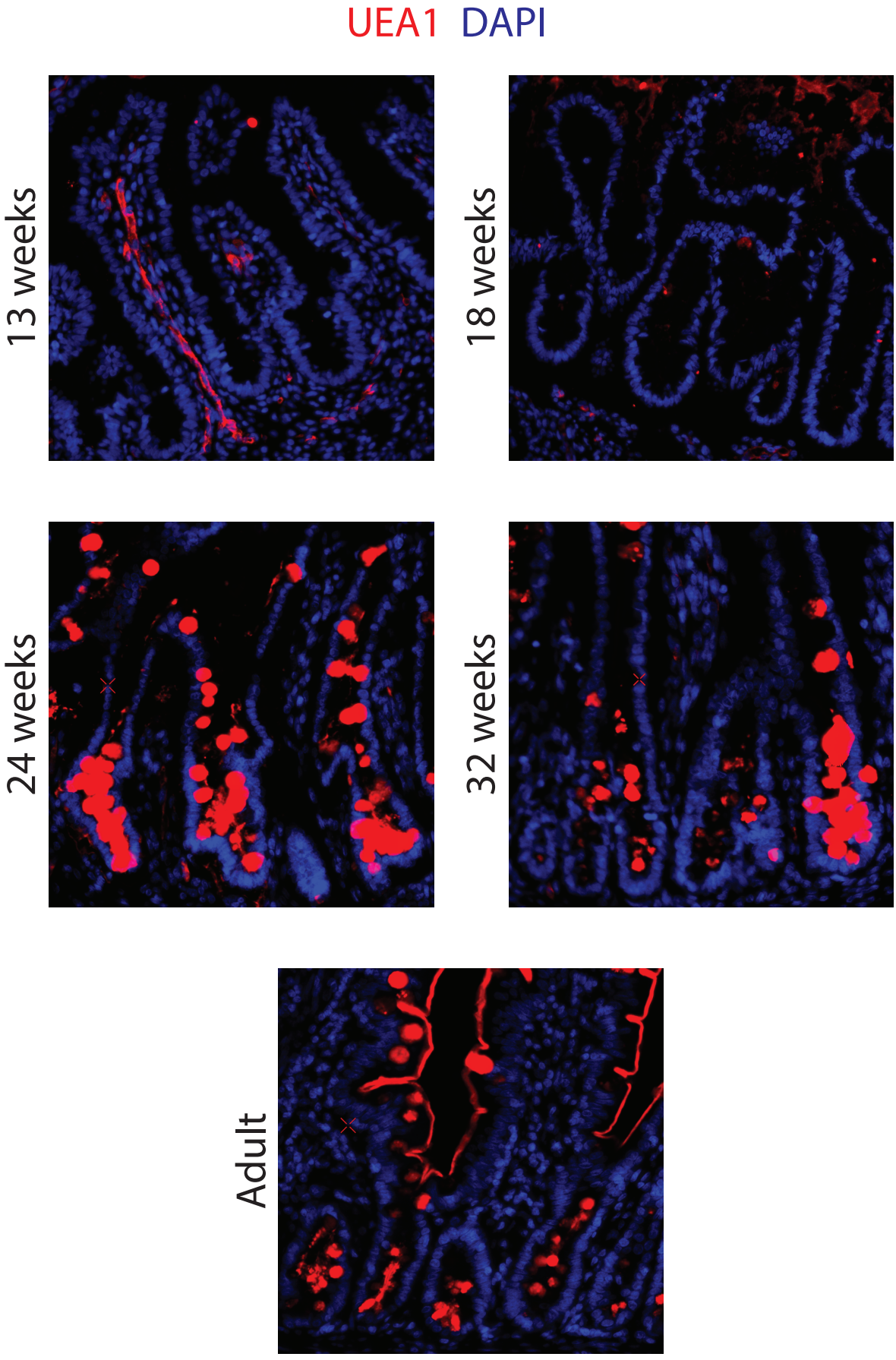

Figure 6 - Fluorescent staining for the lectin UEA1 of gestational and adult human intestine. Scale bar 50µm.

Figure 7

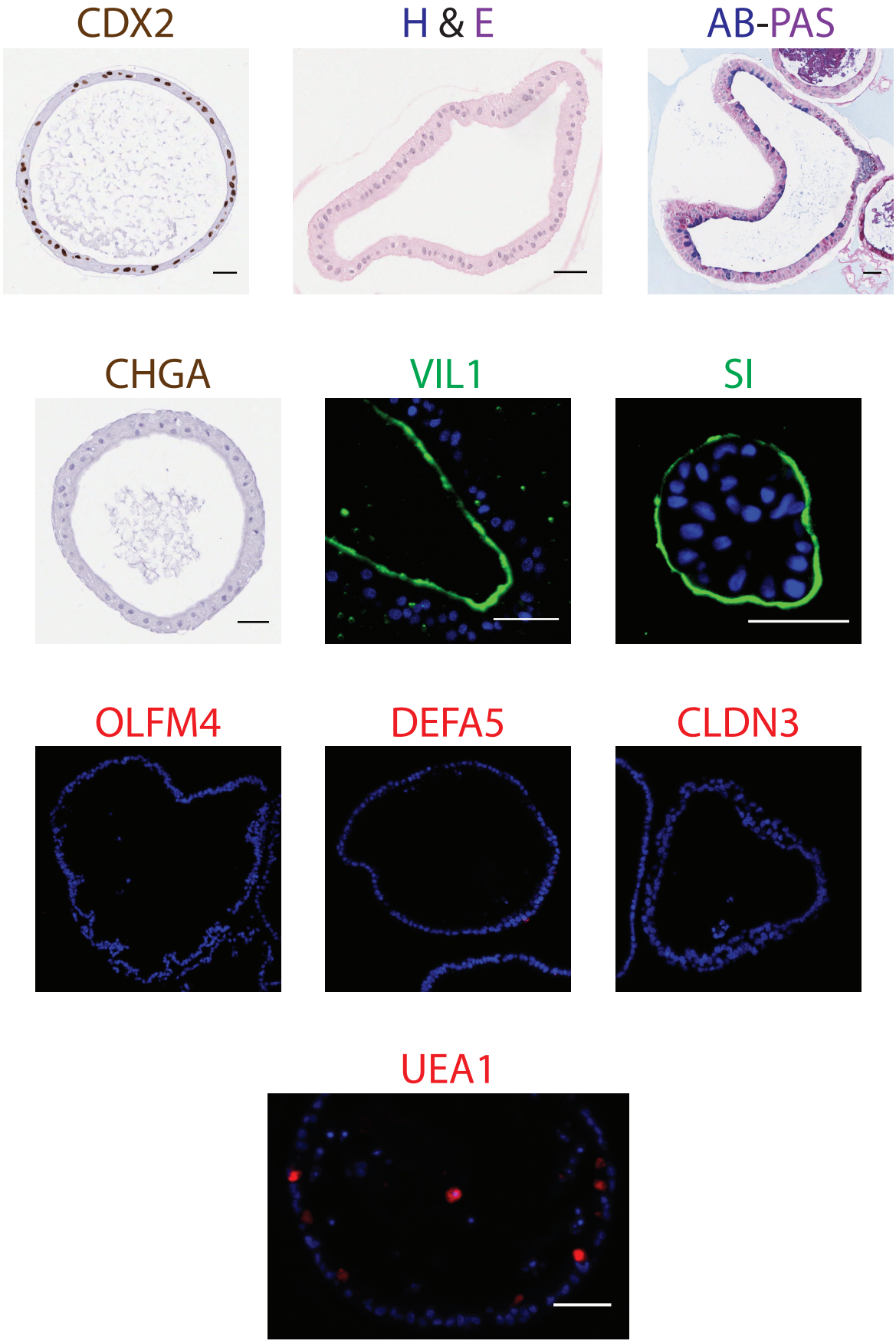

Figure 7 - Immunostaining of hEnS for markers of intestinal maturation. Scale bar 50µm.

Figure S1

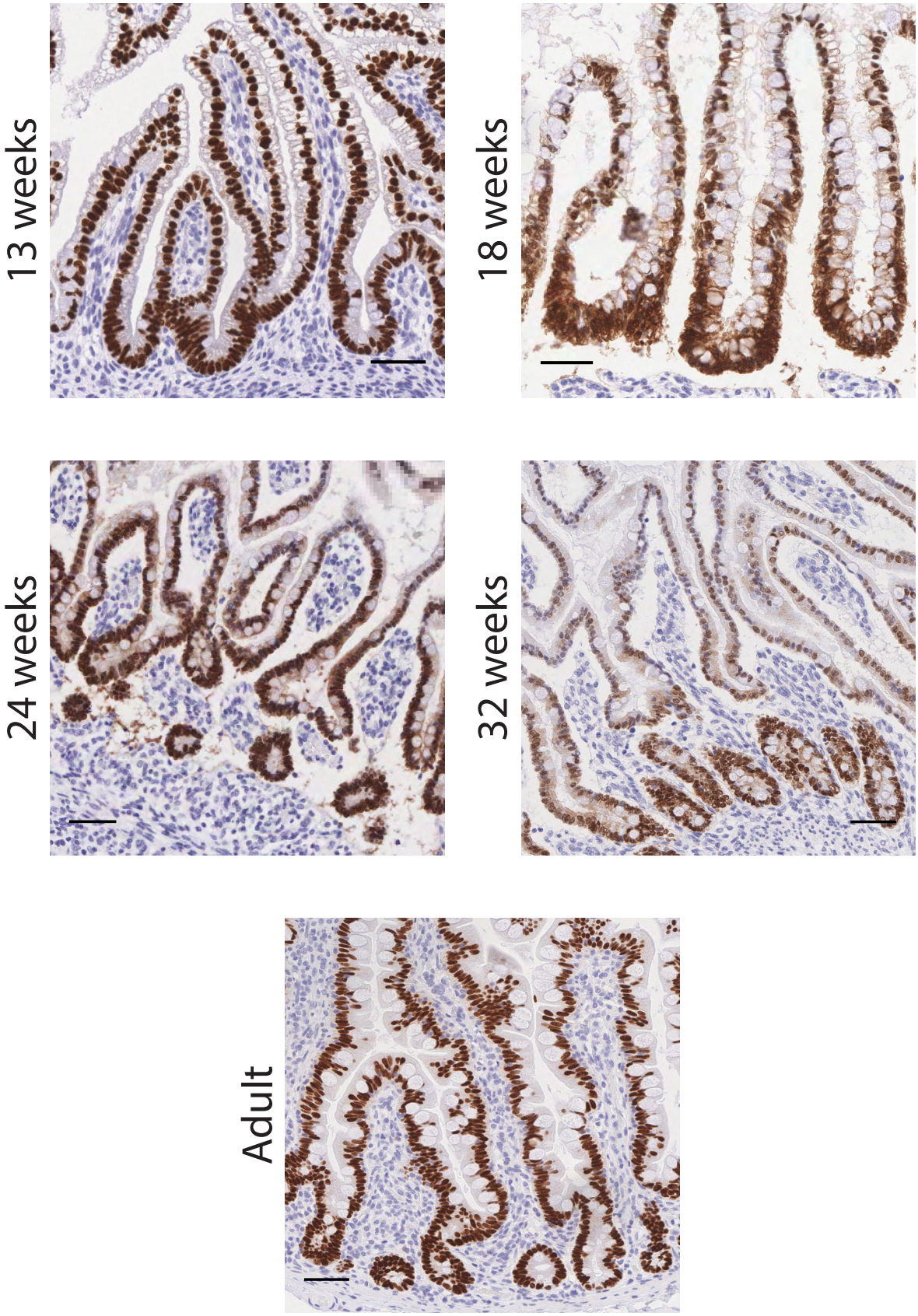

Figure S1 - Chromogenic IHC staining for CDX2 of gestational and adult human intestine. Scale bar 50µm.

Figure S2

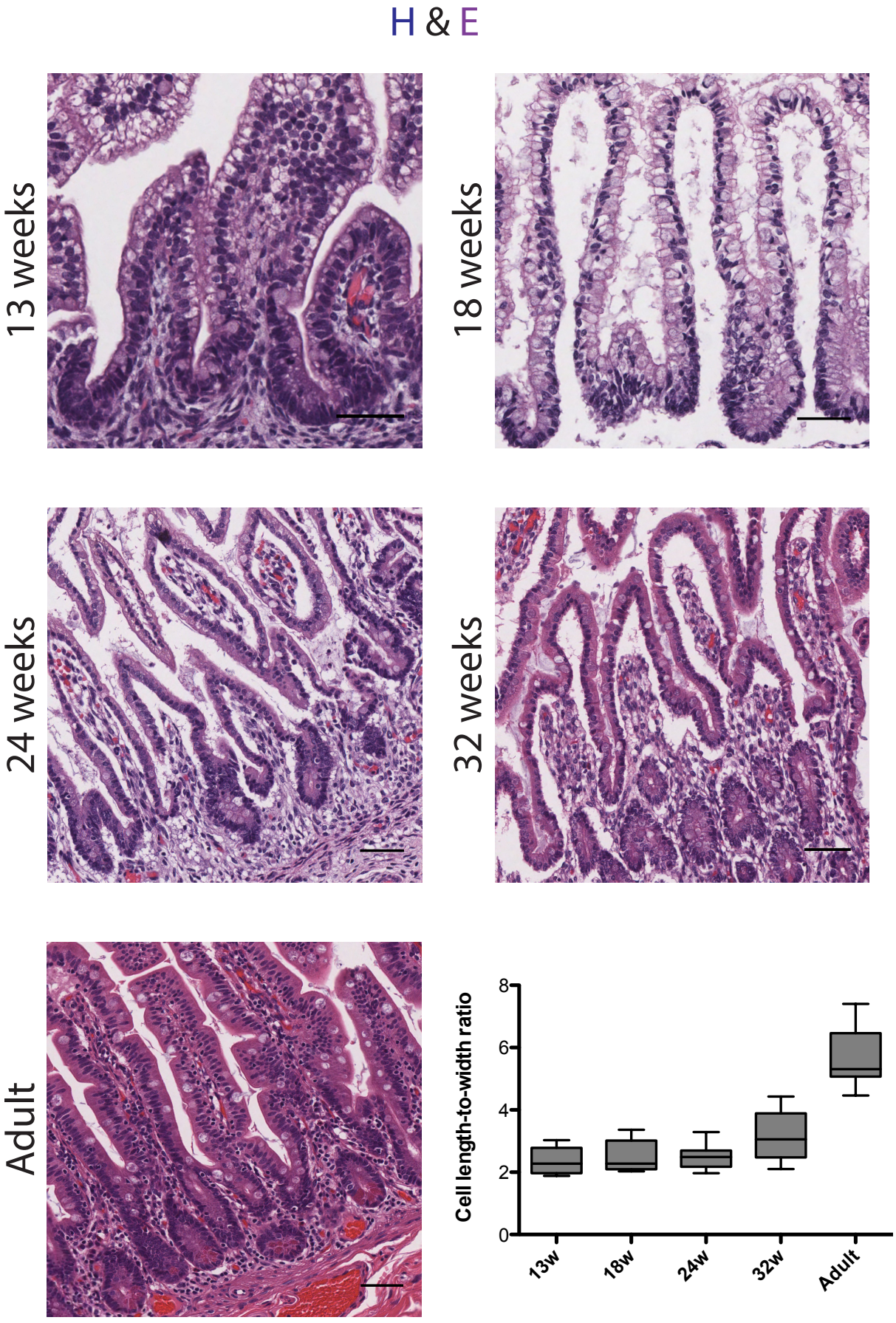

Figure S2 - H&E staining of gestational and adult human intestine, and measurement of average cell length-to-width ratio (mean ± SEM). Scale bar 50µm.

Figure S3

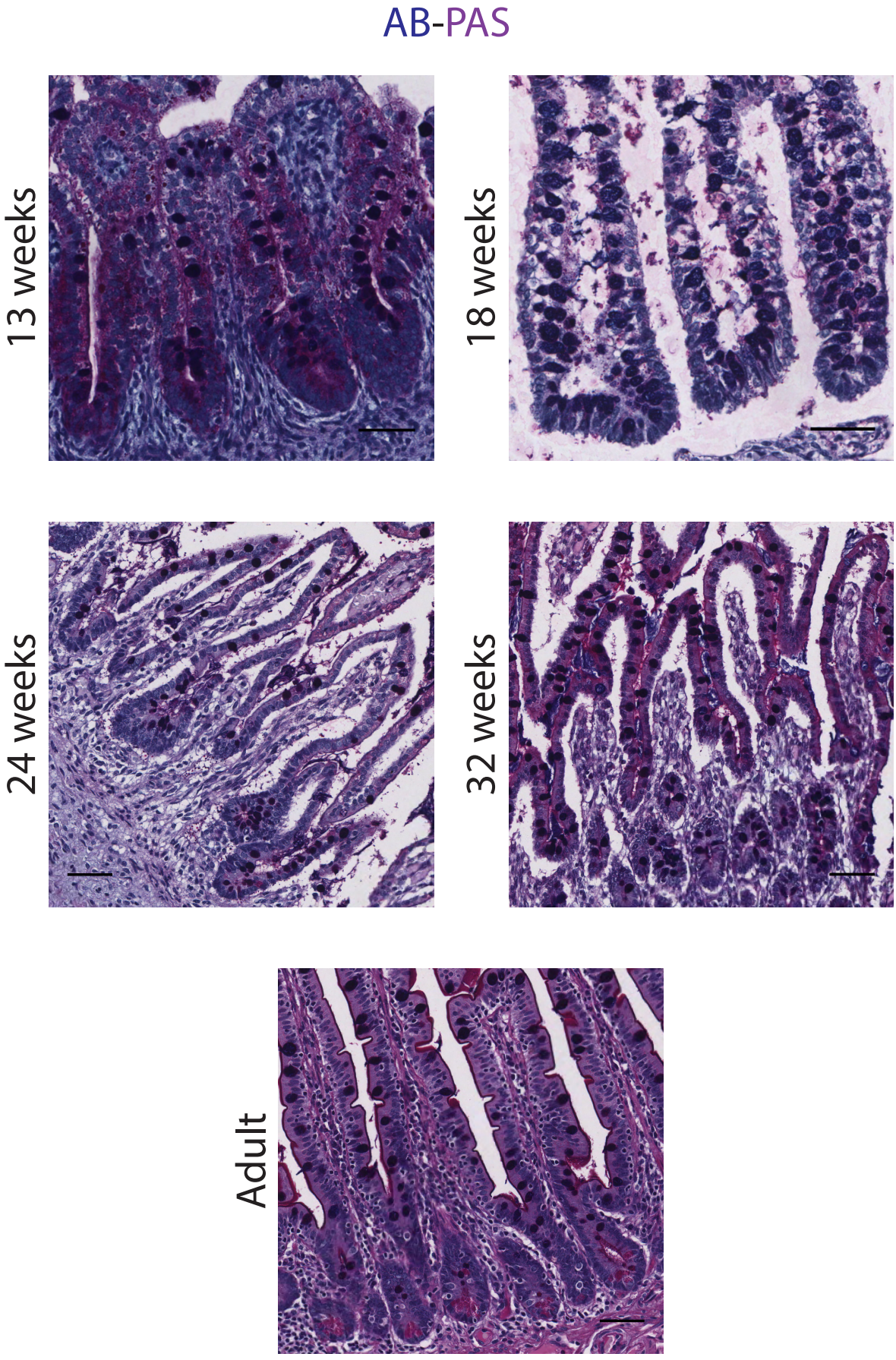

Figure S3 - AB-PAS staining of gestational and adult human intestine. Scale bar 50µm.

Chapter 2.4 – Modeling bacterial-host interactions and intestinal maturation *in vitro* with hEnS

Preface

This chapter builds on the previous one and addresses aim III of the research goal. The idea of this part of the project was conceived during the publication of the work presented in Chapter 2.2. This study was done in collaboration with Dr. Michael G. Surette's lab, which provided bacterial strains. Experimental work began in August 2017, and was performed primarily by me with help from undergraduate student Young-Jin Cheon and graduate student Amos Lim from the Draper lab. The work in this part of the project is ongoing and will continue after I depart the lab.

BACKGROUND

Studying intestinal development and maturation is important for understanding which factors lead to a healthy intestine, and for preventing and treating neonatal diseases like NEC and early-onset IBD. Intestinal maturation can be defined as functional changes that occur beyond morphogenesis and differentiation into intestinal cell types, which is marked by changes in expression of key molecular markers, improvement of structural integrity, and host defense. Studies in animals have shown that postnatal intestinal maturation largely depends on the presence of gut microbes and their secreted products. For example, the intestines of germ-free mice colonized with probiotic bacterial strain *Lactobacillus rhamnosus* show improvement in epithelial barrier integrity, marked by emergence of the expression of tight-junction protein Claudin-3 (CLDN3) and reduced intestinal permeability (Patel et al., 2012). Fucosylation is a type of glycosylation where fucose units are added to glycoproteins, which has a protective role in both gut and systemic infection and inflammation by suppressing the virulence of harmful pathogens (Pickard and Chervonsky, 2015). Colonization of the gut with the bacterial species *Bacteriodes thetaiotaomicron* or treatment with bacteria-secreted polyamines has been shown to induce fucosylation of intestinal brush border and mucinous glycoproteins in germ-free mouse and rat models (Biol-N'Garagba et al., 2002; Bry et al., 1996; Capano et al., 1994; Dufour et al., 1988). The use of probiotic bacteria can contribute to proper intestinal maturation in premature infants at risk of NEC or IBD (Alfaleh et al., 2011; Grave et al., 2007; Guandalini, 2010; Klement et al., 2004; Sisk et al., 2007).

Most of the current understanding of human intestinal development and maturation has been extrapolated from studies in animals, but the timeline of intestinal

development between humans and mice is different. Intestinal morphogenesis in humans is complete before birth, whereas in mice it is complete several weeks after birth, coinciding with exposure to enteric bacteria (Chin et al., 2017; McCracken and Lorenz, 2001). In fact, we showed in Chapter 2.3 that multiple protein markers of intestinal maturation emerge before birth in humans, while they have been observed to emerge after birth in mice. Therefore, it is poorly understood whether putative maturation-inducing factors discovered in animal models have a similar effect in humans.

An *ex vivo* approach using human tissues is needed to study intestinal maturation in humans. Intestinal organoids derived from hPSCs *in vitro* mimic native intestinal architecture, function, are germ-free and typically fetal-like (Finkbeiner et al., 2015; Fordham et al., 2013; Spence et al., 2011), representing a more physiological model of the developing intestine in contrast to their primary adult counterparts or immortalized cell lines. Advantages of a germ-free system are that it provides a blank slate for studying interactions with bacteria, and avoids heterogeneity that may exist among different patient-specific organoids due to the influence of a unique microbiome. hPSC-derived intestinal organoids have been used to model the interaction of *E.coli* and *Salmonella enterica* with the intestine to mostly study the role of these pathogens in modulating innate immunity (Forbester et al., 2015; Hill et al., 2017). In the context of maturation, engraftment of hPSC-derived lung and intestinal organoids under the kidney capsule of mice for several months induces further differentiation and maturation of the organoids, marked by morphological changes and emergence of protein markers observed in adult tissues (Dye et al., 2016; Finkbeiner et al., 2015; Watson et al., 2014). However, the *in vivo* approach has been shown to introduce contaminating cell types into organoids post-

isolation that persist for several passages (Forster et al., 2014), and there is a risk of transmitting zoonotic agents from the animals into organoid cultures. The engraftment-based strategy is largely undefined and does not provide an understanding of the specific factors or interactions that stimulate maturation. Therefore, using organoid models to study the role of enteric bacteria in intestinal maturation remains largely unexplored. Since hEnS are fetal-like and germ-free, they represent a valuable model system for studying early host-microbe interactions and intestinal maturation.

RESULTS

In Chapter 2.2, we established populations of hEnS and showed that they respond to signaling cues consistent with intestinal epithelial function and can be cultured long-term. We also showed that hEnS provided a model for studying functional gastrointestinal responses by testing their ability to elicit an innate immune response when treated with LPS or enteric pathogens (Nadkarni et al., 2017). Our next work was to demonstrate the utility of hEnS in modeling host-microbe interactions and intestinal maturation.

Development of an automated hEnS imaging assay to measure responses to exogenous factors

The complexity of the gut microbiome requires an assay to test individual bugs and bacterial products that modulate intestinal maturation. We therefore set out to design a hEnS screening platform to enable such testing. We first developed an automated hEnS imaging assay to determine the effects of growth factors and bacterial products on hEnS-

forming frequency and size. These properties were previously measured manually using tools on ImageJ. However, this was not feasible for experiments that would include several wells and conditions, and therefore required the measurement process to be automated. Calcein-based imaging of hEnS was used for automated quantitation of number and size of spheres generated per well (Dekkers et al., 2013). Calcein AM is a non-fluorescent cell-permeant dye that is converted to a green fluorescent calcein in live cells. Brightfield and calcein images of wells **(Figure 1A)** were captured on the Operetta High-Content Imaging System (PerkinElmer) in the SCC-RI. Dr. Tony Collins wrote a script for the software Acapella, taking into account the size range of the spheres, which automatically counted and measured properties like area and roundness. We optimized a number of parameters: plate format (96-well plate), number of cells seeded per well (5k), volume of Matrigel which houses the hEnS (60µL), lack of feeder cells, calcein AM dose (1µM), and scanning distance (700µm). Other useful information about hEnS structure could also be collected from images of calcein-stained hEnS populations such as internal density **(Figure 1B)**, a relative measure of lobulation and proliferative ability (Sato et al., 2011). The mean integrated density of complex budding structures was about double that of cystic spheroids that were composed of a thinner epithelium **(Figure 1C**).

We first sought to evaluate our hEnS imaging assay by testing growth factors/compounds with known impact on intestinal stem cells. Inhibition of the Rho-associated protein kinase (ROCK) pathway promotes cell survival and proliferation (Nadkarni et al., 2017; Watanabe et al., 2007). Treatment of hEnS throughout culture for 14 days with Y-27632, a ROCK inhibitor, generated slightly more spheres than control samples and which were larger in size **(Figures 2A-B)**. Addition of SU5402, an inhibitor

of EGFR, FGFR and VEGFR receptors, and LPS which induces apoptosis (Munshi et al., 2002; Xaus et al., 2000), halved the sphere-forming efficiency and those that formed were significantly smaller in size **(Figures 2A-B)**. The detrimental activity of LPS on sphere numbers and size was less severe when treated for a shorter duration **(Figures 2C-D)**. Addition of sodium butyrate, a short-chain fatty acid (SCFA) and an inhibitor of intestinal stem cell proliferation (Kaiko et al., 2016), reduced sphere-forming efficiency in a dose-dependent manner, while sodium acetate and sodium propionate had visibly less impact **(Figures 2E-F**) (Kaiko et al., 2016). Therefore, our hEnS imaging assay accurately detected responses to factors that have known activity on intestinal stem cells.

Using the hEnS imaging assay to measure responses to enteric bacterial exposure

After validating the hEnS imaging assay using compounds, hEnS were treated with commensal isolates of enteric bacteria to determine their effect on hEnS-forming frequency **(Figure S1)**. This work was done in collaboration with Dr. Michael Surette, whose lab provided heat-killed bacteria and supernatants. Since hEnS were being co-cultured for 14 days with bacteria, heat-killed cells were used in our experiments to avoid the adverse effects that live dividing cells would have on hEnS mortality. Although this is a limitation of the model in recapitulating the interaction *in vivo*, heat-inactivated bacteria have been shown to be just as effective as live bacteria in inducing innate immune responses and intestinal maturation in animal models (Hill et al., 2017; Li et al., 2009; Patel et al., 2012). Also, bacterial supernatants, or the decanted media in which bacterial strains were grown, were tested against heat-killed cells because in theory they contain secreted products. We tested heat-killed *E. coli* at MOIs of 10:1, 100:1 and 1000:1, and

E. coli supernatants at 1%, 5% and 10% of hEnS culture media. All three MOIs slightly reduced the hEnS-forming frequency but the impact of a higher MOI (1000:1) was not more severe than 10:1 or 100:1 **(Figure 3A)**. However, when treated with bacterial supernatant, the hEnS-forming frequency decreased in a concentration-dependent manner **(Figure 3B**), with 10% reducing the frequency by more than half. This suggests that an MOI of 1000:1 for heat-killed bacteria and 5% bacterial supernatant are suitable parameters for allowing enough hEnS to form per well to then harvest and analyze.

We then tested the impact of bacterial pathogenicity on the activity of intestinal stem/progenitor cells by measuring hEnS-forming frequency, which has not been explored in the field. We hypothesized that probiotic bacteria would increase the numbers of spheres produced relative to untreated control, benign bacteria would have no change, and pathogenic strains would reduce the number. Probiotic strain *Lactobacillus rhamnosus* (LrGG), pathogenic strain *Clostridium innocuum*, and a benign strain of *E. coli* were chosen. hEnS precursor cells treated with 5% supernatant in the hEnS culture media of LrGG and *E. coli* throughout culture for 14 days only slightly reduced hEnS-forming frequency compared to untreated control, whereas treating with *Clostridium innocuum* did not give rise to any spheres **(Figure 3C)**. This data shows that the hEnS imaging assay may be used in characterizing the impact of bacterial strains on hEnS formation.

hEnS treated with probiotic bacteria show increased CLDN3 expression

Using organoid models to study the role of enteric bacteria in intestinal maturation has not been explored. We asked if hEnS maturation can be induced *in vitro*

upon treatment with probiotic bacteria. Improvement of epithelial barrier integrity is one measure of intestinal maturation. A previous study showed that the intestines of germ-free mice when treated with heat-inactivated cells of the probiotic strain LrGG had increased expression of the tight-junction marker CLDN3 in the intestinal epithelium at the transcript and protein level, which is a mechanism of epithelial barrier tightening (Patel et al., 2012). Similarly, we found that treating hEnS with bacterial supernatant (5%) or heat-killed cells (MOI of 1000:1) of *LrGG* induced an increase in transcript levels of *CLDN3* **(Figure 3D)**. However, CLDN3 protein expression was not detected in *LrGG*-treated and untreated hEnS via immunofluorescence (data not shown).

Penetrating the hEnS epithelial barrier with fluorescent polymers to measure diffusion

In the native intestine, bacteria interact with the apical surface of the epithelium. In hEnS, this is equivalent to the luminal space. Microinjection of heat-killed bacteria into hEnS may be used as a validation assay for bacterial infiltration of the intestinal epithelium. As a technical demo, we showed that the lumen of hEnS could be microinjected with a fluorescently-tagged polymer FITC-Dextran-4kDa (FD4) **(Figure S2A)**, and that FD4 particles largely remained inside the spheres for 9 hours **(Figure S2B)**. Treatment with 2mM EGTA, a chelator of calcium ions, after 9 hours induced damage to the epithelium and resulted in most FD4 seeping out **(Figure S2B)**. We also showed that treating intact spheres with 2mM EGTA while also administering 1mg/ml FD4 for 1 hour at 37°C permitted FD4 entry into the spheres to some extent, whereas untreated spheres took up little to no FD4 **(Figures S2C-D)**.

DISCUSSION

Chapter 2.4 focused on exploring bacterial-host interactions and intestinal maturation using hEnS as a model system. The establishment of an automated hEnS imaging assay is important for consistent, reproducible measurements, surveying large libraries of bacteria and compounds, and accelerating research in this area. The imaging assay proved successful for rapidly taking measurements of hEnS-forming frequency and size in our initial experiments where hEnS were treated with compounds and bacterial supernatants.

We found that an MOI of 1000:1 for heat-killed bacteria and 5% bacterial supernatant are suitable parameters for allowing enough hEnS to form per well. However, we noticed in some experiments that hEnS populations became unhealthy, and a fraction of spheres underwent necrosis, due to stress from prolonged exposure to heat-killed cells or bacterial supernatant. Therefore, hEnS culture conditions need to be optimized such that they survive bacterial treatment long enough to be harvested for analysis including transcript and protein expression analysis.

One of the major limitations of our model is that hEnS are exposed to bacteria on the basal side instead of the apical side, which is how the interaction occurs *in vivo*. The results of hEnS microinjection with FD4 are a technical demo for validation assays of microinjecting heat-killed bacteria into the hEnS lumen to recapitulate bacterial interaction with the apical surface of intestinal epithelium. Nevertheless, our hEnS imaging assay which utilizes a culture system in which hEnS are embedded in a 3D gel layer overlayed with media proved to be effective in generating responses to exogenous factors including bacteria, and simplifies large-scale screening of factors on hEnS

populations. Microinjection of heat-killed bacteria into the lumen of hEnS may be used as a back up for validation.

Majority of the data in Chapter 2.4 is preliminary, so experiments need to be repeated to determine if consistent results are obtained, and for statistical analysis. It should be noted that most of the work in Section 2 was performed on hEnS derived from the H1 human ESC line, so it is important to test hEnS from additional hPSC lines to ensure that experimental results are not unique to one line.

As mentioned earlier, the majority of literature focuses on intestinal maturation studies performed *in vivo* in animals, leading to the identification of specific maturation-inducing microbes (Biol-N'Garagba et al., 2002; Bry et al., 1996; Dufour et al., 1988; Patel et al., 2012). It needs to be determined whether maturation can be induced *ex vivo* in primary mouse or rat fetal enterospheres using the same stimuli that were tested *in vivo* to understand if other components or cell types systemically available participate in the maturation process, and are not captured in an *in vitro* epithelial organoid model. If this is the case, it is a limitation of using organoids alone in the dish for asking such questions, and a potential solution would be to co-culture organoids with the supporting cell types accordingly. These include intestinal fibroblasts, which are adjacent to intestinal crypts *in vivo* and secrete growth factors towards the epithelium. Also, as mentioned earlier, since the timeline of intestinal development between humans and mice is different (Chin et al., 2017; McCracken and Lorenz, 2001), the response to individual stimuli may also be different between the species. For example, while CLDN3 protein expression in epithelial tight junctions emerges in the post-natal murine intestine upon exposure to probiotic

LrGG (Patel et al., 2012), we showed in Chapter 2.3 that CLDN3 expression in the human intestine begins before birth.

Finally, we need to more accurately gauge the current developmental status of our established hEnS cultures. One way to achieve this is to do RNA-Seq of our hEnS and compare them with a recently published GEO dataset that consists of primary enterospheres from human fetuses ranging from 11 to 22.5 weeks' gestational age (Senger et al., 2018), as well as functional assays across a range of stages to describe when human intestinal tissue gains functional properties.

EXPERIMENTAL PROCEDURES

Note: See Chapter 2.2 Experimental Procedures about hEnS generation and qRT-PCR.

Use of hEnS imaging assay

hEnS were cultured in a 96-well format (5k cells seeded per well) in a 60µL 3D gel volume per well (30µL of hEnS culture media + 30µL of Growth factor-reduced Matrigel), and overlaid with 60µL of hEnS culture media after 30 minutes of gel polymerization at 37°C. In preparation for imaging, overlaid media was replaced with fresh media containing Calcein-AM (ThermoFisher; 1µM in total well volume) and incubated at 37°C for 30 minutes. Plate(s) was imaged on the Operetta High-Content Imaging System (PerkinElmer) at 2x mag in brightfield and FITC channels, at a scanning distance along the z-axis of 700µm. A script was written by Dr. Tony Collins from the SCC-RI at McMaster University for the software Acapella, which took into account the

size range and shape of the hEnS, and was used for automatically counting sphere numbers and measuring properties like sphere area and roundness.

Treatment of hEnS with compounds and bacteria

Compounds or bacterial supernatants were added to hEnS cells in overlaid media after gel polymerization, while heat-killed bacteria were added at a given MOI into the gel at the time of seeing before gel polymerization. Bacterial strains were cultured by Dr. Michael Surette's lab in cooked meat broth (Sigma) from which bacterial supernatants and heat-killed cells were made. Both were tested for growth to ensure that no living bacterial cells were present.

Figure 1

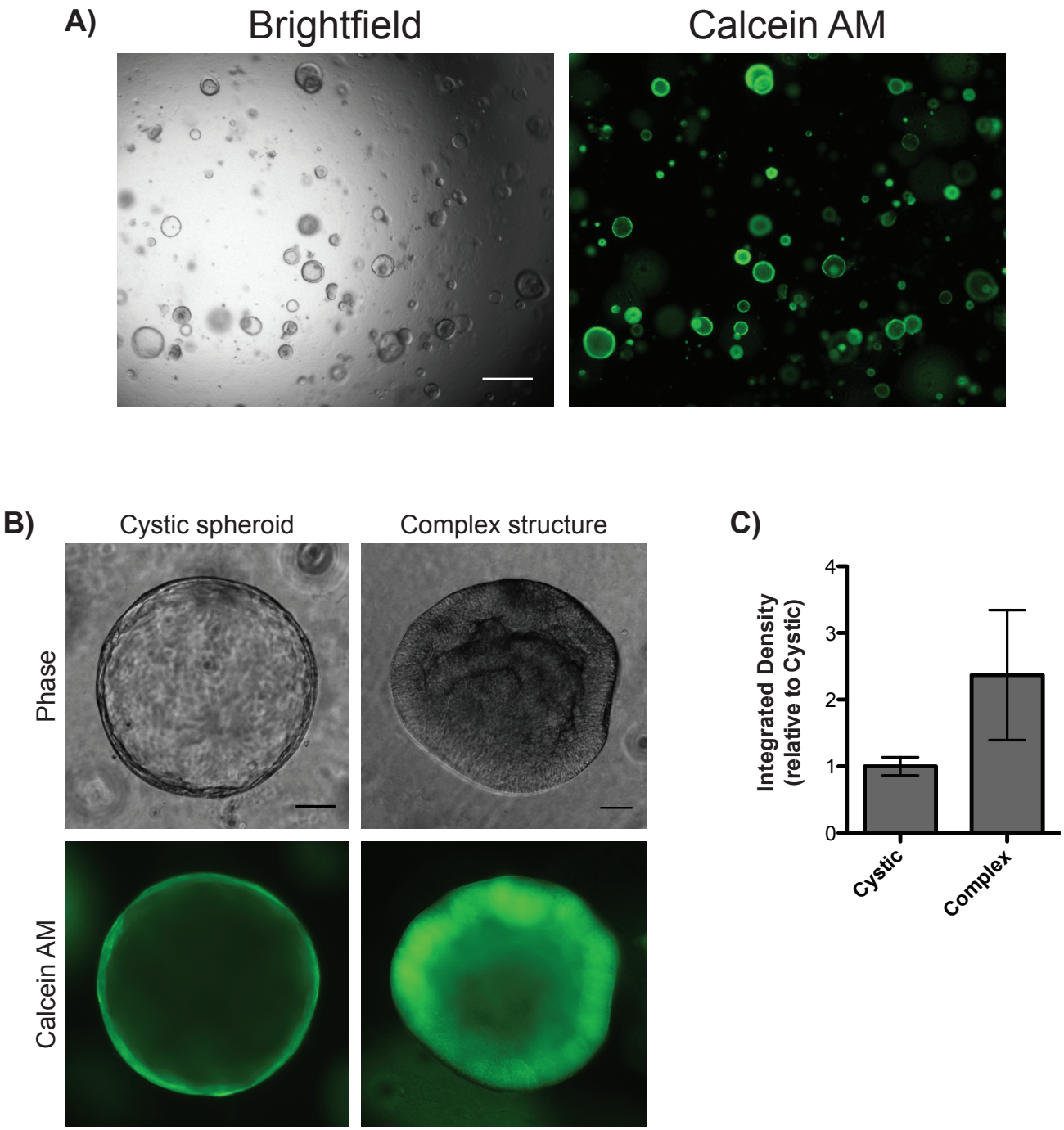

Figure 1 – Calcein-based imaging of hEnS.
A) Representative brightfield (left) and calcein (right) images of hEnS populations.
B) Comparison of cystic spheroids and complex structures stained with calcein.
C) Mean integrated density inside cystic spheroids versus complex structures (mean +/- SEM).
Scale bars: 400 µm (A) and 50 µm (B).

Figure 2

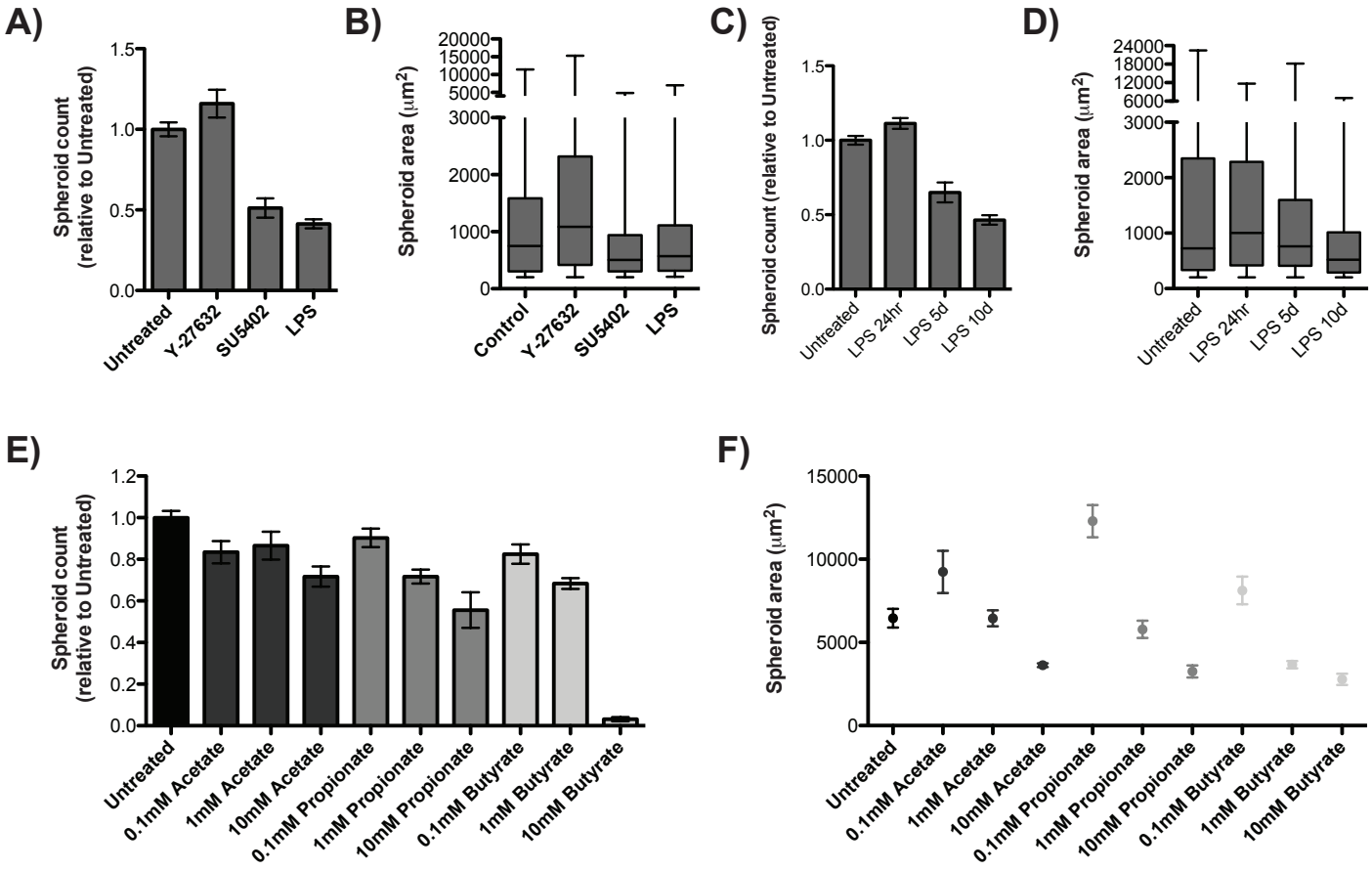

Figure 2 – Use of Calcein AM-based automated imaging assay to measure hEnS-forming frequency and area upon treatment with various compounds.

A) Relative hEnS numbers produced and **B)** sizes (area) upon treatment with basic compounds (mean +/- SEM, n = 1 experiment with 3 technical replicates).

C) Relative hEnS numbers produced and **D)** sizes (area) upon treatment with LPS for different durations (mean +/- SEM, n = 1 experiment with 3 technical replicates).

E) Relative hEnS numbers produced and **F)** sizes (area) upon treatment with three doses each of the SCFAs acetate, propionate and butyrate (mean +/- SEM, n = 1 experiment with 3 technical replicates).

Figure 3

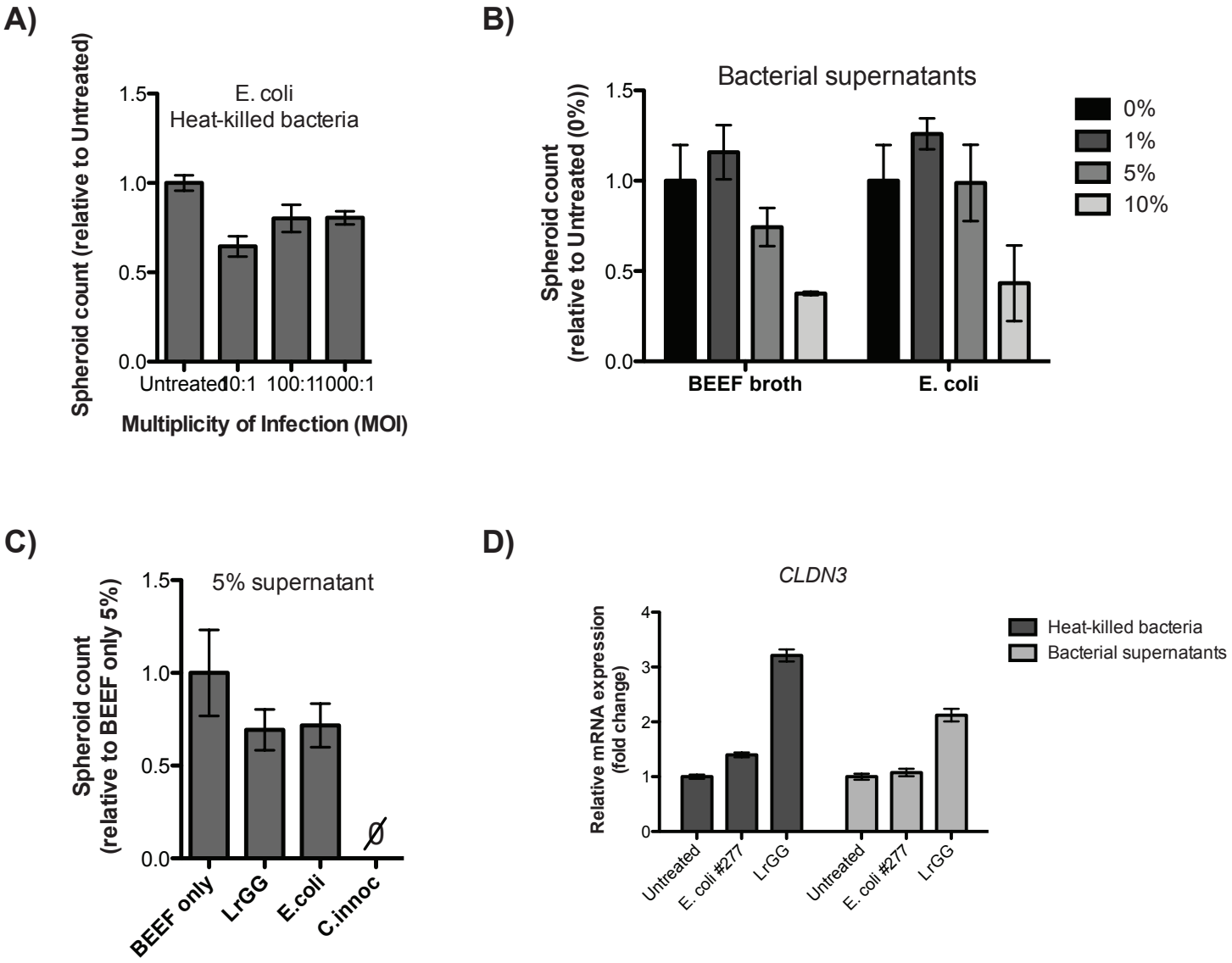

Figure 3 - Impact of heat-killed bacteria and supernatants on hEnS properties.
A) Relative hEnS numbers produced when treated with heat-killed *E. coli* at MOIs of 10:1, 100:1 or 1000:1 (mean +/- SEM, n = 1 experiment with 3 technical replicates).
B) Relative hEnS numbers produced when cultured with different proportions (1%, 5% or 10%) of cooked meat broth or *E. coli* supernatant in the culture media (mean +/- SEM, n = 1 experiment with 3 technical replicates).
C) Relative hEnS numbers produced upon treatment with 5% bacterial supernatant in the culture media of *LrGG, E. coli* and *C. innocuum* (mean +/- SEM, n = 1 experiment with 3 technical replicates).
D) Relative transcript expression levels of *CLDN3* in hEnS treated with supernatants (5%) or heat-killed cells (1000:1) of *E. coli* and *LrGG*; normalized to GAPDH expression (values represent linear fold change, n = 3 independent experiments).

Figure S1

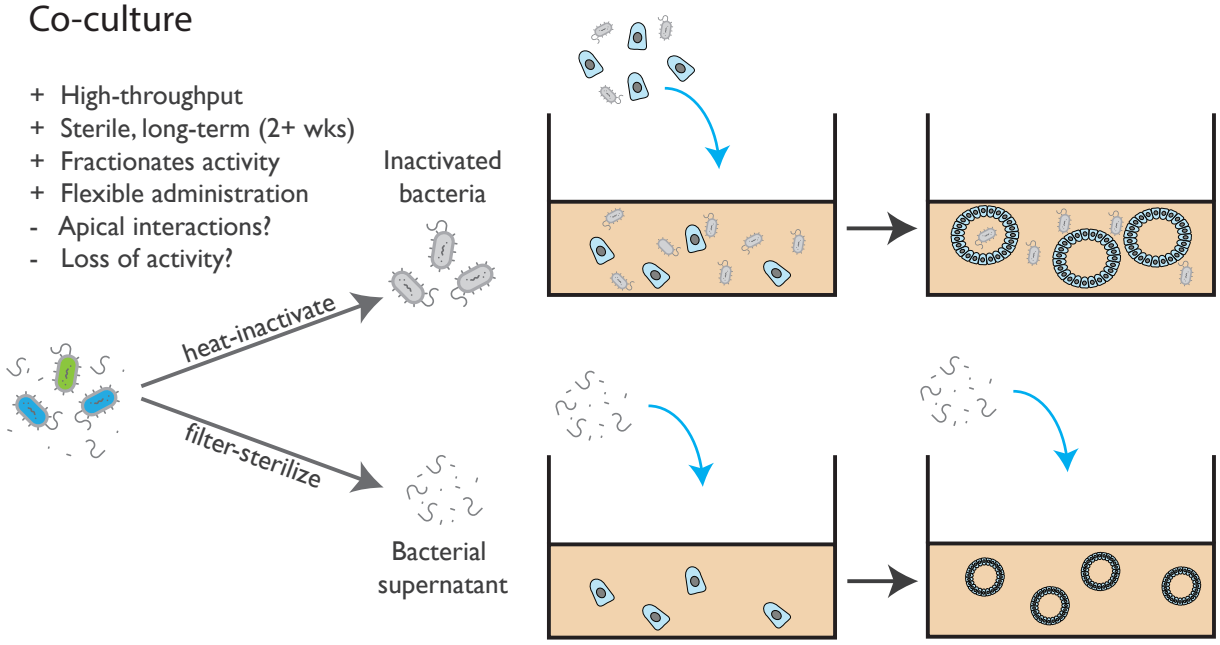

Figure S1 – Schematic of hEnS co-culture with heat-killed bacteria and supernatants.
Heat-killed bacteria were introduced with hEnS precursor cells into the gel layer at the time of seeding before gel polymerization. Bacterial supernatants were mixed with the culture media that was overlayed on top of the gel layer after polymerization.

Figure S2

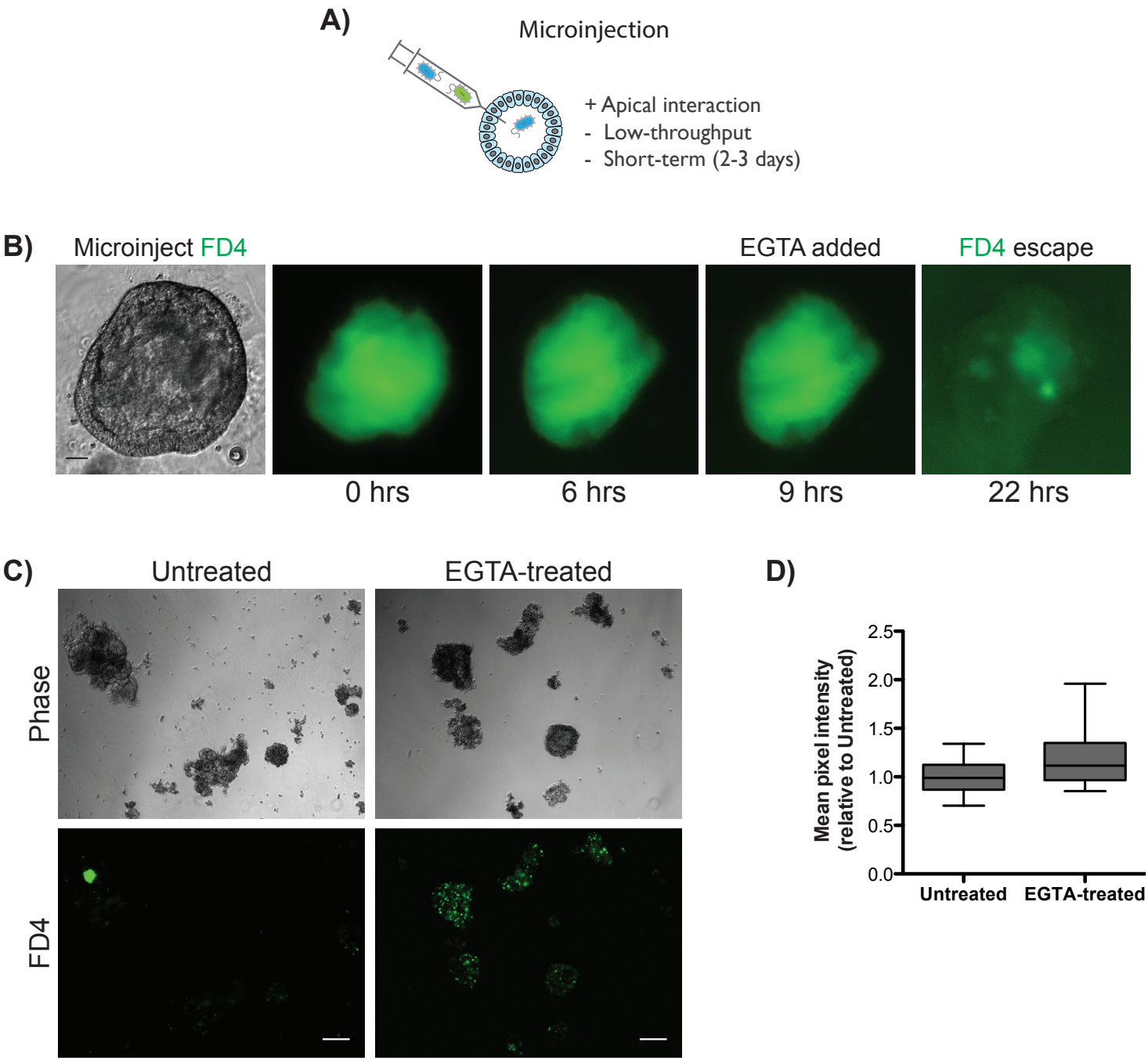

Figure S2 - Analysis of hEnS permeability to FITC-Dextran-4kDa (FD4).
A) Schematic of microinjection into hEnS.
B) Microinjected FD4 persists inside hEnS for at least 9 hours, but escapes after treatment with EGTA.
C) Representative images of hEnS incubated with FD4 with or without simultaneous EGTA treatment for 1 hour.
D) Mean pixel intensity (FD4) for untreated and EGTA-treated hEnS (mean +/- SEM).
Scale bars: 50 µm (A) and 200 µm (B).

Chapter 2.5 – Future Directions and Concluding Remarks

Future Directions

There are a number of avenues for this project that intend to be pursued after the experimental work described at the end of Chapter 2.4 is complete. First, via our collaboration with Dr. Michael Surette, we have access to many commensal bacterial strains isolated from the human intestine (in the form of heat-killed cells as well as cultured supernatants), many of which have not been properly characterized for their impact on the intestinal epithelium. The assay developed here now enables experimental determination of their effect on hEnS formation and growth, and whether they induce an innate immune response.

Due to the fetal nature of hEnS, they provide a unique opportunity to model fetal intestinal diseases *ex vivo*. One particular disease that I am interested in modeling with hEnS is familial multiple intestinal atresia (FMIA). FMIA is an inherited disease where atresia, which is closing of the intestinal tube, occurs at multiple locations throughout the intestine (Cole et al., 2010). It affects newborns at birth and has poor prognosis, with most patients dying within the first two years of life, and can re-occur later in life in individuals that initially survive. The genetic basis of FMIA is mutation(s) in the *TTC7A* gene (Samuels et al., 2013). hEnS represent the ideal structural tissue type for modeling FMIA in the dish because hEnS resemble cysts with a visible lumen, mimicking a cross-section of the intestinal tube. I hypothesize that while normal hEnS are open cysts, hEnS derived from FMIA-hPSCs would develop as closed structures, recapitulating the phenotype observed *in vivo*. Since FMIA is a monogenic disease, instead of going through the time-consuming and challenging process of obtaining primary cells from

patients with FMIA and deriving patient-specific iPSCs, a mutation in the *TTC7A* gene can be engineered in normal human ESCs, iPSCs, or directly in hEnS using genome-editing techniques like CRISPR/Cas9 (Cong and Zhang, 2015). This has been done previously for iPSC-based modeling of other monogenic diseases such as cystic fibrosis (*CFTR* mutations), spinal muscular atrophy (*SMNI* mutations), and Hutchinson-Gilford progeria syndrome (*LMNA* mutations) (Spitalieri et al., 2016). Although FMIA has been previously modeled *ex vivo* using primary enteroid cultures from patient biopsies (Bigorgne et al., 2014), hPSC-derived hEnS may provide further insights into the onset of the disease, such as how mutations in *TTC7A* affect intestinal differentiation itself, and would represent a simple proof of principle study showing the utility of hEnS in modeling disease.

Concluding Remarks

We have developed a functional physiologically relevant model of the human intestinal epithelium from hPSCs. Our work adds to recent advances in *in vitro* 3D culture technologies, and contributes to the field of stem cells in regenerative medicine. Overall, the utilities of hPSC-derived organoid cultures are only beginning to be explored. They will continue to be used in a range of applications all the way from studying basic biology to tissue replacement therapy.

REFERENCES

Alfaleh, K., Anabrees, J., Bassler, D., and Al-Kharfi, T. (2011). Probiotics for prevention of necrotizing enterocolitis in preterm infants. Cochrane Database Syst. Rev. CD005496.

Bigorgne, A.E., Farin, H.F., Lemoine, R., Mahlaoui, N., Lambert, N., Gil, M., Schulz, A., Philippet, P., Schlesser, P., Abrahamsen, T.G., et al. (2014). TTC7A mutations disrupt intestinal epithelial apicobasal polarity. J. Clin. Invest. *124*, 328–337.

Biol-N'Garagba, M.-C., Greco, S., George, P., Hugueny, I., and Louisot, P. (2002). Polyamine participation in the maturation of glycoprotein fucosylation, but not sialylation, in rat small intestine. Pediatr. Res. *51*, 625–634.

Bry, L., Falk, P.G., Midtvedt, T., and Gordon, J.I. (1996). A model of host-microbial interactions in an open mammalian ecosystem. Science *273*, 1380–1383.

Capano, G., Bloch, K.J., Schiffrin, E.J., Dascoli, J.A., Israel, E.J., and Harmatz, P.R. (1994). Influence of the polyamine, spermidine, on intestinal maturation and dietary antigen uptake in the neonatal rat. J. Pediatr. Gastroenterol. Nutr. *19*, 34–42.

Chin, A.M., Hill, D.R., Aurora, M., and Spence, J.R. (2017). Morphogenesis and maturation of the embryonic and postnatal intestine. Semin. Cell Dev. Biol. *66*, 81–93.

Cole, C., Conrad, C., Freitas, A., Clifton, M.S., and Durham, M.M. (2010). Hereditary multiple intestinal atresias: 2 new cases and review of the literature. J. Pediatr. Surg. *45*, E21-24.

Cong, L., and Zhang, F. (2015). Genome engineering using CRISPR-Cas9 system. Methods Mol. Biol. Clifton NJ *1239*, 197–217.

Dekkers, J.F., Wiegerinck, C.L., de Jonge, H.R., Bronsveld, I., Janssens, H.M., de Winter-de Groot, K.M., Brandsma, A.M., de Jong, N.W.M., Bijvelds, M.J.C., Scholte, B.J., et al. (2013). A functional CFTR assay using primary cystic fibrosis intestinal organoids. Nat. Med. *19*, 939–945.

Dufour, C., Dandrifosse, G., Forget, P., Vermesse, F., Romain, N., and Lepoint, P. (1988). Spermine and spermidine induce intestinal maturation in the rat. Gastroenterology *95*, 112–116.

Dye, B.R., Dedhia, P.H., Miller, A.J., Nagy, M.S., White, E.S., Shea, L.D., and Spence, J.R. (2016). A bioengineered niche promotes in vivo engraftment and maturation of pluripotent stem cell derived human lung organoids. ELife *5*.

Finkbeiner, S.R., Hill, D.R., Altheim, C.H., Dedhia, P.H., Taylor, M.J., Tsai, Y.-H., Chin, A.M., Mahe, M.M., Watson, C.L., Freeman, J.J., et al. (2015). Transcriptome-wide

Analysis Reveals Hallmarks of Human Intestine Development and Maturation In Vitro and In Vivo. Stem Cell Rep. *4*, 1140–1155.

Forbester, J.L., Goulding, D., Vallier, L., Hannan, N., Hale, C., Pickard, D., Mukhopadhyay, S., and Dougan, G. (2015). Interaction of Salmonella enterica Serovar Typhimurium with Intestinal Organoids Derived from Human Induced Pluripotent Stem Cells. Infect. Immun. *83*, 2926–2934.

Fordham, R.P., Yui, S., Hannan, N.R.F., Soendergaard, C., Madgwick, A., Schweiger, P.J., Nielsen, O.H., Vallier, L., Pedersen, R.A., Nakamura, T., et al. (2013). Transplantation of expanded fetal intestinal progenitors contributes to colon regeneration after injury. Cell Stem Cell *13*, 734–744.

Forster, R., Chiba, K., Schaeffer, L., Regalado, S.G., Lai, C.S., Gao, Q., Kiani, S., Farin, H.F., Clevers, H., Cost, G.J., et al. (2014). Human Intestinal Tissue with Adult Stem Cell Properties Derived from Pluripotent Stem Cells. Stem Cell Rep. *2*, 838–852.

Gjorevski, N., Sachs, N., Manfrin, A., Giger, S., Bragina, M.E., Ordóñez-Morán, P., Clevers, H., and Lutolf, M.P. (2016). Designer matrices for intestinal stem cell and organoid culture. Nature *539*, 560–564.

Grave, G.D., Nelson, S.A., Walker, W.A., Moss, R.L., Dvorak, B., Hamilton, F.A., Higgins, R., and Raju, T.N.K. (2007). New therapies and preventive approaches for necrotizing enterocolitis: report of a research planning workshop. Pediatr. Res. *62*, 510–514.

Guandalini, S. (2010). Update on the role of probiotics in the therapy of pediatric inflammatory bowel disease. Expert Rev. Clin. Immunol. *6*, 47–54.

Hill, D.R., Huang, S., Nagy, M.S., Yadagiri, V.K., Fields, C., Mukherjee, D., Bons, B., Dedhia, P.H., Chin, A.M., Tsai, Y.-H., et al. (2017). Bacterial colonization stimulates a complex physiological response in the immature human intestinal epithelium. ELife *6*.

Kaiko, G.E., Ryu, S.H., Koues, O.I., Collins, P.L., Solnica-Krezel, L., Pearce, E.J., Pearce, E.L., Oltz, E.M., and Stappenbeck, T.S. (2016). The Colonic Crypt Protects Stem Cells from Microbiota-Derived Metabolites. Cell *165*, 1708–1720.

Klement, E., Cohen, R.V., Boxman, J., Joseph, A., and Reif, S. (2004). Breastfeeding and risk of inflammatory bowel disease: a systematic review with meta-analysis. Am. J. Clin. Nutr. *80*, 1342–1352.

Li, N., Russell, W.M., Douglas-Escobar, M., Hauser, N., Lopez, M., and Neu, J. (2009). Live and Heat-Killed *Lactobacillus rhamnosus* GG: Effects on Proinflammatory and Anti-Inflammatory Cytokines/Chemokines in Gastrostomy-Fed Infant Rats. Pediatr. Res. *66*, 203–207.

McCracken, V.J., and Lorenz, R.G. (2001). The gastrointestinal ecosystem: a precarious alliance among epithelium, immunity and microbiota. Cell. Microbiol. *3*, 1–11.

Munshi, N., Fernandis, A.Z., Cherla, R.P., Park, I.-W., and Ganju, R.K. (2002). Lipopolysaccharide-induced apoptosis of endothelial cells and its inhibition by vascular endothelial growth factor. J. Immunol. Baltim. Md 1950 *168*, 5860–5866.

Mustata, R.C., Vasile, G., Fernandez-Vallone, V., Strollo, S., Lefort, A., Libert, F., Monteyne, D., Pérez-Morga, D., Vassart, G., and Garcia, M.-I. (2013). Identification of Lgr5-independent spheroid-generating progenitors of the mouse fetal intestinal epithelium. Cell Rep. *5*, 421–432.

Nadkarni, R.R., Abed, S., Cox, B.J., Bhatia, S., Lau, J.T., Surette, M.G., and Draper, J.S. (2017). Functional Enterospheres Derived In Vitro from Human Pluripotent Stem Cells. Stem Cell Rep.

Patel, R.M., Myers, L.S., Kurundkar, A.R., Maheshwari, A., Nusrat, A., and Lin, P.W. (2012). Probiotic Bacteria Induce Maturation of Intestinal Claudin 3 Expression and Barrier Function. Am. J. Pathol. *180*, 626–635.

Pickard, J.M., and Chervonsky, A.V. (2015). Intestinal fucose as a mediator of host-microbe symbiosis. J. Immunol. Baltim. Md 1950 *194*, 5588–5593.

Samuels, M.E., Majewski, J., Alirezaie, N., Fernandez, I., Casals, F., Patey, N., Decaluwe, H., Gosselin, I., Haddad, E., Hodgkinson, A., et al. (2013). Exome sequencing identifies mutations in the gene TTC7A in French-Canadian cases with hereditary multiple intestinal atresia. J. Med. Genet. *50*, 324–329.

Sato, T., Vries, R.G., Snippert, H.J., van de Wetering, M., Barker, N., Stange, D.E., van Es, J.H., Abo, A., Kujala, P., Peters, P.J., et al. (2009). Single Lgr5 stem cells build crypt-villus structures in vitro without a mesenchymal niche. Nature *459*, 262–265.

Sato, T., Stange, D.E., Ferrante, M., Vries, R.G.J., Van Es, J.H., Van den Brink, S., Van Houdt, W.J., Pronk, A., Van Gorp, J., Siersema, P.D., et al. (2011). Long-term expansion of epithelial organoids from human colon, adenoma, adenocarcinoma, and Barrett's epithelium. Gastroenterology *141*, 1762–1772.

Senger, S., Ingano, L., Freire, R., Anselmo, A., Zhu, W., Sadreyev, R., Walker, W.A., and Fasano, A. (2018). Human Fetal-Derived Enterospheres Provide Insights on Intestinal Development and a Novel Model to Study Necrotizing Enterocolitis (NEC). Cell. Mol. Gastroenterol. Hepatol. *5*, 549–568.

Sisk, P.M., Lovelady, C.A., Dillard, R.G., Gruber, K.J., and O'Shea, T.M. (2007). Early human milk feeding is associated with a lower risk of necrotizing enterocolitis in very low birth weight infants. J. Perinatol. *27*, 428–433.

Spence, J.R., Mayhew, C.N., Rankin, S.A., Kuhar, M., Vallance, J.E., Tolle, K., Hoskins, E.E., Kalinichenko, V.V., Wells, S.I., Zorn, A.M., et al. (2011). Directed differentiation of human pluripotent stem cells into intestinal tissue in vitro. Nature *470*, 105–109.

Spitalieri, P., Talarico, V.R., Murdocca, M., Novelli, G., and Sangiuolo, F. (2016). Human induced pluripotent stem cells for monogenic disease modelling and therapy. World J. Stem Cells *8*, 118–135.

Stelzner, M., Helmrath, M., Dunn, J.C.Y., Henning, S.J., Houchen, C.W., Kuo, C., Lynch, J., Li, L., Magness, S.T., Martin, M.G., et al. (2012). A nomenclature for intestinal in vitro cultures. Am. J. Physiol. Gastrointest. Liver Physiol. *302*, G1359-1363.

Watanabe, K., Ueno, M., Kamiya, D., Nishiyama, A., Matsumura, M., Wataya, T., Takahashi, J.B., Nishikawa, S., Nishikawa, S., Muguruma, K., et al. (2007). A ROCK inhibitor permits survival of dissociated human embryonic stem cells. Nat. Biotechnol. *25*, 681–686.

Watson, C.L., Mahe, M.M., Múnera, J., Howell, J.C., Sundaram, N., Poling, H.M., Schweitzer, J.I., Vallance, J.E., Mayhew, C.N., Sun, Y., et al. (2014). An in vivo model of human small intestine using pluripotent stem cells. Nat. Med. *20*, 1310–1314.

van de Wetering, M., Francies, H.E., Francis, J.M., Bounova, G., Iorio, F., Pronk, A., van Houdt, W., van Gorp, J., Taylor-Weiner, A., Kester, L., et al. (2015). Prospective derivation of a living organoid biobank of colorectal cancer patients. Cell *161*, 933–945.

Xaus, J., Comalada, M., Valledor, A.F., Lloberas, J., López-Soriano, F., Argilés, J.M., Bogdan, C., and Celada, A. (2000). LPS induces apoptosis in macrophages mostly through the autocrine production of TNF-alpha. Blood *95*, 3823–3831.

Zorn, A.M., and Wells, J.M. (2009). Vertebrate endoderm development and organ formation. Annu. Rev. Cell Dev. Biol. *25*, 221–251.